Cellulose and Pectin Aerogels : Towards their nano-structuration

Cyrielle Rudaz

ParisTech
INSTITUT DES SCIENCES ET TECHNOLOGIES
PARIS INSTITUTE OF TECHNOLOGY

MINES ParisTech

École doctorale n° 364 : Sciences Fondamentales et Appliquées

Doctorat ParisTech

T H È S E

pour obtenir le grade de docteur délivré par

l'École nationale supérieure des mines de Paris

Spécialité " Sciences et Génie des Matériaux "

présentée et soutenue publiquement par

Cyrielle RUDAZ

Le 6 décembre 2013

Cellulose and Pectin Aerogels: Towards their nano-structuration

Aérogels à base de cellulose et pectine : Vers leur nano-structuration

Directrice de thèse : **Tatiana BUDTOVA**

Jury

Mme Irina Smirnova, Professeur, Technische Universität Hambourg	Rapporteur
M. Jacques Desbrières, Professeur, IPREM, Université de Pau	Rapporteur
M. Falk Liebner, Ass.Prof.Dr, University of Natural Resources and Life Sciences Vienna	Examinateur
M. Bernard Yrieix, Docteur, EDF R&D	Examinateur
M. Arnaud Rigacci, Docteur HDR, Persée, Mines ParisTech	Examinateur
Mme Tatiana Budtova, Docteur HDR, Cemef, Mines ParisTech	Examinatrice

T H È S E

MINES ParisTech
CEMEF – UMR CNRS 7635
Rue Claude Daunesse - CS 10207
06904 Sophia-Antipolis Cedex

Remerciements

Ce travail de thèse a été réalisé au Centre de Mise en Forme des Matériaux (Cemef) de Mines-ParisTech à Sophia-Antipolis au sein du pôle « Polymères et Composites ». Il a été financé par l'Agence Nationale de la Recherche (ANR) dans le cadre du projet Nanocel.

Je souhaiterais tout d'abord remercier chaleureusement ma directrice de thèse Tatiana Budtova. Merci Tania de ta confiance, ta grande disponibilité, tes encouragements et ton soutien. J'ai tellement appris à tes côtés !

Je remercie également les membres du jury d'avoir accepté d'évaluer mon travail de thèse : Irina Smirnova et Jacques Desbrières d'avoir été rapporteurs ainsi qu'à Falk Liebner, Arnaud Rigacci et Bernard Yrieix d'avoir été examinateurs. Merci pour la passionnante discussion sur les aérogels et l'intérêt que vous avez porté à mon travail.

Je suis reconnaissante aux partenaires du projet Nanocel pour cette collaboration de trois ans. Merci en particulier à Sylvie Etienne-Calas, Rémi Courson et Laurent Bonnet du laboratoire Charles Coulomb de l'Université de Montpellier pour les nombreuses caractérisations structurales, leur réactivité et leur professionnalisme; à Hébert Sallée du CSTB pour les mesures thermiques, sa disponibilité et sa gentillesse.

J'adresse mes sincères remerciements à Pierre Ilbizian du centre Persée de Mines ParisTech pour le séchage supercritique mais surtout pour son écoute et ses nombreux encouragements. Je remercie également les autres membres de Persée, comme Arnaud Rigacci et Sandrine Berthon-Fabry pour nos échanges scientifiques passionnants et enrichissants. Enfin, j'exprime ma gratitude à Noémie Diascorn pour les nombreux brainstormings qui ont permis d'explorer de nouvelles voies, mais aussi sa disponibilité et son amitié.

Je souhaite exprimer mes remerciements à tous ceux du Cemef qui m'ont aidée à caractériser ces nouveaux biomatériaux. Je pense notamment à Suzanne Jacomet qui m'a tellement appris sur le MEB, à Christophe Pradille et Gilbert Fiorucci pour leur constante bonne humeur et nos fous rires pendant les essais mécaniques.

Je remercie chaleureusement les membres permanents du pôle Polymères et Composite et en particulier Edith Disdier, pour tout ce qu'elle m'a appris sur la sécurité au laboratoire, sa gentillesse et son important soutien moral. Merci également à tous les membres de l'atelier, Marc, Eric, Simon et Francis mais aussi Gaby, Thierry pour leur aide précieuse et leur grande gentillesse. Je suis reconnaissante à Françoise Trucas et Marie-Françoise Guénégan pour leur disponibilité, leur soutien et leur sympathie.

Merci à tous doctorants et post-doctorants que j'ai rencontré pendant ces trois année de thèse et qui m'ont permis de passer des moments agréables : mes deux collègues de bureau les plus géniales Edwige et Valentine, mes amies de Pilates Steph et Noémie et aussi François, Théo, Benjamin, Romain, Seb, Vincent, Thibaut, Nicolas, Georg, Yann, Margot …

Enfin, je remercie sincèrement mes parents et ma sœur pour m’avoir toujours soutenue et encouragée pendant toutes ces années d’étude. Et merci à Clément pour son soutien.

Table of contents

Abbreviations

Experimental parameters

$_{wt}$%: weight percent
ρ_{bulk} (g/cm^3): bulk density
$\rho_{skeletal}$ (g/cm^3): skeletal (or solid) density
ε (%): porosity
S_{BET} (m²/g): specific surface area
$D_{p\ mean}$ (nm): mean pore diameter
$D_{p\ max}$ (nm): maximum of pore size
FWHV (nm): full width at half value of a distribution

E (MPa): Young modulus
σ_{yield} (MPa): yield stress
ε_{yield} (%): yield strain
ε_d (%): densification strain
$W_{40\%}$ (kJ/m^3): absorbed energy from 0 to 40% strain
$W\varepsilon_d$ (kJ/m^3): absorbed energy from 0 to ε_d

$\lambda_{effective}$ (W.m^{-1}.K^{-1}): total or effective thermal conductivity
λ_{solid} (W.m^{-1}.K^{-1}): thermal conductivity of the solid phase
λ_{gas} (W.m^{-1}.K^{-1}): thermal conductivity of the gaseous phase
$\lambda_{radiative}$ (W.m^{-1}.K^{-1}): thermal conductivity of radiative transfer

R_{rel}: relative concentration of epichlorohydrin in the reaction medium
%SR: swelling ratio

η (Pa.s): viscosity
[η] (mL/g): intrinsic viscosity
G’ (Pa): elastic modulus
G’’ (Pa): viscous modulus

Materials

CA: cellulose acetate
DMSO: dimethylsulfoxide
ECH: epichlorohydrin
EMIMAc: 1-ethyl-3-methylimidazolium acetate
HM or LM pectin: high or low methoxy pectin

Techniques

BET: method of Brunauer-Emmett-Teller for specific surface area
BJH: method of Barrett, Joyner and Halenda for pore size distribution
EDS: Energy-dispersive X-ray spectroscopy
SEM: Scanning Electron Microscope

Articles and Communications from this work

This work has led to two articles published in international journals and three others are currently in preparation. Several communications (oral presentations and posters) were given at national and international conferences.

Articles

Hall, C. A., Le, K. A., Rudaz, C., Radhi, A., Lovell, C. S., Damion, R. A., Budtova, T., Ries, M. E. (2012). Macroscopic and microscopic study of 1-ethyl-3-methyl-imidazolium acetate-water mixtures. *The Journal of Physical Chemistry*. B, 116(42), 12810–8.

Rudaz, C., & Budtova, T. (2013). Rheological and hydrodynamic properties of cellulose acetate/ionic liquid solutions. *Carbohydrate Polymers*, 92(2), 1966–71.

Oral presentations

Rudaz, C., Budtova, T., Matrices cellulosiques « hybrides » à base de solutions de cellulose dans liquides ioniques, 11ème Journée du G.F.P. Méditerranée, Sophia-Antipolis, France, 14th September 2011.

Rudaz, C., Liu, W., Sescousse, R., Budtova, T., Aerocellulose and its hybrids from cellulose dissolved in ionic liquid, 2nd EPNOE International Polysaccharide Conference "Polysaccharides as source of advanced and sustainable products", Wageninen, the Netherlands, 29 August- 2 September 2011.

Rudaz, C., Budtova, T., Hybrid ultra-light cellulose-based materials from cellulose-ionic liquid mixtures, "A Greener Chemistry for Industry", Lille, France, 12-14 December 2011.

Rudaz, C., Courson, R., Etienne-Calas, S., Budtova, T., Ultra-light and porous polysaccharide-based materials, EUPOC 2012 – Porous Polymer-based systems: from design to application, Gargnano, Italy, 3-7 June 2012.

Rudaz, C., Courson, R., Etienne-Calas, S., Budtova, T., Aerocellulose: an ultra-light and porous cellulose. Influence of processing parameters on fine morphology, International conference on Bioinspired and Biobased Chemistry and Materials, Nice, France, 3-4 October 2012.

Le, K-A., Rudaz, C., Budtova, T., Phase diagram and solubility limit of cellulose in ionic liquid in the presence of co-solvents, DMSO and water, 3rd International Cellulose Conference ICC2012, Sapporo, Japan, 10-12 October 2012.

Rudaz, C., Pour, G., Budtova, T., Séminaire sur les matériaux architecturés multifonctionnels pour l'efficacité énergétique du bâtiment, Collège de France- Paris, France, 1st March 2013.

Rudaz, C., Courson, R., Etienne-Calas, S., Budtova, T., Aeropectin, an aerogel-like ultra-light and highly porous pectin as promissing thermal insulating material, European Polymer Federation conference (EPF), Pisa, Italy, 16-21 June 2013.

Rudaz, C., Etienne-Calas, S., Courson, R., Bonnet, L., Sallée, H., Budtova, T., Tunable Aerocellulose morphology by cellulose cross-linking, 3rd EPNOE International Polysaccharide Conference "Polysaccharides and Polysaccharide-derived products from basic science to applications", Nice, France, 21-24 October 2013.

Rudaz, C., Etienne-Calas, S., Courson, R., Bonnet, L., Sallée, H., Budtova, T., Aeropectin, a new promising thermal insulating material, 3rd EPNOE International Polysaccharide Conference "Polysaccharides and Polysaccharide-derived products from basic science to applications", Nice, France, 21-24 October 2013.

Posters

Rudaz, C., Budtova, T., Polysaccharides-based aerogels, 1st EPNOE CSA Industrial Meeting, Sophia-Antipolis, France, 7th March 2012.

Rudaz, C., Budtova, T., Polysaccharides-based aerogels, 1st Aerocoins workshop on "Superinsulation Aerogels Materials for Energy Efficiency", Sophia-Antipolis, France, 19th June 2012.

Rudaz, C., Liu, W., Le, K-A., Budtova, T., Cellulose forming by dissolution in ionic liquids: aerogels, films and hybrid materials, GDR BioMatPro. Journée sur les Liquides Ioniques et leurs applications pour la transformation et valorisation des lignocelluloses, Reims, France, 10th October 2012.

Résumé du travail de thèse

Introduction générale

La plupart de nos industries et systèmes de production d'énergie reposent sur la pétrochimie. Depuis la fin du 19ème siècle, le pétrole a été extrait en très grande quantité et est devenu une ressource de plus en plus rare, ce qui augmente grandement son prix. Les carburants issus du pétrole produisent lors de leur combustion des gaz à effet de serre, principaux responsables du réchauffement climatique et d'autres importants problèmes environnementaux. Il est donc nécessaire de trouver des alternatives durables pour réduire notre consommation en ressources fossiles. La biomasse est particulièrement intéressante car elle représente une immense source de carbone renouvelable pour de nombreuses applications, comme les carburants ou les produits chimiques. L'élaboration de nouveaux matériaux, biosourcés avec un faible impact environnemental et des propriétés similaires aux matériaux synthétiques, est l'un des enjeux majeurs pour l'avenir.

Le Conseil Européen a adopté en 2007 trois objectifs principaux à l'horizon 2020, appelés le « triple 20 » : la réduction des gaz à effet de serre de 20%, l'augmentation de la part des énergies renouvelables de 20%, et l'amélioration de l'efficacité énergétique de 20%. Une des voies les plus prometteuses pour atteindre ces objectifs est de diminuer significativement la consommation énergétique des bâtiments. Des isolants thermiques améliorés et efficaces permettraient d'apporter une solution durable aux pertes énergétiques. L'amélioration de l'isolation peut se faire par l'augmentation de l'épaisseur d'isolant utilisé mais cela réduit fortement la surface habitable des logements. Une deuxième approche est de développer de nouveaux matériaux avec une très bonne capacité d'isolation, en dessous de celle de l'air, 0.025 $W.m^{-1}.K^{-1}$. Ces matériaux sont appelés super-isolants thermiques.

Les aérogels sont des matériaux extrêmement poreux et ultra-légers. Ils ont une structure poreuse très fine avec des pores de quelques dizaines de nanomètres. Ils sont généralement obtenus par séchage au CO_2 supercritique. Les aérogels peuvent être inorganiques (à base de silice) ou organiques (exemple du résorcinol-formaldehyde). Ils possèdent une très faible conductivité thermique et sont souvent super-isolants, mais ils sont relativement fragiles (aérogel de silice) ou toxiques (aérogels organiques). Une nouvelle voie de recherche a été récemment menée dans le but de développer des matériaux de type aérogels, biosourcés et super-isolants. Ainsi des aérogels à base de cellulose ou de ses dérivés, ou d'autres polysaccharides ont été investigués (par exemple dans les articles Fischer, Rigacci, Pirard, Berthon-Fabry, & Achard, 2006; García-González, Alnaief, & Smirnova, 2011; Gavillon & Budtova, 2008; Liebner et al., 2009, 2010; Mehling, Smirnova, Guenther, & Neubert, 2009; Sescousse, Gavillon, & Budtova, 2011). Les aérogels à base de cellulose ont été plus particulièrement étudiés et peuvent être classés en deux catégories :

- à partir de *cellulose I*, comme la cellulose bactérienne ou la cellulose avec une nano- ou micro fibrillation. Le précurseur d'aérogel est un réseau de nanofibres de cellulose I gonflé d'eau et séché par $scCO_2$.
- à partir de *cellulose II*, obtenu par le procédé de dissolution-coagulation. Il est appelé « aérocellulose ». Différents solvants de la cellulose peuvent être utilisés (NMMO, 8%NaOH-eau, thiocyanate de calcium, liquides ioniques).

Les aérogels de cellulose peuvent être une solution innovante pour fabriquer des biomatériaux à haute valeur ajoutée, notamment dans le milieu de l'isolation thermique. Est-il possible d'élaborer des matériaux biosourcés, super-isolants, mécaniquement résistants avec un faible impact environnemental ? Ce travail de thèse contribue modestement à répondre à cette question. Il est à l'interface entre de nombreux domaines comme la physico-chimie des polymères, la science des aérogels et des polysaccharides ainsi que la compréhension des relations structure-propriétés.

Le but de ce travail de thèse se distingue en deux voies:
- Evaluer les propriétés thermiques des aérocelluloses et optimiser leurs morphologies pour obtenir si possible des propriétés super-isolantes.
- Avoir une vision plus large des propriétés des aérogels à base de polysaccharides et montrer leur fort potentiel comme biomatériaux dans diverses applications.

La première voie va se concentrer sur une meilleure compréhension de la morphologie de l'aérocellulose pour atteindre des propriétés super-isolantes. Le but est d'affiner la structure poreuse par deux stratégies différentes : la réticulation chimique de la cellulose et la formation de réseaux interpénétrés à base de cellulose.
La seconde voie va étudier d'autres sources de polysaccharides, comme la pectine et d'en préparer des matériaux proches des aérogels, appelés « aéropectine ».

Le principe de préparation des aérocelluloses et des aéropectines est présenté sur la Figure 1. Le polysaccharide est tout d'abord dissout dans un solvant. La solution obtenue peut gélifier au cours du temps. Le gel ou la solution est ensuite coagulée dans un bain de non-solvant. Le polysaccharide précipite en formant une structure poreuse et le solvant de dissolution est libéré dans le bain de coagulation. Le polysaccharide ainsi coagulé est gonflé par le non-solvant et séché par CO_2 supercritique.

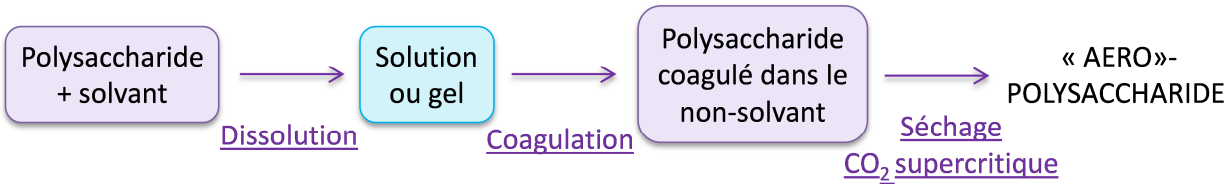

Figure 1 : Schéma de préparation de bio-aérogels: l'aérocellulose et l'aéropectine.

Chaque étape dans l'élaboration de ces "bio-aérogels" sera considérée. La compréhension des propriétés des solutions seront étudiées par rhéologie. L'influence du fluide utilisé pour le bain de coagulation sur la morphologie finale sera discutée. La cinétique de gélification dans le cas de certaines solutions de cellulose sera évaluée. Une analyse détaillée de la structure des bio-aérogels sera réalisée par pycnométrie à poudre ou à mercure, porosimétrie à mercure (technique développée pour les aérogels fragiles), l'adsorption d'azote et le microscope électronique à balayage. Les propriétés mécaniques et thermiques seront également étudiées et les relations

structure-propriétés discutées. Pour les aérogels à base de mélanges de polymères, les interactions entre les différents composants seront investiguées.

Cette thèse a été réalisée dans le cadre du projet ANR « Nanocel ». L'objectif de ce projet était d'élaborer et caractériser des matrices cellulosiques nano-structurées pour une super-isolation thermique. Il rassemblait un consortium de 8 partenaires, industriels et académiques, avec chacun un rôle bien défini :
- Les centres Cemef et Persée de Mines ParisTech: Elaboration d'aérogels à base de cellulose ou d'acétate de cellulose et analyse de cycle de vie
- Laboratoire Charles Coulomb (L2C) - Université de Montpellier: Caractérisations structurales
- CSTB, Grenoble: Caractérisations thermiques
- NeoTIM, Albi: Caractérisations thermiques
- Cethil-Insa Lyon: Modélisation des transferts thermiques dans les aérogels
- CEA, Marcoule: Optimisation du séchage supercritique
- EDF R&D, Moret-sur-Loing: Caractérisations thermo-hydriques.

Chapitre I : Etat de l'art

Le chapitre I fait état de l'art sur la structure et la mise en forme de deux polysaccharides, la cellulose et la pectine, pour obtenir des aérogels ou « aéro-polysaccharides ».
La cellulose est le polymère le plus abondant sur Terre et l'un des composants majeurs du bois, coton, lin, etc. Elle est constituée d'un assemblement d'unités anhydroglucose (AGU). Elle possède un grand nombre de liaisons hydrogènes qui lui confère une grande stabilité chimique mais peu de solvants sont capables de la dissoudre. Ce sont souvent des solvants complexes, toxiques avec une faible capacité de dissolution. Depuis une dizaine d'années, des études ont montré le fort intérêt des liquides ioniques dans la dissolution de la cellulose. Ils ont une faible tension de vapeur, sont stables thermiquement et chimiquement et peuvent dissoudre jusqu'à 30% de cellulose. Ils sont largement utilisés pour la fonctionnalisation de la cellulose. Cependant, à l'heure actuelle, ils sont encore très onéreux et doivent être d'une grande pureté pour éviter des réactions secondaires.

La pectine est constituée d'un arrangement d'unités d'acide D-galacturonique qui peuvent être partiellement estérifiées. On distingue deux catégories de pectines selon le degré d'estérification: celle à haut degré d'estérification (HM) (au-delà de 50%) et à faible degré d'estérification (LM) (en-dessous de 50%). La pectine est extraite principalement des écorces d'agrumes ou de marc de pomme. Les pectines HM peuvent être dissoutes dans une solution aqueuse acide. Les groupes carboxyl sont alors sous leur forme protonée ce qui diminue les répulsions électrostatiques et augmente la formation de liaisons hydrogènes. Un gel physique est ainsi formé. Les pectines LM gélifient et forment un complexe avec des cations divalents.

Ce chapitre aborde également la préparation d'aérogels. Ce sont des matériaux très légers et poreux, souvent séchés par CO_2 supercritique. Le plus utilisé est l'aérogel de silice : c'est un materiau nano-structuré, avec une densité d'environ 0.1 g/cm^3, une haute surface spécifique 800-

900 m^2/g et une très basse conductivité thermique (0.015-0.02 $W.m^{-1}.K^{-1}$). Le principe de la « super-isolation » a été décrit : elle présente une conductivité thermique totale en dessous de 0.025 $W.m^{-1}.K^{-1}$. La conductivité thermique se distingue en trois composantes : la conduction de la phase solide, de la phase gazeuse et l'effet radiatif. Le contrôle de la morphologie avec des pores de taille inférieure au libre parcours moyen des molécules d'air (70 nm) permet de diminuer significativement la contribution de la phase gazeuse, par effet Knudsen, et d'atteindre des propriétés super-isolantes.
Les études sur les aérogels à base de polysaccharides, comme la cellulose, la pectine, l'alginate ou l'amidon, sont peu nombreuses mais montrent un très grand potentiel avec des morphologies intéressantes. Différentes applications des aérogels à base de polysaccharides ou « aéro-polysaccharides » peuvent être envisagées comme la libération contrôlée de médicaments ou l'isolation thermique.

Chapitre II: Matériaux et méthodes

La préparation des « aéro-polysaccarides » est réalisée en plusieurs étapes comme montré sur la Figure 1: le polysaccharide (cellulose ou pectine) est dissout dans un solvant puis coagulé dans un bain de non-solvant (typiquement eau ou éthanol) et séché par CO_2 supercritique.
Les propriétés des solutions, comme la cellulose dans les liquides ioniques ou ses mélanges avec l'acétate de cellulose, ont été étudiées par rhéologie.
Les aérocelluloses et les aéropectines ont été observées par microscope électronique à balayage (MEB) et caractérisées par leur densité apparente (par pycnométrie au mercure ou à poudre) et de squelette (par pycnométrie à l'hélium), leur surface spécifique (par adsorption de N_2 et la méthode BET) et leur distribution de taille de pores (par porosimétrie mercure ou désorption de N_2 et la méthode BJH). Ces mesures ont été réalisées au laboratoire Charles Coulomb de l'Université de Montpellier ainsi qu'au centre Persée-Mines ParisTech.

Les aéropolysaccharides ont également été testés mécaniquement par compression uniaxiale et caractérisées par leur module d'Young et leur contrainte de plasticité. Le modèle de mousses décrit par Gibson et Ashby a été utilisé en première approximation.

Enfin, la conductivité thermique totale ainsi que ses différentes contributions (solide, gaz et radiatif) des aérocelluloses et aéropectines ont été mesurées par thermofluxmètre ou par la méthode du fil chaud. Ces mesures ont été réalisées au CSTB de Grenoble ainsi qu'au centre Persée-Mines ParisTech.

Chapitre III: Propriétés structurales et thermiques des aérocelluloses préparées dans différents solvants : 8%NaOH-eau, EMIMAc et EMIMAc/DMSO

L'élaboration des aérocelluloses par la dissolution de cellulose dans des solvants comme 8%NaOH-eau et les liquides ioniques ainsi que leurs caractérisations ont été étudiées précédemment. Le liquide ionique, l'acétate de 1-éthyl-3-méthylimidazolium (EMIMAc), permet de dissoudre une quantité importante de cellulose mais la solution résultante est hautement visqueuse. De plus, EMIMAc réagit de manière exothermique avec l'eau du bain de coagulation créant de gros macropores dans la structure poreuse de la cellulose coagulée. Nous avons donc investigué l'addition d'un co-solvant, le diméthylsulfoxide (DMSO) à l'EMIMAc et montré qu'il diminue grandement la viscosité et l'apparition des macropores dans les aérocelluloses. Le diagramme de phase de cellulose-EMIMAc-DMSO a été établi et montre qu'il est encore possible de dissoudre de fortes concentrations de cellulose (~ 20_{wt}%) avec 30-40_{wt}% DMSO ajoutés à l'EMIMAc.

Nous avons comparé les propriétés structurales de 5_{wt}% aérocellulose préparées dans différents solvants : 8%NaOH-eau, EMIMAc et 60_{wt}% EMIMAc - 40_{wt}% DMSO. Elles présentent toutes une grande porosité (>90%). La densité apparente de l'aérocellulose à partir d'EMIMAc/DMSO est légèrement plus élevée que pour EMIMAc grâce à la diminution des macropores. Les distributions de tailles de pores sont relativement similaires pour les aérocelluloses préparées à partir de liquides ioniques mais sont plus larges que pour les aérocelluloses à partir de 8%NaOH. La concentration en cellulose modifie grandement la morphologie de l'aérocellulose finale. La densité apparente augmente linéairement avec la concentration en cellulose et aucune différence n'est observée entre les solvants EMIMAc ou EMIMAc/DMSO. Les aérocelluloses les plus concentrées (par exemple, à base de 15_{wt}% cellulose) présente une structure poreuse plus fine avec des plus petits pores et plus homogènes par rapport à une aérocellulose moins concentrée comme 5_{wt}%.

Les propriétés thermiques des différentes aérocelluloses ont été étudiées. La conductivité thermique d'une aérocellulose préparée à partir de 5_{wt}% cellulose dans 80_{wt}% EMIMAc- 20_{wt}% DMSO est de 32.8 $mW.m^{-1}.K^{-1}$ pour une densité de 0.18 g/cm^3. Des résultats similaires ont été obtenus pour les aérocelluloses dans 8%NaOH à égale densité (7_{wt}%). L'aérocellulose 5_{wt}% dans 8%NaOH-eau a donné la meilleure conductivité thermique avec 30.8 $mW.m^{-1}.K^{-1}$. Les trois contributions (solide, gaz et radiatif) ont été déterminées. La conduction de la phase gazeuse représente 60% et le transfert radiatif 30% de la conductivité totale. La conductivité de la phase solide a été estimée à 3.5 $mW.m^{-1}.K^{-1}$ pour une densité apparente de 0.18 g/cm^3.

Toutes les aérocelluloses, indépendamment du solvant utilisé donnent des conductivités thermiques supérieures à celle de l'air libre (0.025 $W.m^{-1}.K^{-1}$). Cela est principalement dû à la présence de certains gros pores (avec des tailles au-delà du libre parcours moyen des molécules d'air, 70 nm) et au manque de contrôle de la morphologie pendant la coagulation.

Chapitre IV: Cellulose réticulée- Gels et Aérogels

Pour obtenir de bonnes propriétés thermiques, il est important d'avoir une structure poreuse fine et « nano-structurée ». Nous avons étudié l'influence de la réticulation chimique de la cellulose sur la morphologie des aérocelluloses. La réticulation a été réalisée par l'agent réticulant, l'épichlorhydrine (ECH), dans le solvant 8%NaOH-eau. Le rapport R_{rel} a été défini comme le rapport molaire de la quantité d'ECH sur celle de cellulose et représente la concentration initiale relative en ECH dans le milieu réactionnel. Comme il n'a pas été possible de déterminer précisément le « vrai » degré de réticulation de la cellulose, nous avons préféré utiliser le rapport R_{rel} pour toutes les caractérisations. Les propriétés des solutions de cellulose réticulée et leur gélification ont été étudiées par rhéologie. Le temps de gélification est fortement diminué en présence d'agent réticulant avec un maximum pour $R_{rel} = 0.5$, ce qui montre la compétition entre la gélification physique et la gélification par réticulation chimique. Nous supposons que l'agent réticulant écarte spatialement les chaînes de cellulose ce qui diminue l'association de chaines par liaisons hydrogène. Le temps de gélification des solutions de cellulose réticulée diminue exponentiellement avec la température avec un comportement plus particulier pour la formulation $R_{rel} = 0.5$ qui est moins sensible à la température.

Les solutions de cellulose réticulée ont été coagulées dans l'eau. Le gonflement des celluloses coagulées a été étudié par le degré de gonflement (%SR) en fonction de la concentration en agent réticulant R_{rel}. Il augmente fortement jusqu'à $R_{rel} = 1$ (%SR≈3500) puis diminue à plus haut degré de réticulation (%SR≈1500). Nous supposons que l'addition d'un agent réticulant écarte les chaines de cellulose et permet de créer des pores supplémentaires qui se remplissent d'eau, augmentant ainsi le degré de gonflement. Pour la cellulose coagulée non-réticulée ou faiblement réticulée, les échantillons sont blancs et opaques alors que pour une cellulose plus fortement réticulée les échantillons apparaissent transparents, démontrant une structure plus homogène que ceux non-réticulés.

Les échantillons gonflés dans l'eau ne peuvent pas être directement séchés par $scCO_2$ et une étape supplémentaire d'échange de solvant est nécessaire. Différents liquides ont été testés et le méthanol a été choisi, la contraction des échantillons dans ce solvant étant plus limitée.

Les aérocelluloses réticulées obtenues par séchage supercritique ont été caractérisées et comparées en fonction de la concentration relative d'agent réticulant, R_{rel}. La densité apparente augmente linéairement avec la concentration en épichlorhydrine. La surface spécifique est maximale pour $R_{rel} = 0.5$, ce qui montre une structure plus fine comparée à une aérocellulose non-réticulée. Les distributions de taille de pores sont plus fines pour les aérocelluloses réticulées.

Les aérocelluloses réticulées ont été testées par compression uniaxiale. Les modules d'Young et les contraintes de plasticité ont été déterminés et suivent des lois en puissance $E \sim \rho^{2.4}$ and $\sigma_{plasticité} \sim \rho^{2.2}$. A égale densité, les aérocelluloses réticulées présentent de bien meilleures propriétés mécaniques que celles non-réticulées.

Les propriétés thermiques des aérocelluloses réticulées à 5% cellulose et 7_{wt}% cellulose ont été mesurées. Un minimum de conductivité a été observé pour les formulations avec R_{rel} = 0.5. Les conductivités thermiques totales ont évaluées à 26.2 and 30.7 $mW.m^{-1}.K^{-1}$ pour des aérocelluloses respectivement de 5 et 7_{wt}%. Ces formulations présentent la plus fine structure (la plus haute surface spécifique), ce qui confirme l'idée que d'améliorer la structure poreuse vers une nano-structuration donne de meilleures propriétés thermiques. La réticulation de la cellulose a permis de s'approcher du domaine de la super-isolation (25 $mW.m^{-1}.K^{-1}$).

Enfin, nous avons étudié et comparé différents modes de séchage des aérocelluloses réticulées : par séchage évaporatif, cryo-dessication et séchage par CO_2 supercritique. Les « xéro-celluloses » obtenues par séchage évaporatif sont très peu poreuses. Les « cryo-celluloses » sont hautement poreuses et extrêmement légères mais présentent de très larges macropores et des inhomogénéités par rapport aux « aéro-celluloses » séchées par CO_2 supercritique.

Chapitre V: Hybrides à base de cellulose préparés dans les liquides ioniques

La deuxième stratégie pour obtenir des aérocelluloses plus finement structurées a été d'investiguer la préparation d'hybrides avec d'autres polymères dans le but de faire des réseaux interpénétrés. Deux polymères ont été étudiés : l'acétate de cellulose et la lignine.
L'élaboration d'hybrides de cellulose et d'acétate de cellulose (CA) ne peut se faire que par dissolution dans un solvant commun. L'EMIMAc a été choisi. Des études rhéologiques ont montré que la solution de CA-EMIMAc se comportait classiquement comme une solution de polymère. La viscosité intrinsèque d'acétate de cellulose dans EMIMAc a été déterminée : elle diminue en fonction de la température comme il a déjà été reporté pour les solutions de cellulose-EMIMAc. La concentration de recouvrement de l'acétate de cellulose dans l'EMIMAc est plus grande que pour d'autres solvants organiques (diméthylformamide, tetrachloroéthane et acétone), ce qui montre que la qualité thermodynamique de l'EMIMAc est plus faible. L'énergie d'activation suit une loi en puissance avec la concentration en polymère.

Les mélanges de cellulose et d'acétate de cellulose dans l'EMIMAc ont été étudiés pour des concentrations totales en polymères de 5 et 10_{wt}%. Aucune séparation de phase n'a été observée à l'état liquide. La viscosité du mélange suit une loi de mélange, ce qui montre que les deux polymères coexistent dans le solvant sans interactions entre eux.

Les mélanges de différentes compositions en cellulose et acétate de cellulose ont ensuite été coagulés dans l'eau ou l'éthanol puis séchés par $scCO_2$ pour donner des matériaux « hybrides ». Des morphologies très différentes ont été observées selon les compositions ainsi que des séparations de phases entre les deux polymères. La porosité diminue fortement et les inhomogénéités augmentent avec l'augmentation de la concentration en acétate de cellulose.

Des hybrides secs préparés à partir de solutions de cellulose, lignine (lignosulphonate) et EMIMAc ont aussi été étudiés. La lignine a été lavée par l'eau pendant la coagulation de la cellulose. Lors de la coagulation dans l'éthanol, la lignine reste dans la structure poreuse mais des phases distinctes de celles de la cellulose ont été observées.

Il semble donc assez difficile de préparer des hybrides à base de cellulose qui soient homogènes et présentent des propriétés morphologiques intéressantes.

Chapitre VI: Aéropectine et les hybrides pectine-silice

Nous nous sommes intéressés à un autre polysaccharide, la pectine, et à l'élaboration de l'aérogel correspondant, « l'aéropectine ».
La pectine est dissoute dans une solution acide puis cette solution gélifie au cours du temps. Nous avons étudié l'influence du pH sur la structure du gel de pectine. Pour éviter des inhomogénéités dans le gel, le pH doit être très acide (< 1), et par la suite le solvant 0.5 mol/L HCl a été utilisé. Après un échange progressif de solvant dans l'éthanol, la pectine coagulée est séchée par CO_2 supercritique.
Les aéropectines obtenues sont poreuses (>90%) et très légères. La densité apparente croît linéairement avec la concentration en pectine. La surface spécifique, autour de 250 m²/g, et les distributions de taille de pores sont très proches de celles de l'aérocellulose préparée dans 8%NaOH-eau. Les distributions sont plus fines pour des concentrations en pectine plus élevées. Aucune différence majeure n'a été observée selon la source de la pectine (de marc de pomme ou d'écorce d'agrumes).

Les propriétés mécaniques des aéropectines ont aussi été étudiées par compression uniaxiale. Les modules de Young ainsi que les contraintes de plasticité varient en loi de puissance avec la densité apparente : $E \sim \rho^{1.8}$ and $\sigma_{plasticité} \sim \rho^{3.2}$. Les aéropectines ont été comparées aux aérocelluloses non-réticulées et présentent de meilleures propriétés mécaniques (E et $\sigma_{plasticité}$). Cela peut s'expliquer par les différences de configuration spatiale des macromolécules de cellulose et de pectine.

La conductivité thermique totale des aéropectines a été mesurée : elle diminue avec la diminution de la concentration en pectine. Une aéropectine à 2_{wt}% donne une faible conductivité thermique de 20 $mW.m^{-1}.K^{-1}$. La contribution gazeuse représente la majeure partie de la conductivité thermique totale (autour de 60%) et la conduction de la phase solide a été estimée à 2.8 $mW.m^{-1}.K^{-1}$. Les aéropectines sont les premiers matériaux biosourcés, plus respectueux de l'environnement (sans réticulation chimique), qui soient robustes mécaniquement et qui présentent des propriétés thermiques super-isolantes.

Pour essayer d'abaisser la conductivité des aéropectines, l'air contenu dans la structure poreuse a été remplacé par une phase super-isolante comme l'aérogel de silice : l'idée était de former des hybrides pectine-silice. Pour élaborer ces hybrides, une solution de précurseurs de silice a diffusé à l'intérieur du réseau poreux de la pectine coagulée (gonflée dans l'éthanol). La condensation de

la silice est directement réalisée à l'intérieur du réseau de pectine. La pectine coagulée, chargée de silice, est ensuite séchée par $scCO_2$.
Nous avons d'abord étudié l'influence du temps de diffusion (ou imprégnation), par analyse EDS. Nous avons montré qu'une saturation en silice est observée après 10 heures d'imprégnation.
Les hybrides pectine-silice, séchés par $scCO_2$, ont des rendements d'imprégnation importants, autour de 75% pour une formulation standard d'aérogels de silice et 90% pour une formulation optimisée. Les surfaces spécifiques des hybrides sont beaucoup plus importantes que les aéropectines pures, 700 m^2/g vs 250 m^2/g, ce qui prouve la présence de silice nanostructurée à l'intérieur du réseau de pectine.

Les hybrides pectine-silice ont des conductivités thermiques plus faibles de 4-5 $mW.m^{-1}.K^{-1}$ par rapport aux aéropectines pures. La meilleure formulation donne une conductivité totale de 17 $mW.m^{-1}.K^{-1}$.

Conclusions et Perspectives

Le but de cette thèse a été d'élaborer et de caractériser une nouvelle génération d'aérogels à base de cellulose et de pectine. L'objectif principal était d'obtenir des matériaux « nano-structurés » par la dissolution, coagulation et séchage sous CO_2 supercritique.
Pour la cellulose, plusieurs voies ont été étudiées : l'ajout de co-solvant au liquide ionique (EMIMAc), la réticulation chimique de la cellulose et la création de réseaux interpénétrés avec un second polymère.
Pour la pectine, nous avons investigué la formation d'une structure poreuse à base de pectine pure, sans réticulation chimique, ainsi que des hybrides pectine-silice.
Dans tous les cas, nous nous sommes attachés à corréler les propriétés structurales des aéropolysaccharides à leurs propriétés mécaniques et thermiques.
Ces aérogels sont biosourcés, avec un plus faible impact sur l'environnement, et peuvent être utilisés dans de nombreuses autres applications que l'isolation thermique, telle que la libération contrôlée de médicaments ou en catalyse.

Des améliorations peuvent être encore apportées sur les aérocelluloses réticulées. L'agent réticulant, l'épichlorhydrine est toxique et nocif pour l'environnement. L'étape suivant serait de trouver un autre type de composé, compatible avec les solvants de la cellulose et qui soit plus respectueux de la santé et de l'environnement.
Nous avons utilisé principalement la pectine à haut degré d'estérification. Il peut être envisagé de préparer des gels à partir de pectine faiblement estérifiée et complexée par les cations divalents. Les aéropectines résultantes peuvent présenter des propriétés morphologiques intéressantes.
D'autres polysaccharides peuvent être envisagés pour la préparation d'aérogels comme l'alginate, le carraghénane, la chitine ou le chitosane.
Des hybrides cellulose-silice peuvent présenter également un grand intérêt, notamment pour l'isolation thermique. Deux projets sont en cours à Mines ParisTech sur cette thématique.

General Introduction

Currently, most industries and energy production systems are based on petrochemistry. Many products in our everyday life are petrochemicals such as fuels, plastics, clothes, shampoos, food, medicine… Since the end of the 19th century, crude oil has been extracted in huge quantities, and nowadays it is becoming harder and harder to get petroleum from our natural resources. The price of fossil fuels (like petroleum, coal…) continually rises. Fuels from petroleum produce greenhouse gases (GHG), like carbon dioxide CO_2, when they are burnt. GHG are responsible for global warming and many other environmental issues. It is thus necessary to find long-term alternative solutions to reduce the consumption of non-renewable fossil resources. Biomass is attracting research and industry since it represents a huge source of renewable carbon for fuels, chemicals and materials. The elaboration of bio-based and environmentally friendly materials with similar and better properties as synthetic materials is the one of the major challenge for today and tomorrow.

The European Council adopted, in 2007, three major energy and climate change objectives for 2020: to reduce greenhouse gas emissions by 20%, to increase the share of renewable energy to 20% and to make a 20% improvement in energy efficiency. One of the most promising ways to achieve these objectives is a reduction of the energy consumption of buildings. Efficient and improved thermal insulation materials can bring a sustainable solution to decrease thermal losses of buildings. One of the ways to improve insulation is to install thicker layers of conventional insulation but it will considerably decrease the living area in houses. The second approach is to design new materials with a very low capacity to conduct heat, called thermal conductivity, below the thermal conductivity of the air, 0.025 $W.m^{-1}.K^{-1}$. These materials are called super-insulating materials.

Aerogels are highly porous and ultra-light materials; they have a very fine structure with pores of few tens nanometers. They are usually obtained by drying of wet gels with supercritical CO_2 ($scCO_2$) and in a few rare cases by drying at ambient pressure after gel chemical treatment. Aerogels are often either inorganic (silica) or organic (resorcinol-formaldehyde). They have very low thermal conductivity, generally in the super-insulation domain, but have either poor mechanical properties (silica aerogels) or they are toxic (organic aerogels). One of the ways to solve the problem is to develop a new generation of super-insulating materials that are aerogel-like and based on natural polymers. This has become a “hot” research topic and recently the first aerogels based on cellulose, cellulose derivatives or some other polysaccharides were developed (see, for example, Fischer, Rigacci, Pirard, Berthon-Fabry, & Achard, 2006; García-González, Alnaief, & Smirnova, 2011; Gavillon & Budtova, 2008; Liebner et al., 2009, 2010; Mehling, Smirnova, Guenther, & Neubert, 2009; Sescousse, Gavillon, & Budtova, 2011). Cellulose aerogels seem to be the most studied; they can be classified in two main categories:
- from *cellulose I*, such as bacterial cellulose, nano- or micro-fibrillated cellulose. The precursor of aerogel is a network of cellulose I nanofibers filled with water which is then dried with $scCO_2$.
- from *cellulose II* obtained by dissolution-coagulation route and is called “Aerocellulose”. Various cellulose solvents can be used (NMMO, 8%NaOH-water, calcium thiocyanate, ionic liquids).

Cellulose aerogels can be a promising solution as new high added-value biomaterials, particularly in the thermal insulation domain. The question here is “is it possible to get bio-based super-insulating materials, mechanically robust and with a low environmental impact?” This work makes a small step in trying to answer this question. That is why it is at the interface between polymer chemical physics, aerogel science, polysaccharides and the understanding of structure-properties relationships.

The overall goal of this thesis is double:
- First, we want to evaluate the thermal properties of aerocelluloses and to tune the morphology of cellulose porous materials to obtain, if possible, super-insulation properties.
- Second, we should like to have a larger vision of polysaccharide aerogels properties and to show their high potential as biomaterials for various applications.

Within the first objective we shall focus on a better understanding of aerocelluloses morphology, targeting super-insulation properties. We will try to tune the porous structure by two different strategies: cellulose crosslinking and the formation cellulose-based interpenetrating networks.
Within the second objective we shall investigate other sources of polysaccharides such as pectin and prepare materials that are similar to an aerogel, called “aeropectin”.

The principle of aerocellulose and aeropectin preparation is shown in Figure 2. The polysaccharide is first dissolved in a solvent. The solution obtained may undergo a gelation depending on the polysaccharide and the solvent used. The gel or solution is then placed in a non-solvent coagulation bath where the polysaccharide precipitates forming a porous network. During coagulation the dissolution solvent is released and the non-solvent penetrates into the polysaccharide sample. The coagulated polysaccharide swollen in the non-solvent is finally dried with supercritical CO_2 ($scCO_2$). If the non-solvent is not compatible with $scCO_2$, a solvent exchange step (typically ethanol or acetone) is therefore required before drying.

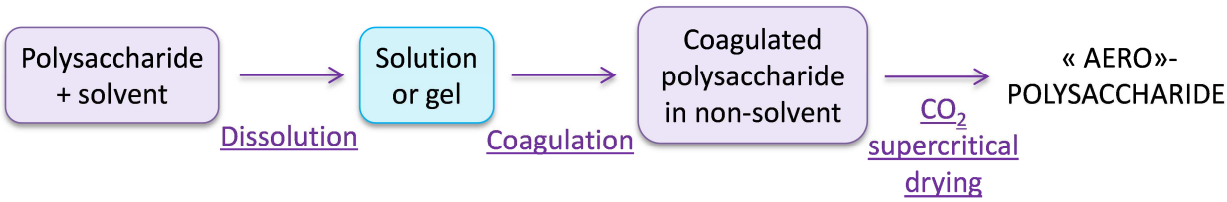

Figure 2 : General preparation of “bio-aerogels”: aerocellulose and aeropectin.

We will study each step of the elaboration of “bio-aerogels”. We shall start from polysaccharide dissolution and understanding solution properties using dynamic and steady state rheology. The influence of the fluid used for coagulation on the final morphology will be discussed. In the case of cellulose solution gelling, the kinetics of gelation will be monitored. A detailed analysis of materials structure and morphology will be performed using powder or mercury and helium pycnometry, mercury porosimetry (approach developed for weak aerogels), nitrogen adsorption and scanning electron microscopy. The mechanical and thermal properties of bio-aerogels will

be studied and structure-properties relationships will be discussed. For aerogels based on polymers mixtures, the interactions between the components will be investigated.

This thesis was performed in the frame of the ANR project “Nanocel”. The road map of this project was to elaborate and characterize super-insulating cellulosic porous matrices (from cellulose or cellulose acetate). It was a consortium of 8 partners, industrial and academic, with different roles:
- Cemef and Persée centers from Mines ParisTech: Elaboration of cellulose-based aerogels and life cycle assessment
- Laboratoire Charles Coulomb (L2C) - University of Montpellier: Structural characterisations
- CSTB (Scientific and Technical Center for Building), Grenoble: Thermal characterisations
- NeoTIM, Albi: Thermal characterisations
- Cethil-Insa Lyon: Numerical modeling of aerogels’ thermal behavior
- CEA, Marcoule: Supercritical drying optimisation
- EDF R&D, Moret-sur-Loing: Thermo-hydric characterisations.

This manuscript is divided is six chapters.
Chapter I deals with the literature review on two polysaccharides used in the work, cellulose and pectin, and their properties and processing. The concept of “aerogel”, as a very porous material dried by supercritical route, will be introduced and illustrated by several examples such as silica aerogels. A more detailed review of aerogels from polysaccharides will be given, with a special focus on cellulose and its derivatives, starches, alginate and pectin. These bio-aerogels have a large range of morphologies and mechanical properties that can be tuned with polysaccharides concentration, different solvents or the addition of cross-linkers. Various applications of these materials will be presented such as controlled drug release and thermal insulation. The notion of super-insulation will be introduced.

Chapter II describes starting materials and experimental methods used during the thesis. The elaboration of bio-aerogels by dissolution-coagulation-supercritical CO_2 drying route is detailed. Structural characterisations techniques, such as helium and mercury pycnometry, mercury porosimetry with the theory of indirect reconstruction of pores distribution, nitrogen adsorption and scanning electron microscopy, will be presented. Mechanical properties of bio-aerogels will be studied by uniaxial compression and a model for foams will be used in a first approximation. The total thermal conductivity as well as the different thermal contributions (solid, gas and radiative) will be investigated by steady-state (heat flow-meter) and transient methods (hot-wire experiments).

Chapter III is dedicated to the comparison of morphology and properties of aerocelluloses prepared from different solvents: 8%NaOH-water and ionic liquids. The solution of cellulose in the ionic liquid, EMIMAc, is highly viscous which is responsible for inhomogeneities in the structure of coagulated cellulose. The addition of a co-solvent, dimethylsulfoxide (DMSO) and its influence on cellulose solutions viscosity will be investigated. A ternary phase diagram cellulose-EMIMAc-DMSO will be built and discussed. The influence of the non-solvent (water or ethanol) used for coagulation on aerocellulose morphology will be studied. Structural

properties (bulk density, specific surface areas and pore size distributions) of aerocelluloses prepared from 8%NaOH-water, EMIMAc and EMIMAc-DMSO will be compared. The thermal properties of aerocellulose will be measured and correlated to the porous structure. It will be shown that it will be not possible to achieve fine morphology with super-insulating properties by only changing the cellulose solvents.

To elaborate "nano-structured" aerocelluloses, the first strategy will be to investigate the chemical cross-linking of cellulose. Chapter IV focuses on the cellulose cross-linking by epichlorohydrin in the solvent 8%NaOH-water. In this solvent, cellulose solution undergoes a physical gelation. The influence of the addition of cross-linker on the cellulose solutions gelation by dynamic rheology will be studied. A competition between physical and chemical gelation mechanisms will be demonstrated. Cross-linked cellulose solutions will be then coagulated in water. The effects of cross-linking on the formation of coagulated cellulose by looking at samples' swelling ratios will be discussed. Several fluids for the solvent exchange step and their influence on the samples texture will be investigated. Samples will be dried with $scCO_2$ to give cross-linked aerocelluloses. Structural properties of these aerogels will be studied depending on the cross-linking ratio. An optimal formulation will be demonstrated to give the finer morphology and reach thermal properties close to super-insulation. Cross-linked aerocelluloses will be tested by uniaxial compression and their mechanical properties will be correlated to the final porous structure.

Chapter V presents the second strategy for the nano-structuration of aerocellulose: creating interpenetrated networks of cellulose with a second polymer. Two polymers will be investigated cellulose acetate and lignin. Cellulose acetate is of special interest as it forms a fine structured aerogel, when chemically cross-linked, with promising thermal properties. Cellulose and cellulose acetate must be processed in the liquid state and EMIMAc is chosen as a common medium. Rheological properties of cellulose and cellulose acetate in EMIMAc will be characterised and potential interactions between these two polymers will be evaluated. Solutions will be coagulated in various fluids (water and ethanol) and dried by $scCO_2$. Dried cellulose-based hybrids (with lignin or cellulose acetate) will be characterised as a function of their composition. It will be shown that a phase separation between the two components occurs during coagulation step.

Chapter VI focuses on another polysaccharide, pectin and the pectin-based aerogel "Aeropectin". Pectin will be dissolved in an acidic aqueous solution and will gel in time. The gelation as a function of the solvent pH will be briefly discussed. Gelled pectin will be coagulated in ethanol and dried by $scCO_2$. The influence of pectin sources (apple pomace and citrus peel) and concentrations on structural properties (bulk and skeletal densities, specific surface areas and pores size distribution) of aeropectins will be studied and compared to aerocelluloses. Mechanical behaviour will be evaluated by uniaxial compression and correlated to bulk densities. Effective thermal conductivities will be measured and discussed as a function of pectin concentrations. The different thermal contributions, solid, gas and radiative, will be determined and related to the porous structure of aeropectins.

Silica aerogel is known to be one of the best super- insulating materials. In order to improve thermal properties of aeropectins, the elaboration of hybrid pectin-silica aerogels will be investigated. The idea is to use coagulated pectin as a porous matrix where silica aerogel is formed *in situ*. The diffusion of silica precursors into the pectin scaffold with time will be studied. The maximum silica impregnation quantity that can be reached depending on pectin concentration and silica aerogel formulation will be evaluated. Coagulated pectin, loaded with silica, will be dried by $scCO_2$. Hybrid pectin-silica aerogels will be characterised by their bulk density, specific surface areas and scanning electron microscopy. Their thermal conductivity will be measured and correlated to the impregnation efficiency.

Finally, conclusions are drawn and suggestions for further work are proposed.

Bibliography

Fischer, F., Rigacci, A., Pirard, R., Berthon-Fabry, S., & Achard, P. (2006). Cellulose-based aerogels. *Polymer*, *47*(22), 7636–7645.

García-González, C. A., Alnaief, M., & Smirnova, I. (2011). Polysaccharide-based aerogels—Promising biodegradable carriers for drug delivery systems. *Carbohydrate Polymers*, *86*(4), 1425–1438.

Gavillon, R., & Budtova, T. (2008). Aerocellulose: new highly porous cellulose prepared from cellulose-NaOH aqueous solutions. *Biomacromolecules*, *9*(1), 269–77.

Liebner, F., Haimer, E., Potthast, A., Loidl, D., Tschegg, S., Neouze, M.-A., Wendland, M., et al. (2009). Cellulosic aerogels as ultra-lightweight materials. Part 2: Synthesis and properties. *Holzforschung*, *63*(1), 3–11.

Liebner, F., Haimer, E., Wendland, M., Neouze, M.-A., Schlufter, K., Miethe, P., Heinze, T., et al. (2010). Aerogels from unaltered bacterial cellulose: application of $scCO_2$ drying for the preparation of shaped, ultra-lightweight cellulosic aerogels. *Macromolecular bioscience*, *10*(4), 349–52.

Mehling, T., Smirnova, I., Guenther, U., & Neubert, R. H. H. (2009). Polysaccharide-based aerogels as drug carriers. *Journal of Non-Crystalline Solids*, *355*(50-51), 2472–2479.

Sescousse, R., Gavillon, R., & Budtova, T. (2011). Aerocellulose from cellulose–ionic liquid solutions: Preparation, properties and comparison with cellulose–NaOH and cellulose–NMMO routes. *Carbohydrate Polymers*, *83*(4), 1766–1774.

Chapter I

State of the art:

Polysaccharides and their aerogels - Structure and applications

Introduction

This chapter is dedicated to review the state of the art on two polysaccharides, cellulose and pectin, as well as their aerogels and their potential applications.

In a first part, we will present in more details cellulose, its structure and its peculiar properties. We will show the two major industrial cellulose processings, Viscose and Lyocell. We will compare some cellulose solvents and introduce ionic liquids (IL) as powerful cellulose solvents. We will discuss their major advantages and drawbacks for industrial applications and their potential improvements.

The second part will be focused on pectin. We will present its structure, its extraction from citrus peel or apple pomace. We will describe its gelation mechanism in the presence of an acid or divalent cations.

We will introduce in a third part the concept of aerogel, as a very porous material dried by supercritical route. The most famous aerogel, silica aerogel, will be briefly described. Then a review of aerogels from polysaccharides will be given, with a special focus on cellulose and its derivatives, starches, alginate and pectin. Because of the polysaccharides great diversity, aerogels from polysaccharides or “aero-polysaccharides” have a large range of morphologies and mechanical properties that can be tuned with polysaccharides concentration, the addition of cross-linkers or different solvents.

We will show that polysaccharide aerogels present a large porosity, high specific surface areas and pores with sizes of few tens nanometers. A large range of applications can therefore be foreseen. Two of them will be enlightened in this chapter: drug release and building thermal insulation. In the latter application, the concept of “superinsulation” will be introduced and discussed.

Introduction

Ce chapitre fait l'état de l'art sur deux polysaccharides, la cellulose et la pectine, ainsi que sur leurs aérogels associés et leurs applications potentielles.

Dans un premier temps, la cellulose, sa structure et ses propriétés seront détaillées. Les deux principaux procédés industriels de mise en forme de la cellulose, Viscose et Lyocell seront présentés. Les différents solvants de la cellulose seront comparés et les liquides ioniques seront plus particulièrement étudiés : leurs avantages et inconvénients ainsi que leurs éventuelles améliorations.

La pectine sera ensuite présentée par sa structure et son extraction à partir d'écorces d'agrumes et de marc de pomme. Sa gélification en présence d'une solution acide ou de cations divalents sera décrite.

Le concept d'aérogel, comme un matériau très poreux séché par CO_2 supercritique sera introduit. Les propriétés de l'aérogel de silice seront brièvement décrites. Une étude approfondie des aérogels à base de polysaccharides, en particulier la cellulose, l'amidon, l'alginate et la pectine, sera menée et montrera la grande diversité des morphologies et des propriétés mécaniques des « aéro-polysaccharides » obtenues selon la concentration en polysaccharides, l'addition d'agents réticulant ou le solvant utilisé.

Grâce à leurs propriétés intéressantes, comme leur porosité, leur grande surface spécifique et leurs pores de quelques dizaines de nanomètres, les « bio-aérogels » peuvent être utilisés dans diverses applications, telle que la libération contrôlée de médicaments ou l'isolation thermique. La notion de « super-isolation » thermique sera introduite.

1. Polysaccharides: Structure and properties

1.1 General description

Polysaccharides (or polymerized sugars) are long chains of monosaccharides repeating units (sugars) linked by glycosidic bonds. Their general chemical formula is $(C_x(H_2O)_y)_n$ where n may vary from 40 to 3000 (called the degree of polymerisation, DP). They can be classified in two groups: homopolysaccharides when the monomer (monosaccharide) is single (such as cellulose) or heteropolysaccharides with different linked monosaccharides (e.g. alginate, made of 1,4-β-D-mannuronic acid and α-L-guluronic acid). Their various chemical compositions give them a large range of structures and properties. Polysaccharides serve in living organisms either for the storage of energy, for example, starch and glycogen (storage form of glucose); or as structural components, such as cellulose in plants and chitin in invertebrate animal with external skeleton (insects or crustaceans).

An example of monosaccharide is glucose. In its conformation as a ring form (Figure I. 1) the carbon C_1 is asymmetrical and is called anomeric carbon. The –OH group on the carbon C_1 may have and two configurations: if the –OH substituent stands on the same side of the ring as the carbon C_6 the configuration is called β-position, otherwise if it is on the opposite site, it is called α-position.

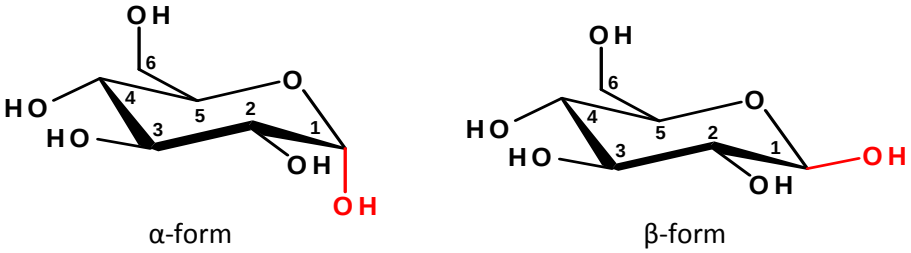

Figure I. 1 : The two isomers of glucose.

In polysaccharides such as amylose or cellulose, glucose units are linked together by a 1,4 glycosidic bond. It means that the hydroxyl group of the carbon C_1 on the first monosaccharide forms a hemiacetal with the carbon C_4 of the second monomer. 1,4 bond can be either α or β. Cellulose has a β-1,4 linkage. As a result of the bond angles, cellulose is mostly a linear chain. On the contrary, amylose is based on a α-1,4 glycosidic bond which gives a coiled spring spatial representation (Figure I. 2).

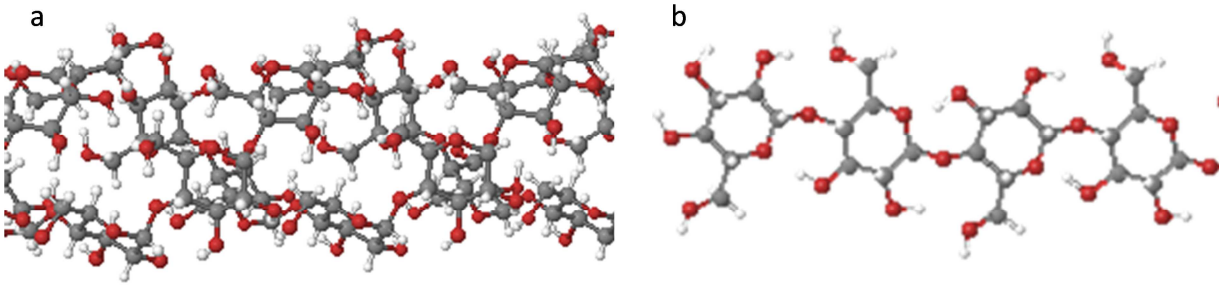

Figure I. 2 : (a) cellulose (b) starch-amylose spatial representation.

The most common polysaccharides are cellulose (from cotton, wood, flax…), amylose and amylopectin (potato, cassava, rice, wheat, maize…), chitin (animal-based polysaccharides, found in cell walls of mushrooms and in the "shell" of arthropods: shellfish, insects), carrageenans (mosses and seaweeds), pectins (fruits and vegetables: citrus peel or apple pomace)…
Cellulose and pectin will be described in more details in the two following sections.

1.2 Cellulose

1.2.1 Stucture of cellulose

Cellulose is the most abundant renewable polymer and is the main component of plant cell walls. Lignocellulosic materials, like wood, contain cellulose, hemicellulose, lignin and other small amounts of extractives in various proportions depending on the plant. Table I. 1 gives different sources of lignocellulosic material and their cellulose content (Klemm, Philipp, Heinze, Heinze, & Wagenknecht, 1998). The degree of polymerisation DP (the number of anhydroglucose units in a chain) depends on the sources as well and varies from 1000 to 30 000 (about 50-15 000 nm of chain length). After isolation, DP is around 800-3000 (Krassig, 1993).

Table I. 1 : Cellulose content in various lignocellulosic sources

Cellulose sources	$_{wt}$% cellulose
Wood	40-50
Bagasse	35-45
Bamboo	40-55
Straw	40-50
Flax	70-80
Hemp	75-80
Jute	60-65
Ramie	70-75
Cotton	95

As presented in the previous section, cellulose is a carbohydrate polymer made of repeated β-anhydroglucose (AGU) units covalently linked by an acetal function between the hydroxyl group of C_4 and the C_1. Cellulose is a linear-chain polymer with many hydroxyl groups (3 groups for each AGU). The morphological architecture of a cellulose fiber is shown in Figure I. 3 (Klemm et al., 1998): elementary fibrils are constituted of six glucose chains (with a DP depending on sources) and have typically a size of 4-6 nm and are 10-20 nm long. They are aggregated in microfibrils having a diameter between 2 to 20 nm depending on cellulose origin. Thereafter, the microfibrils are organized in macrofibrils (diameter around 60-360µm) to form the cell wall (Lerouxel, Cavalier, Liepman, & Keegstra, 2006).

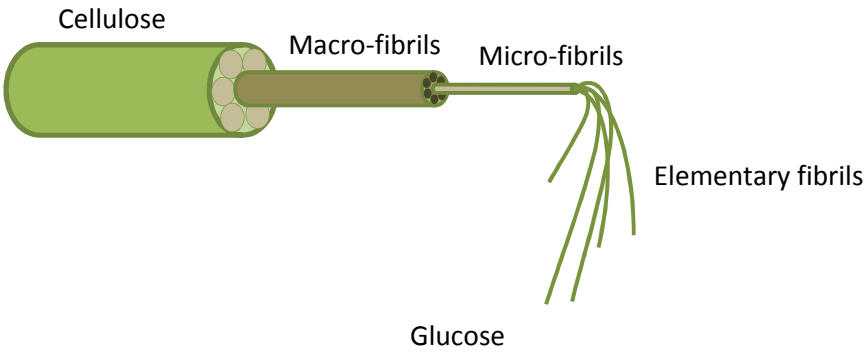

Figure I. 3 : Architecture of a cellulose fiber, adapted from (Klemm et al., 1998).

In cellulose fibers the supramolecular structure is not uniform: low ordered region (called amorphous) coexist with crystalline regions. As cellulose has many hydroxyl groups, a large number of intra- and inter-molecular hydrogen bonds are involved which may have strong effects on physical properties of cellulose: solubility in solvents, low reactivity of hydroxyl groups and crystallinity (Kondo, 1997). These intra- and inter-molecular H-bonds and the linkage β-1,4 give to cellulose a relative stiffness and a rigidity which implies a greater viscosity, crystallisation and fibrillar assemblies (Krassig, 1993).

In the crystal structure, four main polymorphs of cellulose have been discovered: cellulose I, II, III and IV (O'Sullivan, 1997). Cellulose I or native cellulose is the form found in nature but is metastable. It has two different crystal structures I_α (triclinic unit cell) and I_β (monoclinic) alongside each other as confirmed by solid-state ^{13}C-NMR spectroscopy (Atalla & Vanderhart, 1984). Cellulose has two intramolecular hydrogen bonds between –OH of C_3 and the oxygen of C_5 and one between –OH of C_6 and –OH of C_2 (Figure I. 4a, orange line), and has also an interchain H-bonding between the OH of C_6 and the oxygen attached to C_3 of a neighbouring chain (Figure I. 4a, red line). These interactions undergo a structure in layers (Zugenmaier, 2001). Layers are linked together by Van der Waals forces (Figure I. 5a).

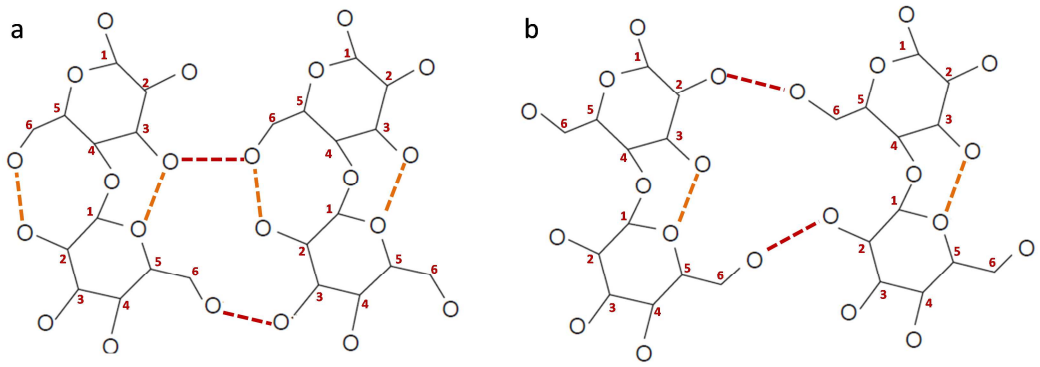

Figure I. 4 : Intra- and inter-molecular hydrogen bonds in cellulose structure

The crystalline structure of cellulose II can be formed from cellulose I by treatment in alkaline media (e.g. aqueous sodium hydroxide) called mercerization, or by regeneration (precipitation) of the dissolved cellulose. Cellulose II has antiparallel chains, the hydroxyl groups are oriented *gauche-trans*: –OH in C_6 is positioned *gauche* to C_5-O_5 and *trans* to C_4-O_4 whereas for cellulose I OH in C_6 is positioned *trans* to C_5-O_5 and *gauche* to C_4-O_4 (Figure I. 4b)(Raymond, Heyraud, Qui, Kvick, & Chanzy, 1995). This modification in configuration modifies greatly the H-bonding system: less intramolecular H-bonds (no bonds between –OH of C_6 and –OH of C_2) but an appearance of hydrogen bonds between molecular layers which confer to cellulose II a greater stability compared to cellulose I (Langan, Nishiyama, & Chanzy, 1999).

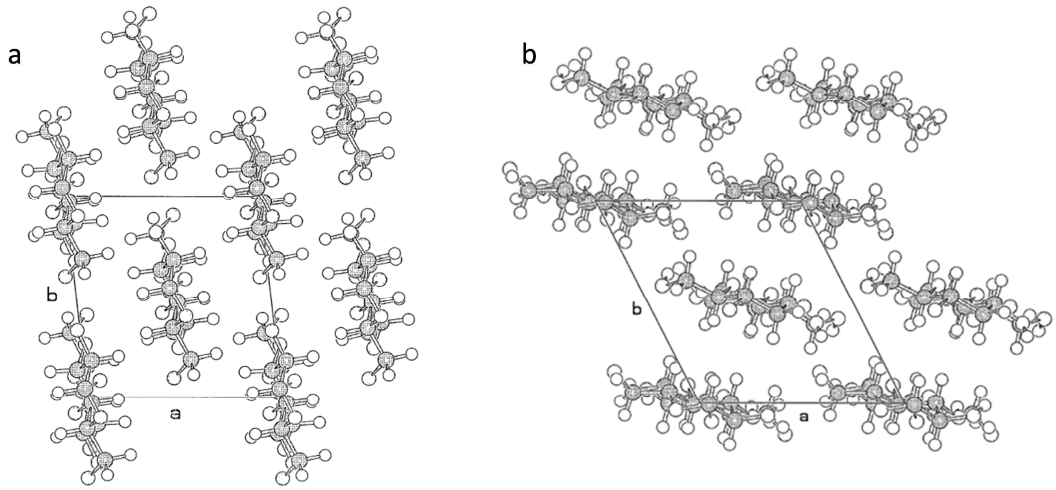

Figure I. 5 : Structure of cellulose in layers (Zugenmaier, 2001). Reprinted from (Zugenmaier, 2001), Copyright (2001), with permission from Elsevier.

Cellulose III is obtained in a reversible process by treatment with liquid ammonia or organic amines such as ethylendiamine followed by washing in alcohol (Sarko, Southwick, & Hayashi, 1976). Cellulose IV may be obtained by a heat treatment of cellulose III (Gardiner & Sarko, 1985).

1.2.2 Cellulose processing

Cellulose cannot melt, since it degrades before melting. In order to process this biopolymer, many studies were devoted to its dissolution. However, cellulose has many intra- and intermolecular hydrogen bonds (see previous section) which gives a great stability but only few solvents were able to break the H-bonding system and to dissolve cellulose. Some of them are represented in Figure I. 6.

The dissolution of cellulose in a solution of lithium chloride LiCl in *N*,*N*-dimethylacetamide (DMAc) has been investigated in details (Burchard, 2003; Dawsey & McCormick, 1990; Potthast, Rosenau, Buchner, & Röder, 2002; Ramos, Assaf, El Seoud, & Frollini, 2005). It has been shown that hydrogen bonds are created between hydroxyl protons of cellulose with chloride ions. Tetrabutylammonium fluoride trihydrate in dimethylsulfoxide (DMSO/TBAF) efficiently dissolves cellulose and is mainly used for synthesising cellulose derivatives (Ciacco, Liebert, Frollini, & Heinze, 2003; Ramos, Frollini, & Heinze, 2005).

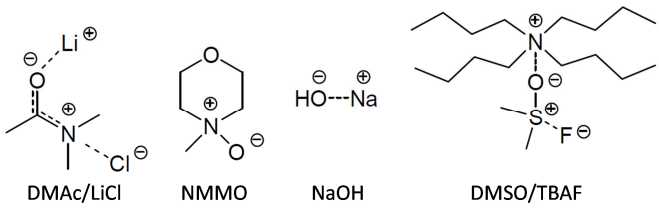

Figure I. 6 : Common cellulose solvents

Other solvents have been widely studied, such as *N*-methylmorpholine-*N*-oxide (NMMO), NaOH-water and will be described in more details in next sections. However, all these solvents present major drawbacks such as either toxicity, or low solubility power or certain decomposition of cellulose. In the last decade, a new category of cellulose solvents were investigated: ionic liquids. They have improved physical and chemical properties and a great cellulose dissolution capacity.

1.2.2.1 Viscose process

The viscose process is the oldest and still the more used for production of regenerated cellulose such as fibers, films, membranes or sponges, with more than 2.2 millions of tons (Klemm, Heublein, Fink, & Bohn, 2005) (Figure I. 7).

(1) The first step of this process is the treatment of cellulose by sodium hydroxide (NaOH) at 17-20% in water which forms alkali-cellulose complex and fibers start to swell and become more accessible to chemical reagents.

(2) Carbon disulfide (CS_2) is added and alkali-cellulose is converted into cellulose xanthogenate. These substituents force the cellulose chains to separate, reducing the intermolecular hydrogen bonds.

(3) This new cellulose derivative is soluble in aqueous sodium hydroxide solution and forms a viscous solution (viscose solution).

(4) Various techniques can be used for shaping cellulose depending on the application: spinning for fibers (Rayon fibers for example), casting for films (Cellophane), and making 3D objects with the addition of porophores for sponges…
(5) Cellulose xanthate is precipitated in regeneration baths, and CS_2 and other sulphur-based by-products are released and the final regenerated cellulose is obtained.

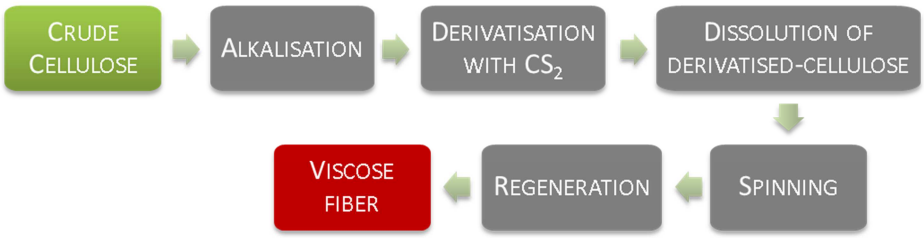

Figure I. 7 : Viscose process.

However, the viscose process requires a complex processing, high quality dissolving pulp and releases in the atmosphere extremely toxic gases such as CS_2 or H_2S. Several improvements were developed for reducing the consumption of chemicals and gas release but alternative processes, simpler with neither derivatisation nor environmentally hazardous chemicals, need to be found.

1.2.2.2 NMMO/Lyocell process

Gränacher and Sallman in 1939 (Graenacher & Sallmann, 1939) were the first to study the dissolution of cellulose in tertiary amine oxides but it is only in the beginning of 1980s that intensive research on producing cellulosic fibers from amine oxide-cellulose mixtures was carried out (Chanzy, Nawrot, Peguy, Smith, & Chevalier, 1982; Chanzy, Peguy, Chaunis, & Monzie, 1980). The most promising amine oxide–based cellulose solvent is NMMO (*N*-metylmorpholine-*N*-oxide) mixed with water, NMMO monohydrate. Because of the high polarity of N-O bond, NMMO has a high hydrophilicity and strong tendency to form hydrogen bonds. NMMO disrupts the hydrogen bonds in cellulose network and forms complexes with new H-bonds between cellulose and the solvent (Harmon, Akin, Keefer, & Snider, 1992). A phase diagram was built for the ternary system cellulose-NMMO-Water (Rosenau, Potthast, Sixta, & Kosma, 2001). Water and cellulose are in competition for hydrogen bonding with NMMO. In only a limited range of compositions and temperatures NMMO-water mixture is able to dissolve cellulose: on one hand, water content below 10% requires a very high temperature for melting NMMO-water which may degrade cellulose; on the other hand, with more than 25% of water NMMO-water is not a cellulose solvent anymore (Cuissinat & Navard, 2006). Therefore optimised water content was established at about 13.3%. Reaction side-products during cellulose dissolution in NMMO monohydrate have been widely studied by Rosenau et al. (Rosenau et al., 2001).

Spinning cellulose dissolved in NMMO monohydrate is now an industrial process called Lyocell (Lenzing, Austria) (Figure I. 8). Cellulose fibers are directly obtained from the cellulose-NMMO solutions without any derivatization (contrary to the Viscose process with alkalization and

xanthanation). The main advantages of the Lyocell process are a lower number of processing steps, a low toxicity and biodegradability of NMMO and its efficient recovery (99% of NMMO can be completely recycled). Unlike the viscose process, the Lyocell technology may use a large range of cellulose fibre variety (paper grade pulp, cotton, waste paper…). The major drawback of Lyocell fibers, used mainly in the textile industry, is their relatively low surface energy, which makes it difficult for dyes to bind to it. They also have a tendency towards fibrillation in the wet state but this problem is almost solved by functionalising surface of fibers.

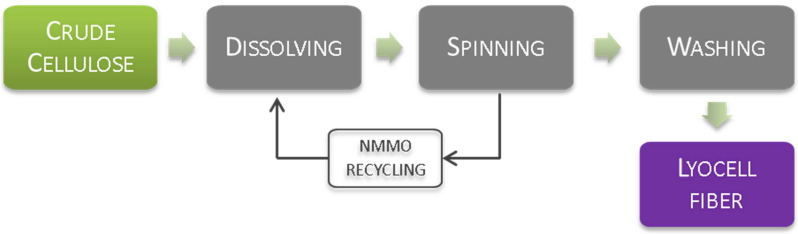

Figure I. 8 : Lyocell process.

1.2.2.3 Dissolution of cellulose in NaOH-water

Studies of cellulose and aqueous solutions of sodium hydroxide started back in the nineteenth century with the Viscose process and were focused on the dissolution of cellulose xanthate and the mercerisation process. The latter is a treatment of native cellulose with concentrated caustic alkaline solution (18-20%) which improves smoothness, dye intake and mechanical properties of cotton fibers. Mercerisation plays a role in the morphological change in cell wall cotton: crystalline structure of cellulose I changes into cellulose II. However, mercerisation is not a dissolution process; it results in cellulose fibre highly swollen state with a rather complex modification of morphology and of crystalline structure of cellulose.

In the 1930s, Davidson and a few years later Sobue showed that it is possible to dissolve cellulose in an aqueous solution of sodium hydroxide. Davidson (Davidson, 1934, 1936) found that up to 80% of cellulose (of a low molar mass) may be dissolved in 10% NaOH-water at low temperature of -5°C. He noticed that when the chain length decreases solubility increases and concluded that it is probably impossible to dissolve unmodified (with higher molar mass) cellulose. Sobue (Sobue, Kiessig, & Hess, 1939) explored the whole cellulose-NaOH-water ternary phase diagram (Figure I. 9) and showed that a rather limited range of NaOH concentrations (7-10%) and temperature (-5°C - 0°C) can dissolve cellulose.

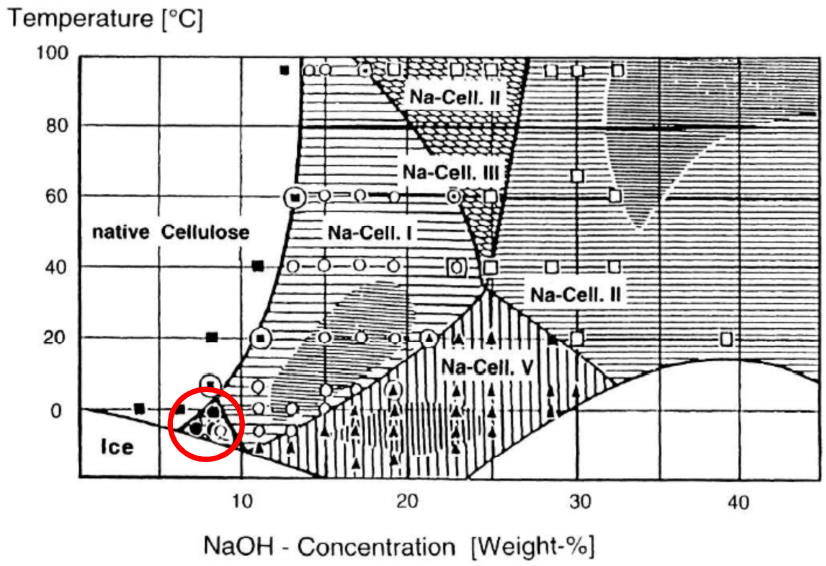

Figure I. 9 : Phase diagram of the cellulose/NaOH/water system as function of NaOH concentration and temperature: different types of Na-cellulose complexes, adapted from (Sobue et al., 1939).

An important breakthrough in cellulose dissolution in NaOH was made in 1980s by a group of Japanese researchers from Asahi Chemical Industry and Co. In a series of papers they intensively studied cellulose dissolution mechanism using various approaches such as IR, ^{13}C-NMR or X-ray (Kamide, Okajima, & Kowsaka, 1992; Kamide, Okajima, Matsui, & Kowsaka, 1984; Kamide, Saito, & Kowsaka, 1987; Yamada, Kowsaka, Matsui, Okajima, & Kamide, 1992; Yamane, Saito, & Okajima, 1996; T Yamashiki, Saitoh, Yasuda, Okajima, & Kamide, 1990; Takashi Yamashiki et al., 1988). The intramolecular hydrogen bond between O_3-H---O_5 (Figure I. 4) has been identified as the bond to be weakened for a dissolution of cellulose in NaOH-water system. Isogai and Atalla (Isogai & Atalla, 1998) managed to dissolve cellulose from various sources in aqueous NaOH. First a suspension of cellulose in 8.5% NaOH solution is frozen at -20°C which is then allowed to thaw at room temperature to obtain a gel-like material. Water is then added to give a solution of 2% cellulose in 5% NaOH-water.
However, aqueous NaOH presents major drawbacks as a cellulose solvent for an industrial process. First the maximum cellulose concentration dissolved is rather limited (<7-9%) (Egal, Budtova, & Navard, 2007) and cellulose solutions are instable and gel with time and temperature (Roy, Budtova, & Navard, 2003). Secondly, the process requires important source of energy to cool down the solution to -6°C or even -20°C if freezing-thawing is performed.

Additives were studied to enhance stability and solubility of cellulose-NaOH solutions. Urea/NaOH/water and thiourea/NaOH/water were shown to be a direct solvent of cellulose and to improve cellulose dissolution (Zhang, Ruan, & Gao, 2002; Zhou, Zhang, & Cai, 2004). Cai claimed that at low temperature alkali hydrates, urea hydrates and free water make a sort of envelope around cellulose molecules destroying intra- and intermolecular hydrogen bonds and reduce cellulose self-association (Cai & Zhang, 2005; Cai, Zhang, et al., 2008). Urea was shown not to interact with cellulose and its role is believed to bind water, making cellulose-NaOH links more stable (Cai, Zhang, et al., 2008; Egal, Budtova, & Navard, 2008).

Zinc oxide (ZnO) was also investigated and was shown to improve cellulose dissolution. One reason was explained by the stronger hydrogen bonds between cellulose and $Zn(OH)_4^{2-}$ as compared to hydrated NaOH (Yang, Qin, & Zhang, 2011). ZnO has an influence for delaying gelation of cellulose-NaOH solutions improving their stability (Liu, Budtova, & Navard, 2011). ZnO is also believed to act as a water "binder".
However, the maximal concentration of cellulose remains low (around 10%) even with additives and gelation may be delayed but not avoided.

1.2.2.4 Dissolution of cellulose in Ionic Liquids

It has been shown above that a limited amount and rather complex solvents are able to dissolve cellulose. Some of them are either toxic or volatile or cannot dissolve a large concentration of cellulose. Dissolution of cellulose has an important interest as it is the first step to shape cellulose into fibers, films, sponges or beads and also for syntheses of cellulose derivatives.
Ionic liquids (IL) have been under intense research over the past decade as new solvents for cellulose. They are defined as molten salts with melting points below 100°C. They have numerous attractive properties such as chemical and thermal stability and low vapour pressure and other physical and chemical characterisations may be tuned by the choice of cations and anions. The first description of cellulose dissolution in IL (benzylpyridinium chloride, a quaternary ammonium salt) dates back to 1934 (Graenacher, 1934) but it is in 2002 that Swatloski et al. reported that imidazolium-based IL, such as 1-butyl-3-methylimidazolium chloride (BMIMCl) were able to dissolve cellulose in high concentration without pre-activation (Swatloski, Spear, Holbrey, & Rogers, 2002). In the following years, many other cellulose-dissolving IL were reported, mainly based on dialkylimidazolium or pyridinium cations and chloride and acetate as anions. The most common IL are BMIMCl, 1-allyl-3-methylimidazolium chloride (AMIMCl) or 1-methyl-3-methylimidazolium acetate (EMIMAc) (Figure I. 10).

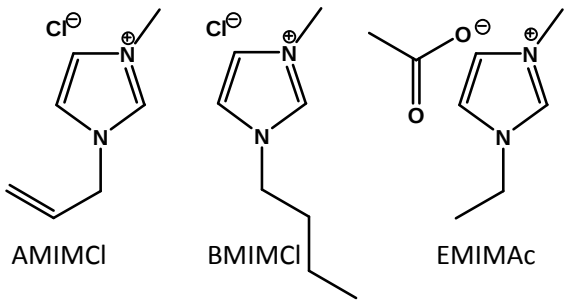

Figure I. 10 : Most common cellulose-dissolving ionic liquids.

The dissolution of cellulose in IL is rather simple and occurs without derivatisation (except minor acetylation at end groups in EMIMAc (Ebner, Schiehser, Potthast, & Rosenau, 2008; Karatzos, Edye, & Wellard, 2011)). Its mechanism is not well known yet. It is thought that anions and cations are involved in the dissolution. Cation such as imidazolium acts as the electron acceptor and may interact with the oxygen atom of cellulose whereas chloride or acetate anion is the electron pair donor and may bind the hydrogen of cellulose. These interactions result in the decrease of cellulose inter- and intra-hydrogen bonds enhancing cellulose solubility. It had been confirmed by ^{1}H-NMR that interactions occur between chloride anions or acetate anions

and cellulose hydrogen atoms of hydroxyls and between the aromatic protons in cations $[BMIM]^+$ or $[EMIM]^+$ and oxygen (Feng & Chen, 2008; Remsing, Swatloski, Rogers, & Moyna, 2006; Zhang et al., 2010) (Figure I. 11). A screening of more than 2000 ionic liquids was performed with a COSMOS-RS model (Conductor-like Screening Model for Realistic Solvation) which is in a good agreement with experimental data available in the literature (Kahlen, Masuch, & Leonhard, 2010). They also showed that anions are mainly responsible for IL dissolving power and gave potential optimised cellulose solvents. Gupta et al. predicted by molecular dynamic simulations that 1-n-butyl-3-imidazolium acetate (BMIMAc) has the strongest capacity to break hydrogen-bonds in cellulose (Gupta, Hu, & Jiang, 2011).

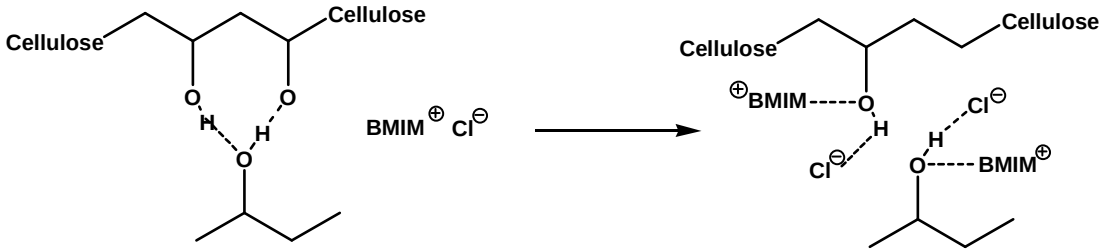

Figure I. 11 : Posssible dissolution mechanism of cellulose in BMIMCl, adapted from (Feng & Chen, 2008).

The understanding of cellulose-IL solutions rheological properties is crucial for all the cellulose process: from dissolution (handling of the solutions, design of reaction vessels pipe systems…) to the final product (spinning of fibers, chemical derivatisation…). Shear flow properties of cellulose-IL solutions were investigated as a function of cellulose concentration and temperature (Collier, Watson, Collier, & Petrovan, 2008; Haward, Sharma, Butts, McKinley, & Rahatekar, 2012; Kosan, Michels, & Meister, 2008; Sammons, Collier, Rials, & Petrovan, 2008). More detailed and complete studies on cellulose hydrodynamic properties were carried out for AMIMCl (Kuang, Zhao, Niu, Zhang, & Wang, 2008), EMIMAc (Gericke, Schlufter, Liebert, Heinze, & Budtova, 2009; Sescousse, Le, Ries, & Budtova, 2010) and BMIMCl (Sescousse et al., 2010) in dilute and semi-dilute states. Solubility of cellulose in these IL is very high with cellulose concentrations of 10-20$_{wt}$% and a maximum predicted to be around 27$_{wt}$% (Lovell et al., 2010). In contrast to many common liquids, IL viscosities are at least two orders of magnitudes higher which may be a disadvantage for cellulose processing (Gericke et al., 2009). It has also been reported that the intrinsic viscosity of cellulose-IL solutions decreases with increasing temperature, showing a decrease of the thermodynamic quality of the solvent (therefore a decrease in solubility) (Gericke et al., 2009).

Cellulose dissolution in ionic liquids is very promising and opens new perspectives as higher cellulose solubility can be reached. A large range of cellulose shaping has been under research to produce fibers with similar properties as Lyocell fibers (Kosan et al., 2008), films (Cao, Li, Zhang, Zhang, & He, 2010), or porous monoliths (Sescousse, Gavillon, & Budtova, 2011; Tsioptsias, Stefopoulos, Kokkinomalis, Papadopoulou, & Panayiotou, 2008). IL are also widely studied as a reaction media for the homogeneous synthesis of cellulose derivatives (El Seoud, Koschella, Fidale, Dorn, & Heinze, 2007; Gericke, Fardim, & Heinze, 2012; Köhler, Liebert, & Heinze, 2008; Pinkert, Marsh, Pang, & Staiger, 2009).

However, even if IL have demonstrated a huge potential for cellulose chemistry, several drawbacks become apparent that need to be solved for an industrialisation of cellulose-IL-based processes.

First the purity of IL is a key factor. Residues of unreacted starting materials or side products may be present in IL (Keil, Kick, & König, 2012), which have a strong effect on cellulose derivatization (especially if carried out in anhydrous conditions) or decrease IL cellulose dissolution power. Purification techniques of IL have been improved in the recent years with grades of ≥ 98-99%. However, EMIMAc is known to be of rather low purity between 90 and 95%. The presence of water plays also an important effect. Water is cellulose non-solvent and precipitates cellulose from the solutions. IL absorb high amounts of moisture present in the air. The mixing of water and EMIMAc is exothermal, and it has been shown that these two fluids interact without the formation of new compounds (Hall et al., 2012). It has been reported that cellulose-EMIMAc solutions tolerate up to 15% of water in dilute cellulose solutions without altering their rheological properties (Le, Sescousse, & Budtova, 2011).

IL are believed to be thermally stable to 400°C and chemically inert. However, some recent studies have tempered these assertions especially for imidazolium-based IL. They can participate in derivatization reactions and may induce the formation of unexpected products (Chowdhury, Mohan, & Scott, 2007; Sowmiah, Srinivasadesikan, Tseng, & Chu, 2009). EMIMAc for example, may undergo self-deprotonation leading to a formation of carbene species. These carbenes can react with end-group of cellulose in its aldehyde form (Figure I. 12). It has also been claimed that side reactions as acetylation of cellulose by EMIMAc might occur confirming that IL are “non-innocent” solvents (Ebner et al., 2008; Karatzos et al., 2011).

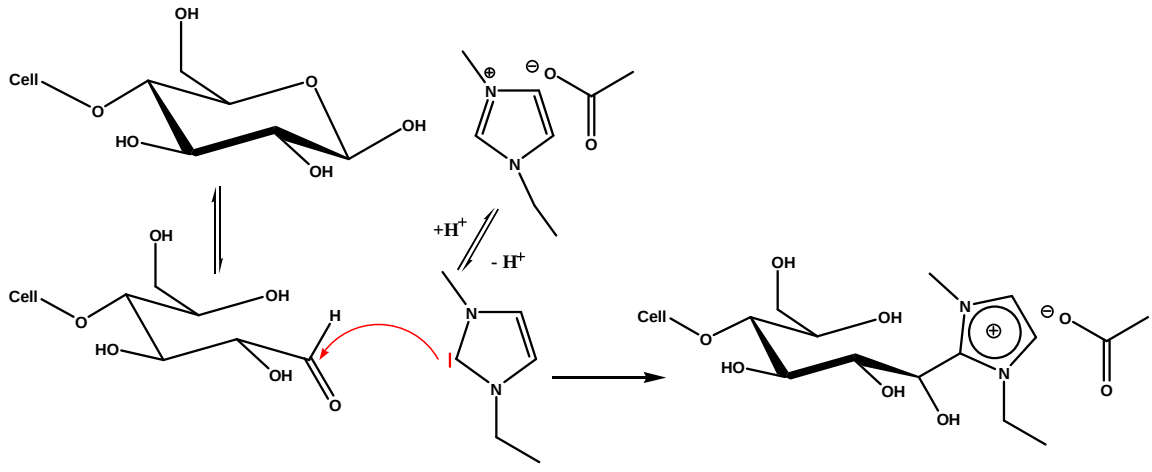

Figure I. 12 : Possible side reaction observed during the dissolution of cellulose in EMIMAc, adapted from (Gericke et al., 2012).

IL demonstrated chemical decomposition at lower temperatures than stated especially in the presence of impurities (Kosmulski, Gustafsson, & Rosenholm, 2004). Onset temperature for the chemical decomposition were determined for EMIMAc at 181°C and 179°C for BMIMCl (Wendler, Todi, & Meister, 2012). However, it is well beyond the usual temperature for cellulose dissolution (Gericke et al., 2009; Sescousse et al., 2010).

IL are said to be “green solvents” thanks to their physical and chemical interesting properties, their stability and their high cellulose dissolution capacity. However, few studies were carried out on their toxicity (Welton, 2011). The toxicity strongly depends on the nature of the cation and its alkyl chain lengths and anions (Docherty & Kulpa, Jr., 2005; Jastorff et al., 2005).
A life cycle analysis of cellulose dissolution with BMIMCl was performed and compared to the one for NMMO/H_2O process (Righi et al., 2011). Laboratory scale studies showed promising features for highly concentrated cellulose solutions, no production of dangerous by-products (such as C_2S or heavy metals) and simple and fast processes decreasing the electric energy consumption. For these two solvents, the major contribution to environmental impacts come from starting materials syntheses (for BMIMCl, the synthetic pathway to imidazolium cation) which require long supply chains from natural resources, a large amount of organic materials, energy and solvents.
Taking into account the high production costs of IL and their environmental and safety issues, an efficient recycling of IL is one of the key parameter. IL have mostly a very low vapor pressure; thus volatile impurities such as methylimidazolium, alkylation agents or water can be removed by distillation techniques or by active carbon and molecular sieves (Keil et al., 2012), but they are energy intensive processes. Recycling IL can become extremely difficult depending on impurities such as bases (Gericke et al., 2012).

Further investigations and a complete evaluation of ecological and economical aspects are required to move cellulose dissolution in IL towards an industrial scale, especially on the IL recycling and purification.

1.3 Pectin

1.3.1 Origin and structure of pectin

Pectin is widely present in many terrestrial plants and is found in the middle lamellae and primary cell walls where it helps to bind cells altogether. It is also associated to other chemical components of cell membrane such as cellulose, hemicellulose or lignin via chemical or physical bonds. Depending on the nature, the age and part of plants, a wide range of structures and chemical compositions of pectin is observed. According to the age of the plant, pectin can be found in two forms, one is *propectin* (insoluble and linked to other components) and the other is *pectic acid* which is soluble in water. Protopectin is gradually converted into pectic acid in time by enzymes, pectinase and pectinesterase. In this process of ripening, cells become separated from each other as the middle lamellae breaks down and the fruit becomes softer.

Pectin is a linear polymer of α-(1-4) D-galacturonic acid repeated units (Figure I. 13). As shown in the previous section, α-chains have a spatial configuration as a coil. Carboxylic acid functions may be esterified by methanol during the biosynthesis (Mohnen, 2008). The degree of esterification (DE) is defined as the number of esterified acid functions for 100 units of galacturonic acid on the main chain. *High Methoxy* (HM) pectins have a DE>50 and *Low Methoxy* (LM) pectin a DE<50 (Figure I. 13). Acid functions are usually neutralised by mono- or divalent cations such as sodium, potassium, calcium or ammonium salts.

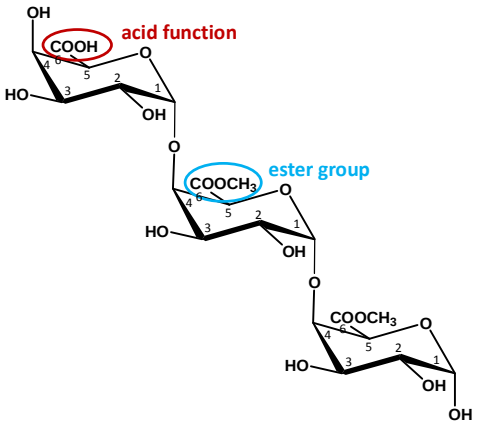

Figure I. 13 : Structure of pectin.

Some ramifications made of short chains of sugars as galactanes, arabanes or xylanes, or acetyl groups may be branched on hydroxyl groups C_2 or C_3 on the main chain. The regular structure of galacturonic acid chains is also interrupted by the presence of β-L Rhamnose (on C_1 and C_2) units which cause deviations called “pectic elbows” (Figure I. 14). This flexibility in the chain easies the formation of a tridimensional network and the gelation process (Mohnen, 2008; Sila et al., 2009).

In summary, pectin is characterised by its galacturonic acid content, the length of its chains (molecular mass) and the degree of substitution or degree of esterification (DE).

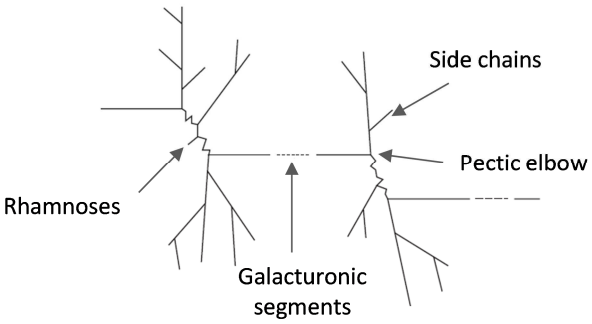

Figure I. 14 : Schematic representation of a pectin molecule, adapted from (Tilly, 2010).

1.3.2 Pectin extraction

Pectin is mainly extracted from dried citrus peel or apple pomace, by-products of juice industry, since they have a high content in protopectin and pectic acid. First, the starting materials are placed in a hot dilute acid bath with a pH of 1.5-3.5 for several hours (Figure I. 15). Protopectin loses some of its branching and its chain length and converts into pectic acid which is dissolved into water. Remaining solids are separated and the solution extracted is clarified and concentrated in vacuum. Pectin is then precipitated by adding an alcohol (usually ethanol or isopropanol). The precipitate is washed, dried under vacuum and grinding to obtain a fine powder. Temperature, pH and hydrolysis time can be careful controlled to tune the DE.

Extracted pectins have usually a DE between 55 and 75% (HM pectins) (May, 1990; Tilly, 2010).

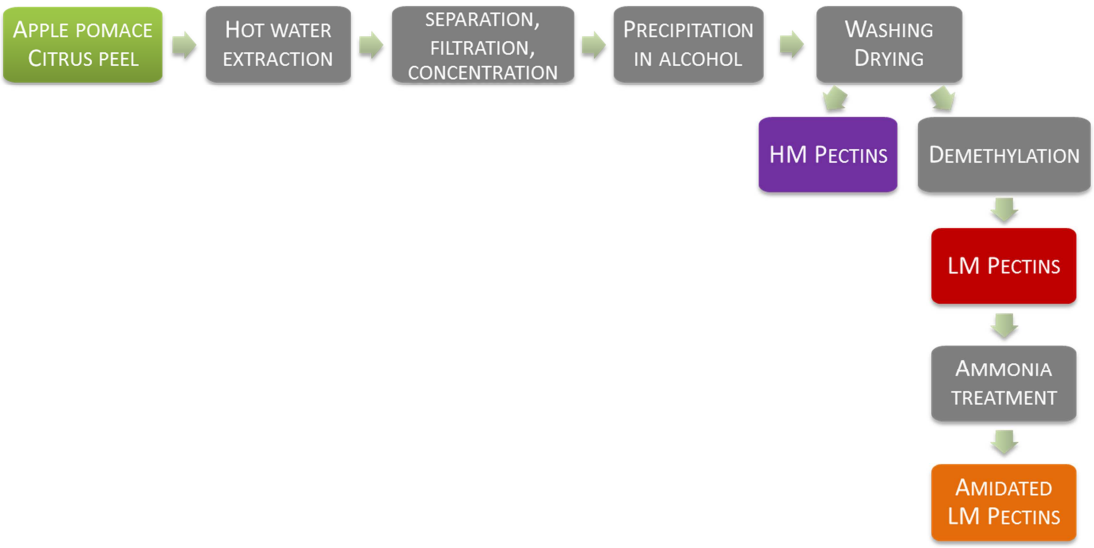

Figure I. 15 : Process for extracting pectin.

Low methoxy pectins (LM) can be obtained either by acid or alkaline hydrolysis of HM pectins. Amidated (-NH_2 groups instead of -OCH_3) LM pectins can also be produced from HM pectins by alkaline hydrolysis using ammonia solution.
Final products are carefully analysed to produce a constant quality since the pectin content of raw materials can be various.

1.3.3 Physical properties and applications

Pectin is well known for its ability to form gels. Depending on the DE, mechanisms of gelation and properties of gels are different. A gel is a three-dimensional network of polymeric molecules immersed in a liquid solvent. The presence of “pectic elbows” prevents having long junction zones or pectin total precipitation and improves the formation of a network.

1.3.3.1 Gelation mechanism of HM pectins

Hydrogen bonds and hydrophobic interactions (due to the methyl groups of esters) are mainly responsible for the gelation of HM pectin. Gelation is improved by the addition of acid and sugars (Oakenfull, 1992; Oakenfull & Scott, 1984).
By decreasing pH (typically below 3), all carboxylic groups are under the acidic form COOH, i.e. non-ionised, which decreases electrostatic repulsions between polymer chains and improves their association. In addition, more H-bonds are formed between methoxyl, carboxyl and hydroxyl groups (Figure I. 16).

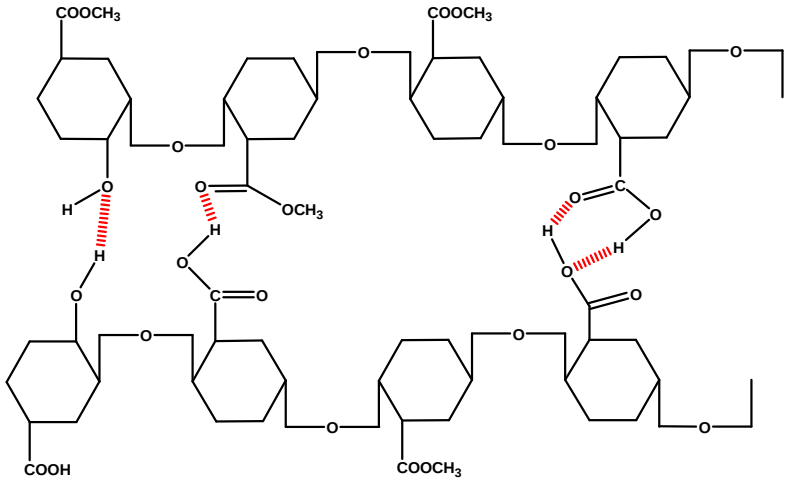

Figure I. 16 : Hydrogen bonds network in pectin at low pH, adapted from (Tilly, 2010).

The addition of sucrose (at a concentration above 55_{wt}%) improves greatly the gel formation (Thakur, Singh, & Handa, 1997). It acts as a dehydrating agent by decreasing the water activity. Therefore, chains become closer which enhance H-bonding network. It also plays the role of stabilising junction zones with hydrophobic interactions (mainly Van der Waals bonds between methoxyl groups), by increasing the number of galacturonic units involved.
Several intrinsic and extrinsic factors influence greatly rheological properties of pectin solutions and gels (Evageliou, Richardson, & Morris, 2000; Löfgren, Guillotin, Evenbratt, Schols, & Hermansson, 2005), for example sources of pectin and its DP give different gels textures; gelation time and gel strength are inversely proportional to pH (Tilly, 2010).

1.3.3.2 Gelation mechanism of LM pectins

For low esterified (LM) pectins, hydrophobic interactions are rather weak and pectin gels only in the presence of divalent cations such as Ca^{2+}. The mechanism of gelation was found to be similar to that of alginate. It relies mainly on the well-known “egg-box” model (Grant, Morris, Rees, Smith, & Thom, 1973) and it involves junction zones of associated galacturonic units linked intermolecularly through electrostatic and ionic bonding of carboxylic groups. (Figure I. 17). The oxygen atoms of the hydroxyls groups (on C_2 and C_3), oxygen atom in the ring and the oxygen on the glycosidic bonds participate in the bonding process through their free-electron pairs (Kohn, 1987). The bonds are stable when there are at least seven consecutive carboxyl groups (Powell, Morris, Gidley, & Rees, 1982).

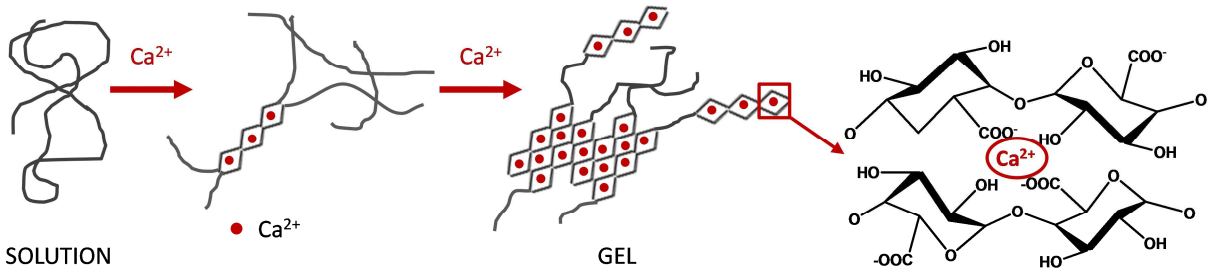

Figure I. 17 : Schematic representation of LM pectins gelation by calcium ions: the "egg box" packing, adapted from (Sriamornsak, 2003; Tilly, 2010).

The gel is a network of cross-linked pectin molecules. The cross-links formed by ionic bonds are strong. The gel formed is less elastic than the one formed by H-bonds. Again, sources of pectin have major impacts on gelation. For example, free carboxylic acids are dispatched in blocks along the chain for citrus pectin and randomly for apple pectin (Tilly, 2010). pH and calcium concentration also play an important role (Capel, Nicolai, Durand, Boulenguer, & Langendorff, 2006; Fraeye et al., 2010). Gel strength increases with increasing Ca^{2+} or pectin concentration. Sugar addition is not essential for pectin gelation but small amounts (10-20%) of sugars tend to decrease syneresis and add firmness to gels (Sriamornsak, 2003).
Amidation (formation of an amide function $COONH_2$) increases the gelling ability of LM-pectin since amidated pectins need less calcium to gel as far as there are less free carboxylic acid groups (May, 1990).

Due to their various functionalities, pectins (conventional or amidated) are widely used in food industry such as fruit-based preparations and sauces, icings, fillings or sweets. HM-pectins are mainly used for jams and sweets and for stabilising fruit drinks. LM-pectins applications are wider since they are less sensitive to pH and raw materials. They are used as a gelling agent for fillings, toppings or fruits yaourts.
Pectin gels have found a large range of applications in pharmaceutics as drug controlled release matrices (Sriamornsak, 2003).

2. Aerogels and porous polysaccharides

2.1 Generalities on aerogels

The term aerogel was first introduced by Kistler in 1930s to design gels in which the liquid was replaced with a gas, with very moderate shrinkage of gel solid network. (Kistler, 1931, 1932). No official definition exists for aerogels and they refer generally to dried gels with a very high porosity (>90%), low apparent densities and large specific surface areas . Supercritical drying is a classical technique for making aerogels. Other techniques, such as freeze-drying or ambient pressure drying in special conditions, leading to materials similar to aerogel, can also be used in some cases. Supercrititical drying remains the "reference" technique for making aerogels, both organic and inorganic.

During classical evaporative drying, the liquid which is contained inside pores, starts to evaporate. The cohesive intermolecular forces within the liquid become lower than the adhesive intermolecular forces between the liquid and the solid. This difference in specific energy of the liquid-vapor interface and the solid-liquid interface creates a concave meniscus. Pore walls are submitted to capillary forces (Figure I. 18): with the liquid evaporation, the meniscus curvature increases and forces may be strong enough to crack the solid or to provoke a strong contraction and even pore collapse. Capillary pressure can be expressed by the Young-Laplace equation (Equation (I. 1)).

$$p_C = \frac{2\gamma \cos\theta}{R} \quad \text{(I. 1)}$$

with γ the surface tension between the evaporating liquid and gas phase
θ the angle between the contact angle formed between the solid and the liquid (forming the meniscus) (Figure I. 18)
R the characteristic pore radius.

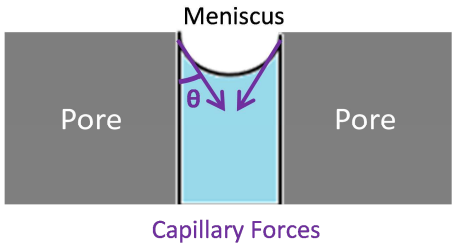

Figure I. 18 : Illustration of capillary forces during drying.

To avoid the capillary forces, it is necessary to suppress the liquid/gas surface tension. One way is to transform the liquid inside pores to a supercritical fluid with a null surface tension. A supercritical fluid is a fluid in its supercritical state and has properties midway between a liquid and a gas (Figure I. 19). It has the density of a liquid but expands like a gas. Supercritical drying consists in putting the material is such conditions that the pressure and temperature exceed the critical temperature T_c and critical pressure P_c of the liquid trapped in the gel pores. Supercritical CO_2 is usually used as its T_c and P_c are easily reachable: P_c = 72.8 bar and T_c = 31.1°C.

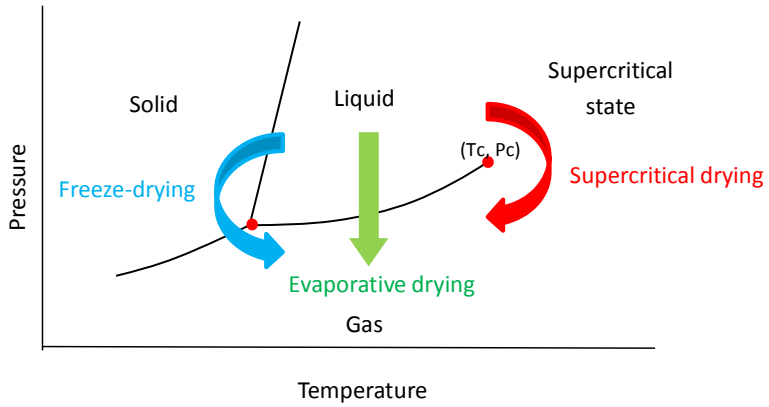

Figure I. 19 : Different drying processes. Above the critical temperature (T_c) and pressure (P_c) is the domain of supercritical conditions.

Classical aerogels are prepared by the polymerization "sol-gel" process which is a method for producing solid materials from small molecules. For example, for silica aerogels, particles dispersed in a colloidal solution (a sol) undergo chemical cross-linking (often a series of hydrolysis and polymerization) to form a continuous three-dimensional network extending throughout the liquid (a gel) (Figure I. 20). The gel is washed with ethanol several times and dried by supercritical CO_2 to give an aerogel.

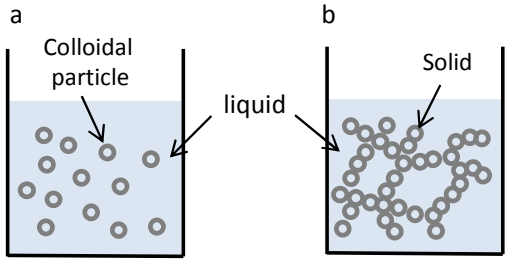

Figure I. 20 : the sol-gel process: sol (a); gel (b).

This route is widely used for inorganic gels. Sol-gel precursors can be metallic salts MX_n or more recently alkoxides $M(OR)_n$ (Pierre & Pajonk, 2002). Silica aerogels are the most common aerogels and are extensively studied and used (see next section).
Pekala and his co-workers studied organic aerogels from resorcinol/formaldehyde and melamine/formaldehyde (Pekala, 1989). These organic aerogels were shown to be less brittle than inorganic ones. They also can be converted into carbon aerogels through pyrolysis (Pekala et al., 1998).

More recently, ultra-porous organic aerogel-like materials from polysaccharides were prepared (Fischer, Rigacci, Pirard, Berthon-Fabry, & Achard, 2006; García-González, Alnaief, & Smirnova, 2011; Gavillon & Budtova, 2008; Mehling, Smirnova, Guenther, & Neubert, 2009; Quignard, Valentin, & Di Renzo, 2008; White, Budarin, & Clark, 2010). They present similar interesting structural properties as silica aerogels, i.e. low density, rather high specific surface area (but slightly lower than silica aerogels) and porosity. However, the process of gelation is

rather different from the sol-gel route. Polysaccharides are already polymers and the gel formation can be via two processes: *physical gel* refers to a gel formed by entanglements or weak forces (e.g. hydrogen bonds) between polymeric chains; and *chemical gel* where a cross-linking occurs between chains by coupling agent or cross-linker promoters. For some polysaccharides there may even be no gelation at all: for example, wet cellulose monoliths network is formed simply by cellulose coagulation from solution into non-solvent.

It seems therefore relevant to make a distinction between porous structure prepared by conventional sol-gel route and the one prepared from entangled polymers. Even if the "polysaccharide aerogel" expression is widely used in literature, a different notation will be used for porous materials from polysaccharides physical gels, taken from (Gavillon & Budtova, 2008; Innerlohinger, Weber, & Kraft, 2006). The prefix "Aero"- followed by the name of the polysaccharide, e.g. "Aero-cellulose", will be preferred.

2.2 Silica aerogels

Silica aerogels are the most studied aerogel materials.
Its preparation is via the sol-gel route with the creation of siloxane bridges (-Si-O-Si-) between Si atoms delivered by precursor molecules. The Si precursors are frequently alkoxides $Si(OR)_4$ with R=alkyl chain and OR=alkoxide group. Often, R is a methyl group $-CH_3$ and the alkoxide is called TetraMethOxySilane (TMOS) or R is an ethyl group $-CH_2-CH_3$ and the alkoxide is TetraEthOxySilane (TEOS). Si alkoxides are usually dispersed in ethanol or isopropanol and are pre-polymerized to small extent (oligomers). Their polymerization is carried out by simultaneous hydrolysis (Figure I. 21a) and polycondensation of water (Figure I. 21b) and alcohol (Figure I. 21c).

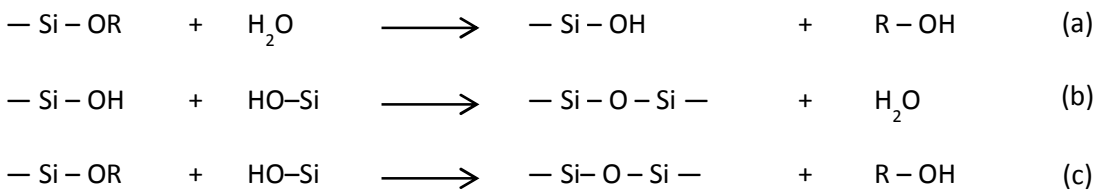

Figure I. 21 : Synthesis of silica polymers chains.

It is catalyzed either by bases (ammonia) or acids (HCl). Under acidic catalysis, hydrolysis and condensation lead to weakly branched structures whereas basic conditions favours cross-linking and lead to denser gels with broader pores size distribution.
Silica aerogels have interesting structural properties (Pierre & Rigacci, 2011; Soleimani Dorcheh & Abbasi, 2008). They have a skeletal density around 2 g/cm^3 close to the one of amorphous silica (ρ_s=2.2 g/cm^3). They are ultra-porous (with porosity above 90%) and ultra-light with bulk density varying from 0.003 to 0.35 g/cm^3. Their specific surface are exceeding 600 m²/g reaching sometimes 1000 m²/g. Silica aerogels are mesoporous with pores size typically from 5 to 100 nm and an average pore diameter between 20 and 40 nm (Figure I. 22).

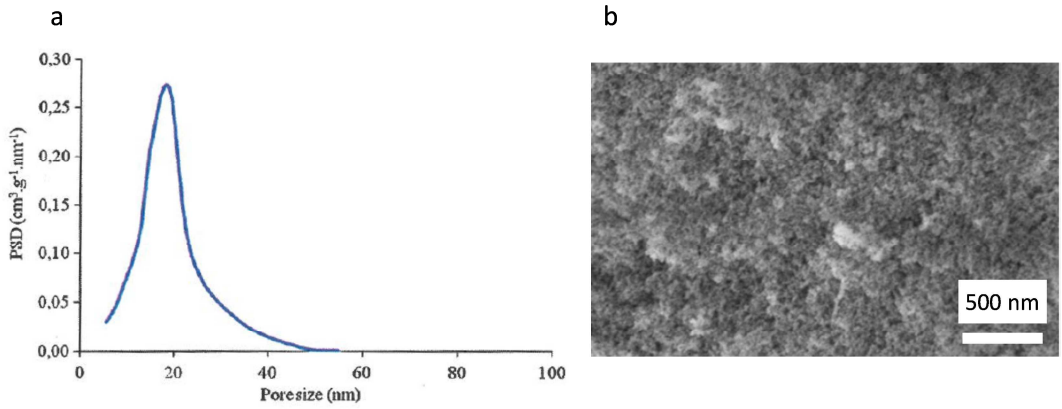

Figure I. 22 : Pore size distribution of a silica aerogel with a bulk density of 0.15 g/cm^3 obtained by non-intrusive mercury porosimetry (Pierre & Rigacci, 2011) with kind permission from Springer Science and Business Media (a); SEM image of a silica aerogel with a bulk density of 0.18 g/cm^3 (Koebel, Rigacci, & Achard, 2012) with kind permission from Springer Science and Business Media. (b).

After supercritical drying, silica aerogels still contain some residual reactive groups, such as alkoxy and hydroxyl groups, which give certain hydrophilicity. However, for many applications, it is necessary to have hydrophobic materials that do not absorbing humidity. Hydrophobisation of silica aerogels was widely studied (Anderson & Carroll, 2011). Briefly, the pore surface of silica aerogels is covered with non-polar functions such as –Si-CH_3 by silylation (Figure I. 23).

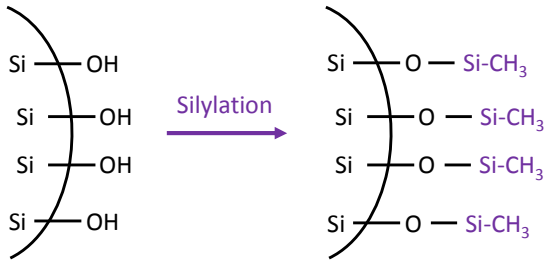

Figure I. 23 : Hydrophobisation of silica aerogel by silylation.

Due to their nanostructure, silica aerogels present very interesting physical properties. They are known for their very low thermal conductivity, 0.015 W.m^{-1}.K^{-1}, and they are thus one of the best thermal insulating materials (see section 3.2). They are optically transparent and they present potential application for opaque or transparent insulating component (Figure I. 24).

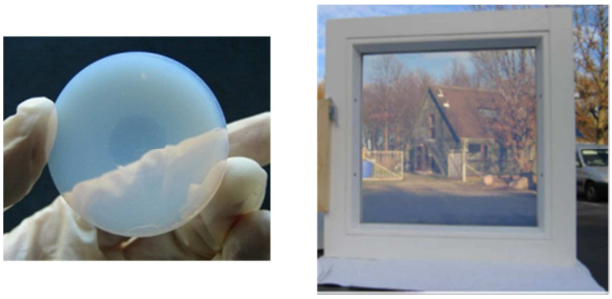

Figure I. 24 : Transparency of silica aerogel and its potential for transparent insulation glazing (Koebel et al., 2012) with kind permission from Springer Science and Business Media.

Aerogels have also a large range of other applications (Akimov, 2003; Pierre & Pajonk, 2002): for gas or liquid purification, for adsorption of spills, for catalysis, for space industry as a trap for space dust particles ("Stardust" project) or as an effective insulating materials of the Mars Rover.

2.3 Polysaccharides-based aerogels

Polysaccharides-based aerogels are a kind of "third generation" aerogels succeeding the silica and synthetic polymer-based ones. Polysaccharide aerogels (or aero-polysaccharides) have somewhat similar structural and mechanical properties as compared to their inorganic and synthetic polymer counterparts, but have a major advantage of being bio-based and their preparation does not involve toxic components.
In this section, different types of polysaccharides aerogels will be presented (from cellulose, starch, alginate and pectin) in order to illustrate the variety of aerogel morphologies that can be achieved and the different mechanisms involved in their preparation.

Aerogel-like cellulose is usually prepared from cellulose II but it can also be prepared from cellulose I such as bacterial cellulose (Liebner et al., 2010) or nanofibrillated cellulose (Kettunen et al., 2011). The obtained aerocelluloses have very low densities of 0.008 g/cm^3 (10 times lower than other aerocelluloses), a specific surface area of 200 m²/g and very large pores but also smaller macropores similar to aerocelluloses from cellulose II. Aerogels of chitin or chitosan are also under intensive research (Chang, Chen, & Jiao, 2008; El Kadib & Bousmina, 2012; Robitzer, Renzo, & Quignard, 2011; Silva, Duarte, Carvalho, Mano, & Reis, 2011; Tsioptsias, Michailof, Stauropoulos, & Panayiotou, 2009; Valentin, Bonelli, Garrone, Di Renzo, & Quignard, 2007; Valentin, Molvinger, Quignard, & Brunel, 2003). They will not be presented in details in this section.

2.3.1 Aerogels from cellulose and its derivatives

The preparation of cellulose (cellulose II) aerogel-like materials, so-called Aerocellulose (Innerlohinger et al., 2006), comprises the following steps:
- dissolution of cellulose in a direct solvent
- casting (films, monoliths, beads),
- coagulation in a non-solvent (water or alcohols),

- drying either by freeze-drying (cryogel) or supercritical drying (aerogel-like).

When coagulation process occurs in water, the latter is replaced by a $scCO_2$-miscible organic solvent (acetone or alcohol) before supercritical drying. Aerocelluloses are made only of cellulose and no chemical cross-linker or stabiliser of cellulose network is used. The porous network is formed by entangled coagulated cellulose chains either from a solution (cellulose dissolved in NMMO or ionic liquid) or from a physical gel (cellulose in NaOH-water). Various shapes can be prepared depending on applications such as monoliths or beads.
Various solvents of cellulose were used for preparing aerocellulose: calcium thiocyanate (Jin, Nishiyama, Wada, & Kuga, 2004), NMMO (Innerlohinger et al., 2006; Liebner et al., 2009), LiCl/DMAc (Duchemin, Staiger, Tucker, & Newman, 2010), 8%NaOH-water (Cai, Kimura, Wada, Kuga, & Zhang, 2008; Gavillon & Budtova, 2008) or ionic liquids (Deng, Zhou, Du, Van Kasteren, & Wang, 2009; Sescousse et al., 2011; Tsioptsias et al., 2008). Depending on the drying methods, different morphologies are obtained: by freeze drying cryogels have large pores and low specific surface compared to aerogels dried by supercritical drying (Duchemin et al., 2010; Hoepfner, Ratke, & Milow, 2008; Jin et al., 2004). This morphology is not in the scope of our work and thus will not be further discussed. Only aerogels obtained via supercritical drying will be presented in the following.
The solvent of cellulose has a strong impact on the final morphology of aerocelluloses. Two types of structures can be differentiated: a “fibrous network”-like and a “globular”-like. A network structure is observed for gelled (in 8%NaOH or $Ca(SCN)_2$ or solidified (NMMO monohydrate) cellulose solutions (Figure I. 25).

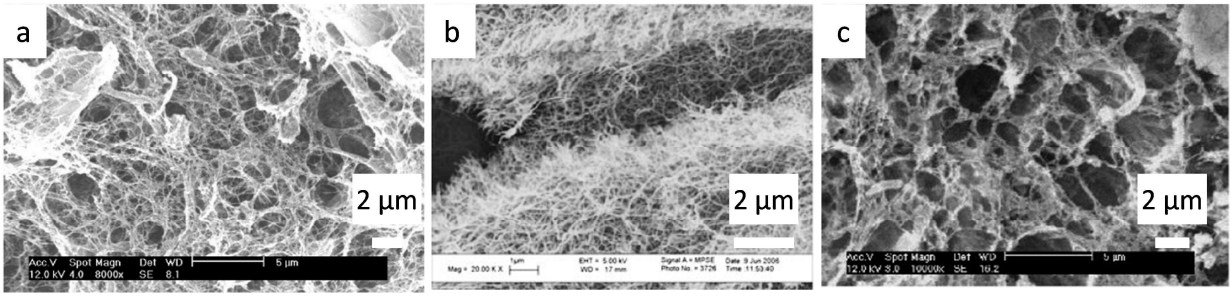

Figure I. 25 : SEM images of aerocelluloses “network-like” from different solvents. 5% cellulose Avicel-8%NaOH-water (Gavillon & Budtova, 2008) (a); 2%cellulose-$Ca(SCN)_2.4H_2O$ (Hoepfner et al., 2008) with kind permission from Springer Science and Business Media. (b); 3%cellulose-82% solid NMMO-15%water (Gavillon & Budtova, 2008) (c). Reprinted with permission from (Gavillon et al., 2008). Copyright (2008) American Chemical Society.

A globular morphology is obtained when solutions are coagulated directly from the liquid state (molten NMMO monohydrate or ionic liquids as EMIMAc) (Figure I. 26).

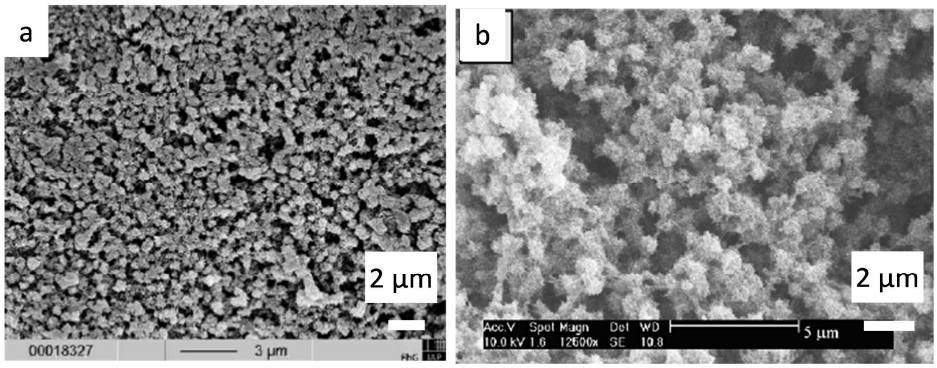

Figure I. 26 : SEM images of aerocelluloses "globular-like" from different solvents. 3%cellulose-molten 82% NMMO-15%water (Gavillon & Budtova, 2008) (a). Reprinted with permission from (Gavillon et al., 2008). Copyright (2008) American Chemical Society; 3% cellulose Avicel-Ionic liquid EMIMAc (Sescousse et al., 2011) (b). Reprinted from (Sescousse et al., 2011), Copyright (2011), with permission from Elsevier.

These differences in morphologies may be explained by the state of the cellulose solution before the coagulation step (Sescousse et al., 2011). For molten NMMO and EMIMAc-cellulose solutions, cellulose is homogeneously distributed and phase separation occurs in one step (spinodal decomposition) which creates small spheres (Biganska & Navard, 2009). On the other hand, a gelation occurs for cellulose-NaOH-water solutions (where cellulose chains reorganize and self-associate) so a micro-phase separation occurs before coagulation (Figure I. 27).

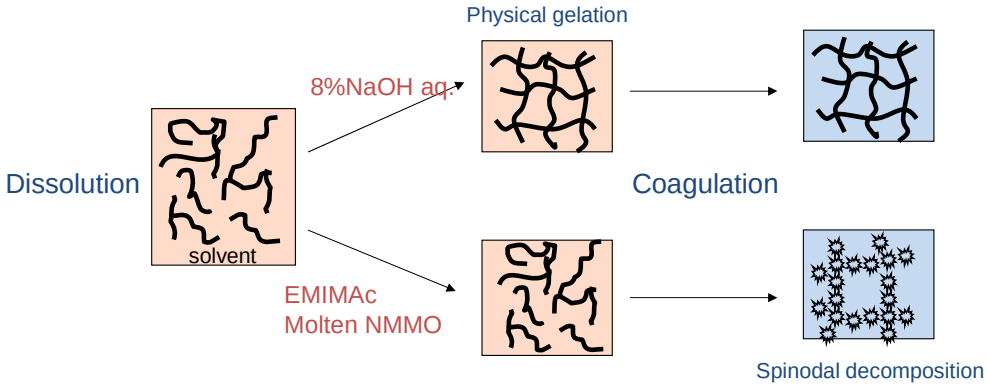

Figure I. 27 : Two mechanisms for a network or globular aerocellulose morphologies.

It has been shown that during coagulation and even supercritical drying, samples of aerocellulose tend to shrink and the resulting volume can be lowered as 30-40% (Innerlohinger et al., 2006). But shrinkage can be considerably decreased by increasing the cellulose content. Having higher cellulose concentration favours higher mechanical stability in the porous network (Innerlohinger et al., 2006; Liebner et al., 2009).

The densities of aerocelluloses depend on the initial cellulose concentration (in solution). It was demonstrated that bulk densities are directly proportional to cellulose concentration independently of the solvent used (Hoepfner et al., 2008; Innerlohinger et al., 2006; Liebner et al., 2009; Sescousse et al., 2011). Figure I. 28 displays this relationship between density and

cellulose concentration. It has to be noted that density increases with the molecular weight of the cellulose (shown by arrows).

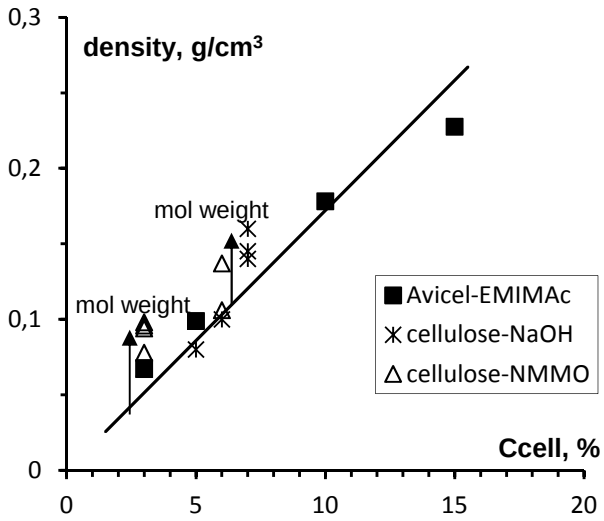

Figure I. 28 : Aerocellulose densities as a function of cellulose concentration. Graphic is taken from (Wendler et al., 2013) based on data of (Gavillon & Budtova, 2008; Liebner et al., 2009; Sescousse & Budtova, 2009; Sescousse et al., 2011)

Aerocelluloses with initial cellulose concentration between 0.5 and 15_{wt}% give densities around 0.03-0.4 g/cm^3 and specific surfaces of 100-400 m²/g (Table I. 2). Thus the structural properties of aerocelluloses can be easily tuned by adjusting cellulose concentration. For all aerocelluloses presented in Table I. 2, nitrogen sorption isotherms at 77K were performed and the latter showed a isotherm type IV typical for a mesoporous structure (see Chapter II). The overall pore size distribution is wide: from few nanometers to few microns.

Table I. 2 : Summary of aerocelluloses densities and specific surfaces.

% $C_{cellulose}$	Solvent	Density (g/cm^3)	S_{BET} (m²/g)	References
0.5-13	NMMO.H_2O	0.1-0.4	100-400	(Innerlohinger et al., 2006)
4-6	NaOH-urea	0.13-0.27	260-400	(Cai, Kimura, et al., 2008)
1-7	LiOH-urea	0.03-0.58	290-480	(Cai, Kimura, et al., 2008)
1.73	AMIMCl	0.058	315	(Tsioptsias et al., 2008)
0.5-3	$Ca(SCN)_2.4H_2O$	0.01-0.06	200-220	(Hoepfner et al., 2008)
3	NMMO.H_20	0.046-0.069	190-310	(Liebner et al., 2009)
5	NaOH	0.10-0.30	200-300	(Gavillon & Budtova, 2008; Gavillon, 2007)
3-15	EMIMAc	0.13-0.38	128-228	(Sescousse, 2010)

Mechanical behavior of aerocelluloses was also investigated by (Sescousse et al., 2011) via uniaxial compression tests. Young modulus E and yield stress σ_{yield} were determined from the curve stress-strain. For an aerocellulose with a density of 0.1 g/cm^3 the modulus is about 3-5

MPa for cellulose-NaOH-water or cellulose-EMIMAc. The yield stress is around 0.1-0.2 MPa. Young modulus was plotted as a function of the bulk density according to the model of foams by (Gibson & Ashby, 1999). A power-law is found to be $E \sim \rho^3$ (Sescousse et al., 2011; Wendler et al., 2013). The model by Gibson and Ashby predicts an exponent 2 for foams. The exponent 3 in Young modulus-density correlation was already reported for silica (Alaoui, Woignier, Scherer, & Phalippou, 2008) and resorcinol-formaldehyde (Pekala, Alviso, & LeMay, 1990) aerogels and is probably due to structural defects appearing during the sol-gel process or the cellulose coagulation.

Cellulose derivatives for making aerogels, in particular, cellulose ester, were also studied (Fischer et al., 2006; Tan, Fung, Newman, & Vu, 2001). Cellulose acetate was cross-linked by isocyanate using a tin-based catalyst (Fischer et al., 2006). By varying cellulose acetate concentration and the degree of cross-linking, cellulose acetate aerogel morphology and properties (bulk density, porous volume, pore size distribution…) were tuned. These aerogels have rather low densities (0.2 g/cm^3), high specific surface areas (140-250 m^2/g) and a meso- and macroporous structure (pores from few nanometers to few hundreds nanometers, (Figure I. 29).

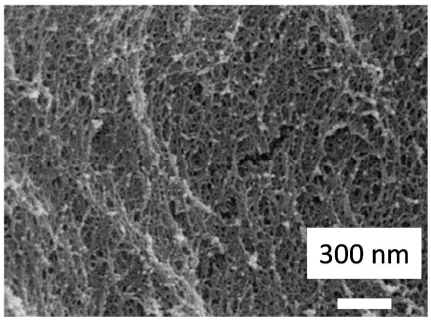

Figure I. 29 : SEM image of cellulose acetate aerogel (Fischer et al., 2006). Reprinted from (Fischer et al., 2006), Copyright (2006), with permission from Elsevier.

2.3.2 Aerogels from starch

As cellulose, starch is also one of the major sources of polysaccharides. It is composed of amylose (linear chain of repeated units of glucose) and amylopectin (branched chains of glucose) (Figure I. 30). The ratio between these two components strongly depends on starch sources. Usually starch contains 70-85% amylopectin.

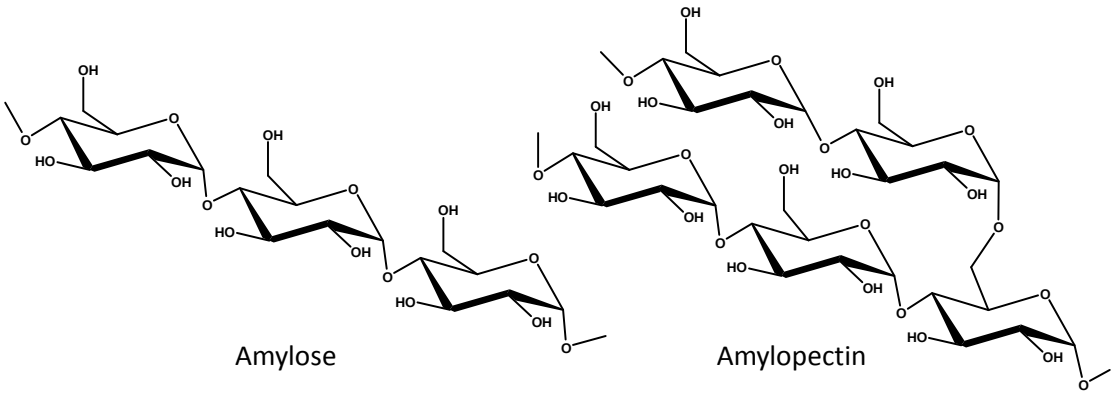

Figure I. 30 : Structure of main macromulecules composing starch : amylose linear chain and amylopectin branched chain.

Aerogels from starch are prepared in a different way as compared with cellulose, according to the specificity of starch gelation. First, starch undergoes *gelatinisation process*: granules are swelling in hot water and then bursting with amylose leaching out. The next step is starch *retrogradation* when a hydrogel is formed upon cooling and ageing. Gelation is mainly influenced by amylose content and the temperature of gelatinisation. Then after several exchanging water by CO_2-compatible liquids, coagulated starch is dried with $scCO_2$ to give "Aerostarch" (Glenn & Stern, 1999; Mehling et al., 2009).
Various shapes can be prepared depending on applications such as monoliths or beads (Figure I. 31).

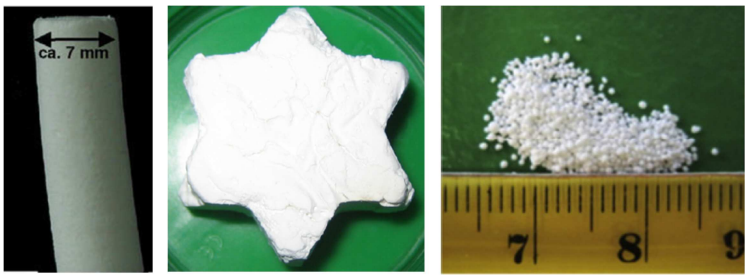

Figure I. 31 : Various shapes of aerostarch (García-González et al., 2011; García-González, Uy, Alnaief, & Smirnova, 2012; Mehling et al., 2009). Reprinted from (García-Gonzalez et al., 2011), Copyright (2011); from (García-Gonzalez et al., 2012), Copyright (2012); from (Mehling, 2009), Copyright (2009), with permission from Elsevier.

Starch gel shrinkage is observed during retrogradation, solvent exchange and supercritical drying. The volume can decrease down to 35-40% of the initial volume for wheat and corn starch (Glenn & Stern, 1999) and 23% for potatoes starch (Mehling et al., 2009). The morphology of aerostarch can be tuned by the temperature of gelatinisation. Higher temperature results in more rigid gel structure and a denser network. At lower temperatures, smaller crystals appear during the retrogradatation and they are more favourable for having higher specific surface areas (Mehling et al., 2009) (Figure I. 32).

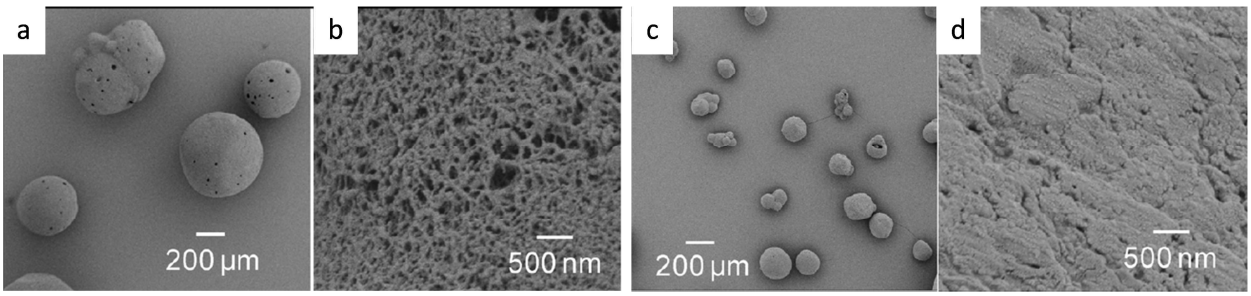

Figure I. 32 : Influence of gelatinisation temperature on the morphological structure of aerostarch: T=120°C (a and b) and T= 140°C (c and d) (García-González et al., 2011). Reprinted from (García-Gonzalez et al., 2011), Copyright (2011), with permission from Elsevier.

Aerostarch presents a mesoporous structure and its properties depending on starch source are summarised in Table I. 3. Starches concentrations may vary from 1 to 20_{wt}%. Bulk densities are about 0.25-0.30 g/cm^3 (for 8% starch concentration) for wheat and corn starches and 0.46 g/cm^3 (for a 10% starch) from potatoes starch. For high amylose corn or maize starch, bulk densities are much lower (0.16 to 0.34 g/cm^3). Specific surface areas are smaller as compared with aerocelluloses and vary from 50 to 180 m²/g; they also strongly depend on starch various sources. Specific surface area decreases with the increase of starch content (Miao et al., 2008).

Table I. 3 : Summary of aerostarch structural properties.

% C $_{starch}$	Starch Sources	Density (g/cm^3)	S_{BET} (m²/g)	References
8	Wheat	0.26	116	(Glenn & Stern, 1999)
8	Corn	0.29	50	(Glenn & Stern, 1999)
8	High Amylose Corn	0.16	145	(Glenn & Stern, 1999)
11.1	Potatoes	0.46	73	(Mehling et al., 2009)
11.1	High Amylose Maize	0.34	90	(Mehling et al., 2009)
4.7	High Amylose Corn	-	184	(White, Budarin, Luque, Clark, & Macquarrie, 2009)
15	Non-specified	-	119	(Miao et al., 2008)
20	Non-specified	-	99	(Miao et al., 2008)
25	Non-specified	-	55	(Miao et al., 2008)

SEM images of various aerostarches are reported in Figure I. 33. A network of small interconnecting strands interrupted by starch granule remnants is observed. With higher amylose content, the porous structure is less disturbed by the presence of starch granule remnants.

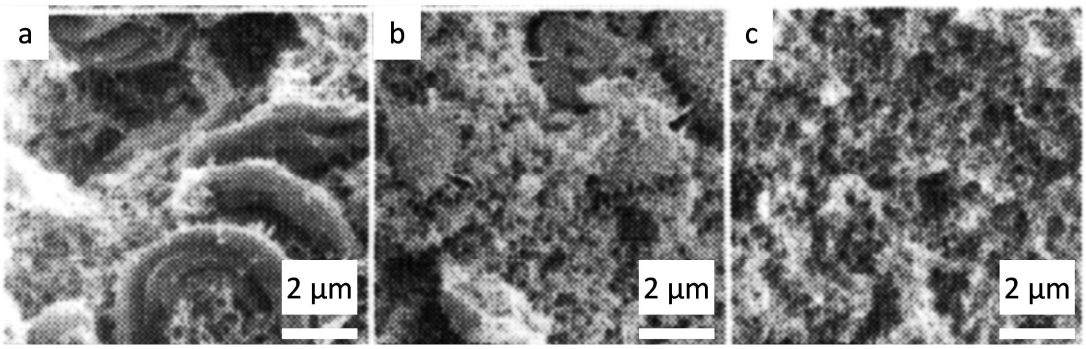

Figure I. 33 : SEM images of aerostarches from wheat starch (a); corn starch (b); high amylose corn starch (c), adapted from (Glenn & Stern, 1999).

As the starch concentration increases, the porous structure is denser with slimmer entangled strands (Figure I. 34). Aerostarches are highly porous with pores varying from few nanometers to few microns, for a large range of sources and concentrations.

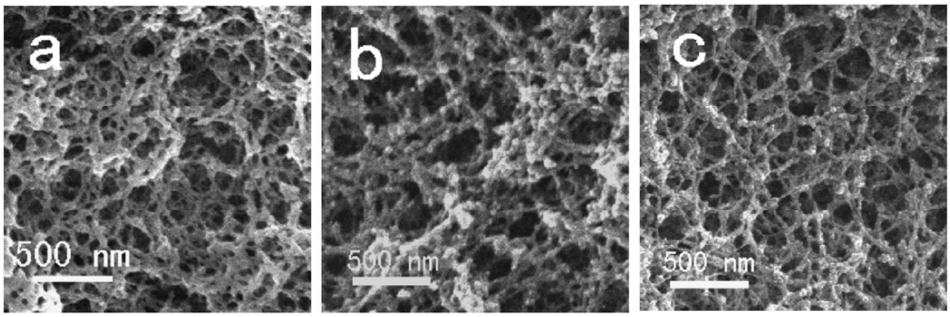

Figure I. 34 : SEM images of aerostarch from 25_{wt}% (a); 20_{wt}% (b); 15_{wt}% (c) of starch (Miao et al., 2008). Reprinted from (Miao et al., 2008), Copyright (2008), with permission from Elsevier.

Aerostarches also present interesting mechanical and thermal properties (Glenn & Stern, 1999) and they are summarised in Table I. 4. Their thermal conductivity seems promising and they can be used as an insulating material. They have a Young modulus E in uniaxial compressive tests between 5 and 30 MPa depending on starch source. Amylose content seems to have an impact on the mechanical behavior of aerostarches. Amylopectin appears to give strength to the porous materials. Compressive stress is claimed to increase almost linearly with the bulk densities of aerostarches (Figure I. 35) (Glenn & Stern, 1999) but it looks more like a power law dependence (with $\sigma \sim \rho^{2.1}$, data extracted from Figure I. 35).

Table I. 4 : Mechanical and thermal properties of aerostarches (Glenn & Stern, 1999).

Starch sources	E (MPa)	λ (mW/m.K)
Wheat starch	21	36
Corn starch	32	33
High amylose corn starch	5	24

However, as some aerostarches seem to be relatively inhomogeneous (Figure I. 33), values of Young modulus and thermal conductivity have to be taken with care. They may vary greatly depending on samples.

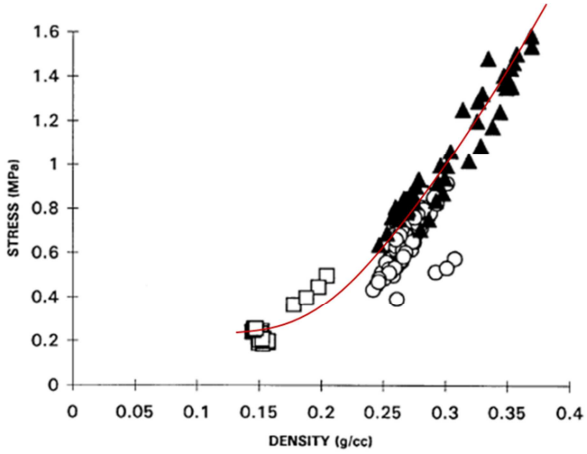

Figure I. 35 : Compressive stress as a function of bulk density for aerostarch, adapted from (Glenn & Stern, 1999).

2.3.3 Aerogels from alginate and pectin

Pectin and alginate can also form porous materials and aerogels. Because their gelation is very similar, the structure and properties of pectin and alginate aerogels will be reviewed together. As well as pectin, alginates are widely used as thickeners in the food industry, as matrices for encapsulation of drugs, proteins or enzymes.

Alginate (usually sodium alginate) is the basic form of alginic acid. It is produced by brown algae. It consists of a copolymer of 1,4-β-D-mannuronic acid and α-L-guluronic acid of various compositions and sequences (Figure I. 36). The gelation of alginate is similar to LM pectin and involves the cross-linking of alginate by divalent cation (Ca^{2+} usually) following the "egg box" model (Figure I. 17). Alginic acid gels can also be formed by lowering the pH of a Na-alginate solutions (Na^{+} cations are replaced by protons) or from native alginic acid (White, Antonio, et al., 2010) similarly to HM pectin. In this case gelation occurs via hydrogen bonds and a physical gel is formed.

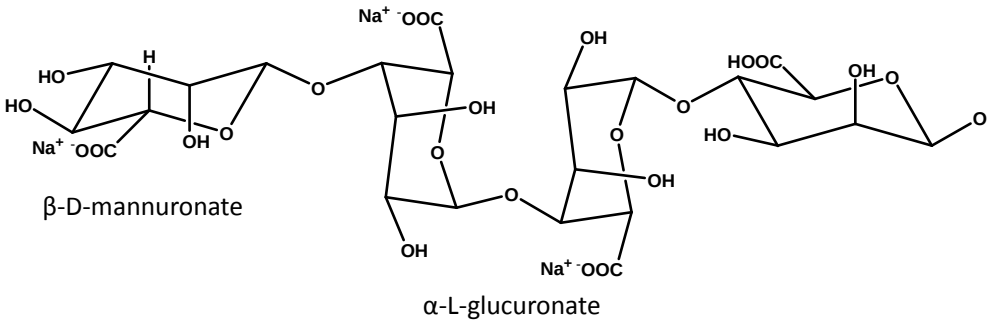

Figure I. 36 : Alginate structure.

Quignard's group (Quignard et al., 2008; Robitzer, David, Rochas, Di Renzo, & Quignard, 2008; Robitzer, David, Rochas, Di Renzo, & Quignard, 2008; Valentin, Molvinger, Quignard, & Di Renzo, 2005) has widely studied the properties of alginate aerogels prepared from a solution of 2_{wt}% alginate in distilled water added to a solution of $CaCl_2$ (0.24 M) to form a hydrogel of alginate. The hydrogel is then immersed in a CO_2-compatible solvent like alcohols and dried by $scCO_2$. Volume contraction is also observed (about 20%) during the solvent exchange and the supercritical drying. It can be limited by preferring progressive increase of the alcohol content in exchange baths than a direct immersion (Mehling et al., 2009; Robitzer et al., 2008). Various shapes can be forms such as beads (Deze, Papageorgiou, Favvas, & Katsaros, 2012; Valentin et al., 2005) or monoliths (Mehling et al., 2009) (Figure I. 37).

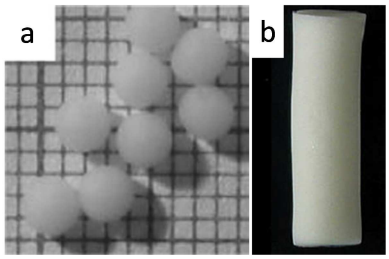

Figure I. 37 : Various shapes of alginate aerogel: beads (a) (Robitzer et al., 2008). Reprinted with permission from (Robtizer et al., 2008). Copyright (2008) American Chemical Society; monolith (b) (Mehling et al., 2009). Reprinted from (Mehling, 2009), Copyright (2009), with permission from Elsevier.

The adsorption-desorption isotherm of N_2 at 77K on alginate aerogel is typical of a type IV isotherm which indicates the presence of mesopores. Structural characteristics seem to be very promising and are summarised in Table I. 5. Densities are relatively low (0.13-0.20 g/cm^3), specific surface areas are between 150-500 m²/g and porosity around 90%. Bulk density is affected by the concentration of calcium. It tends to increase with increasing the amount of Ca^{2+} (Mehling et al., 2009). The specific surface area seems to follow the same tendency, it increases until a maximum at a Ca^{2+} concentration of 0.24 mol/L is reached (Quignard et al., 2008).

Table I. 5 : Structural characterisations of alginate aerogels.

Type of alginate	C %	Gelation method	Density (g/cm^3)	S_{BET} (m²/g)	References
20% guluronate	2%	0.24 M $CaCl_2$	-	342	(Valentin et al., 2005)
45% guluronate	2%	0.24 M $CaCl_2$	-	339	(Valentin et al., 2005)
76% guluronate	2%	0.24 M $CaCl_2$	-	507	(Valentin et al., 2005)
35% guluronate	1%	0.24 M $CaCl_2$	-	385	(Robitzer et al., 2008; Robitzer et al., 2008)
Na-alginate	2%	0.1M $CaCO_3$	0.13	150-300	(Mehling et al., 2009)
Native alginic acid	4.7%	Heating 90°C-2h	0.22	320	(White, Antonio, et al., 2010)
Alginate non specified	2%	0.05 M $CaCl_2$	-	419	(Deze et al., 2012)

SEM images of alginate aerogels are given in Figure I. 38. The morphology is an open network of entangled fibrils. It strongly depends on the initial composition of alginate, i.e the ratio between guluronic and mannuronic acids. The aerogels from guluronic-rich alginates present a more compact nanostructure with fibrils with diameter of 20-30 nm (Figure I. 38d) against 10-15 nm for mannuronic-rich alginate (Figure I. 38a). The size distribution of pores is broad and centred around 40 nm (Robitzer et al., 2008). To the best of our knowledge, no extensive studies on density, porosity, mechanical or thermal properties of alginate aerogels have been reported.

Alginate aerogels have found many applications as a scaffold for drug release (Mehling et al., 2009), for sorption of heavy metals from aqueous solutions (Deze et al., 2012), catalysis (Quignard et al., 2008) or they can be carbonized for electro-chemical applications (White, Antonio, et al., 2010).

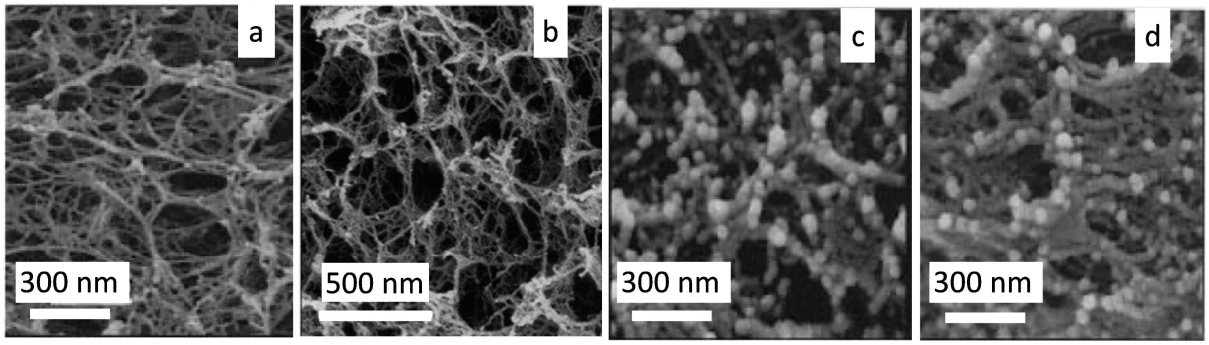

Figure I. 38 : SEM images of alginate aerogels : 20% guluronate (a); 35% guluronate (b); 45% guluronate (c) and 76% guluronate (d).
Pictures a, c and d are taken from (Valentin et al., 2005), reprinted with permission from (Valentin et al., 2005). Copyright (2005) Wiley.
Picture b is taken from (Robitzer et al., 2008), reprinted with permission from (Robtizer et al., 2008). Copyright (2008) American Chemical Society.

Hydrogels of pectin are widely studied and used in food industry (c.f. 1.3). However only few papers reported dried pectin porous materials (Agoudjil et al., 2012; Chen, Chiou, Wang, & Schiraldi, 2013; García-González, Carenza, Zeng, Smirnova, & Roig, 2012; White, Budarin, et al., 2010).
(White, Budarin, et al., 2010) were the first one to report the preparation of “aeropectin”. Two different pathways were explored: native pectin underwent either a thermal gelation (an aqueous solution of pectin was heated at 90°C for 2h) or an acidic gelation (pectin dissolved in an acidic aqueous solution and let gelling for 48h). The hydrogel is then washed with ethanol-water progressive baths (water is gradually replaced by ethanol) and dried by $scCO_2$. Two different morphologies were obtained (Figure I. 39): a powder for the thermal treatment (“thermal aeropectin”) and monolith for acidic gelation (“acidic aeropectin”). SEM images of “thermal aeropectin” showed large irregular agglomerated particles (about 50 µm), composed of overlapping folded sheets of polysaccharide (Figure I. 39a). “Thermal aeropectin” has a density of 0.20 g/cm^3 and a specific surface area of 485 m^2/g. Contrary to “thermal aeropectin”, SEM images of “acidic aeropectin” revealed a high porosity with interconnected “fibers” composing a network (Figure I. 39b). The N_2 adsorption-desorption showed an isotherm of type IV typical of

mesoporous structure. This aeropectin is very light, 0.07 g/cm^3 for a pectin concentration of 4.8$_{wt}$% and a specific surface of 200 m²/g.

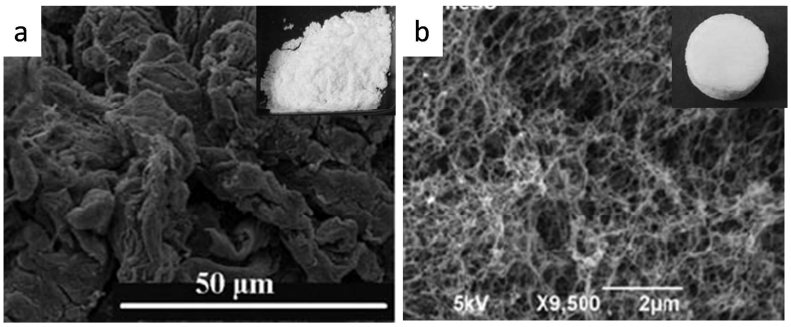

Figure I. 39 : SEM images of aeropectin prepared from thermal gelation(a); acidic gelation (b) (White, Budarin, et al., 2010). Reprinted with permission from (White et al., 2010). Copyright (2010) Wiley.

(García-González et al., 2012) also prepared aeropectin from HM pectin with a different process but obtained similar results. They dissolved 6$_{wt}$% pectin in water (for 24 h) which is then heated at 40-60°C for 30 min and ethanol is added under stirring. The mixture is let gelling for 24h. After ethanol washing and scCO_2 drying the aeropectin obtained presents a low bulk density 0.08 g/cm^3 and a rather large specific surface 247 m²/g.

To the best of our knowledge, no paper was reported on “pectin aerogel” prepared from a divalent cation cross-linked hydrogel. One paper claims to prepare pectin cryogels (freeze-dried) from the gelation of pectin without and with cation cross-linking (various cations such as Na^+, Ca^{2+} and Al^{3+} were investigated) (Chen et al., 2013). First, they studied the influence of pectin concentration on density and Young modulus (in compression) for non-cross-linked cryogels. Bulk densities are very light from 0.03 to 0.16 g/cm^3 for 5 to 15$_{wt}$% pectin and seem to increase linearly with polymer concentration. Mechanical properties are improved as the Young modulus increases from 0.04 MPa for 2.5$_{wt}$% pectin in solution to 12 MPa for 12.5% solution. SEM images of pectin cryogels are given in Figure I. 40. Layered structures are observed. As pectin concentration increases, the thickness of layers increases as well without a change in the overall morphology (Figure I. 40a and b). For 15$_{wt}$% the morphology exhibited a network structure with pores of few tens microns (Figure I. 40c). Authors believed that it is due to the high viscosity solutions at high pectin concentration. Growth of ice crystals during the freezing is retarded by the viscosity.

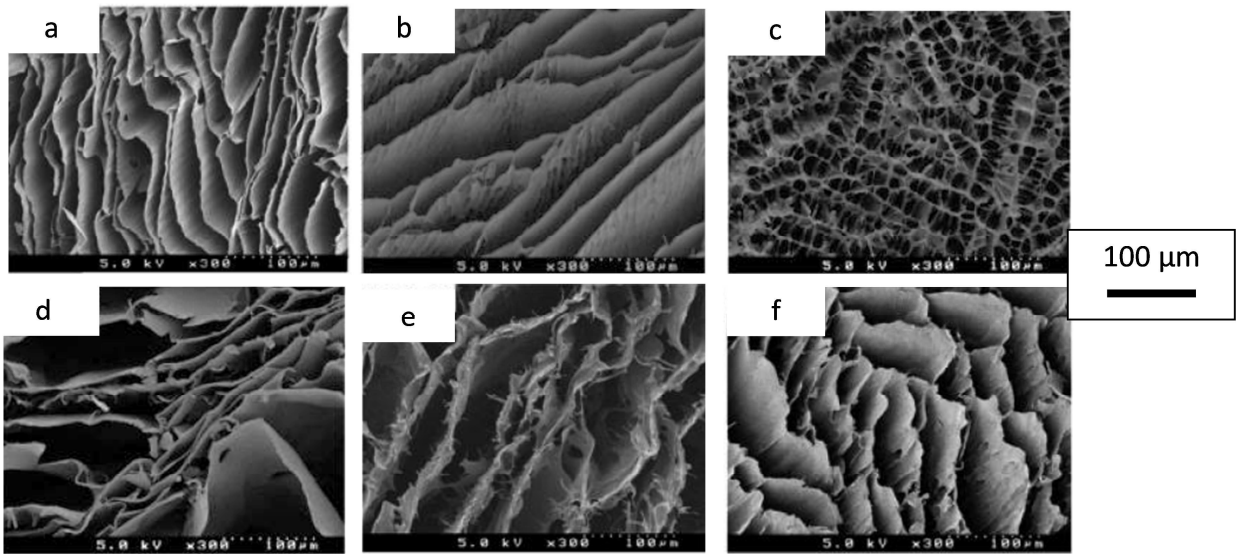

Figure I. 40 : SEM images of pectin cryogels : 5_{wt}% (a); 10_{wt}% (b); 15_{wt}% (c); 5_{wt}%+0.001mol/g Na^{+} (d); 5_{wt}%+0.001mol/g Ca^{2+} (e); 5_{wt}%+0.001mol/g Al^{3+} (f) (Chen et al., 2013). Reprinted with permission from (Chen et al., 2013). Copyright (2013) American Chemical Society.

The addition of cations changes the mechanism of gelation and the structural properties of pectin cryogels may be different. Three different cations were chosen: a monovalent Na^{+}, a divalent Ca^{2+} and a trivalent Al^{3+}. Sodium showed no ability to cross-link pectin (as it is well-known in the literature). Densities are not affected by the addition of Ca^{2+} whereas moduli increase. A cryogel with 5_{wt}% pectin and 0.001 mol/g of $CaCl_2$ has a density of 0.06 g/cm^3 and Young modulus increases from 0.07 to 1.2 MPa. Al^{3+} has less impacts on the morphology; densities and moduli are similar (0.06 g/cm^3 and 0.50 MPa). SEM images of 5_{wt}% pectin cryogels cross-linked with these three cations are reported in Figure I. 40d-f. Layered structures are still visible but have "rougher" surfaces when Ca^{2+} (Figure I. 40e) and Al^{3+} (Figure I. 40f) are used.

Polysaccharides have a great diversity (chemical functions, spatial conformations…) and thus "aeropolysaccharides" are with a large range of morphologies, densities and mechanical properties that can be tuned with polysaccharide type and concentration, the addition of cross-linkers or different solvents. The diversity of aeropolysaccharides gives therefore a large potential of applications.

3. Applications of porous polysaccharides

Applications of porous polysaccharides are numerous due to their high specific surface areas, high porosity and their lightness. Two applications will be described in this section: controlled drug release and thermal insulation. Other applications in catalysis or biomedical scaffolds can also be envisaged (Quignard et al., 2008).

3.1 Drug release

First, silica aerogels were investigated as additives for cosmetics, as a matrix for biomedical or pharmaceutical applications (Smirnova, 2011). For example, they were studied as drug carriers. They present a large specific surface area which allows a higher loading capacity of a drug, a faster dissolution rate compared to the solid forms of the drug and an efficient absorption by the body. Also, hydrophilic silica aerogels fracture completely when they are placed in water, due to the capillary forces (exerted by the surface tension when a liquid enters the pores of the aerogel). Drug molecules absorbed on the aerogel porous structure are immediately surrounded by water molecules thus they are rapidly dissolved and released. By functionalising silica to produce hydrophobic silica aerogels, the release of drugs is slowed down due to a slower permeation of water into the porous structure. The aerogel surface functionalization may allow tuning the drug release depending on applications, i.e. hydrophilic silica aerogel for rapid release or hydrophobic silica aerogel for more "long-term" release system.

Unfortunately silica aerogels do not fulfil all the requirements for pharmaceutical industry, as biocompatibility and biodegradability. They are biocompatible but not biodegradable. Polysaccharides aerogels are of particular interest for drug-delivery thanks to their low toxicity. In the previous sections it was shown that it is possible to produce highly porous materials with large specific surface areas from polysaccharides (see section 2.3). Loading of aeropolysaccharides with drugs and their release have been recently studied by Smirnova's group, from aerostarch and aeroalginate (Mehling et al., 2009). Two different pathways of drug loading were used. The first one is an *adsorption from the liquid phase*, during the solvent exchange. The second one is an *adsorption from supercritical solutions*. In the latter case, the drug is dissolved in $scCO_2$ and is adsorbed during the $scCO_2$ drying.

Two different starches were studied as release matrix: one from potato and the other one with a high amylose content called Eurylon7. Depending on the adsorption technique two different drugs were used. Paracetamol was chosen for adsorption from ethanol exchange bath (since it has a low solubility in $scCO_2$) and ibuprofen for adsorption from $scCO_2$. The adsorption process does not seem to have an influence on the maximum drug loading. For potato starch 10% of ibuprofen or paracetamol can be loaded and 22-25% for Eurylon7. One potential explanation for the difference in loading from these two starches is a finer pore size distribution for Eurylon7 as compared to potato starch. Alginate aerogel was also investigated as a drug carrier for ibuprofen and showed a similar to Eurylon7 loading (21-26%).

The release kinetics from the polysaccharides matrices is relatively different (Figure I. 41). The release of paracetamol from the two aerostarches is completed after 2 hours (Figure I. 41a), whereas the release of ibuprofen is largely dependent on starch source: a fast release for Eurylon7 and a longer one for potato starch (Figure I. 41b).The dissolution of ibuprofen from alginate aerogel is very fast, almost similar to silica aerogels.

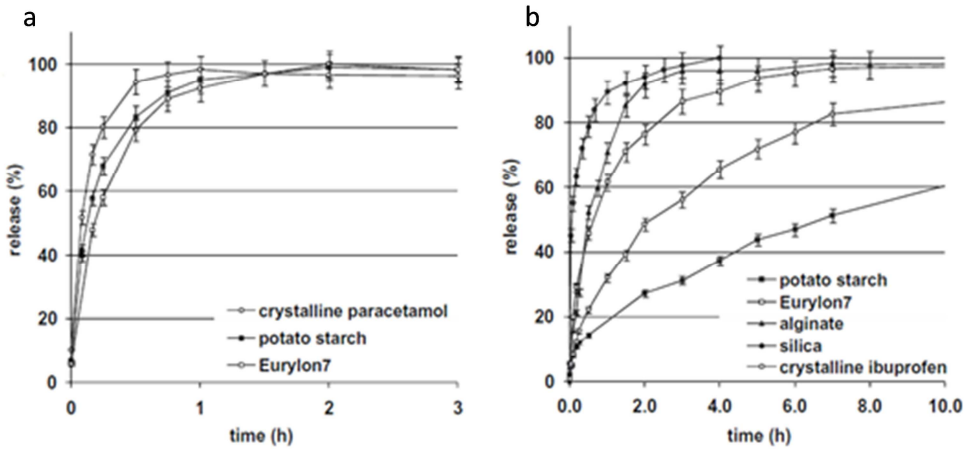

Figure I. 41 : Release kinetics for different aerogels: paracetamol release from aerostarches (a); ibuprofen release from aerostarches and alginate aerogels (b) (Mehling et al., 2009). Reprinted from (Mehling, 2009), Copyright (2009), with permission from Elsevier.

3.2 Thermal insulating properties of aerogels

3.2.1 General aspects of heat transfer in aerogels

Heat transfer in porous materials, such as aerogels, is described by the equation of heat transfer. Equation (I. 2) shows the conservation of energy and Equation (I. 3) is the Fourier's law which defines the thermal conductivity as the ratio between heat flux density and the local temperature gradient.

$$\nabla \vec{q} + \Phi = \rho . c . \frac{\partial T}{\partial t} \quad \text{(I. 2)}$$

$$\vec{q} = -\lambda \nabla T \quad \text{(I. 3)}$$

with q the heat flux density, λ the thermal conductivity, ρ the bulk density, c specific heat, Φ heat source and T the local temperature.

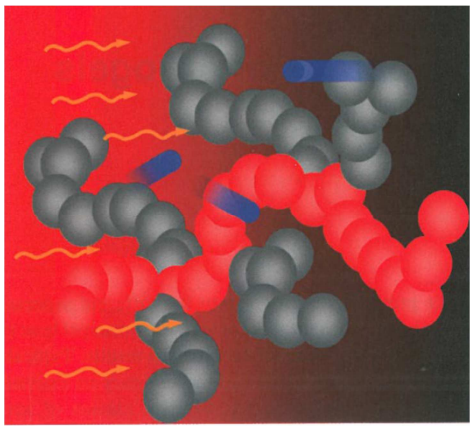

Figure I. 42 : Heat transfer mechanisms in an aerogel : by the solid backbone (red chain), by thermal radiation (wavy yellow arrows) and by the gaseous phase present in the porous structure (blue points) (Ebert, 2011), with kind permission from Springer Science and Business Media.

Heat transfer in aerogels is based on three inputs and is illustrated in Figure I. 42: heat conduction via the *solid backbone*, heat transfer within the *gaseous phase* present in the porous structure and *radiative* heat transfer. The total (or often called effective) thermal conductivity can be decomposed according to Equation (I. 4).

$$\lambda_{effective} = \lambda_{solid} + \lambda_{gas} + \lambda_{radiative} \quad \text{(I. 4)}$$

In aerogels, it is usually admitted that coupling between different heat transfer modes and the convection of gas within the porous structure are negligible.

3.2.1.1 Solid thermal conductivity

The heat transfer of the solid depends on the skeleton structure, its spatial arrangement and its chemical composition. Under a temperature gradient, heat is transferred by diffusing phonons (molecular vibrations of the material) via the chains of the aerogel backbone. The diffusion of phonons is given by Equation (I. 5).

$$\lambda_{solid} = \frac{1}{3}\,\rho_0 . c_V . \nu_0 . l_{ph} \quad \text{(I. 5)}$$

with λ_{solid} the solid thermal conductivity ($W.m^{-1}.K^{-1}$);
ρ_0 the density of the solid phase ($kg.m^{-3}$);
c_V the specific heat at constant volume ($J.kg^{-1}.K^{-1}$);
ν_0 the average velocity of the elastic waves within the solid phase ($m.s^{-1}$);
and l_{ph} the average mean free path of phonons (m).

λ_{solid} of aerogels is expected to be reduced compared to non-porous materials, because of the large amount of pores which restrict the propagation of phonons in the aerogel backbone.
It was shown empirically that for materials such as silica aerogels, solid phase contribution follows a scaling law as a function of the density (Equation (I. 6)). The factor C is expected to

depend on the connectivity of particles in aerogels and their tortuosity and the exponent is α ≈1.5 (Fricke, Lu, Wang, Büttner, & Heinemann, 1992; Lu, Nilsson, Fricke, & Pekala, 1993).

$$\lambda_{solid} = C\ \rho^{\alpha} \tag{I. 6}$$

3.2.1.2 Gaseous thermal conductivity

The heat transfer by conduction in a gaseous phase is due to elastic collisions of gas molecules. In porous materials, it is characterised by the Knudsen number K_n which is the ratio of the free mean path l_g of the gas molecules and the pore diameter d (Equation (I. 7)).

$$K_n = \frac{l_g}{d} \tag{I. 7}$$

The free mean path is calculated according to Equation (I. 8). At 300K and 1 bar, l_g for air molecules is ≈ 70 nm.

$$l_g = \frac{k_B\ T}{\sqrt{2}\ \pi\ \delta^2\ P} \approx 70\ nm \tag{I. 8}$$

with k_B the Boltzmann constant ($1.38.10^{-23}$ $J.K^{-1}$) ; T temperature (K) ; δ diameter of gas molecules ($\delta=3.7.10^{-10}$ m for air) and P the pressure of gas ($N.m^{-2}$).

The gas heat transfer is described by Equation (I. 9).

$$\lambda_{gas} = \frac{\lambda_{g0}.\varepsilon}{1 + \alpha\ K_n} = \frac{\lambda_{g0}.\varepsilon}{1 + \alpha\ \frac{l_g}{d}} \tag{I. 9}$$

with ε the porosity (usually ε=1),
λ_{g0} the thermal conductivity of free air (= 0.025 $W.m^{-1}.K^{-1}$),
α coefficient depending on the type of gas and interactions between the gas and the solid structure.

For Kn<<1, i.e when the average pore size is significantly larger than the mean free path of the gas molecules, gas molecules have collisions predominantly with themselves as if they are not confined (free gas); thus the gas conductivity equals 0.025 $W.m^{-1}.K^{-1}$.

When Kn>>1, i.e d<l_g, gas molecules have collisions mainly with the solid backbone and λ_{gas} decreases significantly. This phenomenon is called the *Knudsen effect* (Figure I. 43);

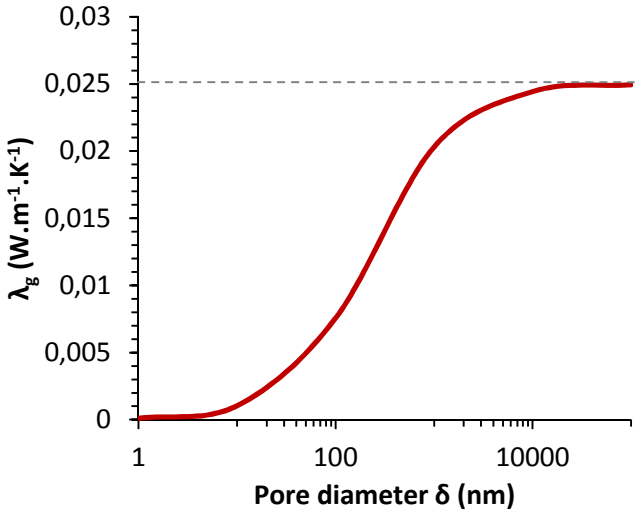

Figure I. 43 : Knudsen effect- significant decrease of the gas conductivity due to air confinement in the pores.

Pore size is thus a very important factor for reducing the gaseous thermal conductivity.

3.2.1.3 Radiative thermal conductivity

Electromagnetic radiations arriving on a material can be reflected, absorbed or transmitted depending on the optical thickness τ of the material. This latter can be transparent, semi-transparent or opaque to radiations. Most organic aerogels are optically thick for thermal radiations with τ>>1, which means than the mean free path of infrared photons $l_{ph\text{-}ir}$ is smaller than the geometrical thickness, $\tau = e/l_{ph\text{-}ir}$. In this case the radiative conductivity is described by Equation (I. 10).

$$\lambda_{radiative} = \frac{16}{3} n^2 . \sigma . \frac{T^3}{E_x} \qquad \text{(I. 10)}$$

with σ the Stefan-Boltzman constant ($\sigma=5.67.10^{-8}$ $W.m^{-2}.K^{-4}$),
n the mean index of refraction of the material,
T the mean radiative temperature (K),
E_x the specific extinction coefficient (m^{-1}).
It is known that the specific extinction coefficient is proportional to the bulk density of the aerogel, therefore $\lambda_{radiative} \propto \frac{1}{\rho}$.

To improve the thermal insulation properties of aerogels, so-called infrared opacifiers are embedded into aerogels matrix to enhance optical thickness and to reduce radiative heat transfer. Highly absorbing or scattering particles, such as carbon black or titanium dioxide, are integrated to the aerogel structure in a low concentration without significantly increasing the solid thermal conductivity of the backbone (Figure I. 44).

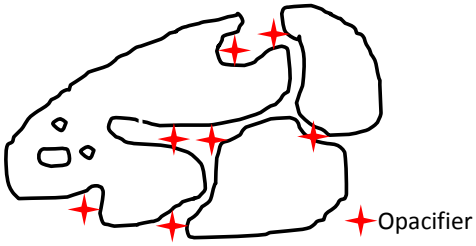

Figure I. 44 : Aerogel structure with infrared opacifiers.

3.2.2 Super-insulation

The thermal conductivity λ ($W.m^{-1}.K^{-1}$) is an intrinsic material property and gives information as defined by the heat flow through a piece of material with an area A and a thickness e and an effective difference temperature ΔT between two surfaces.
Metals are good thermal conductors with λ of few tens to hundreds $W.m^{-1}.K^{-1}$; glass, sand or minerals have λ around few units $W.m^{-1}.K^{-1}$ and typical thermal insulators exhibit λ below 0.1 $W.m^{-1}.K^{-1}$ (Figure I. 45).

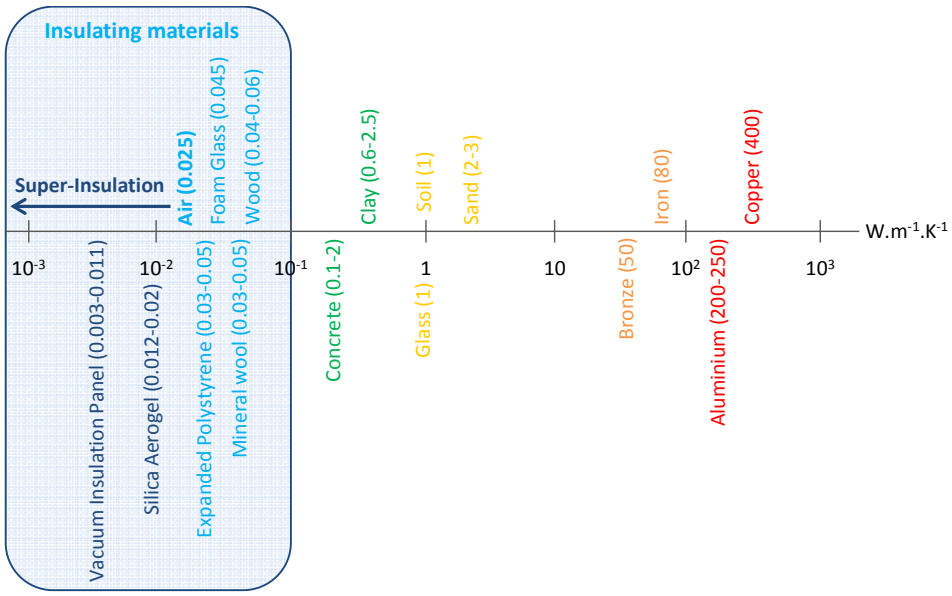

Figure I. 45 : Thermal conductivities of some materials.

Conventional insulating materials are mineral wool or glass wool which have λ ≈ 0.030-0.045 $W.m^{-1}.K^{-1}$, and expanded polystyrene (EPS) or extruded polystyrene (XPS) with λ ≈ 0.030-0.050 $W.m^{-1}.K^{-1}$.

Building insulation is a key factor for the decrease of CO_2 emissions and energy consumption, as required by the 2020 European program. In France, energy regulations called "Réglementation Energétique RT 2012" (http://www.developpement-durable.gouv.fr/-Batiment-et-construction-.html) requires for new constructed buildings a thermal resistance, defined by Equation (I. 11), above $R \geq 4$ for walls and floors and $R \geq 8$ for attics.

$$R = \frac{e}{\lambda} \quad \text{(I. 11)}$$

with λ the thermal conductivity of the material and e its thickness.

For conventional insulating materials, with λ ≈ 0.035 $W.m^{-1}.K^{-1}$, the thickness needs to be at least 14 cm to respect the regulation RT 2012 (R = 4) (Table I. 6).
For improving building insulation, we can either increase the thickness of the insulation but it will decrease the living space, or we can decrease the thermal conductivity. *"Superinsulation"* or "high-performance insulation" is defined by a thermal conductivity λ below *0.025* $W.m^{-1}.K^{-1}$ (thermal conductivity of free air) (Koebel et al., 2012) and it is thus a very promising solution for insulation.

Table I. 6 : Thickness of insulation for R = 4.

Type of insulation	Insulation	λ ($W.m^{-1}.K^{-1}$)	Thickness (cm)	
Conventional Insulation	Mineral Wool	0.040	16	
	Expanded Polystyrene	0.035	14	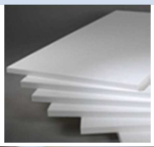
Superinsulation	Silica aerogels	0.015	6	
	VIP	0.008	3	

Three families of products are considered as superinsulating: aerogels, vacuum insulating panels (VIP) and vacuum glazing. Aerogels such as silica aerogels have a thermal conductivity between 0.01 and 0.02 $W.m^{-1}.K^{-1}$ and VIP of 0.003 to 0.01 $W.m^{-1}.K^{-1}$. The decrease of thermal conductivity allows to have much thinner insulation, $e_{aerogels}$ = 6 cm and e_{vip} = 3 cm for getting R = 4.

3.2.2.1 Vacuum Insulating panels (VIP) and vacuum glazing (VG)

Vacuum Insulating panels (VIP) and vacuum glazing (VG) offer an excellent thermal conductivity because of the massive reduction of heat transport by gas molecules. This reduction is done by the evacuation of the gas inside the porous core of VIP or the glazing cavity of VG.
VIP is made of a core of pressed mesoporous powder (e.g. fumed silica) wrapped in a multi-layered aluminium barrier foil and evacuated below 1 hPa pressure and sealed. VG is made of two glass panels separated by a thin gap and held together by a hermetic edge seal. The pressure inside the cavity is required to be below 10^{-1}-10^{-2} Pa for an optimal performance.

The main drawbacks of evacuated systems as VIP is that they are quite sensitive to ageing and have to be correctly implemented and mounted (no screws for example). Damage such as ageing, loss of integrity and delamination, increases dramatically the pressure of gas inside the structure and so does the thermal conductivity. For VG, the lack of suitable and resistant edge sealing greatly limit their commercialisation.

3.2.2.2 Superinsulation at atmospheric pressure (SIAP)

Aerogels are non-evacuated (at atmospheric pressure) superinsulation materials.
Silica aerogels (c.f. 2.2) are widely studied. As shown in Figure I. 22, pores are mainly below 40 nm. This nanostructuration dramatically decreases the gas conduction λ_{gas} (Knudsen effect) and gives a lower than air effective thermal conductivity.

Silica aerogels can be divided into three classes:
- *Monolithic aerogels*: large, thick (above 1 cm) and homogeneous blocks of aerogel (see Figure I. 24).
- *Divided materials*: finely divided aerogels with diameters below 1cm for granules or 1mm for powders.
- *Composite materials*: an additive, such as fibers or blankets, is introduced either during the sol-gel or in the gel as a second distinctive phase.

Monoliths are interesting for their optical and thermal properties for highly insulating windows. However, they are still expensive to produce and it is very hard to obtain large crack-free plates of silica aerogels. The problem is that silica aerogels are extremely fragile materials and break upon very low stress. Several national and European research programs are currently running for improving the method of production and its cost and mechanical properties of silica aerogels.

Chemical surface modification of silica (Figure I. 23) allows drying aerogels by evaporative route but gives granular pieces of material. Packed beds of granular beads present efficient thermal conductivities (slightly higher than monoliths).
The North American company Cabot Corporation has developed a family of silica aerogels called Nanogel™ and now sold them under the name Lumira™. Nanogel granules can be directly used as superinsulating filling materials (such as daylighting panels, Figure I. 46a) but also for more specific applications such as pipe-in-pipe and cryogenic insulation systems.
Granular transparent aerogels are easier to handle and are poured as powder. Nanogel products are used for daylighting applications. A cavity, for example between to glass plates, can be filled with granular aerogels and a highly insulating window is produced (Figure I. 46a). Contrary to monoliths, granules are not optically transparent and the optical effect is more like “milky glass”.

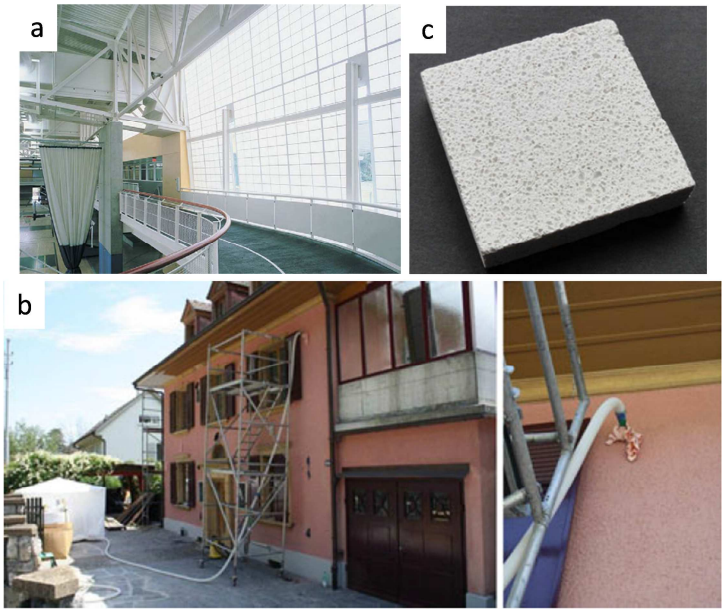

Figure I. 46 : Different application examples of granular silica aerogels: daylighting panels (a); retrofitting of insulation of old buildings (b); and rendering system (c). Pictures a) is taken from (Baetens, Jelle, & Gustavsen, 2011). Reprinted from (Baetens et al., 2011), Copyright (2011), with permission from Elsevier. Pictures b) and c) are taken from (Koebel et al., 2012) with kind permission from Springer Science and Business Media.

Granular aerogels are also used for the retrofitting of cavity walls. A packed bed of granules is directly injected into the cavity wall construction (Figure I. 46b). After retrofitting the thermal resistance is dramatically improved from 1 to 5 $W^{-1}.m^2.K$ (Koebel et al., 2012).

The recent promising application is in the field of making insulating plaster and rendering systems (Figure I. 46c).

Monoliths and granular silica aerogels have, however, severe mechanical limitations such as their poor flexibility. New composites, such as aerogel infused blankets have been recently developed (Figure I. 47a). The silica sol is cast onto a very porous material made of unwoven mineral fibers, silica is gelled and the composite is dried by supercritical CO_2, or more recently by evaporative drying when silica is hydrophobised. The fibers allow to keep a cohesion and give material a real flexibility (Figure I. 47b). Their major drawback is that silica is released from blankets in the form of dust.

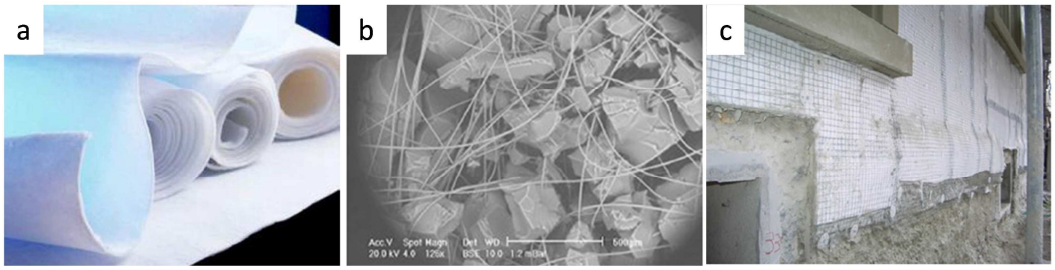

Figure I. 47 : Silica aerogel-based blankets from Aspen Aerogel (a) (Baetens et al., 2011), reprinted from (Baetens et al., 2011), Copyright (2011), with permission from Elsevier; SEM image of a blanket with ρ = 0.1g.cm^3 and λ_{eff} = 0.014 W.m^{-1}.K^{-1} (b) (Koebel et al., 2012) ; retrofit wall insulation with Spaceloft blankets (c) (Koebel et al., 2012) with kind permission from Springer Science and Business Media.

The main manufacturer of silica aerogel-blankets is Aspen Aerogels company with their product Spaceloft for building insulation. Spaceloft is used for the retrofitting of old buildings where the exterior façade must be maintained and the insulation layer must be put inside and thus be as thin as possible (Figure I. 47c). In a demonstration project in Zurich, the original wall was stripped of its rendering and two Spaceloft blankets with a thickness of 10 mm thick each, were glued on. The structure was covered with 30 mm of standard insulating rendering. The thermal resistance of the system was evaluated at R=2.5 (1/3 higher than the original value). However, due to dusting, workers have to wear protective safety gear (Koebel et al., 2012).

Silica aerogels and VIP are still expensive compared to conventional insulating materials. As an example, silica aerogels costs 4000$/m^3 (in 2008) compared to less than 100$ for typical insulation. But aerogels have major advantages that may counterbalance their high price, such as space saving in habitations, reducing operating costs, longevity and chemical resistance (Koebel et al., 2012). The aerogel insulation market is believed to grow fast in the next decades which will drop aerogel price towards 1500$/m^3 (prediction in 2020) and will become much more competitive.

Polysaccharide aerogels may also have a high potential as thermal insulation as they present pores from few nanometers to few hundred nanometers and better mechanical resistance than silica aerogels (no dusting). However, so far very few studies are found in literature on the thermal conductivity of aeropolysaccharides (Cai et al., 2012).

Conclusions

This chapter reviewed the state of the art on the structure and processing of two polysaccharides, cellulose and pectin as starting components for making aerogels-like materials, called “Aero-polysaccharides”.

Cellulose is made of repeated units of anhydroglucose (AGU) and is widely found in nature in wood, cotton, flax… It has numerous hydroxyl groups that create an important hydrogen bonds network conferring to cellulose a great stability. However, only few solvents are able to dissolve efficiently cellulose. They are often rather complex and toxic with low cellulose dissolution power.

Two main cellulose industrial processes were presented.
Viscose process is the most widely used for making fibers, films, sponges. It is based on cellulose derivatisation and regeneration in a non-solvent. It is a complex and polluting process with emissions of toxic gases.
Cellulose fibers produced by the *Lyocell process* are directly obtained from dissolution of cellulose in NMMO without derivatisation. It tolerates a large range of cellulose raw materials and is less toxic than the Viscose process.

In the laboratory scale another solvent is promising 7-10% aqueous NaOH solutions. Additives as urea or ZnO are under research to limit solution ageing (gelation).
Ionic liquids (IL) are of particular interest for cellulose dissolution. They have low vapor pressure, chemical stability and higher dissolution power of cellulose than conventional solvents. Many rheological studies of solutions IL-cellulose allow a better understanding of dissolution mechanism. IL are particularly interesting for cellulose chemistry (derivatisation). Their main drawbacks so far are their price, their purity, their energetic recycling and the lack of data on their toxicity.

Pectin is made of D-galacturonic acid repeated units that can be esterified. Two types of pectin are found depending on the degree of esterification: high methoxy (HM) and low methoxy-pectin (LM). Pectin is found in dried citrus peel or apple pomace and extracted by hot dilute acidic solution. HM pectins are mostly obtained. LM pectins are obtained by hydrolysis either in acidic or basic media of HM pectins.
When HM pectin is dissolved in an acidic aqueous solution, its carboxyl groups are protonated. They decrease electrostatic repulsions and increase hydrogen bonds creating a physical gel.
LM pectin gelation occurs when divalent cations are added. The mechanism of gelation is known as the “egg box” model.
Pectin is mainly used in food industry as gelling agents.

Aerogels
Aerogels as highly porous and light materials, usually dried by supercritical CO_2, were introduced. The most famous aerogel based on silica was reported. It presents interesting

structural properties such as high specific surface areas and mesoporous morphology. Its main disadvantages are their relative fragility and its dusting.

We investigated therefore the preparation of porous materials from polysaccharides as a new generation of aerogels. We reviewed cellulose-based aerogels and the influence of the dissolution solvent in the final morphology. Cellulose porous materials prepared from ionic liquids-cellulose solutions were partially studied but seem particularly interesting.
Only one paper reported pectin aerogel-like materials.
Other polysaccharides were studied as starch and alginate but this literature review showed that very few articles relate their preparation and their morphological characterisations.

The preparation and the complete structural, mechanical and thermal characterisations of cellulose and pectin-based porous materials were a challenge.

Applications
Because of aerogels interesting structural properties, many applications were foreseen. We reviewed only two of them: drug release and thermal insulation.

Polysaccharides have low toxicity and are usually biocompatible which made them excellent candidates for drug release. Starch and alginate aerogels-like were studied and presented very interesting release kinetics for various drugs.

We reviewed general theories on heat transfer into an insulating material. The three main contributions were described as the conduction of the solid and gaseous phases and the radiative transfer. We gave thermal conductivities of a range of conventional insulating materials. They usually are around 0.035-0.050 $W.m^{-1}.K^{-1}$.
Recent regulations require improvements on building insulation. New materials with “super-insulating” properties, defined with a thermal conductivity below 0.025 $W.m^{-1}.K^{-1}$, present a high potential on the insulation market. Silica aerogels have excellent thermal insulating properties with thermal conductivity of 0.015 $W.m^{-1}.K^{-1}$. Their nanostructuration allows decreasing the conductivity of the gaseous phase (Knudsen effect). They start to be used as daylighting panels, retrofitting insulation of buildings or rendering systems. However, the price of silica aerogels remain important compared to conventional insulating materials and their poor mechanical resistance (dusting) requires wearing protective safety gear.

Very few studies are found in literature on thermal properties of polysaccharides porous materials. Polysaccharides-based aerogels may have a high potential for insulation applications. They are usually biobased with low toxicity, widely available and present interesting structural properties.

Bibliography

Agoudjil, N., Sicard, C., Jaouen, V., Garnier, C., Bonnin, E., Steunou, N., & Coradin, T. (2012). Design and properties of biopolymer–silica hybrid materials: The example of pectin-based biodegradable hydrogels. *Pure and Applied Chemistry*, *84*(12), 2521–2529.

Akimov, Y. (2003). Fields of application of aerogels (review). *Instruments and Experimental Techniques*, *46*(3), 287–299.

Alaoui, A. H., Woignier, T., Scherer, G. W., & Phalippou, J. (2008). Comparison between flexural and uniaxial compression tests to measure the elastic modulus of silica aerogel. *Journal of Non-Crystalline Solids*, *354*(40-41), 4556–4561.

Anderson, A., & Carroll, M. (2011). Hydrophobic Silica Aerogels: Review of Synthesis, Properties and Applications. In M. A. Aegerter, N. Leventis, & M. M. Koebel (Eds.), *Aerogels Handbook SE - 3* (pp. 47–77). Springer New York..

Atalla, R. H., & Vanderhart, D. L. (1984). Native Cellulose: A Composite of Two Distinct Crystalline Forms. *Science*, *223*(4633), 283–285.

Baetens, R., Jelle, B. P., & Gustavsen, A. (2011). Aerogel insulation for building applications: A state-of-the-art review. *Energy and Buildings*, *43*(4), 761–769.

Biganska, O., & Navard, P. (2009). Morphology of cellulose objects regenerated from cellulose–N-methylmorpholine N-oxide–water solutions. *Cellulose*, *16*(2), 179–188.

Burchard, W. (2003). Solubility and solution structure of cellulose derivatives. *Cellulose*, *10*(3), 213–225.

Cai, J., Kimura, S., Wada, M., Kuga, S., & Zhang, L. (2008). Cellulose aerogels from aqueous alkali hydroxide-urea solution. *ChemSusChem*, *1*(1-2), 149–54.

Cai, J., Liu, S., Feng, J., Kimura, S., Wada, M., Kuga, S., & Zhang, L. (2012). Cellulose-silica nanocomposite aerogels by in situ formation of silica in cellulose gel. *Angewandte Chemie*, *51*(9), 2076–9.

Cai, J., & Zhang, L. (2005). Rapid dissolution of cellulose in LiOH/urea and NaOH/urea aqueous solutions. *Macromolecular bioscience*, *5*(6), 539–48.

Cai, J., Zhang, L., Liu, S., Liu, Y., Xu, X., Chen, X., Chu, B., et al. (2008). Dynamic Self-Assembly Induced Rapid Dissolution of Cellulose at Low Temperatures. *Macromolecules*, *41*(23), 9345–9351.

Cao, Y., Li, H., Zhang, Y., Zhang, J., & He, J. (2010). Structure and properties of novel regenerated cellulose films prepared from cornhusk cellulose in room temperature ionic liquids. *Journal of Applied Polymer Science*, *116*(1), 547–554.

Capel, F., Nicolai, T., Durand, D., Boulenguer, P., & Langendorff, V. (2006). Calcium and acid induced gelation of (amidated) low methoxyl pectin. *Food Hydrocolloids*, *20*(6), 901–907.

Chang, X., Chen, D., & Jiao, X. (2008). Chitosan-based aerogels with high adsorption performance. *The Journal of Physical Chemistry. B*, *112*(26), 7721–5.

Chanzy, H., Nawrot, S., Peguy, A., Smith, P., & Chevalier, J. (1982). Phase behavior of the quasiternary system N-methylmorpholine-N-oxide, water, and cellulose. *Journal of Polymer Science: Polymer Physics*, *20*(10), 1909–1924.

Chanzy, H., Peguy, A., Chaunis, S., & Monzie, P. (1980). Oriented cellulose films and fibers from a mesophase system. *Journal of Polymer Science: Polymer Physics*, *18*(5), 1137–1144.

Chen, H.-B., Chiou, B.-S., Wang, Y.-Z., & Schiraldi, D. a. (2013). Biodegradable pectin/clay aerogels. *ACS applied materials & interfaces*, *5*(5), 1715–21.

Chowdhury, S., Mohan, R. S., & Scott, J. L. (2007). Reactivity of ionic liquids. *Tetrahedron*, *63*(11), 2363–2389.

Ciacco, G., Liebert, T., Frollini, E., & Heinze, T. (2003). Application of the solvent dimethyl sulfoxide/tetrabutyl-ammonium fluoride trihydrate as reaction medium for the homogeneous acylation of Sisal cellulose. *Cellulose*, *10*(2), 125–132.

Collier, J. R., Watson, J. L., Collier, B. J., & Petrovan, S. (2008). Rheology of 1-butyl-3-methylimidazolium chloride cellulose solutions. II. Solution character and preparation. *Journal of Applied Polymer Science*, *111(2)*, 1019–1027.

Cuissinat, C., & Navard, P. (2006). Swelling and Dissolution of Cellulose Part 1: Free Floating Cotton and Wood Fibres in N-Methylmorpholine-N-oxide–Water Mixtures. *Macromolecular Symposia*, *244*(1), 19–30.

Davidson, G. F. (1934). 12- The dissolution of chemically modified cotton cellulose in alkaline solutions. Part I- In solutions of sodiul hydroxide, particularly at temperatures below the normal. *Journal of the Textile Institute Transactions*, *25*(5), T174–T196.

Davidson, G. F. (1936). 10- The dissolution of chemically modified cotton cellulose in alkaline solutions. Part II- A comparison of the solvent action of solutions of lithium, sodium, potassium, and tetramethylammonium hydroxides. *Journal of the Textile Institute Transactions*, *27*(4), T112–T130.

Dawsey, T. R., & McCormick, C. L. (1990). The Lithium Chloride/Dimethylacetamide solvent for cellulose: A Literature Review. *Journal of Macromolecular Science, Part C: Polymer Reviews*, *30*(3-4), 405–440.

Deng, M., Zhou, Q., Du, A., Van Kasteren, J., & Wang, Y. (2009). Preparation of nanoporous cellulose foams from cellulose-ionic liquid solutions. *Materials Letters*, *63*(21), 1851–1854.

Deze, E. G., Papageorgiou, S. K., Favvas, E. P., & Katsaros, F. K. (2012). Porous alginate aerogel beads for effective and rapid heavy metal sorption from aqueous solutions: Effect of porosity in Cu^{2+} and Cd^{2+} ion sorption. *Chemical Engineering Journal*, *209*, 537–546.

Docherty, K. M., & Kulpa, Jr., C. F. (2005). Toxicity and antimicrobial activity of imidazolium and pyridinium ionic liquids. *Green Chemistry*, *7*(4), 185-189.

Duchemin, B. J. C., Staiger, M. P., Tucker, N., & Newman, R. H. (2010). Aerocellulose based on all-cellulose composites. *Journal of Applied Polymer Science*, *115*(1), 216–221.

Ebert, H.-P. (2011). Thermal Properties of Aerogels. In M. A. Aegerter, N. Leventis, & M. M. Koebel (Eds.), *Aerogels Handbook SE - 23* (pp. 537–564). Springer New York.

Ebner, G., Schiehser, S., Potthast, A., & Rosenau, T. (2008). Side reaction of cellulose with common 1-alkyl-3-methylimidazolium-based ionic liquids. *Tetrahedron Letters*, *49*(51), 7322–7324.

Egal, M., Budtova, T., & Navard, P. (2007). Structure of aqueous solutions of microcrystalline cellulose/sodium hydroxide below 0°C and the limit of cellulose dissolution. *Biomacromolecules*, *8*(7), 2282–7.

Egal, M., Budtova, T., & Navard, P. (2008). The dissolution of microcrystalline cellulose in sodium hydroxide-urea aqueous solutions. *Cellulose*, *15*(3), 361–370.

El Kadib, A., & Bousmina, M. (2012). Chitosan bio-based organic-inorganic hybrid aerogel microspheres. *Chemistry (Weinheim an der Bergstrasse, Germany)*, *18*(27), 8264–77.

El Seoud, O. A., Koschella, A., Fidale, L. C., Dorn, S., & Heinze, T. (2007). Applications of ionic liquids in carbohydrate chemistry: a window of opportunities. *Biomacromolecules*, *8*(9), 2629–47.

Evageliou, V., Richardson, R. K., & Morris, E. R. (2000). Effect of pH, sugar type and thermal annealing on high-methoxy pectin gels. *Carbohydrate Polymers*, *42*(3), 245–259.

Feng, L., & Chen, Z. (2008). Research progress on dissolution and functional modification of cellulose in ionic liquids. *Journal of Molecular Liquids*, *142*(1-3), 1–5.

Fischer, F., Rigacci, A., Pirard, R., Berthon-Fabry, S., & Achard, P. (2006). Cellulose-based aerogels. *Polymer*, *47*(22), 7636–7645.

Fraeye, I., Colle, I., Vandevenne, E., Duvetter, T., Van Buggenhout, S., Moldenaers, P., Van Loey, A., et al. (2010). Influence of pectin structure on texture of pectin–calcium gels. *Innovative Food Science & Emerging Technologies*, *11*(2), 401–409.

Fricke, J., Lu, X., Wang, P., Büttner, D., & Heinemann, U. (1992). Optimization of monolithic silica aerogel insulants. *International Journal of Heat and Mass Transfer*, *35*(9), 2305–2309.

García-González, C. A., Alnaief, M., & Smirnova, I. (2011). Polysaccharide-based aerogels—Promising biodegradable carriers for drug delivery systems. *Carbohydrate Polymers*, *86*(4), 1425–1438.

García-González, C. A., Carenza, E., Zeng, M., Smirnova, I., & Roig, A. (2012). Design of biocompatible magnetic pectin aerogel monoliths and microspheres. *RSC Advances*, *2*(26), 9816.

García-González, C. A., Uy, J. J., Alnaief, M., & Smirnova, I. (2012). Preparation of tailor-made starch-based aerogel microspheres by the emulsion-gelation method. *Carbohydrate Polymers*, *88*(4), 1378–1386.

Gardiner, E., & Sarko, A. (1985). Packing analysis of carbohydrates and polysaccharides. 16. The crystal structures of celluloses IVI and IVII. *Canadian journal of chemistry*, *63*(9), 173–180.

Gavillon, R. (2007). Préparation et caractérisation de matériaux cellulosiques ultra poreux. *PhD thesis*, Ecole des Mines de Paris.

Gavillon, R., & Budtova, T. (2008). Aerocellulose: new highly porous cellulose prepared from cellulose-NaOH aqueous solutions. *Biomacromolecules*, *9*(1), 269–77.

Gericke, M., Fardim, P., & Heinze, T. (2012). Ionic liquids--promising but challenging solvents for homogeneous derivatization of cellulose. *Molecules*, *17*(6), 7458–502.

Gericke, M., Schlufter, K., Liebert, T., Heinze, T., & Budtova, T. (2009). Rheological properties of cellulose/ionic liquid solutions: from dilute to concentrated states. *Biomacromolecules*, *10*(5), 1188–94.

Gibson, L. J., & Ashby, M. F. (1999). *Cellular Solids: Structure and Properties*. Cambridge University Press.

Glenn, G. M., & Stern, D. J. (1999). Starch-based Microcellular Foams., US patent 5,958,589.

Graenacher, C. (1934). Cellulose Solution. US patent 1,943,176.

Graenacher, C., & Sallmann, R. (1939). Cellulose solutions and process of making same. US patent 2,179,181.

Grant, G. T., Morris, E. R., Rees, D. A., Smith, P. J. C., & Thom, D. (1973). Biological interactions between polysaccharides and divalent cations: The egg-box model. *FEBS Letters*, *32*(1), 195–198.

Gupta, K. M., Hu, Z., & Jiang, J. (2011). Mechanistic understanding of interactions between cellulose and ionic liquids: A molecular simulation study. *Polymer*, *52*(25), 5904–5911.

Hall, C. A., Le, K. A., Rudaz, C., Radhi, A., Lovell, C. S., Damion, R. A., Budtova, T., et al. (2012). Macroscopic and microscopic study of 1-ethyl-3-methyl-imidazolium acetate-water mixtures. *The journal of physical chemistry. B*, *116*(42), 12810–8.

Harmon, K. M., Akin, A. C., Keefer, P. K., & Snider, B. L. (1992). Hydrogen bonding Part 45. Thermodynamic and IR study of the hydrates of N-methylmorpholine oxide and quinuclidine oxide. Effect of hydrate stoichiometry on strength of H-O-H…O-N hydrogen bonds; implications for the dissolution of cellulose in amine oxide . *Journal of Molecular Structure*, *269*(1–2), 109–121.

Haward, S. J., Sharma, V., Butts, C. P., McKinley, G. H., & Rahatekar, S. S. (2012). Shear and extensional rheology of cellulose/ionic liquid solutions. *Biomacromolecules*, *13*(5), 1688–99.

Hoepfner, S., Ratke, L., & Milow, B. (2008). Synthesis and characterisation of nanofibrillar cellulose aerogels. *Cellulose*, *15*(1), 121–129.

Innerlohinger, J., Weber, H. K., & Kraft, G. (2006). Aerocellulose: Aerogels and Aerogel-like Materials made from Cellulose. *Macromolecular Symposia*, *244*(1), 126–135.

Isogai, A., & Atalla, R. (1998). Dissolution of cellulose in aqueous NaOH solutions. *Cellulose*, *5*, 309–319.

Jastorff, B., Mölter, K., Behrend, P., Bottin-Weber, U., Filser, J., Heimers, A., Ondruschka, B., et al. (2005). Progress in evaluation of risk potential of ionic liquids—basis for an eco-design of sustainable products. *Green Chemistry*, *7*(5), 362.

Jin, H., Nishiyama, Y., Wada, M., & Kuga, S. (2004). Nanofibrillar cellulose aerogels. *Colloids and Surfaces A: Physicochemical and Engineering Aspects*, *240*(1-3), 63–67.

Kahlen, J., Masuch, K., & Leonhard, K. (2010). Modelling cellulose solubilities in ionic liquids using COSMO-RS. *Green Chemistry*, *12*(12), 2172.

Kamide, K., Okajima, K., & Kowsaka, K. (1992). Dissolution of natural cellulose into aqueous alkali solution: role of super-molecular structure of cellulose. *Polymer Journal*, *24*(1), 71–86.

Kamide, K., Okajima, K., Matsui, T., & Kowsaka, K. (1984). Study on the solubility of cellulose in aqueous alkali solution by deuteration IR and ^{13}C-NMR. *Polymer Journal*, *16*(12), 857–866.

Kamide, K., Saito, M., & Kowsaka, K. (1987). Temperature dependence of limiting viscosity number and radius of gyration for cellulose dissolved in aqueous 8% sodium hydroxide solution. *Polymer Journal*, *19*(10), 1173–1181.

Karatzos, S. K., Edye, L. A., & Wellard, R. M. (2011). The undesirable acetylation of cellulose by the acetate ion of 1-ethyl-3-methylimidazolium acetate. *Cellulose*, *19*(1), 307–312. doi:10.1007/s10570-011-9621-0

Keil, P., Kick, M., & König, A. (2012). Long-Term Stability, Regeneration and Recycling of Imidazolium-based Ionic Liquids. *Chemie Ingenieur Technik*, *84*(6), 859–866.

Kettunen, M., Silvennoinen, R. J., Houbenov, N., Nykänen, A., Ruokolainen, J., Sainio, J., Pore, V., et al. (2011). Photoswitchable Superabsorbency Based on Nanocellulose Aerogels. *Advanced Functional Materials*, *21*(3), 510–517.

Kistler, S. (1931). Coherent Expanded Aerogels and Jellies. *Nature*, *127*(3211), 741–741.

Kistler, S. (1932). Coherent Expanded-Aerogels. *Journal of physical chemistry*, *36*(1), 52–64.

Klemm, D., Heublein, B., Fink, H., & Bohn, A. (2005). Cellulose: fascinating biopolymer and sustainable raw material. *Angewandte Chemie*, *44*(22), 3358–93.

Klemm, D., Philipp, B., Heinze, T., Heinze, U., & Wagenknecht, W. (1998). *Comprehensive Cellulose Chemistry* (Vol. 1). Weinheim, FRG: Wiley-VCH Verlag GmbH & Co. KGaA.

Koebel, M., Rigacci, A., & Achard, P. (2012). Aerogel-based thermal superinsulation: an overview. *Journal of Sol-Gel Science and Technology*, *63*(3), 315–339.

Kohn, R. (1987). Binding of divalent cations to oligomeric fragments of pectin. *Carbohydrate Research*, *160*(0), 343–353.

Kondo, T. (1997). The relationship between intramolecular hydrogen bonds and certain physical properties of regioselectively substituted cellulose derivatives. *Journal of Polymer Science Part B: Polymer Physics*, *35*(4), 717–723.

Kosan, B., Michels, C., & Meister, F. (2008). Dissolution and forming of cellulose with ionic liquids. *Cellulose*, *15*(1), 59–66.

Kosmulski, M., Gustafsson, J., & Rosenholm, J. B. (2004). Thermal stability of low temperature ionic liquids revisited. *Thermochimica Acta*, *412*(1-2), 47–53.

Krassig, H. A. (1993). *Cellulose- structure, accessibility and reactivity*. Gordon and Breach, Amsterdam.

Kuang, Q.-L., Zhao, J.-C., Niu, Y.-H., Zhang, J., & Wang, Z.-G. (2008). Celluloses in an ionic liquid: the rheological properties of the solutions spanning the dilute and semidilute regimes. *The Journal of Physical Chemistry. B*, *112*(33), 10234–40.

Köhler, S., Liebert, T., & Heinze, T. (2008). Interactions of ionic liquids with polysaccharides. VI. Pure cellulose nanoparticles from trimethylsilyl cellulose synthesized in ionic liquids. *Journal of Polymer Science Part A: Polymer Chemistry*, *46*(12), 4070–4080.

Langan, P., Nishiyama, Y., & Chanzy, H. (1999). A Revised Structure and Hydrogen-Bonding System in Cellulose II from a Neutron Fiber Diffraction Analysis. *Journal of the American Chemical Society*, *121*(43), 9940–9946.

Langan, P., Nishiyama, Y., & Chanzy, H. (2001). X-ray structure of mercerized cellulose II at 1 a resolution. *Biomacromolecules*, *2*(2), 410–6.

Le, K. A., Sescousse, R., & Budtova, T. (2011). Influence of water on cellulose-EMIMAc solution properties: a viscometric study. *Cellulose*, *19*(1), 45–54.

Lerouxel, O., Cavalier, D. M., Liepman, A. H., & Keegstra, K. (2006). Biosynthesis of plant cell wall polysaccharides - a complex process. *Current opinion in plant biology*, *9*(6), 621–30.

Liebner, F., Haimer, E., Potthast, A., Loidl, D., Tschegg, S., Neouze, M.-A., Wendland, M., et al. (2009). Cellulosic aerogels as ultra-lightweight materials. Part 2: Synthesis and properties. *Holzforschung*, *63*(1), 3–11.

Liebner, F., Haimer, E., Wendland, M., Neouze, M.-A., Schlufter, K., Miethe, P., Heinze, T., et al. (2010). Aerogels from unaltered bacterial cellulose: application of scCO2 drying for the preparation of shaped, ultra-lightweight cellulosic aerogels. *Macromolecular bioscience*, *10*(4), 349–52.

Liu, W., Budtova, T., & Navard, P. (2011). Influence of ZnO on the properties of dilute and semi-dilute cellulose-NaOH-water solutions. *Cellulose*, *18*(4), 911–920.

Lovell, C. S., Walker, A., Damion, R. a, Radhi, A., Tanner, S. F., Budtova, T., & Ries, M. E. (2010). Influence of Cellulose on Ion Diffusivity in 1-Ethyl-3-Methyl-Imidazolium Acetate Cellulose Solutions. *Biomacromolecules*, 2927–2935.

Lu, X., Nilsson, O., Fricke, J., & Pekala, R. W. (1993). Thermal and electrical conductivity of monolithic carbon aerogels. *Journal of Applied Physics*, *73*(2), 581.

Löfgren, C., Guillotin, S., Evenbratt, H., Schols, H., & Hermansson, A.-M. (2005). Effects of calcium, pH, and blockiness on kinetic rheological behavior and microstructure of HM pectin gels. *Biomacromolecules*, *6*(2), 646–52.

May, C. D. (1990). Industrial pectins: Sources, production and applications. *Carbohydrate Polymers*, *12*(1), 79–99.

Mehling, T., Smirnova, I., Guenther, U., & Neubert, R. H. H. (2009). Polysaccharide-based aerogels as drug carriers. *Journal of Non-Crystalline Solids*, *355*(50-51), 2472–2479.

Miao, Z., Ding, K., Wu, T., Liu, Z., Han, B., An, G., Miao, S., et al. (2008). Fabrication of 3D-networks of native starch and their application to produce porous inorganic oxide networks through a supercritical route. *Microporous and Mesoporous Materials*, *111*(1-3), 104–109.

Mohnen, D. (2008). Pectin structure and biosynthesis. *Current opinion in plant biology*, *11*(3), 266–77.

Oakenfull, D. (1992). The Chemistry of HighMethoxyl Pectins. *The Chemistry and Technology of Pectin* (Academic P., pp. 87–106). Elsevier Science.

Oakenfull, D., & Scott, A. (1984). Hydrophobic Interaction in the Gelation of High Methoxyl Pectins. *Journal of Food Science*, *49*(4), 1093–1098.

O'Sullivan, A. (1997). Cellulose: the structure slowly unravels. *Cellulose*, 173–207.

Pekala, R. W., Alviso, C. T., & LeMay, J. D. (1990). Organic aerogels: microstructural dependence of mechanical properties in compression. *Journal of Non-Crystalline Solids*, *125*(1–2), 67–75.

Pekala, R. W. (1989). Organic aerogels from the polycondensation of resorcinol with formaldehyde. *Journal of Materials Science*, *24*, 3221–3227.

Pekala, R. W., Farmer, J. C., Alviso, C. T., Tran, T. D., Mayer, S. T., Miller, J. M., & Dunn, B. (1998). Carbon aerogels for electrochemical applications. *Journal of Non-Crystalline Solids*, *225*, 74–80.

Pierre, A. C., & Pajonk, G. M. (2002). Chemistry of aerogels and their applications. *Chemical reviews*, *102*(11), 4243–65.

Pierre, A. C., & Rigacci, A. (2011). SiO_2 Aerogels. In M. A. Aegerter, N. Leventis, & M. M. Koebel (Eds.), *Aerogels Handbook SE - 2* (pp. 21–45). Springer New York.

Pinkert, A., Marsh, K. N., Pang, S., & Staiger, M. P. (2009). Ionic liquids and their interaction with cellulose. *Chemical reviews*, *109*(12), 6712–28. doi:10.1021/cr9001947

Potthast, A., Rosenau, T., Buchner, R., & Röder, T. (2002). The cellulose solvent system N, N-dimethylacetamide/lithium chloride revisited: the effect of water on physicochemical properties and chemical stability. *Cellulose*, 41–53.

Powell, D., Morris, E., Gidley, M., & Rees, D. (1982). Conformations and interactions of pectins- II. Influence of Residue Sequence on Chain Association in Calcium Pectate Gels. *Journal of Molecular Biology*, *155*(4), 517–531.

Quignard, F., Valentin, R., & Di Renzo, F. (2008). Aerogel materials from marine polysaccharides. *New Journal of Chemistry*, *32*(8), 1300.

Ramos, L. A., Assaf, J. M., El Seoud, O. A., & Frollini, E. (2005). Influence of the supramolecular structure and physicochemical properties of cellulose on its dissolution in a lithium chloride/N,N-dimethylacetamide solvent system. *Biomacromolecules*, *6*(5), 2638–47.

Ramos, L. A., Frollini, E., & Heinze, T. (2005). Carboxymethylation of cellulose in the new solvent dimethyl sulfoxide/tetrabutylammonium fluoride. *Carbohydrate Polymers*, *60*(2), 259–267.

Raymond, S., Heyraud, A., Qui, D. T., Kvick, A., & Chanzy, H. (1995). Crystal and molecular structure of beta-D-cellotetraose hemihydrate as a model of cellulose II. *Macromolecules*, *28*(6), 2096–2100.

Remsing, R. C., Swatloski, R. P., Rogers, R. D., & Moyna, G. (2006). Mechanism of cellulose dissolution in the ionic liquid 1-n-butyl-3-methylimidazolium chloride: a ^{13}C and $^{35/37}Cl$ NMR relaxation study on model systems. *Chemical communications*, (12), 1271–3.

Righi, S., Morfino, A., Galletti, P., Samorì, C., Tugnoli, A., & Stramigioli, C. (2011). Comparative cradle-to-gate life cycle assessments of cellulose dissolution with 1-butyl-3-methylimidazolium chloride and N-methyl-morpholine-N-oxide. *Green Chemistry*, *13*(2), 367.

Robitzer, M., David, L., Rochas, C., Di Renzo, F., & Quignard, F. (2008). Supercritically-Dried Alginate Aerogels Retain the Fibrillar Structure of the Hydrogels. *Macromolecular Symposia*, *273*(1), 80–84.

Robitzer, M., David, L., Rochas, C., Di Renzo, F., & Quignard, F. (2008). Nanostructure of calcium alginate aerogels obtained from multistep solvent exchange route. *Langmuir : the ACS journal of surfaces and colloids*, *24*(21), 12547–52.

Robitzer, M., Renzo, F. Di, & Quignard, F. (2011). Natural materials with high surface area. Physisorption methods for the characterization of the texture and surface of polysaccharide aerogels. *Microporous and Mesoporous Materials*, *140*(1-3), 9–16.

Rosenau, T., Potthast, A., Sixta, H., & Kosma, P. (2001). *The chemistry of side reactions and byproduct formation in the system NMMO/cellulose (Lyocell process)*. *Progress in Polymer Science* (Vol. 26, pp. 1763–1837).

Roy, C., Budtova, T., & Navard, P. (2003). Rheological properties and gelation of aqueous cellulose-NaOH solutions. *Biomacromolecules*, *4*(2), 259–64.

Sammons, R. J., Collier, J. R., Rials, T. G., & Petrovan, S. (2008). Rheology of 1-butyl-3-methylimidazolium chloride cellulose solutions. I. Shear rheology. *Journal of Applied Polymer Science*, *110*(2), 1175–1181.

Sarko, A., Southwick, J., & Hayashi, J. (1976). Packing Analysis of Carbohydrates and Polysaccharides. 7. Crystal Structure of Cellulose IIII and Its Relationship to Other Cellulose Polymorphs. *Macromolecules*, *9*(5), 857–863.

Sescousse, R. (2010). Nouveaux matériaux cellulosiques ultra-poreux et leurs carbones à partir de solvants verts. *PhD thesis*, Mines ParisTech.

Sescousse, R., & Budtova, T. (2009). Influence of processing parameters on regeneration kinetics and morphology of porous cellulose from cellulose–NaOH–water solutions. *Cellulose*, *16*(3), 417–426.

Sescousse, R., Gavillon, R., & Budtova, T. (2011). Aerocellulose from cellulose–ionic liquid solutions: Preparation, properties and comparison with cellulose–NaOH and cellulose–NMMO routes. *Carbohydrate Polymers*, *83*(4), 1766–1774.

Sescousse, R., Le, K. A., Ries, M. E., & Budtova, T. (2010). Viscosity of cellulose-imidazolium-based ionic liquid solutions. *The Journal of Physical Chemistry. B*, *114*(21), 7222–8.

Sila, D. N., Van Buggenhout, S., Duvetter, T., Fraeye, I., De Roeck, A., Van Loey, A., & Hendrickx, M. (2009). Pectins in Processed Fruits and Vegetables: Part II-Structure-Function Relationships. *Comprehensive Reviews in Food Science and Food Safety*, *8*(2), 86–104.

Silva, S. S., Duarte, A. R. C., Carvalho, A. P., Mano, J. F., & Reis, R. L. (2011). Green processing of porous chitin structures for biomedical applications combining ionic liquids and supercritical fluid technology. *Acta biomaterialia*, *7*(3), 1166–72.

Smirnova, I. (2011). Pharmaceutical Applications of Aerogels. In M. A. Aegerter, N. Leventis, & M. M. Koebel (Eds.), *Aerogels Handbook SE - 31* (pp. 695–717). Springer New York.

Sobue, H., Kiessig, H., & Hess, K. (1939). The cellulose-sodium hydroxide-water system as a function of the temperature. *Z. Physik Chem. B*, *43*, 309–328.

Soleimani D. A.., & Abbasi, M. H. (2008). Silica aerogel; synthesis, properties and characterization. *Journal of Materials Processing Technology*, *199*(1-3), 10–26.

Sowmiah, S., Srinivasadesikan, V., Tseng, M.-C., & Chu, Y.-H. (2009). On the chemical stabilities of ionic liquids. *Molecules (Basel, Switzerland)*, *14*(9), 3780–813.

Sriamornsak, P. (2003). Chemistry of pectin and its pharmaceutical uses: a review. *Silpakorn University International Journal*, *3*(1-2), 206–228.

Swatloski, R. P., Spear, S. K., Holbrey, J. D., & Rogers, R. D. (2002). Dissolution of Cellose with Ionic Liquids. *Journal of the American Chemical Society*, *124*(18), 4974–4975.

Tan, C., Fung, B. M., Newman, J. K., & Vu, C. (2001). Organic Aerogels with Very High Impact Strength. *Advanced Materials*, *13*(9), 644–646.

Thakur, B. R., Singh, R. K., & Handa, A. K. (1997). Chemistry and uses of pectin--a review. *Critical reviews in food science and nutrition*, *37*(1), 47–73.

Tilly, G. (2010). Pectines. *Techniques de l'ingénieur* (ref. article : f5000), 0–12.

Tsioptsias, C., Michailof, C., Stauropoulos, G., & Panayiotou, C. (2009). Chitin and carbon aerogels from chitin alcogels. *Carbohydrate Polymers*, *76*(4), 535–540.

Tsioptsias, C., Stefopoulos, A., Kokkinomalis, I., Papadopoulou, L., & Panayiotou, C. (2008). Development of micro- and nano-porous composite materials by processing cellulose with ionic liquids and supercritical CO_2. *Green Chemistry*, *10*(9), 965.

Valentin, R., Bonelli, B., Garrone, E., Di Renzo, F., & Quignard, F. (2007). Accessibility of the functional groups of chitosan aerogel probed by FT-IR-monitored deuteration. *Biomacromolecules*, *8*(11), 3646–50.

Valentin, R., Molvinger, K., Quignard, F., & Brunel, D. (2003). Supercritical CO_2 dried chitosan: an efficient intrinsic heterogeneous catalyst in fine chemistry. *New Journal of Chemistry*, *27*(12), 1690.

Valentin, R., Molvinger, K., Quignard, F., & Di Renzo, F. (2005). Methods to Analyse the Texture of Alginate Aerogel Microspheres. *Macromolecular Symposia*, *222*(1), 93–102.

Welton, T. (2011). Ionic liquids in Green Chemistry. *Green Chemistry*, *13*(2), 225.

Wendler, F., Schulze, T., Ciechanska, D., Wesolowska, E., Wawro, D., Meister, F., Budtova, T., et al. (2013). Cellulose Products from Solutions: Film, Fibres and Aerogels. In P. Navard (Ed.), *The European Polysaccharide Network of Excellence (EPNOE) SE - 6* (pp. 153–185). Springer Vienna.

Wendler, F., Todi, L.N., & Meister, F. (2012). Thermostability of imidazolium ionic liquids as direct solvents for cellulose. *Thermochimica Acta*, *528*, 76–84.

White, R. J., Antonio, C., Budarin, V. L., Bergström, E., Thomas-Oates, J., & Clark, J. H. (2010). Polysaccharide-Derived Carbons for Polar Analyte Separations. *Advanced Functional Materials*, *20*(11), 1834–1841.

White, R. J., Budarin, V. L., & Clark, J. H. (2010). Pectin-derived porous materials. *Chemistry (Weinheim an der Bergstrasse, Germany)*, *16*(4), 1326–35.

White, R. J., Budarin, V., Luque, R., Clark, J. H., & Macquarrie, D. J. (2009). Tuneable porous carbonaceous materials from renewable resources. *Chemical Society reviews*, *38*(12), 3401–18.

Yamada, H., Kowsaka, K., Matsui, T., Okajima, K., & Kamide, K. (1992). Nuclear magnetic study on the dissolution of natural and regenerated celluloses into aqueous alkali solution. *Cellulose chemistry and technology*, *26*(2), 141–150.

Yamane, C., Saito, M., & Okajima, K. (1996). Industrial preparation method of cellulose-alkali dope with high solubility. *Sen'i Gakkaishi*, *52*(6), 310–317.

Yamashiki, T, Saitoh, M., Yasuda, K., Okajima, K., & Kamide, K. (1990). Cellulose fibre spun from gelatinized cellulose/aqueous sodium hydroxide system by the wet spinning method. *Cellulose Chemistry and Technology*, *24*(2), 237–249.

Yamashiki, Takashi, Kamide, K., Okajima, K., Kowsaka, K., Matsui, T., & Fukase, H. (1988). Some Characteristic Features of Dilute Aqueous Alkali Solutions of Specific Alkali Concentration (2.5 mol l−1) Which Possess Maximum Solubility Power against Cellulose. *Polymer Journal*, *20*(6), 447–457.

Yang, Q., Qin, X., & Zhang, L. (2011). Properties of cellulose films prepared from NaOH/urea/zincate aqueous solution at low temperature. *Cellulose*, *18*(3), 681–688.

Zhang, J., Zhang, H., Wu, J., Zhang, J., He, J., & Xiang, J. (2010). NMR spectroscopic studies of cellobiose solvation in EmimAc aimed to understand the dissolution mechanism of cellulose in ionic liquids. *Physical chemistry chemical physics : PCCP*, *12*(8), 1941–7.

Zhang, L., Ruan, D., & Gao, S. (2002). Dissolution and regeneration of cellulose in NaOH/thiourea aqueous solution. *Journal of Polymer Science Part B: Polymer Physics*, *40*(14), 1521–1529.

Zhou, J., Zhang, L., & Cai, J. (2004). Behavior of cellulose in NaOH/urea aqueous solution characterized by light scattering and viscometry. *Journal of Polymer Science Part B: Polymer Physics*, *42*(2), 347–353.

Zugenmaier, P. (2001). Conformation and packing of various crystalline cellulose fibers. *Progress in polymer science*, *26(9)*, 1341-1417.

Chapter II

Materials and Methods

Introduction

In this chapter, the preparation and characterisations of aeropolysaccharides will be described in details.

First, a presentation of the starting materials, such as pectin, cellulose, lignin and cellulose acetate and their solvents (HCl aqueous solutions, 8%NaOH-water and ionic liquids) will be given.
The preparation of pure porous materials based on cellulose (“aerocelluloses”), on cross-linked cellulose (“cross-linked aerocelluloses”) and on pectin (“aeropectins”) will be described through their main steps: dissolution, coagulation and supercritical drying.

Rheology (steady state and dynamic) will be used as a powerful tool to understand systems in their fluid state, such as cellulose acetate solutions and their mixtures with cellulose. Cross-linked cellulose solutions and their gelation will also be studied by dynamic rheology.

Aeropolysaccharides will be fully characterised.
Their morphology will be evaluated by their skeletal and bulk densities, their specific surface areas and their pore size distributions.

Mechanical properties will be analysed by the Young modulus, yield stress and strain, absorbed energy and densification strain.

Effective thermal conductivity and their three contributions (skeletal, gas and radiative) will be determined by hot-wire or heat flowmeters.

Introduction

Ce chapitre présente la préparation et les méthodes de caractérisation des aéropolysaccharides.

Les matériaux utilisés, comme la pectine, la cellulose, la lignine et l'acétate de cellulose ainsi que leurs solvants respectifs (solution aqueuse de HCl, de NaOH ou les liquides ioniques) seront présentés. La préparation de matériaux poreux à base de cellulose (« aérocelluloses »), de cellulose réticulée (« aérocelluloses réticulées ») et de pectine (« aéropectine ») sera décrite par les principales étapes : dissolution, coagulation et séchage supercritique.

La rhéologie sera utilisée pour mieux comprendre les systèmes dans leur état liquide, comme les solutions d'acétate de cellulose dans les liquides ioniques et leurs mélanges avec la cellulose. La gélification des solutions de cellulose réticulée sera également étudiée par rhéologie oscillatoire.

Les aérogels de cellulose et de pectine seront caractérisés. Leur morphologie sera évaluée par la densité apparente, de squelette, la surface spécifique et la distribution de taille de pores.

Les propriétés mécaniques seront analysées par compression uniaxiale et déterminées par le module de Young, la contrainte de plasticité, l'énergie absorbée au cours de la déformation et l'allongement de densification.

Enfin, la conductivité thermique totale ainsi que ses trois contributions (de la phase solide et gazeuse et du transfert radiatif) seront déterminés par la méthode du fil chaud et par thermo flux-mètre.

1. Starting materials

1.1 Polysaccharides

1.1.1 Microcrystalline cellulose

Microcrystalline cellulose Avicel PH101® was purchased from Sigma-Aldrich and will be called "Cellulose" in the following. It is a purified and partially depolymerised α-cellulose with a degree of polymerisation of 180, given by the manufacturer. First cellulose was extracted from fibres and separated from hemicellulose and lignin; then an acidic hydrolysis at 100°C was carried out to remove the amorphous regions. After purification and drying a white microcrystalline powder Avicel is obtained with a mean size of particles around 50 µm. Figure II. 1 presents a SEM (Scanning Electron Microscopy) image of Avicel.

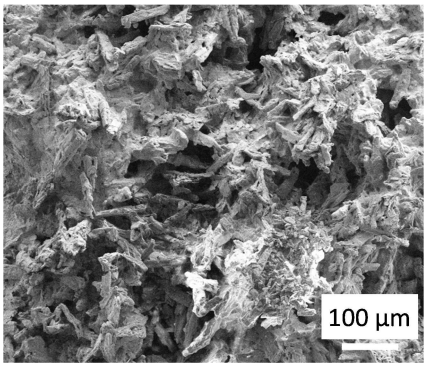

Figure II. 1 : SEM image of Avicel microcrystalline cellulose

1.1.2 Pectin

Two sources of pectin was studied and purchased from Sigma-Aldrich. One was extracted from citrus peel and the other from apple pomace. In both pectins, the proportion of galacturonic acid is above 74% with at least 6.7% of methoxy groups as given by the manufacturer. For citrus peel pectin no information was given on the degree of esterification (DE) whereas for apple pomace DE was evaluated between 72 and 76%.
(Synytsya, 2003) studied by FT-Raman and FT-IR spectroscopy different kind of pectins: pure polygalacturonic acid, potassium pectate, methylated and acetylated pectins. Based on their measurements, major signals can be easily attributed.

Table II. 1 : Major FT-IR signals for polygalacturonic acid (called H-pectin), potassium pectate, methylated pectate (Me-pectate) (Synytsya, 2003), citrus and apple pectin (from Figure II. 2)

H-Pectin	K-Pectate	Methyl-pectin	Citrus pectin	Apple pectin	Assignments
3493	3425		3392	3413	ν (OH)
		2970			ν_{as} (CH_3)
2942	2941		2927	2930	ν (CH)
		2865			ν_{s} (CH_3)
2653					ν $(OH)_{COOH}$
1762					ν $(C=O)_{COOH}$
		1734	1740	1738	ν (C=O)
	1633		1608	1611	ν_{as} (COO^-)
		1444	1441	1440	δ_{as} (CH_3)
	1419		1408	1408 (weak)	ν_{s} (COO^-)
1253	1236		1230	1228	δ (CH)

Figure II. 2 gives the spectrum of pure citrus peel and apple pomace pectin. A strong band centered at 1740 cm^{-1} was assigned to C=O stretching of esterified groups -$COOCH_3$ and an intense band at 1610 cm^{-1} was assigned to carboxylic ions (COO^-).
By using the peak height of these bands at 1740 and 1610 cm^{-1}, DE can be calculated with the following equation (Chatjigakis, Pappas, & Polissiou, 1998; Gnanasambandam, 2000; Urias-Orona et al., 2010):

$$DE = \frac{height\ of\ esterified\ carboxyl\ groups}{(height\ of\ esterified\ carboxyl\ groups + height\ of\ free\ carboxyl\ groups)} \quad \text{(II. 1)}$$

With Equation (II. 1), we were able to evaluate a citrus peel pectin DE_{citrus} = 54% and an apple pomace pectin DE_{apple} = 72%, the latter being consistent with the value given by the manufacturer. In both cases, pectins are qualified as high-methoxy (HM) pectins.

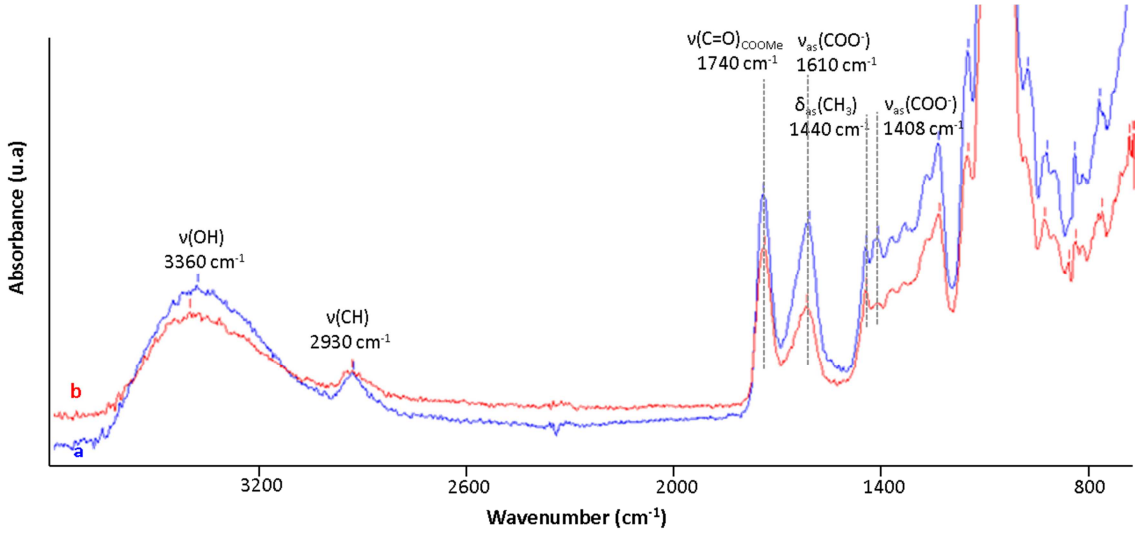

Figure II. 2 : FTIR spectrum of pectin from citrus peel (a) and apple pomace (b).

1.1.3 Cellulose acetate

Cellulose acetate was purchased from Sigma-Aldrich with molecular weight M_n ~ 50 000 g/mol and between 39.2 and 40.2$_{wt}$% of acetyl content, as given by the provider, which is equivalent to an average degree of substitution DS = 2.44.

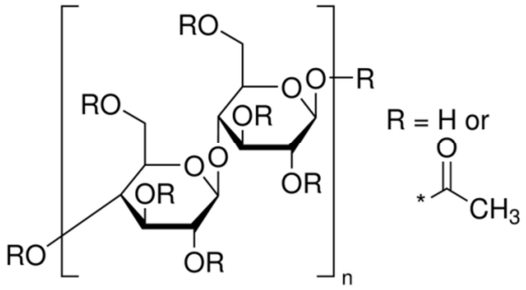

Figure II. 3 : Cellulose acetate.

1.1.4 Lignin

Lignin was obtained from Tembec. It was a lignosulfonate type called ARBO C12 with a molar mass of 30 000 g/mol.

1.2 Solvents

1.2.1 NaOH-water

Sodium hydroxide in pellets with a purity > 97% was supplied by Merck. Distilled water was used to prepare the solutions. 18$_{wt}$% NaOH in water solutions was prepared at room temperature and cooled down to -6°C for a direct use in the dissolution of cellulose (see 2.1.2.1).

1.2.2 Ionic liquids and co-solvent DMSO

The ionic liquid 1-ethyl-3-methyl imidazolium acetate (called EMIMAc in the following) was received from BASF and kept under an azote atmosphere to avoid air humidity. The purity is above 90%.

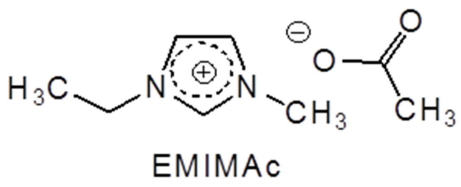

Figure II. 4 : Ionic Liquid 1-ethyl-3-methyl imidazolium acetate.

Dimethylsulfoxide (DMSO) was purchased from Sigma-Aldrich with a purity >99%.

1.2.3 HCl

Hydrochloric solution at 4.0 mol/L was purchased from Sigma-Aldrich. Solutions with different concentrations were obtained by diluting 4.0 mol/L HCl with distilled water.

1.2.4 Coagulation bath

For coagulation baths, distilled water and different alcohols, pure ethanol (purity > 99%) and pure methanol (purity > 99%), were used.

1.3 Cross-linker of cellulose

Epichlorhydrin or epichlorohydrin (ECH in the following) from Fluka with purity>98% was received from Sigma-Aldrich.

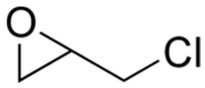

Figure II. 5 : Molecule of epichlorhydrin.

2. General presentation of aeropolysaccharides preparation

Aeropolysaccharide preparation is described in three main steps: dissolution of polysaccharides in a solvent, coagulation of the solution or gel in a non-solvent of polysaccharides and CO_2 supercritical drying (Figure II. 6).

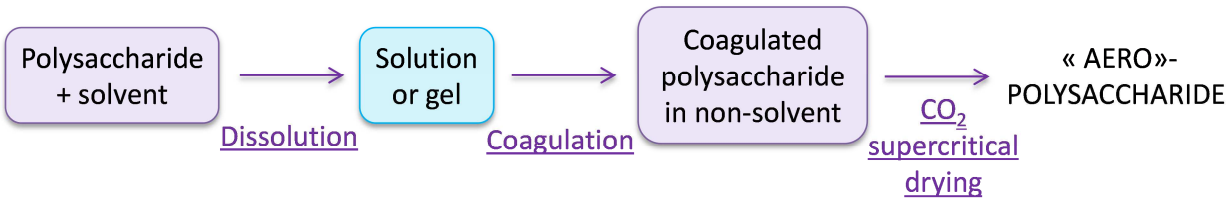

Figure II. 6 : General preparation of aeropolysaccharides.

2.1 Dissolution of polysaccharides

2.1.1 Pre-treatment of polymers before dissolution

Cellulose and cellulose acetate were dried in a vacuum oven at 50°C overnight prior to use. Pectin was used as received.

2.1.2 Dissolution of cellulose or cellulose acetate

Two types of solvents were studied for preparing aerocellulose, an aqueous solution of sodium hydroxide at 8_{wt}% and an ionic liquid EMIMAc, the latter sometimes mixed with DMSO. Cellulose acetate was dissolved in pure EMIMAc.

2.1.2.1 Dissolution in 8%NaOH-water

Cellulose-8%NaOH-water solutions were prepared according to a standard procedure (Egal, Budtova, & Navard, 2007; Gavillon & Budtova, 2008; Sescousse & Budtova, 2009) as followed: cellulose was swollen in distilled water for 2 hours at 5°C. We mixed 18_{wt}% NaOH aqueous solution and swollen cellulose in water with an overhead mixer at 800 rpm for 2 h in a -6°C to get cellulose dissolved in 8_{wt}%NaOH-water. Solutions were poured into moulds and let gelling for 24 h at room temperature.

2.1.2.2 Dissolution of either cellulose or cellulose acetate in EMIMAc

EMIMAc and polymer (cellulose or cellulose acetate) were mixed and stirred in a sealed reaction vessel at 70°C for at least 24 h (checked by optical microscopy) to ensure complete dissolution. Clear solutions were obtained and poured into mould. They were stored at room temperature and protected against moisture absorption.

2.1.2.3 Dissolution of cellulose in EMIMAc-DMSO mixtures

Cellulose is immersed in DMSO at 70°C under moderate stirring (300 rpm) for two hours for letting cellulose swelling. EMIMAc is poured to the mixture and the overall is stirred at 70°C for several days (checked by optical microscopy) to ensure complete dissolution.

2.1.3 Mixing cellulose and cellulose acetate in EMIMAc

Cellulose and cellulose acetate in various proportions ($_{wt}$%) were added simultaneously into the solvent EMIMAc. The mixture was stirred at 70°C in a sealed reaction vessel for least 24. Clear solutions were obtained. They were stored at room temperature and protected against moisture absorption.

2.1.4 Dissolution of pectin

Pectin and HCl solutions (with different concentrations that will be precised for each case) were mixed and stirred vigorously at room temperature for 4 h. Viscous solutions were centrifuged at 6000 rpm for 20 min. They were poured into moulds and let gelling from 24 h to 48h (depending on pectin concentrations).

2.2 Cross-linking of cellulose

2.2.1 Different cellulose gelation mechanisms

In the solvent 8%NaOH-water cellulose undergoes a "physical" gelation, due to chains entanglements (Figure II. 7a). By adding divalent molecules as ECH, cellulose chains will be cross-linked between them. Gelation is also due to the increasing of cross-linking points (Figure II. 7b) forming a "chemical gel".

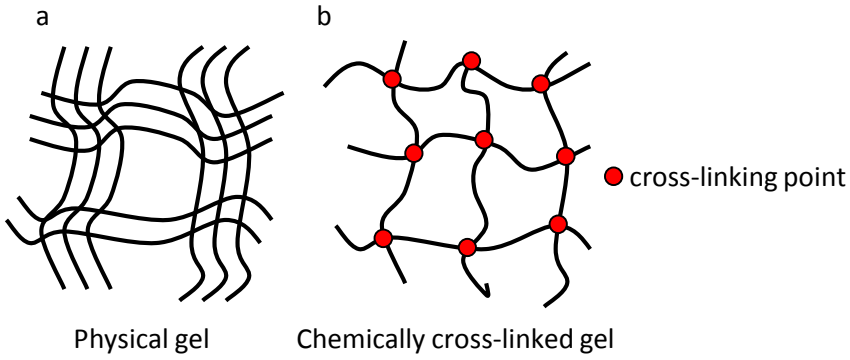

Figure II. 7 : Different types of cellulose gelation: physical (a) and chemical (b).

2.2.2 Cellulose cross-linking in 8% NaOH-water

Cellulose cross-linking was performed in 8_{wt}% NaOH-water solvent and was inspired from (Chang, Zhang, Zhou, Zhang, & Kennedy, 2010; Zhou, Chang, Zhang, & Zhang, 2007). Cellulose solutions were prepared at -6°C and were let warming at room temperature for 2 h. ECH was added dropwise into cellulose solutions. Emulsions obtained were stirred vigorously for 15 min and rapidly poured into moulds. They were let at room temperature gelling for 24 to 48 h.

2.3 Coagulation of polysaccharides in a non-solvent

For cellulose, solutions or gels were immersed in a non-solvent bath (water or ethanol). The volume of the bath is about 5 times higher than cellulose. The solvent is changed every day for at least 5 days. Cellulose coagulation kinetics in water from cellulose-8%NaOH-water (Gavillon & Budtova, 2007; Sescousse & Budtova, 2009) or cellulose-EMIMAc (Sescousse, Gavillon, & Budtova, 2011) were already studied. It was shown that at a given cellulose concentration, the diffusion coefficient of EMIMAc into water D_{EMIMAc} is 4-5 times lower than D_{NaOH}. It means that for a sample with the same geometry the time needed to completely coagulate cellulose will be longer.

The end of coagulation is checked with the pH for cellulose in 8%NaOH-water (pH = 7). For cellulose-IL, it is harder to follow the end of regeneration. We controlled the disappearance of the brown-orange color. However it is known that it is not straightforward to make sure no ionic liquid is trapped inside the structure (Gericke, Fardim, & Heinze, 2012).

For sample coagulation in water a further solvent exchange step is necessary as water is not soluble in supercritical CO_2. Alcohols such as ethanol or methanol were used and will precised for each case.

For pectin, gels are immersed in $50\%_{vol}$ water and $50\%_{vol}$ ethanol bath. The ratio of ethanol in the coagulation bath is then increased progressively to 100% (by 20% increment). Pure ethanol baths are then changed every day for at least 3 days.

Coagulated polysaccharide precursors of aerogel (see Figure II. 6) are ready to be dried. Drying methods will be described in section 4.1.

3. Methods for studies of solutions and gels

3.1 Rheology of cellulose acetate-ionic liquid- solutions and mixtures with cellulose

Measurements of steady state and dynamic rheology of cellulose acetate (CA)/EMIMAc solutions were performed on Bohlin Gemini rheometer equipped with cone-plate geometry (4° – 40 mm) and Peltier temperature control system. Shear rates were varied from 0.01 to 500 s^{-1} and temperatures from 0°C to 80°C. In dynamic mode frequency sweeps were performed at 5 Pa, corresponding to linear visco-elastic regime, in the same temperature range.

Cellulose/cellulose acetate/EMIMAc solutions were studied in steady state rheology on the same rheometer as described above. Shear rates were varied from 0.01 to 500 s^{-1} and temperatures from 0°C to 80°C.

3.2 Use of rheology for the investigation of gelation of cross-liked cellulose

Winter and Chambon (Winter & Chambon, 1986) studied the gelation of chemical cross-linked gels from polydimethylsiloxane (PDMS) and more particularly the determination of gel point (GP).
Briefly, the method is based on following the storage modulus G’ and the loss modulus G” with time at a fixed frequency and stress. At the beginning, the viscous behaviour is predominant (liquid state) thus G” is large and G’ negligible. Close to percolation the molecular weight increases which is reflected by strong increase of G’ while G” is still increasing. The intersection between G’ and G” is the gel point (Figure II. 8).

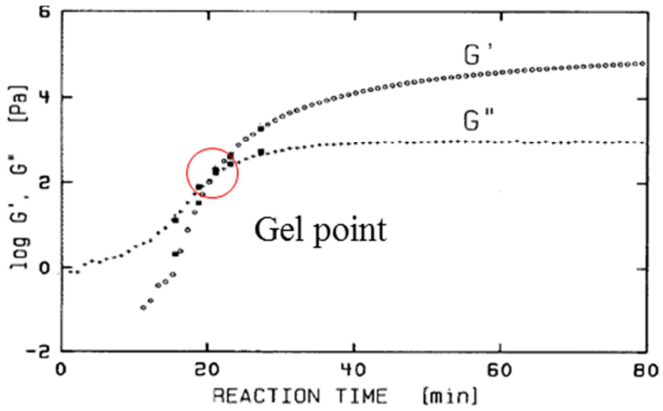

Figure II. 8 : Evolution of G' and G'' as a function of time at a fixed frequency for a PDMS (Winter & Chambon, 1986). Reprinted with permission from (Winters & Chambon, 1986). Copyright (1986), The Society of Rheology.

It is known that cellulose in 8%NaOH-water undergoes a gelation with time and temperature and physical gels are formed. In this work, cross-linker, epichlorhydrin, is added, and cellulose is chemically cross-linked. We measured G' and G" as a function of time and determined gelation point for various compositions of cellulose and cross-linker. All rheological measurements were performed on a Bohlin Gemini rheometer equipped with cone-plate geometry (4° – 40 mm) and Peltier temperature control system, frequency was fixed at 0.1 Hz and stress at 0.01 Pa to ensure being in the linear regime.

3.3 ^{13}C-NMR for the determination of cellulose cross-linking

^{13}C-NMR measurements were carried out on dried cross-linked samples in the laboratory Charles Coulomb of the University of Montpellier in order to study the cellulose cross-linking.

4. Methods for polysaccharides drying

4.1 Drying

Three ways were used for drying polysaccharides: evaporative drying, freeze-drying and supercritical drying. A gel dried by evaporation is called a *xerogel*, by supercritical drying *aerogel* and by freeze drying *cryogel*. Drying will strongly influence polysaccharide morphology and properties.

4.1.1 Supercritical CO_2 drying

Supercritical CO_2 ($scCO_2$ in the following) is easily obtained with a pressure P=72.8 bar and temperature T=31.1°C. The $scCO_2$ drying was performed in the center Persée-Mines ParisTech in Sophia-Antipolis. First, polysaccharide precursors coagulated in alcohols were placed in a 1L

autoclave (Figure II. 9 n°3) containing the same alcohol to avoid samples drying while the autoclave is closing.

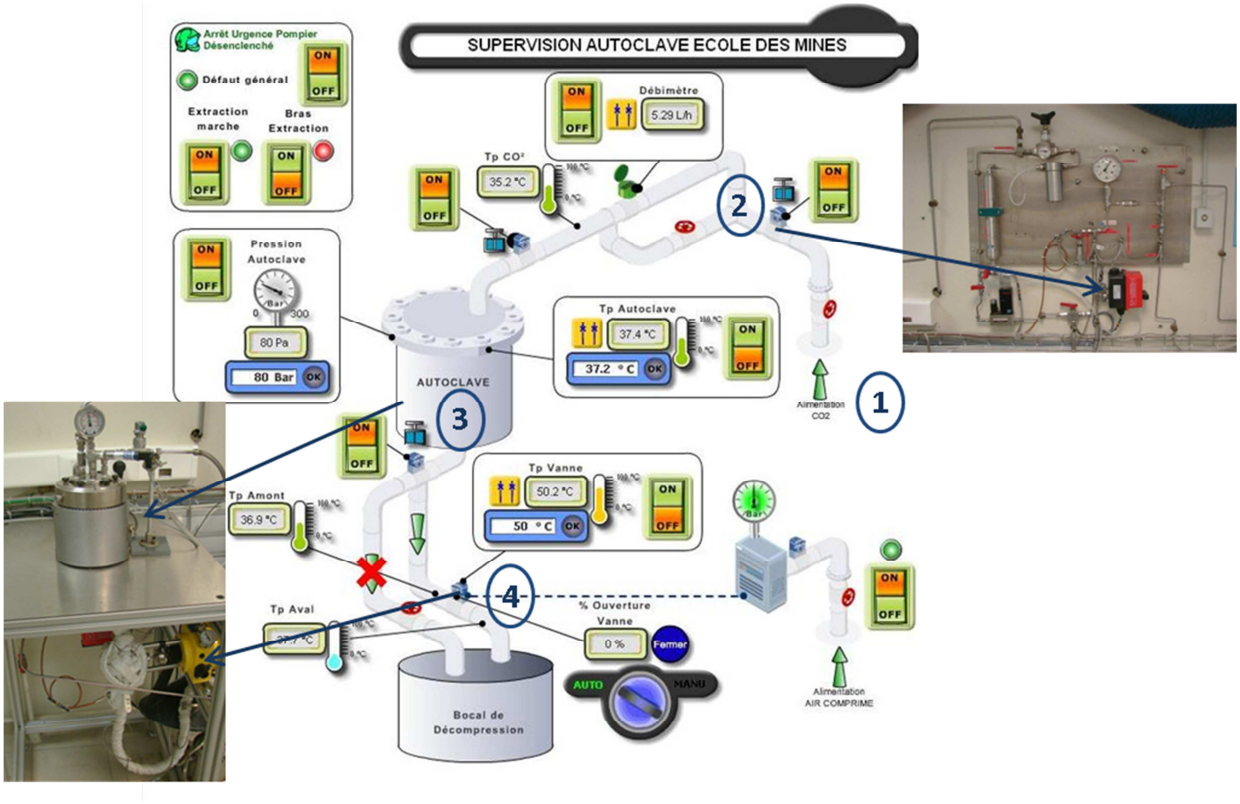

Figure II. 9 : Laboratory-scale supercritical CO_2 drying device in Persée-Mines ParisTech; (1) CO_2 alimentation, (2) Feeding valve, (3) autoclave, (4) depressurization valve. Courtesy of Pierre Ilbizian, Persée-Mines ParisTech.

First the system is pressurized at 50 bars and 37°C with gaseous CO_2. The covering solvent is purged maintaining the pressure and temperature constant with CO_2. Then the system is pressurized at 80 bars and 37°C. CO_2 becomes supercritical and solubilizes the residual solvent inside sample porosity. A dynamic washing step at 80 bars, 37°C with an output of 5kg CO_2/h is carried out for 1 hour. The system is let on a static mode at the same pressure and temperature conditions to allow $scCO_2$ to diffuse and solubilizes solvent even in the nanometric pores for 1-2 hours. The dynamic washing is then starting over with the same CO_2 output for 2 hours. Afterwards, the system is slowly depressurized overnight at 4 bars/h and 37°C and cooled down to room temperature. The autoclave is then opened and samples collected.

4.1.2 Freeze-Drying

When freeze-drying procedure was chosen, cellulose was coagulated in water and no washing in alcohols was performed. These swollen-in-water samples were placed first in a glass beaker. A close contact with glass walls is preferable since it will optimize heat transfer during freezing. Beakers were immersed in either in a liquid nitrogen (-196°C) bath for 3 minutes or in an ethanol bath placed in a freezer for about an hour. Frozen samples were then placed in a freeze-dryer

Cryotec Cosmos 80. Vacuum was slowly made inside the chamber (to avoid cracks). Samples were let drying for 48 hours. Water vapour was condensed in the refrigerated unit (Figure II. 10)

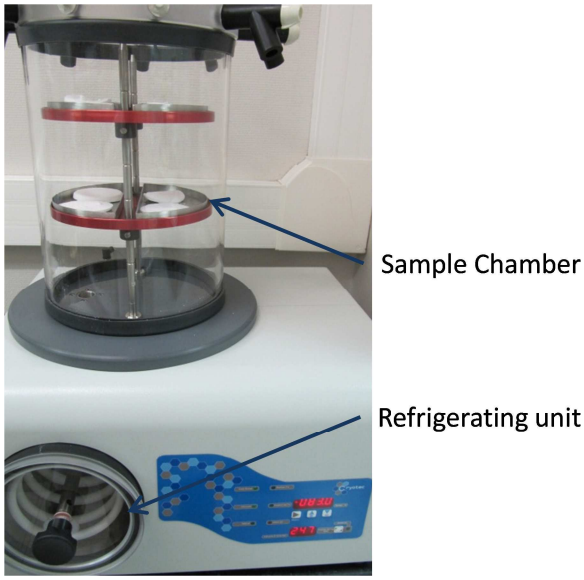

Figure II. 10 : Freeze-drying apparatus.

4.1.3 Evaporative drying

Cellulose coagulated in water was let drying under the extracted hood for 48 hours. They were placed afterwards in a vacuum oven at 60-80°C for at least 48 hours (until the mass of samples are constant) to remove water traces.

4.2 Structural characterisation of solid materials

4.2.1 Bulk and skeletal densities

4.2.1.1 Bulk density

Bulk or envelope density may be measured by two different techniques: a mercury pycnometer or powder envelope density analyser.
By definition, bulk density is calculated by:

$$\rho_{bulk} = \frac{Mass}{Volume} \; of \; sample \qquad \text{(II. 2)}$$

It is straightforward to precisely measure the mass but volume measurement may be tricky for samples with not well defined shape. The two methods used are based on the same principle: measuring a volume difference. In one case we used mercury and in the second one a fine powder of small, rigid spheres having a high degree of flowability and called DryFlo®. For both techniques, we assume that mercury or DryFlo powder at atmospheric pressure will not enter pores smaller than 15 microns in diameter.

Hg pycnometry

The difference in the volume of mercury in the sample chamber with and without the sample is determined and matches the volume of the sample. Density measurements using Hg pycnometry were carried out on a CE Instruments Macropore de Carlos Erba in the laboratory Charles Coulomb (L2C) in Montpellier.

Powder envelope density analyser

In the second method which uses DryFlo® powder, the sample is placed in a chamber with powder that is rotated and agitated while a certain force is applied. The volume difference due to piston displacement at the end of "compaction" with and without the sample at a given force is the volume of the sample.

Bulk density analyser used is a Geopyc 1360 from Micromeritics with DryFlo powder installed in Persée-Mines ParisTech in Sophia-Antipolis (Figure II. 11). A 19.1 mm sample chamber and a force of 25 N are used, particularly optimised for fragile porous materials.

Figure II. 11 : Geopyc 1360 from Micromeritics to measure bulk density of porous materials. The technique is based on measuring a variation of piston displacement without and with the sample in a powder DryFlo.

For pure aerocelluloses from ionic liquids and their hybrids with cellulose acetate, bulk density measurements were carried out on Hg pycnometry (Chapter III and V). Bulk density of all other samples such as cross-linked aerocellulose (Chapter IV) and aeropectin (Chapter V) were measured with Geopyc from Micromeritics (Table II. 2).

For both techniques, very similar results of bulk density are obtained within the experimental errors (less than 10%).

Table II. 2 : Summary of bulk density measurements techniques.

Type of aerogels	Techniques	Chapter
Pure aerocelluloses from ionic liquids	Hg pycnometry	Chapter III
Pure aerocelluloses from NaOH	Geopyc	Chapter III
Cross-linked aerocelluloses	Geopyc	Chapter IV
Hybrid cellulose / cellulose acetate	Hg pycnometry	Chapter V
Aeropectin	Geopyc	Chapter VI

4.2.1.2 Skeletal density

Gas pycnometer is used to determine the skeletal density which represents the "density of solid" without the porous volume. Helium is preferred as it is an inert gas, exhibits ideal gas behaviour and can enter small pores (1Å).
The goal is to measure the volume of only solid part of the sample, i.e to exclude the volume of pores. The instrument determines the volume by measuring the pressure change of helium in a calibrated volume. The volume measured excludes any pore volume accessible to the gas. The skeletal density is obtained by dividing the weight of the sample by the volume measured.
Experiments were carried out on a Micromeritics AccuPyc 1330 Pycnometer in Laboratory Charles Coulomb (L2C) in the University of Montpellier. Samples were degassed at 70°C for 24 hours prior to analysis.

4.2.2 Porosity

Porous materials are defined as materials containing cavities or channels, called pores (voids) filled with air. They are often characterised by their porosity: a measure of the void inside the structure. It is calculated as the ratio between the volume of void space and the total volume (solid + voids). It can also be evaluated with bulk and skeletal densities (Equation (II. 3)).

$$\varepsilon(\%) = \frac{V_{pores}}{V_{total}} = 1 - \frac{\rho_{bulk}}{\rho_{skeletal}} \qquad \text{(II. 3)}$$

A distinction has to be made between open and closed pores (Figure II. 12). Closed pores, contrary to open pores, are not accessible to liquids or gases. The total porous volume is the sum of closed and open pores volumes.

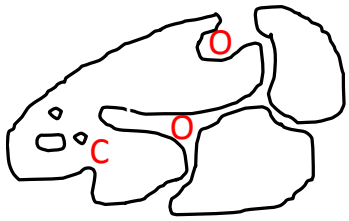

Figure II. 12 : Schematic representation of a porous sample with two different pores: open (O) and closed (C).

The properties of a porous material strongly depend on the geometry and size of pores as well as their distribution. IUPAC classification divides pores sizes in three groups (Sing et al., 1985):

- Macropores are pores with an internal width above 50 nm
- Mesopores with an internal width between 2 and 50 nm
- Micropores with an internal width below 2 nm

4.2.2.1 Gas adsorption

Gas adsorption measurements (in our case nitrogen at 77 K) are used for determining the surface area and pore size distribution of porous materials (Sing et al., 1985).
Gas adsorption is the accumulation of an adsorbable gas (adsorptive or adsorbate) on the surface of a solid (adsorbent) at the gas/solid interface. Two phenomena are possible and have to be distinguished: *physisorption* (caused by Van der Waals interactions between adsorbate and adsorbent) and *chemisorption* (when the adsorbent and adsorbate are linked by valence bonds). Physisorption experiments are carried out at the liquid nitrogen boiling point (77 K) at atmospheric pressure. Adsorption isotherm is a series of equilibrium states between the gas phase (around the sample) and the adsorbed gas phase. Usually adsorption isotherm is experimentally represented by the plot of the adsorbed quantity per gram of adsorbate as a function of equilibrium relative pressure p/p^0 (with p the equilibrium pressure of absorbate gas and p^0 the equilibrium vapour pressure of nitrogen). Adsorption is reversible since physical interactions between the gas adsorbed and the solid are weak. Desorption is the opposite phenomenon. Adsorption isotherm takes into account adsorption and desorption; it is one of the ways to characterize porous materials.

Monolayer adsorption (Figure II. 13) is characterised by one layer of adsorbed gas, or in other words, when all adsorbed molecules are in contact with the surface layer of the solid. Multilayer adsorption occurs when adsorption space may have more than one layer and all the adsorbed molecules are not in contact with the solid surface. Capillary condensation is a phenomenon occurring when the contact angle between a liquid and a solid is lower than 90°C (creation of a meniscus): a gas condenses with a pressure inferior to equilibrium vapour pressure.

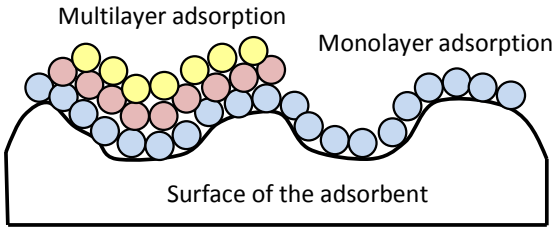

Figure II. 13 : Adsorption mechanism at the surface of adsorbent

4.2.2.2 Classification of adsorption isotherms

Adsorption isotherms are classified with six different standard types according to IUPAC (Sing et al., 1985):

- *Type I isotherm* has a horizontal plateau due to the saturation of the adsorbent even with increasing pressure. It is typical for microporous solids with small external surfaces.
- *Type II isotherm* has a gradual increase of adsorbed quantity with pressure and is obtained for macroporous or non-porous solids. The adsorbed layer is thickening gradually and is typical of multilayer adsorption.
- *Type IV isotherm* is similar to type II for low relative pressure. At higher relative pressure, a saturation plateau is observed with variable length. It is typical for mesoporous adsorbent. A

hysteresis loop is observed during desorption, due to capillary condensation, which is unique to each adsorbate/adsorbent system.
- *Type III and V isotherms* are not common and have a convex plot due to very weak interactions between adsorbate and adsorbent. They are more typical for water vapour adsorption on hydrophobic surface.
- *Type VI isotherm* was observed for adsorption by energetically homogeneous surfaces on which gas layers are successively adsorbed.

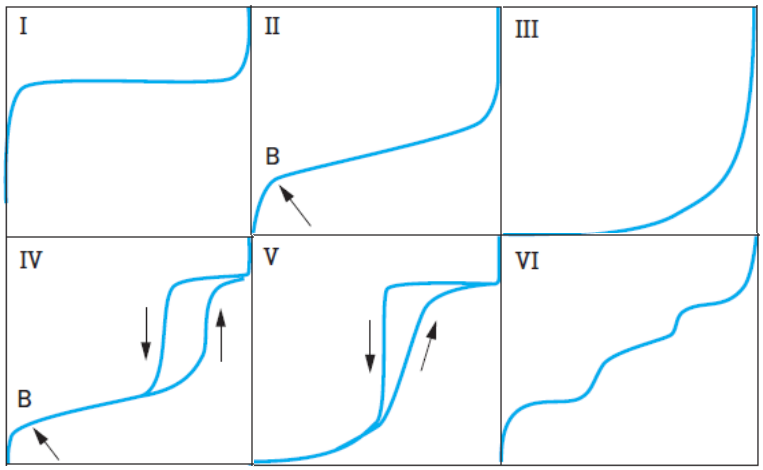

Figure II. 14 : Types of physisorption isotherms (Luciani, Denoyel, & Rouquerol, 2003; Sing et al., 1985).

4.2.2.3 Determination of surface area

Brunauer-Emmett-Teller (BET) gas adsorption method has become the most commonly used for determining surface area of porous solids. In 1938, Stephen Brunauer, Paul Hugh Emmett, and Edward Teller suggested a multilayer adsorption mechanism with several hypotheses: absence of interaction between each adsorption layer, the number of adsorbed layers on a solid is infinite, and the Langmuir theory can be applied to each layer. In the range p/p^0 between 0.05 and 0.3, adsorption isotherm is quasi-linear and a simplified equation is given and known as BET equation:

$$\frac{{}^{p}/_{p^0}}{n^a(1-{}^{p}/_{p^0})} = \frac{1}{n_m^a C} + \left[\frac{C-1}{n_m^a C}\right]\left(\frac{p}{p^0}\right) \qquad \text{(II. 4)}$$

where n_m is the amount of gas absorbed at the relative pressure p/p^0,
p/p^0 is the equilibrium relative pressure,
n^a_m is the monolayer capacity (amount of adsorbate needed to cover the surface with a complete monolayer of molecules).

Specific surface area is known as the surface available to gas adsorption. It is an important parameter to characterise porous materials. It is strongly related to pores size and their distribution: larger pores will give a smaller specific surface whereas smaller pores will give a

larger surface. When the surface is totally covered by adsorbed molecules, specific surface may be determined by:

$$a = \left(\frac{n_m^a}{m_s}\right) N_A \sigma_m \quad \text{(II. 5)}$$

with m_s mass of the adsorbent,
N_A the Avogadro constant,
σ_m is the cross section occupied by each nitrogen molecule and is fixed by IUPAC at σ_m =0.162 nm².

The BET apparatus gives monolayer adsorbed gas volume v^a_m instead of the amount of absorbed molecules n^a_m. These two values are related by

$$n_m^a = \frac{v_m^a}{v_l} \quad \text{(II. 6)}$$

with v_l molar volume of perfect gas equals to 22 414 $cm^3.mol^{-1}$.

Equation (II. 5) may be expressed as

$$S_{BET} = \left(\frac{v_m^a}{m_s}\right) \frac{N_A \sigma_m}{v_l} \quad \text{(II. 7)}$$

By plotting $\frac{p/p^0}{v^a(1-p/p^0)}$ as a function of p/p^0 between 0.05 and 0.3 a straight line is obtained. The constant C and v^a_m are determined (Equation (II. 4) with slope and y-intercept and S_{BET} calculated.

4.2.2.4 Pore size distribution by BJH method

A hystereris is often observed during desorption for type IV isotherm, typical for mesoporous adsorbents. The Barrett, Joyner and Halenda method (or BJH method) gives a pores size distribution of mesopores. It is based on capillary condensation of nitrogen inside mesopores and thus the classical Kelvin law (Equation (II. 8)) is applicable.

$$ln\left(\frac{p}{p^0}\right) = \frac{-2\gamma V_l}{r_K RT} \quad \text{(II. 8)}$$

with γ the surface tension, V_l the molar volume of the adsorbed liquid at temperature T.

This law gives the relation between the pressure *p* of the condensation of gas inside the pore and the radius r_k of the liquid meniscus formed. For nitrogen adsorbed at -196°C the Kelvin law is given by :

$$r_K = -0.415\left(\frac{p}{p^0}\right) \quad \text{(II. 9)}$$

From Equation (II. 8), we can reconstruct a pore size distribution for each relative pressure. Calculations are made preferably on the desorption curve for mesopores with a radius smaller than 50 nm.

4.2.2.5 Apparatus for BET and BJH measurements

Most of specific surface area S_{BET} measurements were carried out on a Micromeritics ASAP 2010 in Laboratoire Charles Coulomb (L2C) in the University of Montpellier.
Measurements on pectin-silica samples (Chapter VI) were performed on a Micromeritics ASAP 2020 in Cemef-Mines ParisTech.

Pore size distribution experiments using BJH method were performed on a Micromeritics ASAP 2020 in Cemef-Mines ParisTech.

4.2.2.6 Samples degassing

Before running adsorption isotherm experiments, all the species that can be physisorbed at the surface of the adsorbent should be removed. This is achieved by outgassing the sample prior to analysis.
For BET experiments in the laboratory L2C in Montpellier, samples are exposed to a high vacuum at 70°C for 24h.
For BET and BJH experiments in Cemef-Mines ParisTech, samples are placed in a high vacuum at 70°C for 5h.

4.2.2.7 Pore size distribution by mercury porosimetry and Pirard's theory

Mercury porosimetry is used to obtain pore size distribution in porous materials. It gives information on mesopores but also on macropores by applying various levels of pressure to a sample immersed in mercury. The pressure applied to fill pores with mercury is inversely proportional to the pores' diameters.

Mercury (Hg) is a non-wetting liquid with high surface tension. The capillary law governing Hg liquid penetration is given by the Washburn equation:

$$L = \frac{4\gamma}{P}\cos\theta \qquad \text{(II. 10)}$$

with L is the pore diameter,
p the applied pressure,
γ the surface tension of mercury,
θ the contact angle between mercury and the porous solid (measured in a separate experiment).

The Washburn equation assumes that all pores are cylindrical. Even if this is rarely true, this equation provides a reliable representation of pores size distribution.

As pressure increases during the experiment, pore size is calculated for each pressure point P and the mercury volume V associated to fill these pores. The dependences of pore volume versus pore size and the total pore volume are obtained.

Unfortunately this method cannot be used for aeropolysaccharides that are contracting under the pressure applied to mercury. Mercury does not enter pores and the volume measured is the difference between sample initial volume and the volume of contracting sample. This has already been reported for aerocellulose (Sescousse et al., 2011) and cellulose acetate aerogels (Fischer, Rigacci, Pirard, Berthon-Fabry, & Achard, 2006).
Pirard and Pirard reported the same for synthetic aerogels and more generally, for hyperporous materials. They demonstrated that the Hg porosimetry theory based on the Washburn's equation cannot be used directly (Pirard, Alié, & Pirard, 2002; Pirard, Blacher, Brouers, & Pirard, 1995; Pirard & Pirard, 1997) because it relies on the fact that Hg intrudes the pores network. The authors showed that the structure of hyperporous materials crushes under the Hg pressure and that the liquid does not intrude pores. They suggested that pore size distribution can be "reconstructed" from the subsequent crashing of pore walls with the buckling theory described by:

$$L = \frac{k}{P^{0.25}} \tag{II. 11}$$

where L is the size of the largest pores remaining after the compression at a pressure P and k the buckling strength constant.

This constant k depends on the material and can be experimentally evaluated by the compression at a pressure P fixed and the measure of the largest pores size remaining by nitrogen adsorption isotherm.

Mercury porosimetry experiments and determination of the buckling constant were kindly carried out in Laboratory Charles Coulomb (L2C) in the University of Montpellier. Two different devices (both from CE instrument) were used to have a pore size distribution from 10 to 400 nm: one with pressure from 0 - 400 kPa (called "Pascal 140") and the other one from 400 kPa - 200MPa ("Pascal 240").

For either BJH measurements or Hg porosimetry, we evaluated and compared typical parameters of pore size distribution:
- the maximum of pore size $L_{p\,max}$ obtained at the maximum of the dV/dL
- the mean pore diameter $L_{p\,mean}$ calculated from Equation (II. 12)

$$L_{p\,mean} = \frac{\sum L_i \times \frac{dV}{dL}_{normalised,i}}{\sum \frac{dV}{dL}_{normalised,i}} \tag{II. 12}$$

- the mean pore diameter $4V/S_{BET}$ calculated according to Equation (II. 13)

$$L_p = \frac{4 \times V_{p\,measured}}{S_{BET}} \quad \text{(II. 13)}$$

- the full width at half value (FWHV) obtained by the difference in pore size at half of the dV/dL max

4.2.3 Scanning Electron Microscopy

4.2.3.1 Principle

A scanning electron microscope (SEM) gives images of a sample surface (topography) by scanning it with a focused beam of electrons. Beam electrons interact with the electrons on the surface, producing various signals (electrons, photons, phonons…) that can be detected.

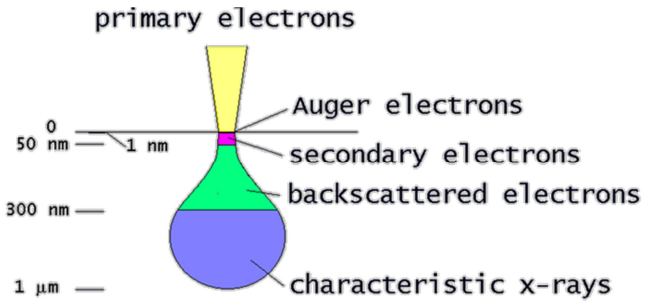

Figure II. 15 : Interaction volume.

When the primary electron beam interacts with the sample, the electrons lose energy within a teardrop-shaped volume known as the *interaction volume* (Figure II. 15). Two types of interactions have to be distinguished: elastic interactions with energy close to incident energy called backscattered electrons coming from deeper inside the sample; and inelastic interactions with a lower energy called secondary electrons and coming from the extreme surface of the sample.
Detection of secondary electrons gives information on the topography whereas detection of backscattered electrons gives the composition of the sample.

4.2.3.2 EDS analysis

Energy-dispersive X-ray spectroscopy (EDS) is an analytical technique used for the elemental analysis of a sample. The electron beam excites the atoms in the sample that produce X-rays to discharge the excess energy. The energy of the X-rays is characteristic of the atoms that produced them, forming peaks in the spectrum. As the electron beam can be precisely controlled, and EDS spectrum can be collected from a selected area of the sample. This technique gives an elemental analysis of a few cubic microns of material.

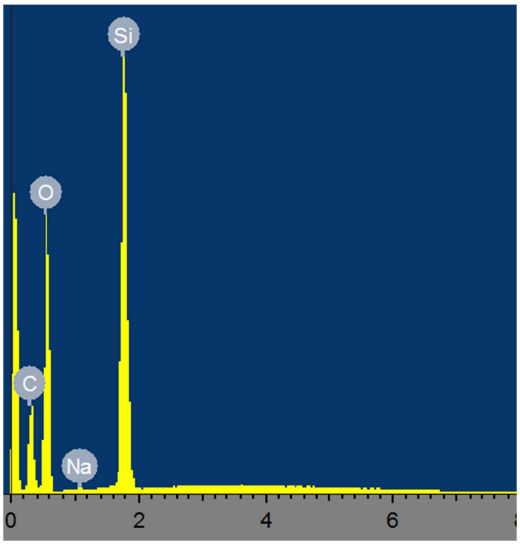

Figure II. 16 : EDS analysis.

EDS analysis was carried out on a XL30 FEI Philipps ESEM (Environmental Scanning Electron Microscopy) in Cemef-Mines ParisTech with an acceleration voltage of 12 keV and a vacuum pressure in the chamber of 0.5mbar (Figure II. 17b).

4.2.3.3 Morphological observations by SEM

SEM observations aerogels morphology were performed on a Supra40 Zeiss SEM FEG (Field Emission Gun) in Cemef-Mines ParisTech, which allows having a high resolution and depth of field (Figure II. 17a). Acceleration voltage was set up at 3 keV and a diaphragm of 20 µm. A fine layer of gold-platinium (few tens of Å) is sputtered onto the surface of samples to prevent accumulation of electrostatic charge at the surface.

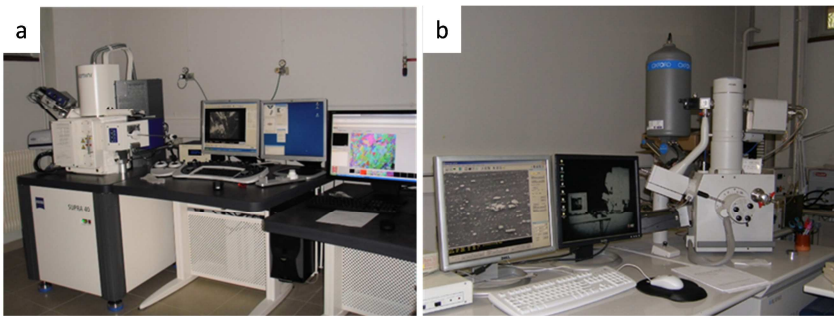

Figure II. 17 : SEM available at Cemef FEG Supra 40 (a) and XL30 ESEM (b).

4.2.4 Fourier Transformed Infrared (FT-IR) Spectroscopy

FT-IR spectroscopy was carried out on a Bruker Tensor 27 spectrometer in Persée-Mines Paristech. Samples were analyzed in attenuated total reflectance mode (ATR) using a Pike MIRacle accessory equipped with a Ge crystal (Pike Technology). The spectrum has been collected 16 times and corrected for the background noise.

4.2.5 Summary of structural characterisations

Various techniques, listed below, were used to have a full characterisation of aeropolysaccharides structure.

- Hg pycnometry or Dryflo powder pycnometry for the apparent or bulk density ρ_{bulk}.
- He pycnometry for skeletal density $\rho_{skeletal}$.
- Adsorption/desorption of N_2 for the information on specific surface S_{BET} and pore size distribution PSD_{BJH}.
- Hg porosimetry for the pores size distribution on a larger range PSD_{Hg}.
- SEM images for morphologies of aeropolysaccharides and elemental analysis.

4.3 Mechanical properties of aeropolysaccharides

Uniaxial compression tests were carried out on Zwick mechanical testing machine in Cemef-Mines ParisTech. Samples were placed between two parallel plates (Figure II. 18).
Planarity and parallelism were verified by a micrometric sensor. Two different load cells were used:

- 100 N for precise measurements of Young modulus
- 2500 N for the complete stress-strain curve.

The tests were performed at room temperature (20-22°C), atmospheric pressure and 30-40% relative humidity. Samples with cylindrical shape and a ratio length/diameter = 3/2 were compressed at a displacement rate of 1 mm/min until 75% of the deformation. (Gavillon, 2007) showed that aerocelluloses compression is slightly dependant of the displacement rate as they are visco-elastic materials. However, differences are not significative due to high experimental errors. We chose to be at 1 mm/min to ensure the same experimental conditions as R.Gavillon for the sake of comparison. A particular attention was given to have two plane and parallel surfaces of a sample. At least 3 samples of the same formulation were tested to ensure reproducibility.

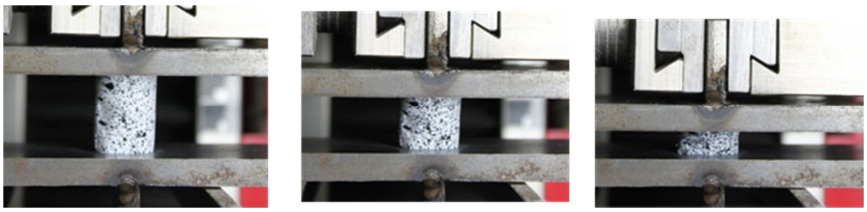

Figure II. 18 : Example of uniaxial compressive test on aerocellulose.

Figure II. 18 shows that the compression is uniform and the cross-section area does not evolve along the test. It has been verified in each aeropolysaccharide. Therefore the stress $\sigma(t)$ is related to the force $F(t)$ divided by the initial cross-section area A_0 (Equation (II. 14))

$$\sigma(t) = \frac{F(t)}{A_0} = \frac{4\,F(t)}{\pi\,d^2} \quad \text{(II. 14)}$$

The deformation is defined as

$$\varepsilon(t) = \frac{l(t) - l_0}{l_0} \quad \text{(II. 15)}$$

with l(t) the length of sample at a time t and l_0 the initial length.

The Poisson's ratio ν gives the information on the transverse deformation of the sample and is calculated according to Equation (II. 16). The deformation was followed by taking regular photos and ν was measured as a function of time.

$$\nu = \frac{transverse\ deformation}{axial\ deformation} = \frac{\frac{L_0 - L}{L_0}}{\frac{l_0 - l}{l_0}} \quad \text{(II. 16)}$$

with L and L_0 are the width of the sample at time t and t=0 respectively.

A stress-strain curve of the compression was recorded. An example of an aeropectin compression is given in Figure II. 19.

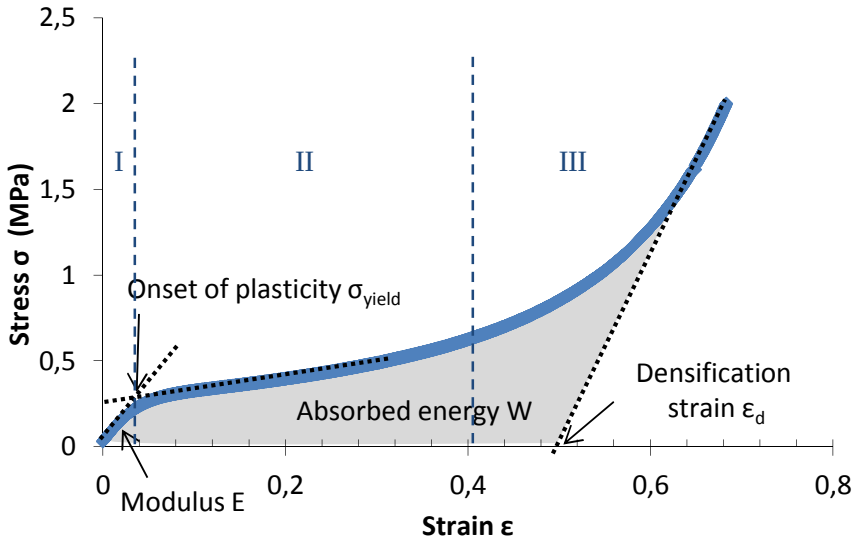

Figure II. 19 : Strain-stress curve for a 0.09g/cm^3 aeropectin.

Three different domains can be distinguished on the stress-strain curve. The response of a porous material to applied force can be schematically presented in (Figure II. 20):

- The first domain corresponds to low and reversible material deformations, it is elastic region (Figure II. 20a). Cell walls bend under the stress but recover when the stress is released. Stress is directly proportional to strain. We define the Young modulus E as the slope in the linear region on the curve σ=f(ε).
- The second domain is when the stress is too strong and cell walls start to collapse by buckling (Figure II. 20b). It is the beginning of plasticity. A plateau is observed (Figure II. 19) called the

plasticity plateau. During this phase the material absorbs energy. We define the onset of plasticity as the yield stress σ_{yield} and the yield strain ε_{yield} and the overall domain I and II is characterized by absorbed energy W (during the elastic and plastic deformation). W is defined as the area under the curve (Equation (II. 17)) from 0 to ε_d strain. In previous data on aerocellulose, the absorbed energy is also calculated from 0 to 40% strain (Gavillon, 2007). Two energies will be then calculated, one $W_{\varepsilon d}$ until ε_d strain, and the second $W_{40\%}$ for the sake of comparison until 40% stain.

$$W_{\varepsilon_d \, or \, \varepsilon_{40\%}} = \int_0^{\varepsilon_d \, or \, \varepsilon_{40\%}} \sigma(x).dx \qquad \text{(II. 17)}$$

- The third and last domain is material densification. Cell walls start to touch each other (Figure II. 20c) and the stress increases extremely fast. The end of the plasticity (domain II and beginning of domain III) is given by the densification strain ε_d.

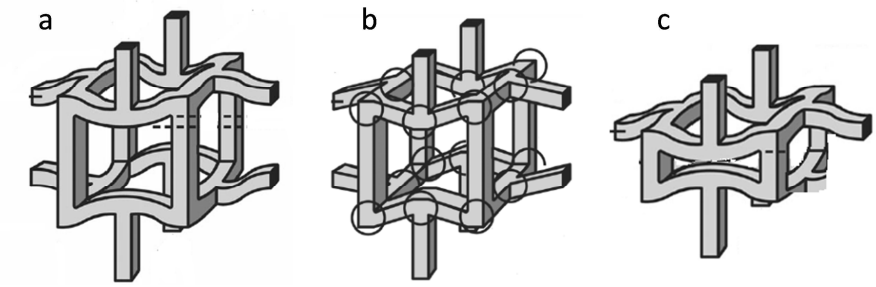

Figure II. 20 : Deformation of cell walls during a uniaxial compressive stress (Gibson & Ashby, 1999).

Gibson and Ashby proposed an open-cell foam model for describing cellular material. Their model predicts a power law dependence of Young modulus (m = 2, Equation (II. 18)) and also yield stress with bulk density (n = 2, Equation (II. 19)).

$$E \sim \rho^m \qquad \text{(II. 18)}$$

$$\sigma \sim \rho^n \qquad \text{(II. 19)}$$

In a first approximation, we will take their approach for describing mechanical behavior of “aeropolysaccharides”.

The power-law dependence with density has already been observed for aerogels: inorganic (silica) and organic (e.g resorcinol-formaldehyde, aerocellulose) (Table II. 3). The exponent is usually close to 3 for Young modulus. One explanation might be inhomogeneities such as dandling branches and end chains formed during gelation. These defects hang off the main skeleton of the network and do not contribute to network elastic properties.

Table II. 3 : Power law dependance of Young modulus and yield stress for various aerogels

Type of aerogel/ type of test	Density g/cm^3	m	n	References
Silica 3-points bending	0.07-0.5	3.7±0.2	2.6±0.2	(Woignier, Reynes, Hafidi Alaoui, Beurroies, & Phalippou, 1998)
Silica compression	0.09-0.25	2.9	-	(Alaoui, Woignier, Scherer, & Phalippou, 2008)
Resorcinol-formaldehyde compression	0.04-0.3	2.7±0.2	2.4±0.3	(Pekala, Alviso, & LeMay, 1990)
Aerocellulose compression	0.08-0.23	2.8	2.2-3	(Gavillon, 2007; Sescousse et al., 2011; Sescousse, 2010)

4.4 Thermal properties of aeropolysaccharides

Thermal conductivities of porous materials have three major contributions: the conduction of the skeleton, of the air confined in pores and radiative (Equation (II. 20)).

$$\lambda_{effective} = \lambda_{skeletal} + \lambda_{gas} + \lambda_{radiative} \quad \text{(II. 20)}$$

Two types of methods exist to measure the thermal conductivity of a sample: steady-state (e.g. heat flow meter) and non-steady-state (e.g. hot-wire) and they will be briefly described below.

4.4.1 Heat Flow meter

A solid disk is placed between two plates, one heated at T_h and called “Hot Plate” and the other cooled or heated to lesser extent at T_c and called “Cold Plate” (Figure II. 21). Temperature of the plates is monitored until they are constant (steady state). Determination of the heat flow through the sample from the Hot Plate towards the Cold Plate is achieved by means of a heat flux sensor (meter). Thermal conductivity is calculated according to Equation (II. 21).

$$\lambda = \frac{Q.d}{A.(T_h - T_c)} \quad \text{(II. 21)}$$

with Q quantity of heat passing through the sample (W)
A area of the sample (m²)
d thickness of the sample (m).

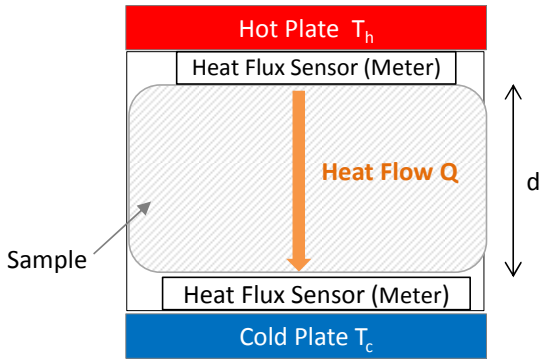

Figure II. 21 : Heat Flow meter device.

Two heat flow meters were used to measure aeropolysaccharide thermal conductivity:
- Laser Comp Fox 150 in Persée Mines ParisTech
- Laser Comp Fox 200 in CSTB, Grenoble. Measurements were kindly performed by Hébert Sallée.
Both set-ups require samples with a large surface of at least 5 cm×5 cm.

Because it is not always straightforward to prepare large, homogeneous aerogels plates without cracks or crinkles for thermal conductivity measurements, CTSB developed a new set-up which requires smaller samples. They conceived an innovative micro thermoflowmeter device, adapted for spherical disks of 4 cm in diameter, which was possible to use directly in their commercial Fox 200 (Figure II. 22).

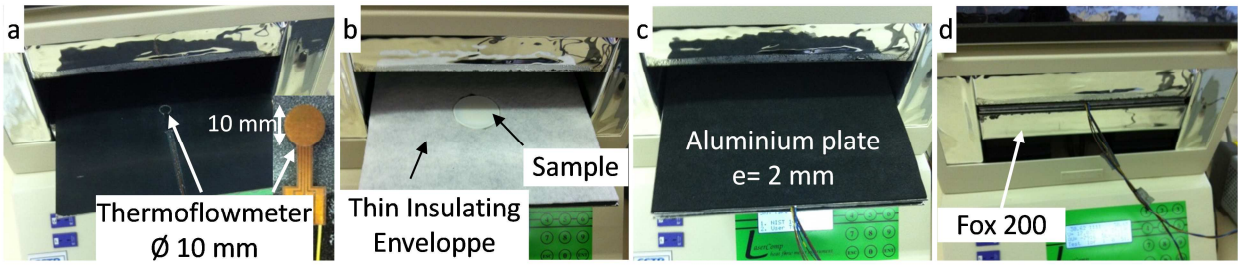

Figure II. 22 : CSTB micro heat flow meter : small thermoflow meters Ø 10mm (a); the sample is embedded in an thin insulating envelope (b), the sample is sandwiched between two aluminium plates with thermoflowmeters (c), the system is directly used in the Fox 200 (d). Courtesy of Hébert Sallée, CSTB, Grenoble.

Two small (10 mm in diameter) thermoflowmeters (Figure II. 22a) are fitted into aluminium plates (Figure II. 22c) of 2 mm thick. The sample is embedded in a thin insulating envelope to limit heat flow leaks and edge effects (Figure II. 22b). Heat flow and temperature are measured simultaneously. All the system is inserted in the Fox 200 (Figure II. 22d) which maintains the thermal regulation. Calibration was performed on samples with known thermal conductivity.

4.4.2 Hot wire method

The hot wire method is a non-steady state (transient) technique based on the measurement of the temperature rise by a thermocouple in a short distance from a linear heat source (hot wire). (Figure II. 23). The heating wire and the temperature sensor are placed between two identical samples with parallel and smooth surfaces, to ensure the best thermal contact.

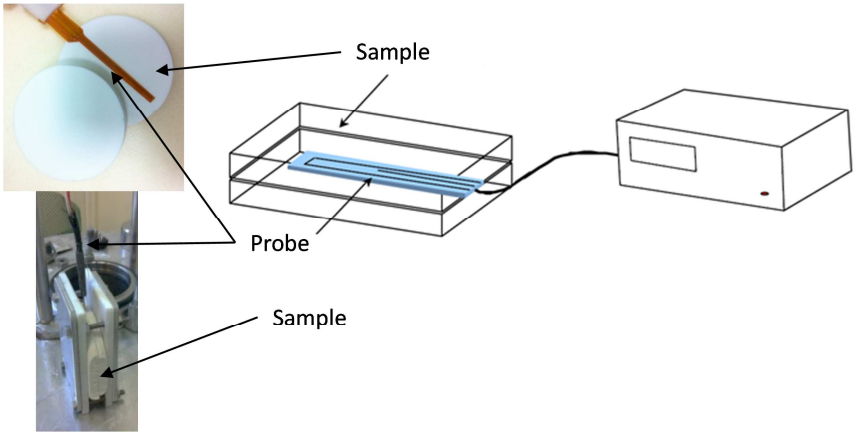

Figure II. 23 : Hot wire device in CSTB-Grenoble. Courtesy of Hébert Sallée.

If the hot wire is far enough from the distance where the measurement takes place, it will be assimilated to an ideal, infinite and long line heat source. Therefore the heat transfer can be monodimensional in cylindrical geometry and the temperature rise be simplified to Equation (II. 22).

$$\Delta T = \frac{Q}{4\pi.\lambda}\ln(\frac{4.a.t}{r^2.C}) \qquad \text{(II. 22)}$$

with Q : quantity of heat production per unit time and per unit length of the heating wire ($W.m^{-1}$)
λ the thermal conductivity ($W.m^{-1}.K^{-1}$),
a thermal diffusivity ($m^2.s^{-1}$) $a = \frac{\lambda}{\rho\, Cp}$ with ρ bulk density ($kg.m^{-3}$) and C_p the heat capacity ($J.kg^{-1}.K^{-1}$),
r: distance between the heating wire and the thermocouple,
C is a constant C≈1.781 ($=e^{\gamma}$ with γ the Euler constant),
and t is time.

The thermal conductivity of the sample can thus be estimated from temperatures T_1 and T_2 taken at different times of measurements t_1 and t_2 by Equation (II. 23).

$$\lambda = \frac{Q}{4\pi}\frac{\ln t_2 - \ln t_1}{T_2 - T_1} \qquad \text{(II. 23)}$$

Transient methods like hot-wire method do not require the signal to wait for a steady-state situation. Instead, the signal is studied as a function of time. The main advantage is that it is

quicker, but it requires identical samples with diameter of at least 6 cm (to be in the approximation of the infinite heating wire).
Measurements were kindly performed by H.Sallée from CSTB, Grenoble.

4.4.3 Measurements of thermal properties of aeropolysaccharides

The effective conductivity of aerocelluloses prepared from ionic liquids was measured by a hot-wire system in CSTB-Grenoble; and aerocelluloses prepared from 8%NaOH was measured by heat flowmeter Fox150 in Persée Mines-ParisTech at 20°C (293 K) (Chapter III).

Aerocelluloses from cross-linked cellulose in NaOH (Chapter IV) and aeropectins (Chapter VI) were analysed by a heat flowmeter Fox150 in Persée-Mines ParisTech and on a Fox 200 adapted to small samples heat flow meter in CSTB-Grenoble (see above for details) at 20°C (293 K).

The radiative contribution $\lambda_{radiative}$ was determined by varying the temperature on the Fox 150 in Persée-Mines ParisTech. The extrapolation of the plot $\lambda = f(T^3)$ towards $T \rightarrow 0$ allows to suppress radiative effect and gives $\lambda_{gas}+\lambda_{solid}$. We can then easily evaluate $\lambda_{radiative}$ by Equation (II. 24).

$$\lambda_{radiative} = \lambda_{effective}\,(293K) - (\lambda_{gas} + \lambda_{solid}) \qquad \text{(II. 24)}$$

The conductivity of solid skeleton λ_{solid} was measured at low pressure (10^{-6} hPa) and low temperature (-118°C) by hot-wire device in CSTB, Grenoble presented in Figure II. 24. The probe and sample are placed in a sphere under vacuum which is then immersed in a liquid nitrogen dewar.

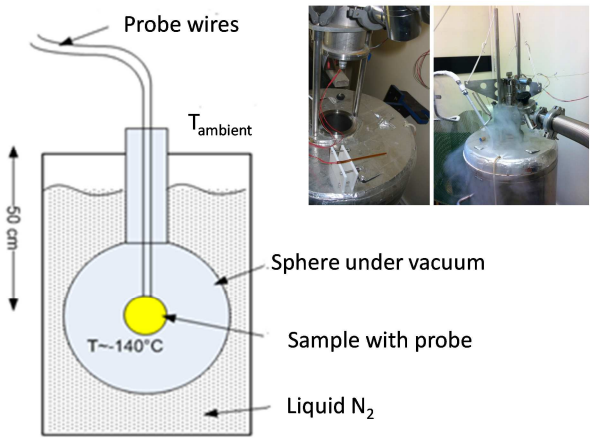

Figure II. 24 : Hot wire apparatus in CSTB for thermal conductivity at low pressure (10^{-6} hPa) and low temperature (-118°C). Courtesy of Hébert Sallée.

Aeropolysaccharides thermal conductivity was also studied as a function of pressure on a hot-wire apparatus in CSTB, Grenoble. The contribution of radiative heat transfer and solid conduction $\lambda_{radiative}+\lambda_{solid}$ was then measured. The solid conductivity λ_{solid} was deduced and compared to the direct measurement at low pressure and temperature.

Conclusions

In this chapter, we reviewed materials for preparing polysaccharides-based porous structures and methods for characterising structurally, mechanically and thermically these "aeropolysaccharides".

First, we presented cellulose, pectin, cellulose acetate and lignin as starting materials and solvents of polysaccharides.
We described the general preparation of aeropolysaccharides from dissolution of polysaccharides, coagulation in a non-solvent and drying with supercritical CO_2.
Each step was detailed: dissolution described by rheology, coagulation in various solvents and drying either by $scCO_2$ or freeze-drying.

Microstructural properties were characterised by texture observed by SEM and by several important parameters: bulk and skeletal densities, specific surface area and pore size distributions.
Bulk densities were determined by two different techniques, Hg pycnometry and powder envelope analyser. Skeletal density was determined by He pycnometry. Specific surface area was calculated from N_2 adsorption and the BET theory. Pore size distributions were evaluated by two different approaches: N_2 desorption by the BJH model and Hg porosimetry with the Pirard's reconstruction.

Mechanical behaviour was studied by uniaxial compressive tests and characteristic parameters as Young modulus, yield stress were determined from the stress-strain deformation curve. We took in a first approximation the model of foams by Ashby and Gibson which gives a power law dependence of Young modulus and yield stress with bulk density.

Thermal conductivities of porous materials have three major contributions: the conduction of the skeleton, of the air confined in pores and radiative. We used two types of methods for measuring the effective (total) thermal conductivity of aeropolysaccharides: heat flowmeter and hot-wire. The radiative heat transfer was determined on heat flowmeter by varying temperature. The contribution of the solid phase was measured by hot-wire at low pressure and low temperature. The conduction of the gaseous phase was then obtained by subtraction of the radiative and solid phase conductivities to the effective conductivity.

Bibliography

Alaoui, A. H., Woignier, T., Scherer, G. W., & Phalippou, J. (2008). Comparison between flexural and uniaxial compression tests to measure the elastic modulus of silica aerogel. *Journal of Non-Crystalline Solids*, *354*(40-41), 4556–4561.

Chang, C., Zhang, L., Zhou, J., Zhang, L., & Kennedy, J. F. (2010). Structure and properties of hydrogels prepared from cellulose in NaOH/urea aqueous solutions. *Carbohydrate Polymers*, *82*(1), 122–127.

Chatjigakis, A., Pappas, C., & Polissiou, M. (1998). FT-IR spectroscopic determination of the degree of esterification of cell wall pectins from stored peaches and correlation to textural changes. *Carbohydrate Polymers*, *37*(4), 395–408.

Egal, M., Budtova, T., & Navard, P. (2007). Structure of aqueous solutions of microcrystalline cellulose/sodium hydroxide below 0°C and the limit of cellulose dissolution. *Biomacromolecules*, *8*(7), 2282–7.

Fischer, F., Rigacci, A., Pirard, R., Berthon-Fabry, S., & Achard, P. (2006). Cellulose-based aerogels. *Polymer*, *47*(22), 7636–7645.

Gavillon, R. (2007). Préparation et caractérisation de matériaux cellulosiques ultra poreux. *PhD thesis*, Ecole des Mines de Paris.

Gavillon, R., & Budtova, T. (2007). Kinetics of cellulose regeneration from cellulose--NaOH--water gels and comparison with cellulose--N-methylmorpholine-N-oxide--water solutions. *Biomacromolecules*, *8*(2), 424–32.

Gavillon, R., & Budtova, T. (2008). Aerocellulose: new highly porous cellulose prepared from cellulose-NaOH aqueous solutions. *Biomacromolecules*, *9*(1), 269–77.

Gericke, M., Fardim, P., & Heinze, T. (2012). Ionic liquids--promising but challenging solvents for homogeneous derivatization of cellulose. *Molecules (Basel, Switzerland)*, *17*(6), 7458–502.

Gibson, L. J., & Ashby, M. F. (1999). *Cellular Solids: Structure and Properties*. Cambridge University Press.

Gnanasambandam, R. (2000). Determination of pectin degree of esterification by diffuse reflectance Fourier transform infrared spectroscopy. *Food Chemistry*, *68*(3), 327–332.

Luciani, L., Denoyel, R., & Rouquerol, J. (2003). Texture des matériaux pulvérulents ou poreux, *Techniques de l'Ingénieur*, 1-24.

Pekala, R. W., Alviso, C. T., & LeMay, J. D. (1990). Organic aerogels: microstructural dependence of mechanical properties in compression. *Journal of Non-Crystalline Solids*, *125*(1–2), 67–75.

Pirard, R, Alié, C., & Pirard, J. (2002). Characterization of porous texture of hyperporous materials by mercury porosimetry using densification equation. *Powder technology*, *128*(2-3), 242–247.

Pirard, R, Blacher, S., Brouers, F., & Pirard, J. P. (1995). Interpretation of mercury porosimetry applied to aerogels. *Journal of Materials Research*, *10*(08), 2114–2119.

Pirard, R., & Pirard, J.-P. (1997). Aerogel compression theoretical analysis. *Journal of Non-Crystalline Solids*, *212*(2-3), 262–267.

Sescousse, R. (2010). Nouveaux matériaux cellulosiques ultra-poreux et leurs carbones à partir de solvants verts. *PhD thesis*, Mines ParisTech.

Sescousse, R., & Budtova, T. (2009). Influence of processing parameters on regeneration kinetics and morphology of porous cellulose from cellulose–NaOH–water solutions. *Cellulose*, *16*(3), 417–426.

Sescousse, R., Gavillon, R., & Budtova, T. (2011). Aerocellulose from cellulose–ionic liquid solutions: Preparation, properties and comparison with cellulose–NaOH and cellulose–NMMO routes. *Carbohydrate Polymers*, *83*(4), 1766–1774.

Sing, K. S. W., Everett, D. H., Haul, R. A. W., Moscou, L., Pierotti, R., Rouquerol, J., & Siemieniewska, T. (1985). Reporting physisorption data for gas/solid systems with special reference to the determination of surface area and porosity. *Pure Appl Chem*, *57*(4), 603–619.

Synytsya, A. (2003). Fourier transform Raman and infrared spectroscopy of pectins. *Carbohydrate Polymers*, *54*(1), 97–106.

Urias-Orona, V., Rascón-Chu, A., Lizardi-Mendoza, J., Carvajal-Millán, E., Gardea, A. A, & Ramírez-Wong, B. (2010). A novel pectin material: extraction, characterization and gelling properties. *International journal of molecular sciences*, *11*(10), 3686–95.

Winter, H., & Chambon, F. (1986). Analysis of linear viscoelasticity of a crosslinking polymer at the gel point. *Journal of Rheology*, *30*(2), 367–382.

Woignier, T., Reynes, J., Hafidi Alaoui, A., Beurroies, I., & Phalippou, J. (1998). Different kinds of structure in aerogels: relationships with the mechanical properties. *Journal of Non-Crystalline Solids*, *241*(1), 45–52.

Zhou, J., Chang, C., Zhang, R., & Zhang, L. (2007). Hydrogels prepared from unsubstituted cellulose in NaOH/urea aqueous solution. *Macromolecular bioscience*, *7*(6), 804–9.

Chapter III

Microstructural and thermal properties of Aerocelluloses from different solvents:

8%NaOH-water, EMIMAc and EMIMAc-DMSO

Introduction

Aerocellulose structure and properties were studied when prepared in either NMMO (Liebner et al., 2009; Sescousse, Gavillon, & Budtova, 2011), 8%NaOH-water (Gavillon & Budtova, 2008; Gavillon, 2007) and ionic liquid EMIMAc (Sescousse et al., 2011; Sescousse, 2010).

Ionic liquids present major advantages such as the high cellulose dissolution power (up to 27-30$_{wt}$%, (Lovell et al., 2010)), very low vapour pressure and high thermal stability (as compared to cellulose). Due to high cellulose-EMIMAc solutions viscosities and the high price of EMIMAc, the addition of co-solvent to ionic liquid was investigated for performing cellulose derivatisation in homogeneous conditions (Gericke, Liebert, Seoud, & Heinze, 2011). DMSO (dimethylsulfoxide) is one of the promising candidates to be mixed with ionic liquid, and recent studies show that DMSO does not modify the ability of EMIMAc to dissolve cellulose (Lv et al., 2012; Le, Rudaz, & Budtova, 2013).

We will study the influence of the addition of DMSO to EMIMAc on the morphological properties of aerocelluloses. We will correlate texture, bulk density, specific surface areas, porosity and pore size distributions with cellulose concentration.

The effective thermal conductivity of aerocelluloses prepared in the solvent EMIMAc/DMSO, will be measured for the first time and compared to aerocelluloses prepared from 8%NaOH. The influence of pore size distributions on thermal properties of aerocelluloses will be discussed.

Introduction

Les propriétés structurales des aérocelluloses préparées dans différents solvants, comme la NMMO (Liebner et al., 2009; Sescousse, Gavillon, & Budtova, 2011), 8%NaOH-eau (Gavillon & Budtova, 2008; Gavillon, 2007) ou les liquides ioniques (Sescousse et al., 2011; Sescousse, 2010), ont déjà été étudiées précédemment.

Les liquides ioniques sont particulièrement intéressants et présentent une importante capacité de dissolution de la cellulose (allant jusqu'à 27-30$_{wt}$%, (Lovell et al., 2010)), une faible tension de vapeur saturante et une grande stabilité thermique. Cependant, les solutions de cellulose-EMIMAc sont hautement visqueuses et onéreuses. L'ajout de co-solvants aux liquides ioniques a été étudié pour dériver la cellulose dans des conditions homogènes (Gericke, Liebert, Seoud, & Heinze, 2011). Le diméthylsulfoxyde (DMSO) est un bon candidat comme co-solvant à l'EMIMAc et de récentes études ont montré qu'il n'altérait pas la capacité de dissolution de l'EMIMAc (Lv et al., 2012; Le, Rudaz, & Budtova, 2013).

L'influence de l'ajout de DMSO à l'EMIMAc sur les propriétés morphologiques des aérocelluloses sera étudiée. La texture, la densité apparente, la surface spécifique, la porosité et la distribution de taille de pores seront comparées en fonction de la concentration en cellulose.

La conductivité thermique des aérocelluloses préparées à partir du solvant EMIMAc/DMSO sera mesurée et comparée à celle des aérocelluloses préparées dans 8%NaOH-eau. L'influence de la distribution de taille de pores sur les propriétés thermiques sera discutée.

1. Importance of co-solvent addition to ionic liquid

1.1 Introduction

In Chapter I, we showed that various morphologies of aerocelluloses can be obtained depending on the solvent: fibrous for 8%NaOH-water and globular from molten NMMO and EMIMAc (Sescousse et al., 2011) (Figure III. 1).

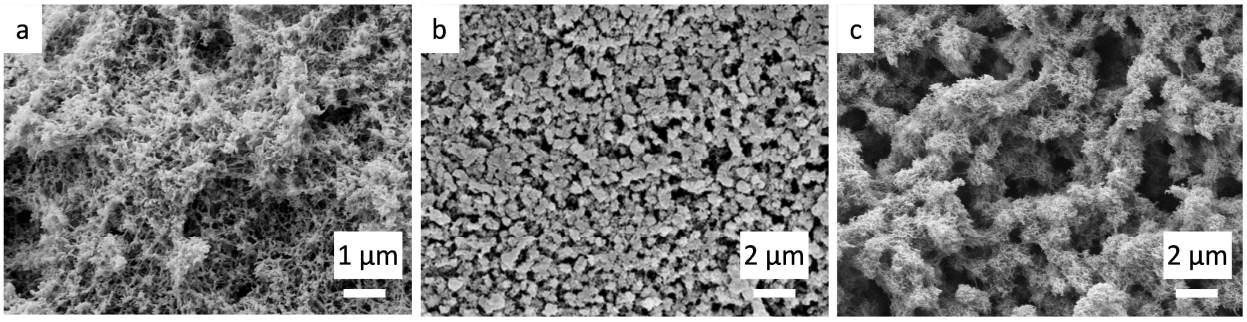

Figure III. 1 : Various morphologies of aerocelluloses from cellulose solutions in 8%NaOH (a); NMMO (b); Ionic Liquid EMIMAc (c) (Sescousse et al., 2011). Reprinted from (Sescousse et al., 2011), Copyright (2011), with permission from Elsevier.

In order to prepare aerocellulose, cellulose-EMIMAc solutions are placed in a coagulation bath, usually water. We looked in details on structure formation during cellulose coagulation from cellulose-EMIMAc in water. It has recently been reported that EMIMAc and water are interacting, without the formation of new compounds, but the mixing of the two fluids is exothermal (Hall et al., 2012). The evolution of mixture (EMIMAc + water) temperature in time from the moment when water is added to EMIMAc is presented in Figure III. 2. As soon as even a small amount of water is added to IL the mixture, temperature increases rapidly and significantly. As an example for water molar ratio of 0.2, temperature raised from 21°C to 30.6 °C in less than 40 seconds. The most pronounced effect was recorded for the mixture with water molar ratio of 0.7 with a temperature increase from 21°C to 57°C.

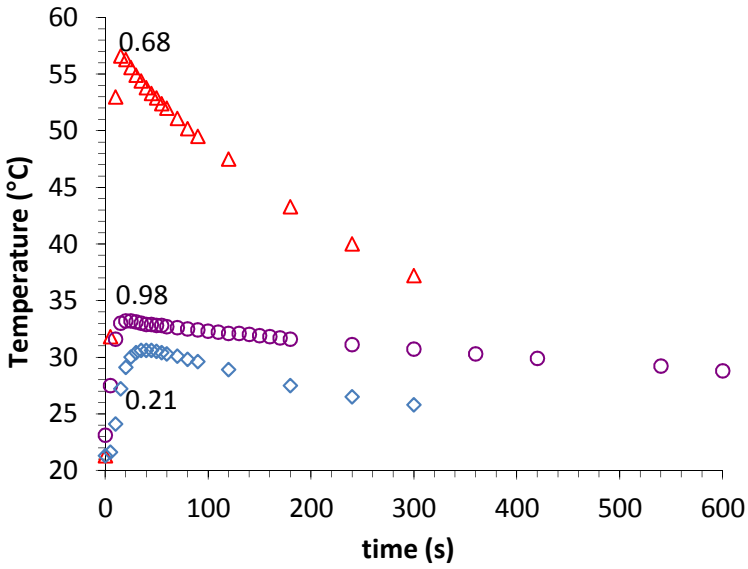

Figure III. 2 : Examples of the evolution of mixture temperature in time for various water mole fractions in the mixture EMIMA/water (Hall et al., 2012).

During coagulation step, EMIMAc is mixed with water, creating strong temperature gradients inside cellulose. This may modify the structure of porous cellulose with the formation of macrochannels or very large macropores. These macropores may be few millimeters large and visible by a naked eye (Figure III. 3a) or few tens of microns as observed by SEM (Figure III. 3c). The mixing of EMIMAc and ethanol is less exothermic thus less heterogeneities are visible in the aerocellulose (Figure III. 3b). These inhomogeneities are more pronounced for high cellulose concentrations (> 5%).

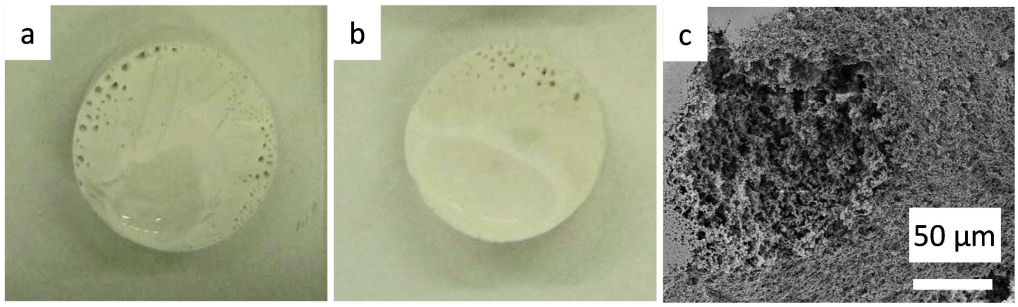

Figure III. 3 : Effects of exothermal reactions between EMIMAc and water on aerocellulose : 20_{wt}% aerocellulose coagulated in water (a); 20_{wt}% aerocellulose coagulated in ethanol (b); SEM images of a macrochannel in a 20_{wt}% aerocellulose coagulated in water (c).

The mixture of cellulose-EMIMAc is highly viscous. For example, the viscosity of a 10_{wt}% polymer-IL solution is about 40 000 times more viscous than water at 20°C (~ 40 Pa.s) (Gericke, Schlufter, Liebert, Heinze, & Budtova, 2009; Sescousse, Le, Ries, & Budtova, 2010). High viscosities of cellulose-ionic liquids solutions create inhomogeneities inside the structure. Air bubbles may be trapped into solutions, even after centrifugation, which weaken the structural and mechanical properties of aerocelluloses.

1.2 DMSO, a smart choice of co-solvent

EMIMAc is still relatively expensive and is a viscous solvent. In order to decrease the viscosity of cellulose-EMIMAc solutions, the addition of a co-solvent was investigated. Dimethylsulfoxide (DMSO) was chosen for several reasons: first it is a cellulose swelling agent but it is not a solvent, it is widely used for chemistry on cellulose derivatives, it is cheap and easily available. Moreover, (Gericke et al., 2011) showed that up to 10 g of DMSO can be dissolved per gram of cellulose solution (at 10_{wt}% in EMIMAc), i.e. 10_{wt}% cellulose can be dissolved in a solvent 8.3% EMIMAc / 91.7% DMSO (Figure III. 4).

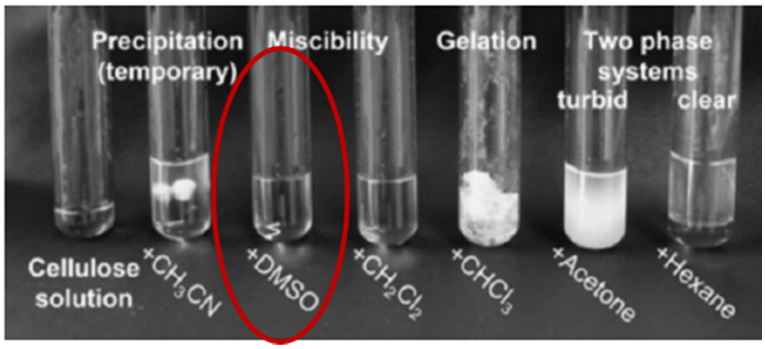

Figure III. 4 : Mixtures of cellulose/EMIMAc solutions with different co-solvents (Gericke et al., 2011). Reprinted with permission from (Gericke et al., 2011). Copyright (2011) Wiley.

The first question to ask is what is the maximal concentration of cellulose that can be dissolved in EMIMAc/DMSO mixture as a function of DMSO concentration? In other words, cellulose/EMIMAc/DMSO phase diagram must be obtained. The work described below was performed in Cemef Mines-Paristech together with another PhD student Kim-Anh Le.

Cellulose-EMIMAc-DMSO solutions, with DMSO ratio varying from 1 to 86_{wt}% in the mixture EMIMAc/DMSO, were carefully analysed with optical microscopy using polarized and non-polarized light in the view of the presence of non-dissolved cellulose. The dissolution of cellulose in EMIMAc/DMSO mixture is presented in Figure III. 5. It shows the decrease of cellulose concentration in solution with the increase of DMSO content, as expected.

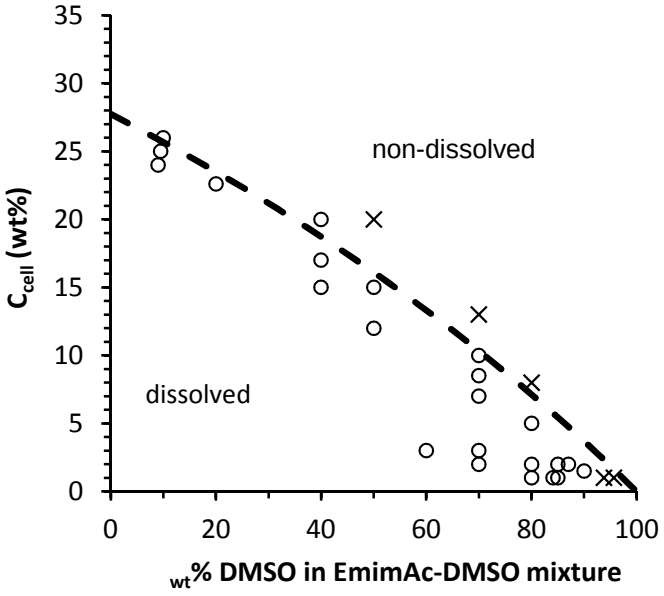

Figure III. 5 : Cellulose solubility in EMIMAc/DMSO mixture.
Crosses correspond to non-dissolved cellulose and open points – to dissolved.
Dashed lines corresponds to 1 anhydroglucose unit binding 2.5 mol of EMIMAc and indicates an approximate boundary between homogeneous (solution) and heterogeneous (presence of non-dissolved cellulose) areas (Le et al., 2013).

Based on the results presented in Figure III. 5, the phase diagram was built (Figure III. 6). For example, the point A has a formulation of 22_{wt}% cellulose – 58_{wt}% EMIMAc – 20_{wt}% DMSO (Equation (III. 1)). We can convert these proportions to the mass ratio of DMSO in the solvent EMIMAc-DMSO by Equation (III. 2). In the example A, the solvent ratio is 74.4_{wt}% EMIMAc/25.6_{wt}% DMSO. In other words, by replacing 25_{wt}% of EMIMAc by DMSO it is still possible to dissolve 20_{wt}%cellulose.

$$X_{cellulose} + X_{DMSO} + X_{EMIMAc} = 100 \quad \text{(III. 1)}$$

$$Y_{DMSO\ in\ the\ solvent} = \frac{X_{DMSO}}{X_{DMSO} + X_{EMIMAc}} \quad \text{(III. 2)}$$

Similarly, the point C gives a formulation of 10_{wt}% cellulose – 25_{wt}% EMIMAc – 65_{wt}% DMSO. Even by having a large proportion of DMSO it is still possible to dissolve 10_{wt}% cellulose.

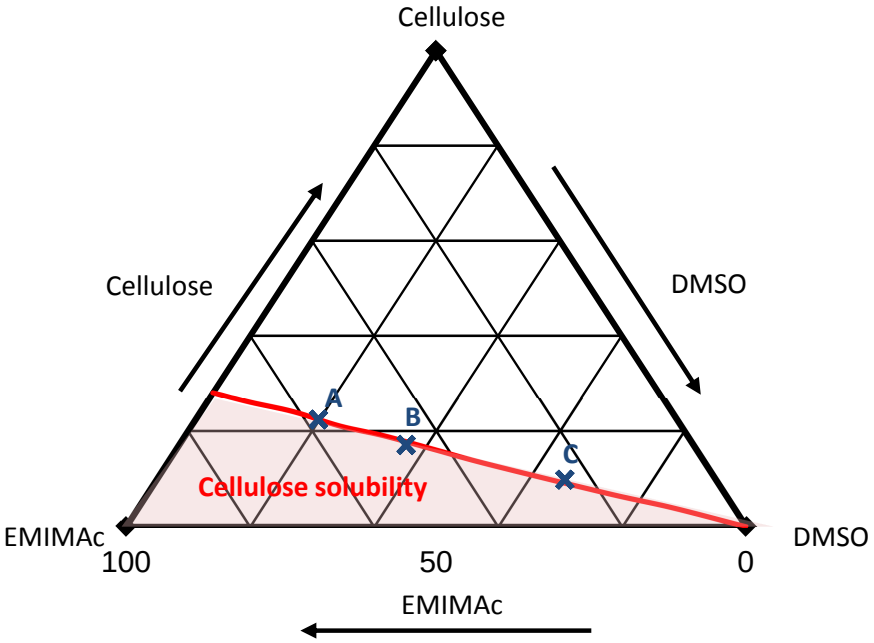

Figure III. 6 : Cellulose solubility phase diagram (shaded area) in EMIMAc-DMSO. Concentrations are in $_{wt}$% (Le et al., 2013).

The viscosity of mixtures EMIMAc/DMSO was also studied (Le et al., 2013). By replacing 40_{wt}% of EMIMAc by DMSO the viscosity is divided by a factor 10: the solution viscosity decreases from 0.1 Pa.s for pure EMIMAc to 0.015 Pa.s for 40%DMSO/60% EMIMAc at 20°C. It should be noted that it is still possible to dissolve almost 20_{wt}% of cellulose (point B in Figure III. 6).

We demonstrated that DMSO allows decreasing cellulose-EMIMAc solutions viscosity while still dissolving high cellulose concentrations. However, we do not have much information on the influence of DMSO on structure formation during cellulose coagulation.

In the next section, we will therefore examine the influence of DMSO on the final morphology of aerocelluloses and we will compare new samples to aerocelluloses prepared from pure EMIMAc and 8%NaOH-water.

2. Microstructural properties of Aerocelluloses

2.1 Influence of DMSO on the aerocellulose texture

The ratio of solvent and co-solvent, 60_{wt}% EMIMAc / 40_{wt}% DMSO, has been carefully chosen to have a compromise between the maximum cellulose concentration possible to dissolve and an optimized viscosity that easies up the process of preparation. The addition of 40%DMSO allows to dissolve 18-20_{wt}% cellulose (Figure III. 6), thus we can easily explore a large range of aerocellulose morphology prepared from solutions from semi-dilute to concentrated states.

Cellulose - 60% EMIMAc / 40% DMSO solutions were prepared and then coagulated either in water or ethanol (c.f. Chapter II). Water is not compatible with supercritical CO_2 and coagulated-in water cellulose was afterwards washed several times with ethanol and dried by $scCO_2$. Structural properties of aerocelluloses, from 5 to 20_{wt}% cellulose, prepared in pure EMIMAc and in a mixture of 60% EMIMAc / 40% DMSO were studied and compared.

Macroscopically, aerocelluloses from EMIMAc/DMSO seem more homogeneous (Figure III. 7). At high concentrations (e.g. 15_{wt}%), cellulose coagulated in ethanol presents no inhomogeneities (Figure III. 7b) and for cellulose coagulated in water the formation of macroscopic holes is significantly decreased (Figure III. 7a). This improvement is mainly due to the decrease of the viscosity of the cellulose-solvent solution and the decrease of interactions between water and EMIMAc as 40% of ionic liquid has been replaced.

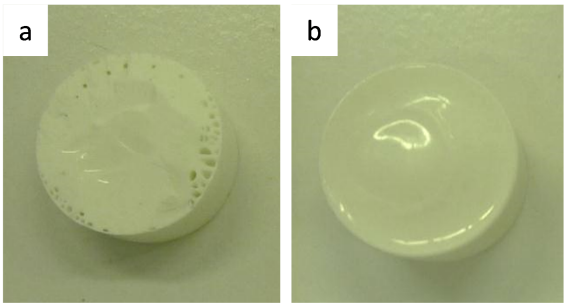

Figure III. 7 : Aerocelluloses prepared from 15_{wt}% cellulose-60%EMIMAc-40% DMSO solutions coagulated in water (a); ethanol (b).

2.2 Comparison of aerocelluloses from different solvents

Bulk and skeletal densities, specific surface areas and porosity of three different kinds of aerocelluloses are presented in Table III.1. They are prepared from:
- dissolution in EMIMAc and coagulation in ethanol,
- dissolution in 60%EMIMAc-40%DMSO and coagulation in ethanol,
- dissolution in 60%EMIMAc-40%DMSO and coagulation in water (then exchanged with ethanol for drying),
- dissolution in 8%NaOH-water and coagulation in water (then exchanged with ethanol for drying).

Table III. 1 : Comparison of 5_{wt}% aerocellulose prepared in EMIMAc (coagulated in ethanol), in 60%EMIMAc/40%DMSO (coagulated in water and ethanol) and in 8%NaOH-water (coagulated in water).

Solvent	EMIMAc	60% EMIMAc/40%DMSO		8%NaOH-water
Coagulation bath	Ethanol	Ethanol	Water	Water
ρ_{bulk} (g/cm³)	0.15	0.17	0.18	0.12
$\rho_{skeletal}$ (g/m²)	1.56	1.54	1.53	1.55
S_{BET} (g/m²)	199	197	246	286
Porosity ε (%)	91%	89%	88%	92%

First, we compared 5_{wt}% aerocellulose prepared in pure EMIMAc and in 60% EMIMAc / 40% DMSO, coagulated in ethanol. Skeletal density is very similar and close to the density of solid cellulose (1.55 g/cm^3) as expected since aerocellulose is only made of cellulose. Porosity is calculated according to Equation (III. 3) (c.f. Chapter II). It is in both cases around 90%.

$$\varepsilon(\%) = 1 - \frac{\rho_{bulk}}{\rho_{skeletal}} \qquad \text{(III. 3)}$$

Specific surface areas are identical for aerocelluloses from EMIMAc and EMIMAc/DMSO solvents. The bulk density of aerocellulose from EMIMAc solutions are slightly lower (ρ = 0.15 g/cm^3) than for EMIMAc/DMSO (ρ = 0.17 g/cm^3). One explanation may be the presence of very large macropores in aerocellulose-EMIMAc that appeared because of air bubbles, compared to the EMIMAc-DMSO counterpart. The presence of “holes” inside the sample obviously enlightens the final material.

We studied also the influence of the coagulation bath, water vs ethanol, on the final morphology of 5_{wt}% cellulose in 60% EMIMAc / 40% DMSO. Bulk and skeletal densities, and porosity are very similar. Specific surface area is slightly higher for the coagulation in water.

Finally, we compared 5_{wt}% aerocellulose from 60% EMIMAc / 40% DMSO and from 8% NaOH-water, both coagulated in water. Aerocellulose from 8% NaOH is also highly porous (> 90%) and presents a lower bulk density, and a higher specific surface area. Aerocellulose from ionic liquids is denser which means that either it has smaller pores or pores walls are thicker than aerocellulose from 8% NaOH. However, as the S_{BET} is lower it seems that the second hypothesis may be more likely.
We studied the texture of aerocelluloses from IL by SEM observations (Figure III. 8). At the same cellulose concentration, aerocellulose from EMIMAc (Figure III. 8a) and from EMIMAc/DMSO (Figure III. 8b) presents exactly the same globular network, and pores sizes appear also very similar.

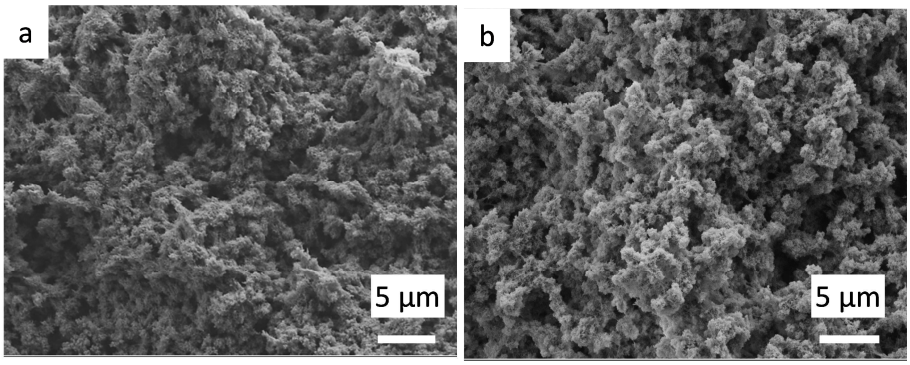

Figure III. 8 : SEM images of aerocellulose prepared from 5_{wt}% cellulose in EMIMAc (a) and in 60% EMIMAc / 40% DMSO (b), coagulated in ethanol.

A more detailed pore size distribution (PSD) was performed by Hg porosimetry in the laboratory L2C in the University of Montpellier. First, the buckling constant k, used in the Pirard's theory (c.f. Chapter II) of pores size "reconstruction" was determined for 5_{wt}% aerocellulose from EMIMAc, coagulated in water resulting in k = 115 nm.MPa$^{0.25}$. Unfortunately, we did not get the buckling constant for 5_{wt}% EMIMAc / DMSO, coagulated in water. Due to their high similarities in structural properties, we opted to use the same value as for 5_{wt}%-EMIMAc aerocellulose. Similarly, we evaluated the buckling constant for 5_{wt}% - 8%NaOH aerocellulose, coagulated in water. Its value is much lower, k = 56 nm.MPa$^{0.25}$.

Figure III. 9 gives the PSD of 5_{wt}% aerocellulose prepared either in EMIMAc, 60% EMIMAc / 40% DMSO or 8% NaOH-water and all coagulated in water.

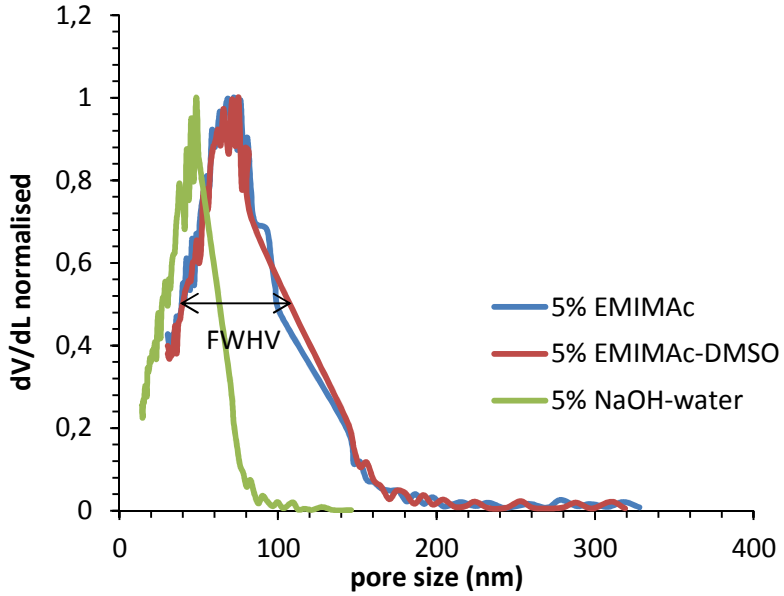

Figure III. 9 : PSD for aerocelluloses from 5_{wt}% cellulose in EMIMAc, 60%EMIMAc/40%DMSO and 8%NaOH-water, coagulated in water.

First, we studied PSD of aerocelluloses from EMIMAc and EMIMAc / DMSO. Classical structural parameters $L_{p\ mean}$, $L_{p\ max}$ and full width at half value (FWHV), presented in Chapter II,

are summarized in Table III. 2. They are very similar, with $L_{p\ max} \approx 75$ nm, $L_{p\ mean} \approx 60$-65 nm and FWHV ≈ 60 nm.

The pore size distribution of aerocellulose prepared in 8%NaOH-water seems narrower with a FWHV of 31 nm, half of IL-based aerocelluloses (Figure III. 9). Aerocellulose prepared from 8% NaOH-water appears to be finer structured compared to EMIMAc-based aerocelluloses which confirms results on specific surface areas. It might be possible that entangled strands of cellulose create smaller pores than a globular morphology of cellulose.

Table III. 2 : PSD data by Hg porosimetry from 5_{wt}% aerocellulose in EMIMAc, 60%EMIMAc/40%DMSO and 8%NaOH-water and coagulated in water.

$\%C_{cellulose}$	Solvent	ρ_{bulk} (g/cm^3)	S_{BET} (m^2/g)	$L_{p\ max}$ (nm)	$L_{p\ mean}$ (nm)	FWHV (nm)
5	EMIMAc	0.114	225	72	65	56
5	EMIMAc/DMSO	0.186	256	75	61	66
5	8%NaOH-water	0.123	286	-	-	31

We showed from morphological characterisations that the addition of DMSO to EMIMAc seems not to have effects on the morphological properties of aerocelluloses.

2.3 Influence of cellulose concentration on the morphology

We studied the influence of cellulose concentration in the solvent 60%EMIMAc-40% DMSO on the texture and structural properties of aerocelluloses. Figure III. 10 shows the evolution of the aerocellulose texture with increasing cellulose concentration from 5 to 15_{wt}%. The structure appears denser and pores seem smaller. At 15_{wt}% cellulose, the globules are not visible and a more homogeneous and compact morphology is observed (Figure III. 10c).

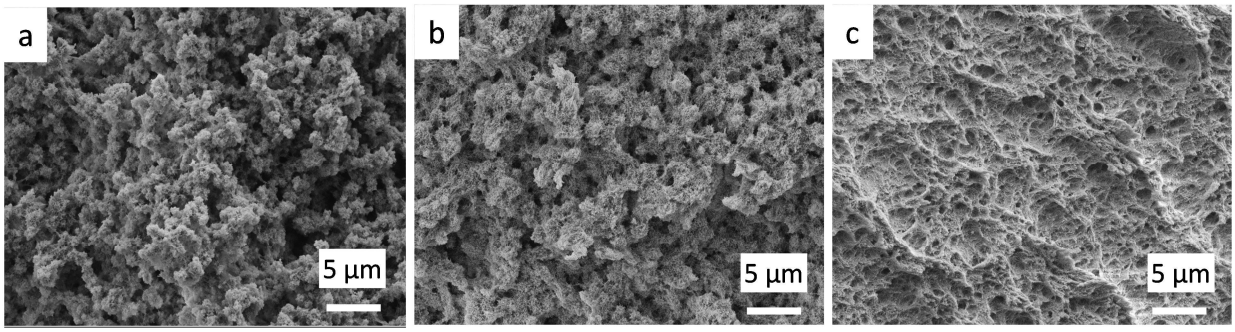

Figure III. 10 : SEM images of aerocellulose prepared from 5_{wt}% (a); 10_{wt}% (b) and 15_{wt}% (c) cellulose in 60wt% EMIMAc/40wt% DMSO, coagulated in ethanol.

The bulk density of aerocelluloses as a function of cellulose concentration is given in Figure III. 11. We compared the influence of the two solvents, pure EMIMAc and 60%EMIMAc-

40%DMSO. No major difference is observed between the two IL systems. Bulk densities increase linearly with cellulose concentration.

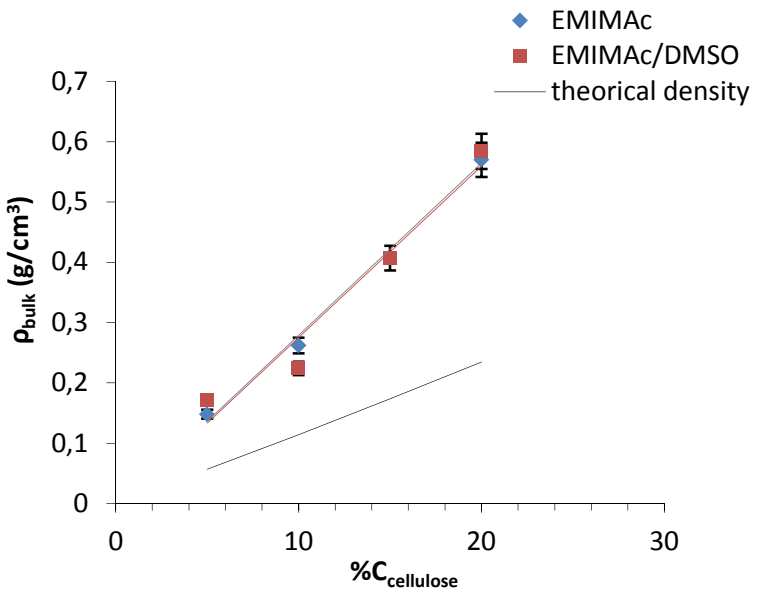

Figure III. 11 : Bulk densities as a function of cellulose concentration for aerocelluloses prepared from 60%EMIMAc/40%DMSO and pure EMIMAc, coagulated in ethanol. A theoretical density for a case of no contraction during all steps of preparation is also added.

We compared bulk densities to the theoretical density ρ_{th}. The latter is calculated according to Equation (III. 4). No contraction means that the volume of the solution (cellulose + solvent) remains constant after drying and the solvent is replaced by air. The final mass is the mass of cellulose + the mass of air that replaced the solvent. We used ρ_{air} = 0.001 g/cm^3, $\rho_{cellulose}$ = $\rho_{skeletal}$ = 1.55 g/cm^3 and ρ_{EMIMAc} = 1.10 g/cm^3.

$$\rho_{th} = \frac{m_{cellulose} + m_{air}}{V_{cellulose+solvent}}$$

$$\rho_{th} = \frac{\%C_{cellulose} + \rho_{air} \times (100 - \%C_{cellulose})}{\frac{\%C_{cellulose}}{\rho_{cellulose}} + \frac{100 - \%C_{cellulose}}{\rho_{EMIMAc}}} \quad \text{(III. 4)}$$

Densities of aerocelluloses in ionic liquids are higher than the theoretical ones mainly due to contraction during the coagulation and scCO$_2$ drying processes.

For a fixed volume, more cellulose is present at high concentrations, therefore the density increases. Figure III. 12 schematises aerocelluloses structure at low and high cellulose concentrations. During coagulation, cellulose chains self-associate. Pores are predicted to be smaller with a larger thickness. The specific surface area is therefore expected to be lower at high cellulose concentrations.

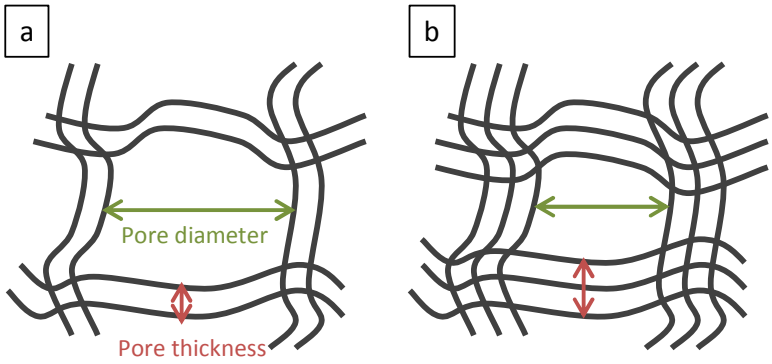

Figure III. 12 : Schematic representations of aerocelluloses structures : from low (a) and high (b) cellulose concentrations.

To confirm our hypothesis, we measured specific surface area by BET and pore size distribution by "reconstruction" from Hg porosimetry (Pirard approach). Both analyses were performed in the laboratory L2C of the University of Montpellier. The influence of cellulose concentration on specific surface area is given in Figure III. 13.

S_{BET} decreases slightly with the increase of cellulose, as an example S_{BET} (5%) = 197 m²/g whereas S_{BET} (20%) = 171 m²/g. It confirms our previous assumption on concentrated aerocelluloses.

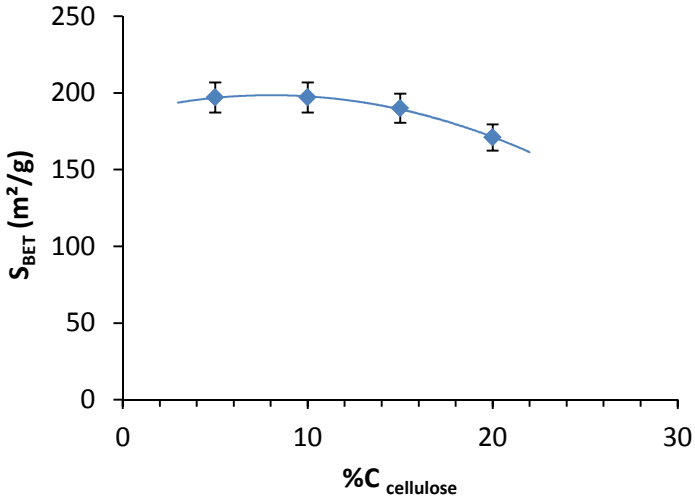

Figure III. 13 : Specific surface area versus cellulose concentration for aerocelluloses from 60%EMIMAc/40% DMSO, coagulated in ethanol.

In order to analyse PSD of aerocellulose as a function of cellulose concentration, the buckling constant must be determined for each concentration as far as wall thickness may increase. As far as the buckling constant was measured only for 5_{wt}% cellulose, unfortunately no comparison of $L_{p\ max}$ and $L_{p\ mean}$ can be performed. What can be compared is the shape and the width of pore size distribution which is independent of the buckling constant. Figure III. 14 presents pore size distributions for 5 and 15_{wt}% cellulose prepared from 60%EMIMAc-40%DMSO mixture with the same buckling constant corresponding to 5% cellulose. The "location" of the distribution for 15% must not be taken into account.

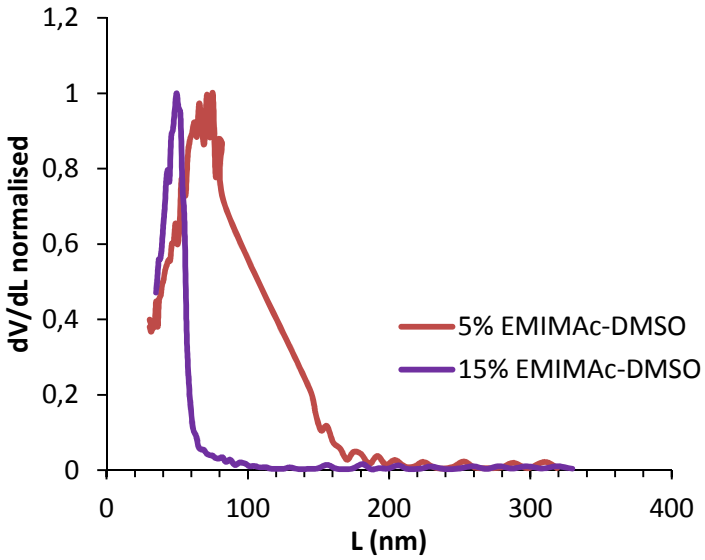

Figure III. 14 : PSD of 5% and 15$_{wt}$% aerocellulose prepared in 60%EMIMAc/40%DMSO.

The FWHV was calculated for both concentrations and is reported in Table III. 3. PSD at higher concentration 15$_{wt}$% is narrower with FWHV=35 nm compared to 74 nm for 5$_{wt}$%. It confirms the previous observations on SEM images.

Table III. 3 : PSD data for 5 and 15$_{wt}$% aerocellulose prepared in 60%EMIMAc/40%DMSO.

%$C_{cellulose}$	Solvent	ρ_{bulk} (g/cm^3)	S_{BET} (m²/g)	FWHV (nm)
5	EMIMAc/DMSO	0.186	256	66
15	EMIMAc/DMSO	0.498	180	20

We showed that cellulose concentration has important effects on the morphological properties of aerocelluloses prepared from 60% EMIMAc/ 40% DMSO, as it was already shown for EMIMAc (Sescousse et al., 2011; Sescousse, 2010). Finally, by changing cellulose concentration, we can easily tune the morphological properties of aerocelluloses depending on the targeted application.

3. Thermal properties of pure aerocelluloses

According to Equation I.5 (Chapter I), thermal conductivity of solid backbone is directly related to the density. To minimise this contribution, a density below 0.15 g/cm^3 will be preferred. We decided therefore to study only aerocellulose at 5$_{wt}$%-7$_{wt}$% cellulose which has a bulk density of 0.12-0.18 g/cm^3 depending on the solvent, EMIMAc / DMSO and 8% NaOH-water.

As it was shown in the previous section, DMSO does not modify morphological properties of aerocelluloses. Using 40% DMSO, the solution of cellulose-EMIMAc-DMSO is slightly too liquid for an easy handling of samples of the coagulation step. Thus we prepared aerocellulose

from a solution 5_{wt}% cellulose dissolved in 80_{wt}% EMIMAc/ 20_{wt}% DMSO and coagulated in ethanol.

The effective thermal conductivities of aerocellulose, prepared either in 80% EMIMAc/ 20% DMSO and 8% NaOH-water, were recorded by two different techniques. They are given in Table III. 4. A direct measurement by hot-wire method was carried out on 5_{wt}% cellulose-IL by Hébert Sallée in CSTB, Grenoble. It gives $\lambda_{effective}$ = 32.8 mW.m^{-1}.K^{-1} for ρ_{bulk} = 0.18 g/cm^3. In Persée Mines-ParisTech, we measured the thermal conductivity of aerocelluloses prepared from 5 and 7_{wt}% in NaOH-water on the heat flowmeter Fox 150 (c.f. Chapter II). We obtained $\lambda_{effective}$ = 30.8 mW.m^{-1}.K^{-1} for ρ_{bulk} = 0.123 g/cm^3 (5_{wt}%) and $\lambda_{effective}$ = 32.2 mW.m^{-1}.K^{-1} for ρ_{bulk} = 0.165 g/cm^3 (7_{wt}%).

Table III. 4 : Thermal characterisations of aerocelluloses from ionic liquid and from 8%NaOH-water. All thermal conductivities are given in mW.m^{-1}.K^{-1}.

$C_{cellulose}$	Solvent	ρ_{bulk} (g/cm^3)	$\lambda_{effective}$ Hot wire CSTB	$\lambda_{effective}$ Fox 150	$\lambda_{gas+solid}$ Fox 150	$\lambda_{radiative}$ Fox 150	λ_{solid} Hot wire CSTB
5	80%EMIMAc-20%DMSO	0.18	32.5	-	-	-	-
5	8%NaOH-water	0.123	-	30.8	21.5	9.3 (30%)	-
7	8%NaOH-water	0.165	-	32.2	23.6	8.6 (27%)	3.2

We plotted effective thermal density as a function of bulk density for aerocelluloses prepared either in ionic liquids or 8%NaOH in Figure III. 15. It decreases with the density no matter the solvent used for aerocellulose preparation. The effective thermal conductivity stands above that of free air (25 mW.m^{-1}.K^{-1}) even at very low density.

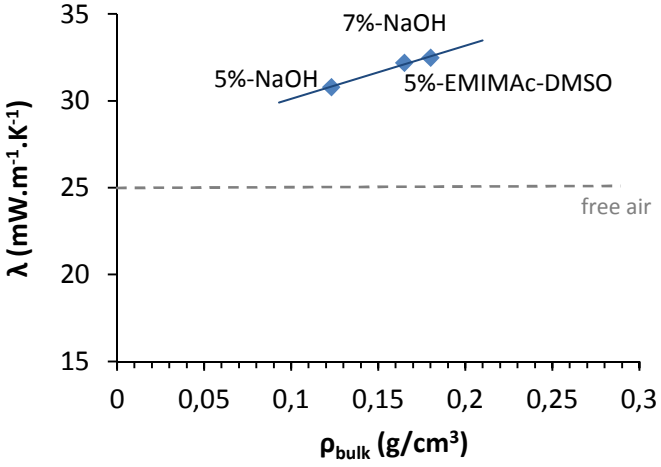

Figure III. 15 : Effective thermal conductivity as a function of bulk density for aerocelluloses from various solvents.

We showed in Chapter I, that pores with size below 70 nm are required to ensure a lower effective thermal conductivity (Knudsen effect). We suppose that macropores present in

aerocellulose structure and observed by SEM, with size of few hundred nm or even few microns, are responsible for higher thermal conductivities.

We studied more precisely the different contributions to the thermal conductivities of aerocelluloses prepared from 8%NaOH-water. We measured the thermal conductivity as a function of temperature on the heat flowmeter Fox 150 in Persée Mines-ParisTech. Results are given in Table III. 4. By extrapolating the curve $\lambda = f(T^3)$ towards $T \rightarrow 0$, we suppressed the contribution of the radiative transfer (c.f. Chapter I) and determined $\lambda_{gas+solid}$. $\lambda_{radiative}$ was then obtained by substraction of $\lambda_{effective} - (\lambda_{gas+solid})$. It contributes at around 30 % of the total thermal conductivity. The decrease of the effective thermal conductivity with density is mainly due to the decrease of the conduction gas + solid (Table III. 4).

Experiments at low pressure (10^{-6} hPa) and low temperature (-118°C) to determine λ_{solid} was carried out on 7_{wt}% cellulose in 8% NaOH-water by hot-wire method in CSTB, Grenoble. We obtained $\lambda_{solid} = 3.2$ mW.m^{-1}.K^{-1} (Table III. 4). We deduced the contribution of the conduction of the gaseous phase to be $\lambda_{gas} = 20.4$ mW.m^{-1}.K^{-1} which represents 63% of the effective thermal conductivity.

The thermal conductivity as a function of pressure for 5_{wt}% aerocellulose prepared in 80% EMIMAc / 20% DMSO was measured by hot wire method in CSTB, Grenoble. $\lambda = f(P)$ is plotted in Figure III. 16. A plateau is observed at low pressure and the value of conductivity is about 12.7 mW.m^{-1}.K^{-1} corresponding to the contribution of $\lambda_{solid}+\lambda_{radiative}$ (c.f. Chapter I). The gas conduction is then evaluated at 19.8 mW.m^{-1}.K^{-1} (by substraction of $\lambda_{effective} - (\lambda_{solid}+\lambda_{radiative})$) and represents 61% of the effective thermal conductivity.

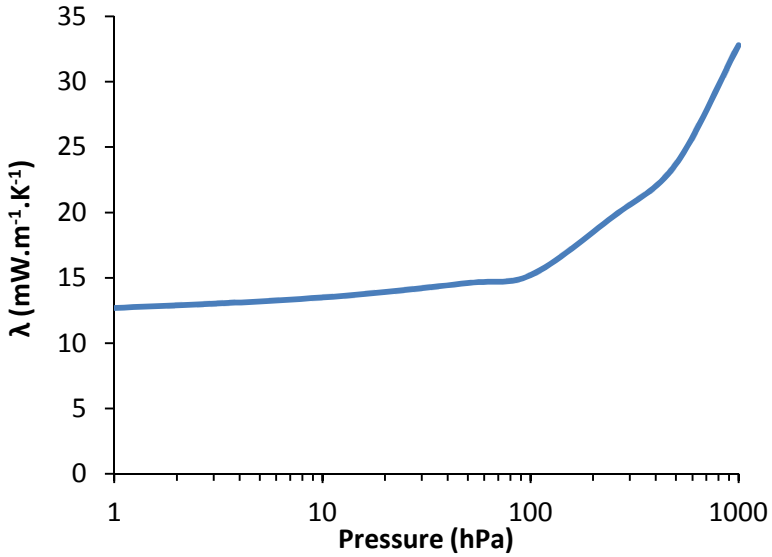

Figure III. 16 : Thermal conductivity as a function of pressure for 5_{wt}% aerocellulose from 80% EMIMAc / 20% DMSO.

We showed that for aerocelluloses from 8% NaOH-water, the radiative conductivity is rather independent on the density. We did not determine $\lambda_{radiative}$ for 5_{wt}% -IL but we suppose that it

should be very similar to aerocelluloses prepared from NaOH solvent, around 30%. We deduced the conductivity of the solid phase from the substraction of ($\lambda_{solid}+\lambda_{radiative}$) – $\lambda_{radiative}$ and obtained λ_{solid} = 12.7-(32.5*30%) ≈ 3 $mW.m^{-1}.K^{-1}$. It is coherent with the direct measurement by hot wire at low temperature and pressure for aerocellulose from 8%NaOH.

Aerocelluloses prepared either in ionic liquids (mixture of EMIMAc and DMSO) and 8% NaOH-water present similar thermal properties, with effective thermal conductivities around 30-32 $mW.m^{-1}.K^{-1}$. Pure aerocelluloses are not therefore super-insulating materials. The main thermal contribution is due to the conduction of the gaseous phase which represents more than 60% of the total conductivity. In order to decrease the gaseous conductivity and thus effective thermal conductivity, it is necessary to improve the porous structure with pores lower than the free mean path of air (70 nm) and to tend towards a nano-structuration.

Conclusions

Aerocelluloses prepared from solvent NaOH-water and ionic liquid EMIMAc were already well characterised in (Gavillon & Budtova, 2008; Sescousse et al., 2011). EMIMAc has this great advantage of dissolving much higher cellulose than in 8%NaOH-water which open new range of properties and morphologies. However, EMIMAc is highly viscous, expensive, and reacts exothermically with water creating large macropores.

The investigation of DMSO as a co-solvent to EMIMAc showed major improvements in the preparation of aerocellulose: decrease of the solvent viscosity and of large macropores. The ternary phase diagram of cellulose-EMIMAc-DMSO displayed that it was still possible to dissolve high cellulose concentrations (~ 20_{wt}%) with 30-40_{wt}% DMSO added to EMIMAc.

We compared structural properties of 5_{wt}% aerocelluloses prepared in different solvents: 8%NaOH-water, EMIMAc and 60_{wt}% EMIMAc / 40_{wt}% DMSO. They present high porosity, above 90%. Skeletal densities appeared to be the same and equals to one of pure cellulose, $\rho_{skeletal}$ = 1.55 g/cm^3. The bulk density of aerocellulose from EMIMAc/DMSO was slightly higher due to the decrease of large pores compared to pure EMIMAc. ρ_{bulk} of aerocellulose from 8%NaOH-water was lower than that from ionic liquid. No significant difference is observed for specific surface areas, for aerocelluloses from EMIMAc or EMIMAc/DMSO but they are lower than for aerocellulose from 8%NaOH. Aerocelluloses from ionic liquids with or without DMSO present similar pores size distributions and are wider than the one from 8%NaOH-water. Aerocellulose from 8%NaOH presents a slightly finer morphology than the one from ionic liquids. We also studied the influence of cellulose concentration on the morphology of aerocelluloses from ionic liquids. The bulk density increased linearly with cellulose concentration with no difference between EMIMAc and EMIMAc/DMSO. More concentrated aerocelluloses (e.g. 15_{wt}%) present a finer porous structure with pores smaller and narrower size distribution compared to 5_{wt}% aerocellulose.

For the first time, thermal properties of aerocelluloses from three different solvents were investigated. The effective thermal conductivity of aerocellulose from 5_{wt}% cellulose- 80_{wt}% EMIMAc/ 20_{wt}% DMSO is 32.8 mW.m^{-1}.K^{-1} for a bulk density of 0.18 g/cm^3. We obtained similar results for aerocellulose from 8%NaOH-water with the same density (7_{wt}% cellulose). The best thermal conductivity was obtained for 5_{wt}% cellulose in 8%NaOH-water and equals to 30.8 mW.m^{-1}.K^{-1}. The three different contributions to the effective thermal conductivity were determined. The conduction of the gaseous phase represents 60% and the radiative transfer 30% of the total conductivity. The conductivity of the cellulose solid phase was estimated at 3.5 mW.m^{-1}.K^{-1} for ρ_{bulk} = 0.18 g/cm^3.

All aerocelluloses, independently of the solvent dissolving cellulose, give thermal conductivity higher than one of free air (25 mW.m^{-1}.K^{-1}). It is due the presence of pores with sizes above the free mean path of air (70 nm) and the lack of control in morphology during the coagulation.

Bibliography

Gavillon, R. (2007). Préparation et caractérisation de matériaux cellulosiques ultra poreux., *PhD thesis*, Ecole des Mines de Paris.

Gavillon, R., & Budtova, T. (2008). Aerocellulose: new highly porous cellulose prepared from cellulose-NaOH aqueous solutions. *Biomacromolecules*, *9*(1), 269–77.

Gericke, M., Liebert, T., Seoud, O. a. El, & Heinze, T. (2011). Tailored Media for Homogeneous Cellulose Chemistry: Ionic Liquid/Co-Solvent Mixtures. *Macromolecular Materials and Engineering*, *296*(6), 483–493.

Gericke, M., Schlufter, K., Liebert, T., Heinze, T., & Budtova, T. (2009). Rheological properties of cellulose/ionic liquid solutions: from dilute to concentrated states. *Biomacromolecules*, *10*(5), 1188–94.

Hall, C. A., Le, K. A., Rudaz, C., Radhi, A., Lovell, C. S., Damion, R. A., Budtova, T., et al. (2012). Macroscopic and microscopic study of 1-ethyl-3-methyl-imidazolium acetate-water mixtures. *The Journal of Physical Chemistry. B*, *116*(42), 12810–8.

Le, K-A., Rudaz, C. Budtova, T. (2013). Phase diagram, solubility limit and hydrodynamic properties of cellulose in binary solvents containing ionic liquid, EmimAc. *Carbohydrate Polymers*, submitted.

Liebner, F., Haimer, E., Potthast, A., Loidl, D., Tschegg, S., Neouze, M.-A., Wendland, M., et al. (2009). Cellulosic aerogels as ultra-lightweight materials. Part 2: Synthesis and properties. *Holzforschung*, *63*(1), 3–11.

Lovell, C. S., Walker, A., Damion, R. A, Radhi, A., Tanner, S. F., Budtova, T., & Ries, M. E. (2010). Influence of Cellulose on Ion Diffusivity in 1-Ethyl-3-Methyl-Imidazolium Acetate Cellulose Solutions. *Biomacromolecules*, 2927–2935.

Lv, Y., Wu, J., Zhang, J. J., Niu, Y., Liu, C.-Y., & He, J. (2012). Rheological properties of cellulose/ionic liquid/dimethylsulfoxide (DMSO) solutions. *Polymer*, *53*(12), 2524–2531.

Sescousse, R. (2010). Nouveaux matériaux cellulosiques ultra-poreux et leurs carbones à partir de solvants verts., *PhD thesis*, Mines ParisTech.

Sescousse, R., Gavillon, R., & Budtova, T. (2011). Aerocellulose from cellulose–ionic liquid solutions: Preparation, properties and comparison with cellulose–NaOH and cellulose–NMMO routes. *Carbohydrate Polymers*, *83*(4), 1766–1774.

Sescousse, R., Le, K. A., Ries, M. E., & Budtova, T. (2010). Viscosity of cellulose-imidazolium-based ionic liquid solutions. *The Journal of Physical Chemistry. B*, *114*(21), 7222–8.

Chapter IV

Chemically cross-linked cellulose: Gels and Aerogels

Introduction

We showed in the previous chapter (Chapter III) that aerocellulose presents a mesoporous structure with pores of tens nanometers but also few larger pores of few hundreds nanometers to few micrometers. We demonstrated that the main thermal contribution of aerocellulose is represented by the conduction of the gaseous phase. Large macropores present in aerocellulose morphology increase the conductivity of the gas phase as their size is higher than the free mean path of air molecules (no Knudsen effect). They are therefore responsible for high effective thermal conductivity of aerocelluloses (around 30-35 $mW.m^{-1}.K^{-1}$).

Thus the next step of our work was focused on the reduction of large macropores in aerocellulose structure. The coagulation of cellulose is an important step, when the porous structure of aerocellulose is formed. Cellulose chains are self-associating without any chemical cross-linking. However, coagulation and the formation of the porous network are not well controlled and therefore a wide range of pores are formed. Classic organic aerogels, for example resorcinol-formaldehyde (Pekala, 1989) or cellulose acetate (Fischer, Rigacci, Pirard, Berthon-Fabry, & Achard, 2006), are chemically cross-linked whereas aerocelluloses are from physical gels. The morphologies of chemical gels are supposed to be more homogeneous and nanostructured. We were thus interested in the possibility of chemically cross-linking cellulose to form new generation of aerocelluloses.

Epichlorohydrin is widely used for chemical cross-linking of polysaccharides. We will study the preparation of cross-linked cellulose by epichlorohydrin in the solvent 8%NaOH-water. Several processes will have to be considered. First, cellulose 8%NaOH-water undergoes a physical gelation due to self-association of cellulose chains. By adding epichlorohydrin, cellulose chains will be chemically cross-linked. We will study the influence of the addition of the cross-linker on the cellulose solutions gelation by rheology. We will carry out dynamic viscoelastic measurements and determine the time of gelation as a function of the cross-linker concentration. We will discuss potential competition between chemical and physical cross-linking.

Cross-linked cellulose gels will be then coagulated in water and we will discuss the effects of cross-linking on the formation of coagulated cellulose by looking at swelling ratios. Finally, we will dry coagulated cross-linked cellulose samples by $scCO_2$. We will study in depth the texture of the new cross-linked aerocelluloses by SEM, their structural properties such as bulk and skeletal densities, porosity, specific surface areas and pore size distribution by Hg porosimetry. We will discuss the influence of cross-linking on these properties.

We will also investigate the mechanical properties of cross-linked aerocelluloses by uniaxial compression. Young modulus, yield stress and strain, densification strain and absorbed energy will be determined. We will correlate structural properties to mechanical behaviour.
Finally, we will study thermal properties of new cross-linked aerocelluloses. First, we will measure their effective thermal conductivity. We will also determine different thermal contributions to have a better understanding of heat transfers through cross-linked aerocelluloses. We will discuss if structural properties improvements allow improving thermal conductivity.

Introduction

Il a été montré au chapitre précédent (Chapitre III) que l'aérocellulose présente une structure mésoporeuse avec des pores de quelques dizaines de nanomètres mais également des pores plus grands, d'une centaine de nanomètres à quelques micromètres. Les macropores présents dans la structure de l'aérocellulose ont une taille bien supérieure au libre parcours moyen des molécules d'air. Ils sont responsables de l'augmentation de la conductivité thermique de la phase gazeuse, (qui représente la majeure partie de la contribution thermique) et donc de la forte valeur de conductivité thermique totale (autour de 30-35 $mW.m^{-1}.K^{-1}$).

Le but de ce travail a été de réduire la présence de gros macropores dans la structure d'aérocellulose. L'étape de coagulation est importante car c'est le moment où la structure poreuse est formée. Les chaines de cellulose s'associent sans aucune réticulation chimique. Cependant cette étape n'est pas bien contrôlée et donne une large gamme de pores.
Les aérogels organiques classiques, comme ceux de résorcinol-formaldelyde (Pekala, 1989) ou à base d'acétate de cellulose (Fischer, Rigacci, Pirard, Berthon-Fabry, & Achard, 2006), sont chimiquement réticulés contrairement aux aérocelluloses qui sont issus de gels physiques. Nous nous sommes donc intéressés à la réticulation chimique de la cellulose pour préparer une nouvelle génération d'aérocelluloses.

L'épichlorhydrine est largement utilisée pour réticuler les polysaccharides. Elle sera utilisée comme agent réticulant de la cellulose dans le solvant 8%NaOH-eau. L'influence de l'épichlorhydrine sera étudiée à toutes les étapes du procédé. La cellulose est connue pour gélifier dans le solvant 8%NaOH-eau mais l'ajout d'agent réticulant risque de jouer sur la gélification physique de cellulose. Des études rhéologiques vont permettre d'étudier le temps de gélification en fonction de la concentration d'agent réticulant. Une éventuelle compétition entre les mécanismes de gélification physique et chimique sera discutée.

Les gels de cellulose réticulée seront ensuite coagulés dans l'eau. Les effets de la réticulation chimique sur la formation de cellulose coagulée seront discutés, notamment en étudiant le degré de gonflement. La cellulose réticulée et coagulée sera séchée par CO_2 supercritique pour donner des aérocelluloses réticulées. Ces nouveaux aérogels seront étudiés en détail en fonction du degré de réticulation: leur texture par MEB, leurs propriétés structurales par leur densités, leur porosité, leur surface spécifiques ainsi que leur distribution de taille de pores.

Les propriétés mécaniques des aérocelluloses réticulées seront également étudiées par compression uniaxiale et les paramètres, comme le module de Young, la contrainte et l'allongement à la plasticité, l'allongement à la densification et l'énergie absorbée, seront déterminés. Les relations structures propriétés seront discutées.

La conductivité thermique totale des aérocelluloses réticulées sera mesurée et les différentes contributions thermiques seront aussi déterminés et apporteront une meilleure compréhension des transferts de chaleur dans la structure poreuse. Les éventuelles améliorations structurales seront corrélées aux propriétés thermiques résultantes.

1. Chemical cross-linking of cellulose in 8%NaOH-water solvent

1.1 Reaction mechanism

Epichlorohydrin (ECH in the following) is well-known as a powerful cross-linker for polysaccharides (Chang, Duan, Cai, & Zhang, 2010; Ciolacu, Oprea, Anghel, Cazacu, & Cazacu, 2012; De Miguel, Rieumajou, & Betbeder, 1999; Delval, Crini, Bertini, Filiatre, & Torri, 2005; Hamerstrand, Hofreiter, & Mehltretter, 1960; Jyothi, Moorthy, & Rajasekharan, 2006). Recently Zhang's group prepared cross-linked cellulose hydrogels with ECH (Chang, Zhang, Zhou, Zhang, & Kennedy, 2010; Zhou, Chang, Zhang, & Zhang, 2007).
ECH is a bifunctional molecule with a function epoxy and chloride (Figure IV. 1).

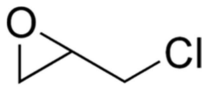

Figure IV. 1 : Epichlorohydrin (ECH).

Cellulose is made of long chains of anhydroglucose units (AGU). ECH can covalently bind two anhydroglucose units of cellulose through a Williamson etherification reaction (Figure IV. 2). Each AGU has three hydroxyl groups on carbons C_2, C_3 and C_6 that can possibly react with ECH. It was shown (and will also be demonstrated in our study) that the cross-linking occurs through OH on C_2 which turned out to be the most reactive as compared to OH-C_6 and OH-C_3 (Luby & Kuniak, 1979).

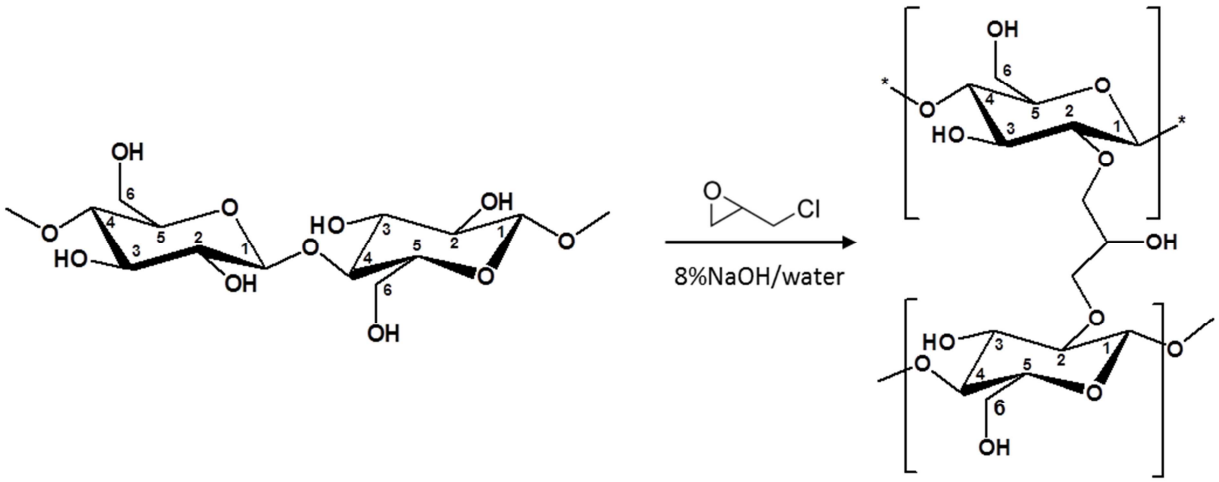

Figure IV. 2 : Mechanism of cellulose cross-linking by epichlorohydrin.

Cellulose undergoes a physical gelation in the solvent 8%NaOH-water with time and temperature increase (Roy, Budtova, & Navard, 2003) Gelation occurs due to cellulose chains self-association since cellulose-cellulose interactions are preferred instead of cellulose-solvent ones; this physical gelation is accompanied by micro-phase separation (gels become opaque). By adding epichlorohydrin, cellulose chains become chemically cross-linked. Two mechanisms are

therefore present and can possibly compete: physical gelation due to chains self-association (Figure IV. 3a) and chemical cross-linking (Figure IV. 3b).

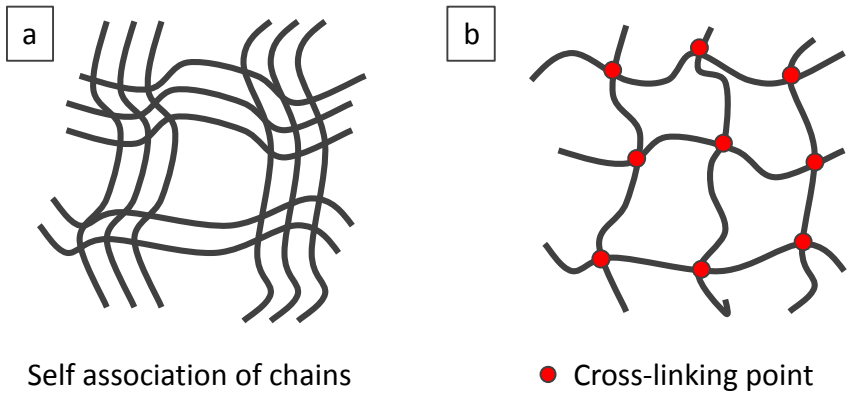

Figure IV. 3 : Two mechanisms of cellulose gelation: physical gelation via self-association of chains (a) and chemical cross-linking (b).

We define the relative ECH concentration in the reaction medium R_{rel} as the molar ratio of ECH to AGU (Equation (IV. 1)).

$$R_{rel} = \frac{n\ mol\ ECH}{n\ mol\ AGU} \quad \text{(IV. 1)}$$

A ratio of 0.5 equals to stoichiometric proportions for one cross-linking point (as represented in Figure IV. 2) that can be called “mono-crosslinking” (Equation (IV. 2)).
However, AGU unit has three hydroxyl groups on C_2, C_3, and C_6 that can potentially react with epichlorohydrin. With a ratio R = 1, two OH groups on AGU are cross-linked (Equation (IV. 3)). With R = 1.5, all cellulose hydroxyl groups will be involved in cross-linkings (Equation (IV. 4)); it is the maximal cross-linking degree that is possible to obtain in the reaction between cellulose and epichlorhydrin;

$$2\ C_6H_{10}O_5 + C_3H_5OCl = C_6H_9O_5 - C_3H_6O - C_6H_9O_5\ "C_{15}H_{24}O_{11}" + HCl \quad \text{(IV. 2)}$$

$$2\ C_6H_{10}O_5 + 2\ C_3H_5ClO = C_{18}H_{28}O_{12} + 2\ HCl \quad \text{(IV. 3)}$$

$$2\ C_6H_{10}O_5 + 3\ C_3H_5ClO = C_{21}H_{32}O_{13} + 3\ HCl \quad \text{(IV. 4)}$$

This ratio R_{rel} has to be distinguished from the cross-linking ratio. It represents the concentration of epichlorohydrin present in the reaction medium and not the effective quantity of cross-links that happen between cellulose and ECH.

1.2 Rheological study of cellulose solutions gelation

As mentioned above, two different mechanisms of cross-linking, physical and chemical, are present during the cellulose cross-linking reaction with ECH. Chemical cross-linking can either enhance or compete with physical gelation. Rheology is a useful tool to evaluate the influence of cross-linking on gelation.
In a recent paper, the chemical cross-linking of cellulose by ECH in the solvent NaOH-water-urea was studied (Qin, Lu, & Zhang, 2013). It was shown that cross-linker concentration, cellulose concentration and temperature play an important role in the gelation mechanism and that the chemical cross-linking induced by ECH decreased significantly the time of cellulose solution gelation. We started our work, cellulose cross-linking by ECH in 8% NaOH-water, before the article (Qin et al., 2013) was published. We studied in details the influence of cross-linker concentration and temperature on the gelation time.

1.2.1 Influence of ECH concentration on gelation

(Qin et al., 2013) studied the rheological behaviour of gelation of cellulose solutions during cross-linking using double concentric cylinder geometry with a gap of 2 mm at a frequency of 6.3 Hz. We performed dynamic viscoelastic measurements with cone-plate geometry at a frequency of 0.1 Hz and stress at 0.01 Pa to ensure being in the linear viscoelastic regime (c.f. Chapter II).

1.2.1.1 Effect of ECH on G' and G" behaviour

The evolution of the two moduli, elastic G' and viscous G", as a function of time for various ratios R_{rel}, was studied at various temperatures and cellulose concentrations. An example for three different cellulose-8%NaOH-water mixtures with different R_{rel} ratios at a given temperature, 22°C, and at a fixed cellulose concentration 4_{wt}% is presented in Figure IV. 4.

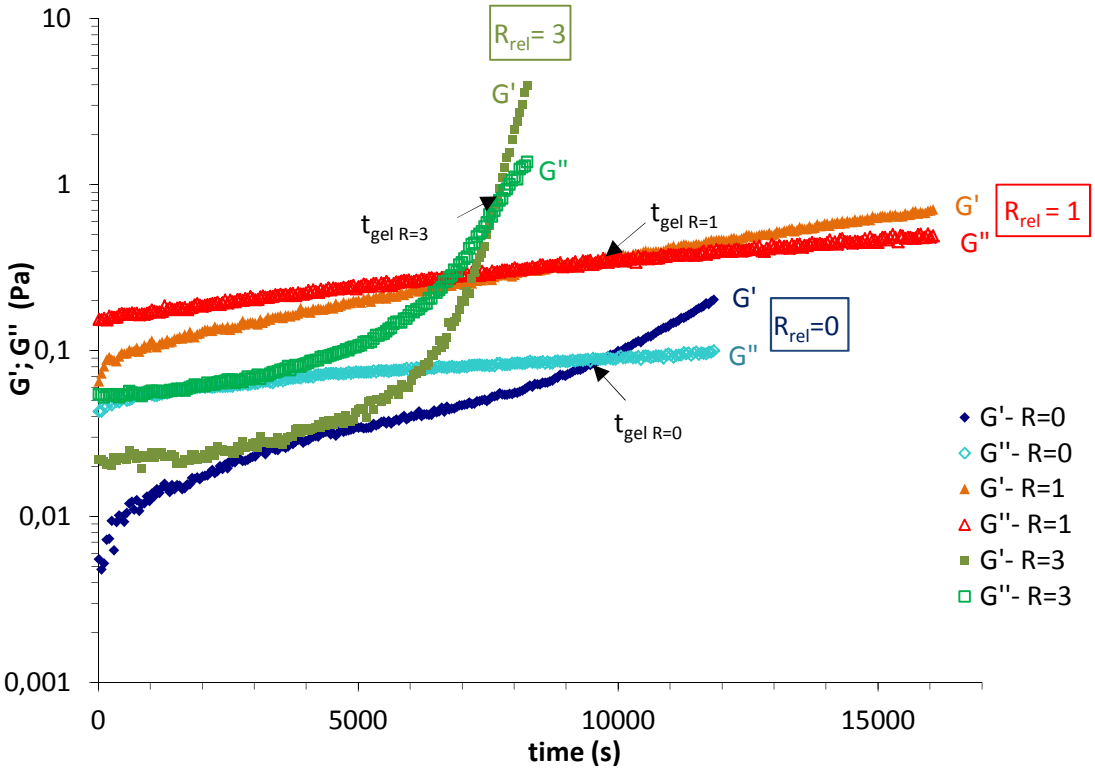

Figure IV. 4 : Elastic (G') and viscous (G'') moduli as a function of time for 4_{wt}% cellulose solution at 22°C with various ECH concentrations in the reaction medium, R_{rel}. (R_{rel}=0 corresponds to cellulose physical gelation without ECH).

At the beginning (low times) G" is higher than G', for all ratio R, indicating a viscous liquid behaviour. Crossovers of G' and G" were observed for all cellulose solutions and the time of gelation was determined at this point (Winter & Chambon, 1986). After the gelation point, G' becomes higher than G" indicating a more elastic behaviour. Viscous G" and elastic G' moduli have rather different shape depending on the R_{rel} ratio.

With low ECH concentration ($R_{rel} \leq 1$) G' and G" increase slowly with time. This behaviour had already been reported for non-crosslinked cellulose ($R_{rel} = 0$) (Roy et al., 2003). At higher cross-linker concentration, G' and G" curves slowly increase with time at the beginning of reaction (below 5000 s), but then sharply increase after G' = G". It shows that a different mechanism than physical gelation is occurring. Unfortunately, it was not possible to wait longer time to eventually see a plateau of G' typical for chemically cross-linked gels as data were scattered due to syneresis.

Similar experiments were performed for 5_{wt}% cellulose-8%NaOH-water solutions and gelation times were recorded. The results showed that cellulose chemical cross-linking has a strong impact on the viscoelastic behaviour of solutions at high cross-linker concentration. The influence of ECH relative concentration on gelation time is presented in details below.

1.2.1.2 Effect of ECH on gelation time

From the curves as presented in Figure IV. 4, we determined gelation time at 22°C for various concentrations of epichlorohydrin, R_{rel} from 0 to 3. Two cellulose concentrations in solution were investigated, 4 and 5_{wt}%. All data are summarised in Figure IV. 5.

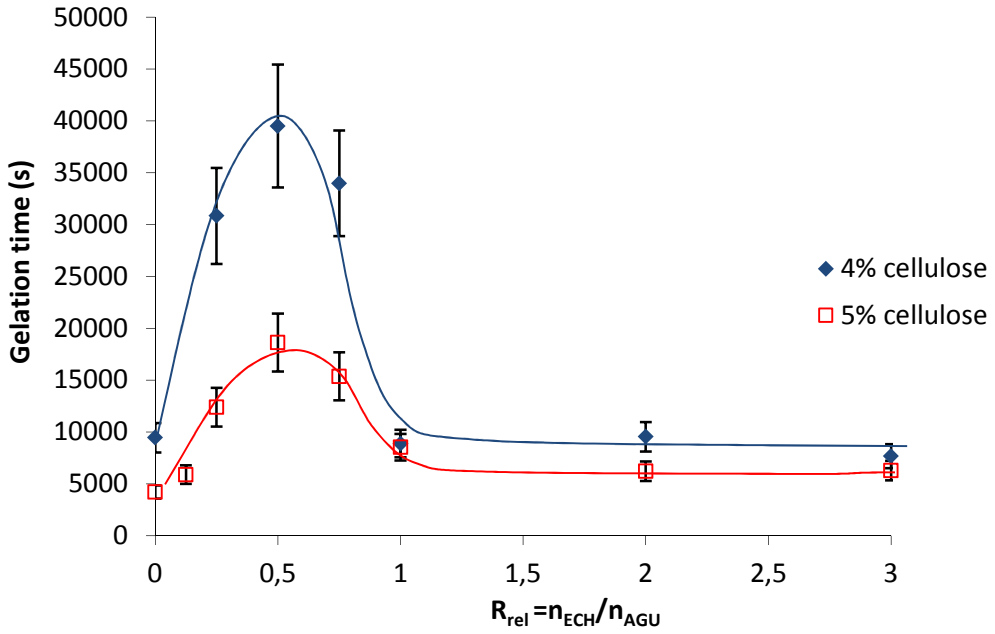

Figure IV. 5 : Gelation time as a function of the ratio R_{rel} for two cellulose concentrations 4 and 5_{wt}% at 22°C. Lines are given to guide the eye.

For both cellulose concentrations, we observed a new and interesting effect: gelation is strongly delayed in the presence of epichlorohydrin and the longest gelation time is at $R_{rel} = 0.5$. This phenomenon is less pronounced for 5_{wt}% as compared to 4_{wt}% cellulose concentration. The ratio $R_{rel} = 0.5$ corresponds to the stoichiometric ratio of ECH to AGU in the reaction medium (what we called "mono-crosslinking", see Figure IV. 2).

We suggest the following interpretation of the delay of cellulose gelation in the presence of cross-linker. Physical gelation is a cooperative reaction: cellulose chains are self-aggregating with time and temperature increase via hydrogen bonding. We suppose that the introduction of a cross-linker, epichlorohydrin, induces a competition between physical and chemical gelation. Epichlorohydrin molecule acts as a "spacer" between cellulose chains preventing cellulose chains self-aggregation (Figure IV. 3). The cooperative reaction of hydrogen bondings is delayed because of spatial constraints. The increase of cellulose concentration increases the probability in chains intra-molecular interactions and thus the delay effect is less marked for 5% cellulose.

A plateau is observed for high ECH ($R_{rel} \geq 1.5$): gelation time in the presence of high amount of ECH is similar to that of non-crosslinked cellulose solution ($R_{rel} = 0$). Above $R_{rel} = 1.5$, if all epichlorohydrin molecules are involved in reaction with cellulose, no more cross-linking is possible as all hydroxyl groups on AGU are already bound. The excess of ECH is not participating to reaction. This explains the independence of gelation time on R_{rel}. Gelation for $R_{rel} \geq 1.5$ is most probably mainly due to chemical cross-linking.

The delay of cellulose gelation in the presence of epichlorohydrin was not reported in ref (Qin et al., 2013). They showed that the gelation time decreased with an increase of ECH concentration. The reason is that they studied the case with $R_{rel} > 2$.

1.2.2 Influence of temperature on gelation time

The influence of temperature on the viscoelastic properties of cellulose-8%NaOH-water solutions in the presence of ECH was studied. Gelation time as a function of temperature for 4_{wt}% cellulose solution is presented in (Figure IV. 6).

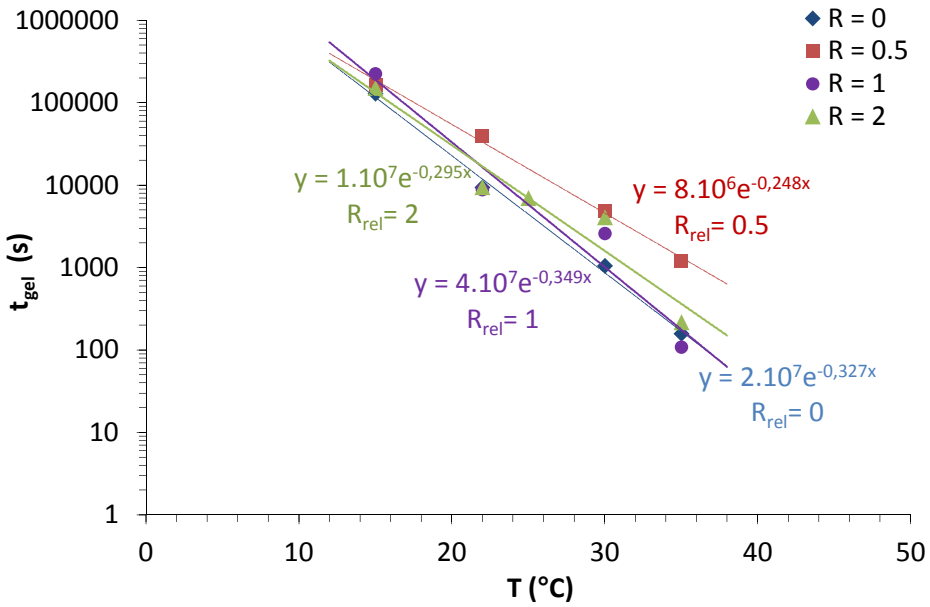

Figure IV. 6 : Gelation time as a function of temperature for 4_{wt}% cellulose solutions with various ECH concentrations in the reaction medium, R_{rel}.

For non-crosslinked cellulose (R_{rel} = 0), it is known that the gelation time t_{gel} decreases with temperature T in an exponential way (Equation (IV. 5)).

$$t_{gel} = A.exp\,(n.T) \qquad \text{(IV. 5)}$$

where A is an empirical adjustable constant.

Gavillon showed that for 5_{wt}% cellulose in 7.6%NaOH-water, n = -0.345 and A = $5.7.10^4$ (Gavillon, 2007). Similar results can be observed for 4_{wt}% in 8%NaOH-water with n = -0.33 (Figure IV. 6). The thermodynamic quality of the solvent NaOH-water decreases with temperature increase. Polymer-polymer interactions are then more favourable and gelation occurs faster at high temperatures.
We looked at the influence of the cross-linker on the gelation as a function of temperature. The values of exponent n were similar within the experimental errors for R_{rel} = 0.5, 1 and 2, except for R_{rel} = 0.5 (Figure IV. 7).

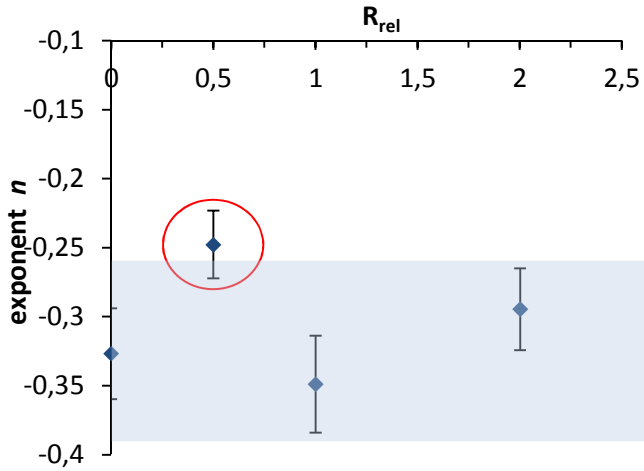

Figure IV. 7 : Exponent *n* of the Equation (IV. 5) as a function of ECH concentration R_{rel} in the reaction medium.

A particular behaviour is again observed for R_{rel} = 0.5, with the exponent *n* being higher than those for the other ECH concentrations. It means that cellulose solution is somewhat slightly less sensitive to temperature increase. Without any cross-linker, temperature increase induces higher chains mobility and thus the probability of the formation of inter- and intramolecular hydrogen bonding is increased. The presence of ECH as a "spacer" between cellulose chains is limiting cellulose-cellulose interactions even with temperature increase. The impact of the solvent quality decrease with temperature becomes less important. At higher ECH concentrations (R_{rel} > 1), cellulose is mostly chemically cross-linked and cellulose-cellulose interactions are important leading to a decrease of gelation time with temperature increase.

2. Characterisation of chemically cross-linked cellulose

2.1 Attempts to determine the degree of cellulose cross-linking

Knowing the degree of cross-linking is important to understand and interpret the properties of gels, coagulated cellulose and dried aerocellulose. To determine the degree of cross-linking, two techniques were used:

- A direct measurement by elemental analysis on dried cross-linked coagulated cellulose
- An indirect measurement by ^{1}H-NMR on the coagulation bath to evaluate non-reacted epichlorhydrin and to deduce the cross-linking ratio.

2.1.1 Determination of cellulose cross-linking by elemental analysis of dried coagulated cellulose

Cellulose was cross-linked with different concentrations of ECH in the reaction medium, R_{rel}. Then, the obtained cellulose gels were coagulated in water. Coagulated cross-linked celluloses were washed in several water baths in order to remove non-reacted ECH and NaOH. Samples were then extracted from the baths and dried by evaporative route in the air at room conditions.

Elemental analysis of dried samples was carried out with the help of the CNRS-Institute of Analytical Sciences. A weight concentration of carbon was measured.

We did this analysis for only one formulation 5_{wt}% cellulose with ECH concentration in reaction medium of R_{rel} = 1. We used 20 g of 5_{wt}% cellulose (i.e. 1 g of cellulose) in 8%NaOH-water in which we added 0.571 g of ECH (R_{rel} = 1). We obtained after drying cross-linked aerocellulose with m_{final} = 1.71 g.
The elemental analysis gave the weight concentration of carbon $\%C_{measured}$ = 34.52%. By using Equations (IV. 6) and (IV. 7), we calculated the mass of carbon for pure aerocellulose and for cross-linked aerocellulose. We calculated therefore the difference in mass of carbon between pure and cross-linked aerocellulose according to Equation (IV. 8) which corresponds to the quantity of ECH that has reacted with cellulose. We evaluated the effective cross-linking ratio $R_{effective}$ (Equation (IV. 9)) and obtained $R_{effective}$ = 0.66. The yield of cross-linking reaction is thus not 100% but 66%.

$$m_C(cellulose) = m_C(R=0) = 6 \times n_{cellulose} \times M_C = 6 \times n_{cellulose} \times 12 \quad \text{(IV. 6)}$$

$$m_C(cellulose\ crosslinked\ with\ R=1) = m_C(R=1) = \frac{\%C_{measured} \times m_{final}}{100} \quad \text{(IV. 7)}$$

$$n_{ECH\ (reacted)} = \frac{n_{C\ R=1} - n_{C\ R=0}}{3} = \frac{m_C(R=1) - m_C(R=0)}{3 \times M_C} \quad \text{(IV. 8)}$$

$$R_{effective} = \frac{n_{ECH\ (reacted)}}{n_{cellulose}} \quad \text{(IV. 9)}$$

Other formulations with various ECH concentrations are currently under research to evaluate more precisely the cross-linking ratio of cellulose.

2.1.2 Determination of cellulose cross-linking by ^{1}H-NMR analysis of coagulation bath

The second set of methods used is an indirect determination of the ECH that had reacted in the cellulose cross-linking reaction.
Cellulose was cross-linked with different concentrations of ECH in the reaction medium. Then, cellulose gels obtained were placed in water for 24 h at room temperature under mild stirring to remove non-reacted ECH and NaOH. The water bath was collected and analysed to determine non-reacted ECH and therefore to deduce ECH that had reacted.

Several techniques were envisaged to determine the concentration of non-reacted ECH in the coagulation bath. As the reaction medium is highly basic, ECH is hydrolysed into glycerol. Glycerol is classically dosed in biochemistry by enzymes. However, due to the high basicity of the medium it was not possible to use this technique.

We tested elemental analysis with the detection of carbon and chlorine. The concentrations of glycerol and chloride anions were too low to be accurately quantified, as it was below the detection concentration.

We opted for determination of glycerol in solution by ^{1}H-NMR. This study was conducted in collaboration with the group of Michael Ries, University of Leeds, UK.
In order to determine ECH concentration in water coagulation bath, a calibration curve must be first built using the correlation between the surface under the corresponding NMR peak and known ECH concentration solutions ("calibration solutions"), separately prepared.

An example of ^{1}H-NMR spectrum of one calibration solution is given in Figure IV. 8. Peaks are identified as the water peak at 4.85 ppm, chemically unique hydrogen of glycerol (H_2) at 3.585 ppm, hydrogens of glycerol H_1 and H_3 at 3.585 ppm and 5.482 ppm, respectively, and the NaOH peak at 2.177 ppm. Each resonance was integrated manually three times and a mean value was taken. Figure IV. 8 shows that the peaks of interest are located on the edge of the water peaks, decreasing the accuracy of the integration.

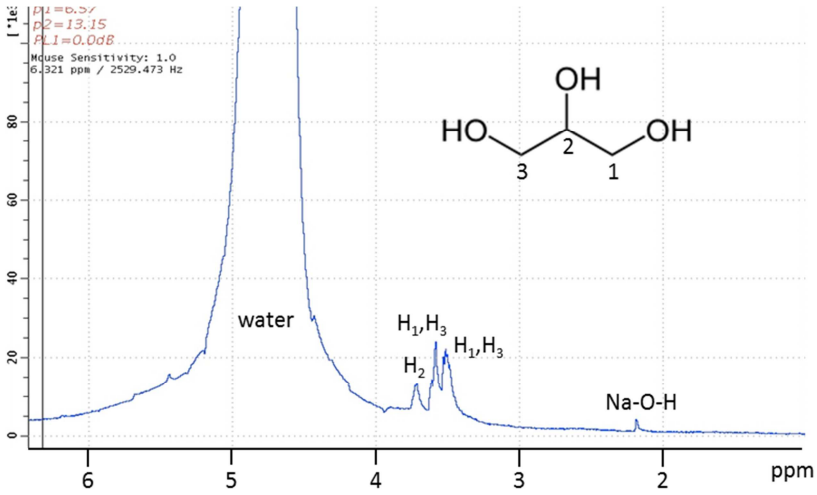

Figure IV. 8 : ^{1}H-NMR spectrum of a coagulation bath from a 5% cellulose.

Then glycerol concentrations were measured using ^{1}H-NMR analysis of coagulation baths collected after immersion of cellulose cross-linked with ECH of various R_{rel} from 0.25 to 4.

For $R_{rel} \leq 1$, the concentration of ECH in the coagulation bath turned out to be higher than the concentration of ECH in the reaction medium which is not possible. This shows the limitation of this method for low concentrations of ECH in the aqueous solutions. For higher R_{rel}, we evaluated the effective R =0.6 for $R_{rel} = 2$ and R=1 for $R_{rel} = 4$.
The yield of etherification (or cross-linking) of cellulose is not 100%, confirming previous observations by elemental analysis. A high amount of epichlorohydrin is required to increase the effective cellulose cross-linking.

As we did not manage to accurately determine the effective cross-linking ratio ($R_{effective}$) of all formulations of cross-linked aerocelluloses, we will use in the following the initial relative ECH concentration in the reaction medium R_{rel} instead of $R_{effective}$.

2.1.3 Analysis of cross-linking with ^{13}C-NMR

Dried cross-linked cellulose samples were analysed by ^{13}C-NMR by Remi Courson and Sylvie Etienne-Calas in the laboratory L2C of the University of Montpellier. Spectra of samples with different relative ECH concentrations in reaction, R_{rel} are given in Figure IV. 9 and are compared to non-crosslinked sample (Figure IV. 9a). Resonance peaks were attributed to C_1 at 105 ppm, C_4 at 85 ppm, C_2, C_3 and C_5 at 75 ppm and C_6 at 62 ppm (Capitani, Del Nobile, Mensitieri, Sannino, & Segre, 2000; Chang, Zhang, et al., 2010). Spectra of cross-linked samples (Figure IV. 9b, c, d) were noticeably broader with the increase of R_{rel}. It is possibly due to the differences in the chemical environment due to the presence of cross-links (Capitani et al., 2000). Signals of C_4 and C_6 were almost merged into the broad resonance peak of $C_{2,3,5}$.

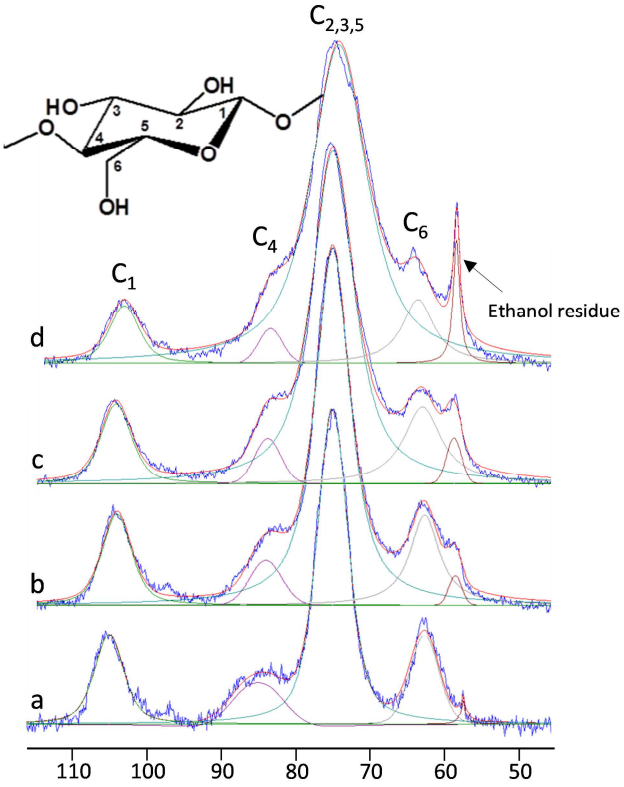

Figure IV. 9 : ^{13}C-NMR spectra of samples from dried 5%cellulose samples: R_{rel} = 0 (non-crosslinked) (a), with R_{rel}=1 (b), R_{rel}=2.5 (c) and R_{rel}=5.1 (d).

Each spectrum was decomposed by Gaussian curves corresponding to each peak and the area under each resonance peak was calculated. We normalised the areas with the area of C_1 signal as it is not affected by chemical cross-linking reaction. The area of signals $C_{2,3,5}$ and C_6 were then plotted as a function of R_{rel} in Figure IV. 10. The peak surface for C_6 is rather independent of R_{rel} whereas the surface for $C_{2,3,5}$ linearly increases with R_{rel}. This quantitative result demonstrates

that cross-linking reaction is more favourable on the hydroxyl group on C_2 and C_3 of AGU than on the hydroxyl group on C_6. This confirmed the previous studies of Luby in which the most reactive hydroxyl groups of cellulose was found to be OH on C_2, followed by OH on C_6 and on C_3 in the crosslinking cellulose reaction with ECH (Luby & Kuniak, 1979).

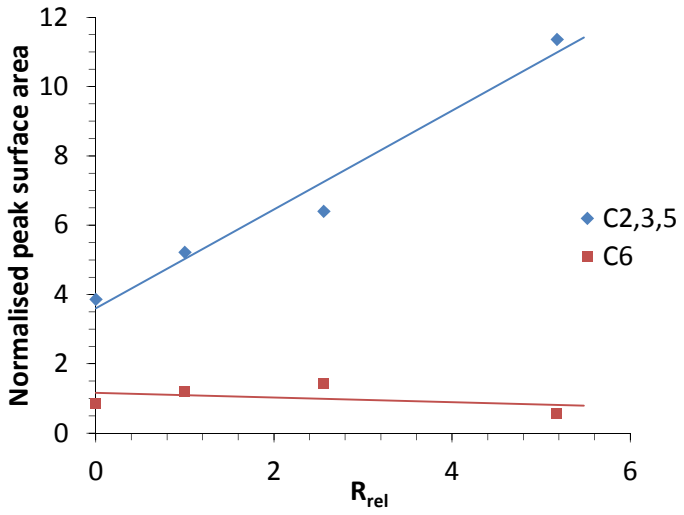

Figure IV. 10 : Normalised areas of peaks $C_{2,3,5}$ and C_6 as a function of the relative concentration of ECH in reaction, R_{rel}.

2.2 Swelling of cross-linked cellulose during coagulation

As shown in the Figure II.6 (Chapter II), cellulose must be coagulated before being dried and obtaining aerocellulose. Coagulation is a very important step: it determines the morphology formation. It is well known that non-crosslinked cellulose gel (obtained via physical gelation of cellulose-NaOH-water solution) slightly shrinks during the coagulation (Gavillon, 2007; Innerlohinger, Weber, & Kraft, 2006). The goal of this part was to investigate the behaviour of cross-linked cellulose during coagulation and to compare it with non-crosslinked cellulose.

It turned out than when placed in water coagulation bath, the behaviour of cross-linked cellulose strongly depends on ECH concentration used for cellulose cross-linking, R_{rel}. We measured the volume variation *%Volume variation* between the gel V_{gel} (gelation after 24h at room temperature) and coagulated cellulose swollen in water $V_{swollen\ in\ water}$ (samples completely washed from NaOH) according to Equation (IV. 10). The volume of gel is measured 24 hours after the gelation of cross-linked cellulose solution. It has to be noticed that the volume of gel does not change in time during gelation and keeps the shape of the mould in which the solution was placed.

$$\%Volume\ variation = \frac{V_{swollen\ in\ water} - V_{gel}}{V_{gel}} \qquad \text{(IV. 10)}$$

A negative volume variation corresponds to a shrinkage and positive to a swelling of cellulose samples.
We studied the variation of volume for gels prepared from two cellulose concentrations, 5 and 7_{wt}% (Figure IV. 11). For both concentrations, we observed that gels with R_{rel} below 0.5 tend to shrink when placed in the coagulation bath. However, the shrinkage is rather limited as compared to non-crosslinked cellulose: the shrinkage decreases from – 33% for R_{rel} = 0 to -11% for R_{rel} = 0.5. If comparing samples prepared from 5 and 7_{wt}% solutions, the contraction is more pronounced for cellulose samples prepared from 5% cellulose. At R_{rel} = 1 – 2 cellulose is strongly swelling: sample volume increases by 20-30% as compared with the gel (Figure IV. 11). This is a very interesting phenomenon that was never reported in literature before.

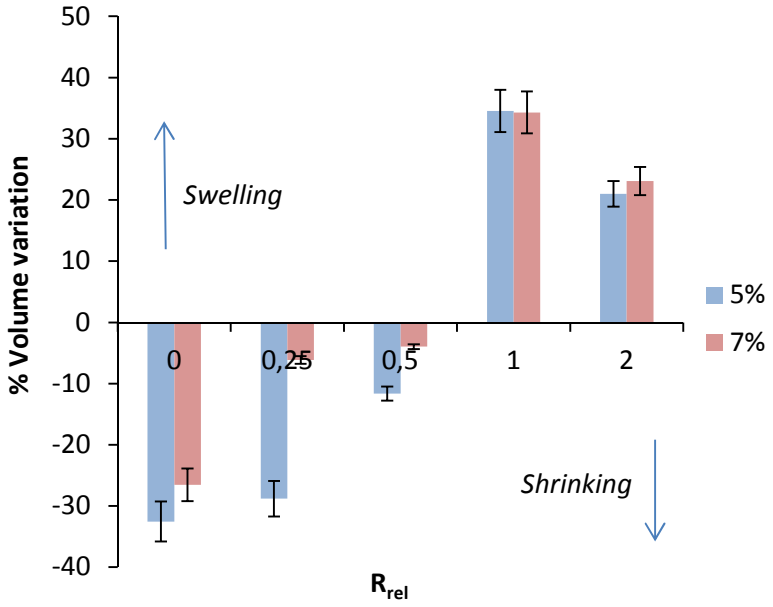

Figure IV. 11 : Volume variation as a function of ECH concentration in reaction, R_{rel}, for 5 and 7_{wt}% cellulose gels.

Usually for samples swollen in water, the relevant parameter is the swelling ratio *%SR* defined by Equation (IV. 11) :

$$\%SR = \frac{W_{swollen} - W_{dried}}{W_{dried}} \qquad \text{(IV. 11)}$$

with $W_{swollen}$ and W_{dried} being the mass of swollen and dried samples, respectively.

Here we analysed the swelling ratio of coagulated cellulose swollen in water for various ECH concentrations in reaction medium R_{rel}. After washing samples from NaOH, they were softly wiped with filter paper and quickly weighted. They were then dried either by evaporative drying (up to constant weight) or freeze-drying and weighted again.
In Figure IV. 12, we plotted %SR as a function of R_{rel} for 5_{wt}% cellulose. The swelling ratio increases dramatically until the maximal value of %SR=3500 for R_{rel} = 1 ($R_{effective}$ = 0.66) and then decreases at higher R_{rel} values, reaching %SR≈1500, which is similar to non-crosslinked

cellulose. The pictures show the visual aspect of coagulated cellulose. Interestingly, with the increase of R_{rel} samples become more and more transparent: for example, samples prepared with R_{rel} = 0 or R_{rel} = 0.25 are opaque whereas with $R_{rel} \geq 2$ they are completely transparent. The "border" between opaque and transparent coagulated swollen cellulose stands between R_{rel} = 1 and 2. The increase of cross-linking thus leads to a more homogeneous structure of coagulated cellulose.

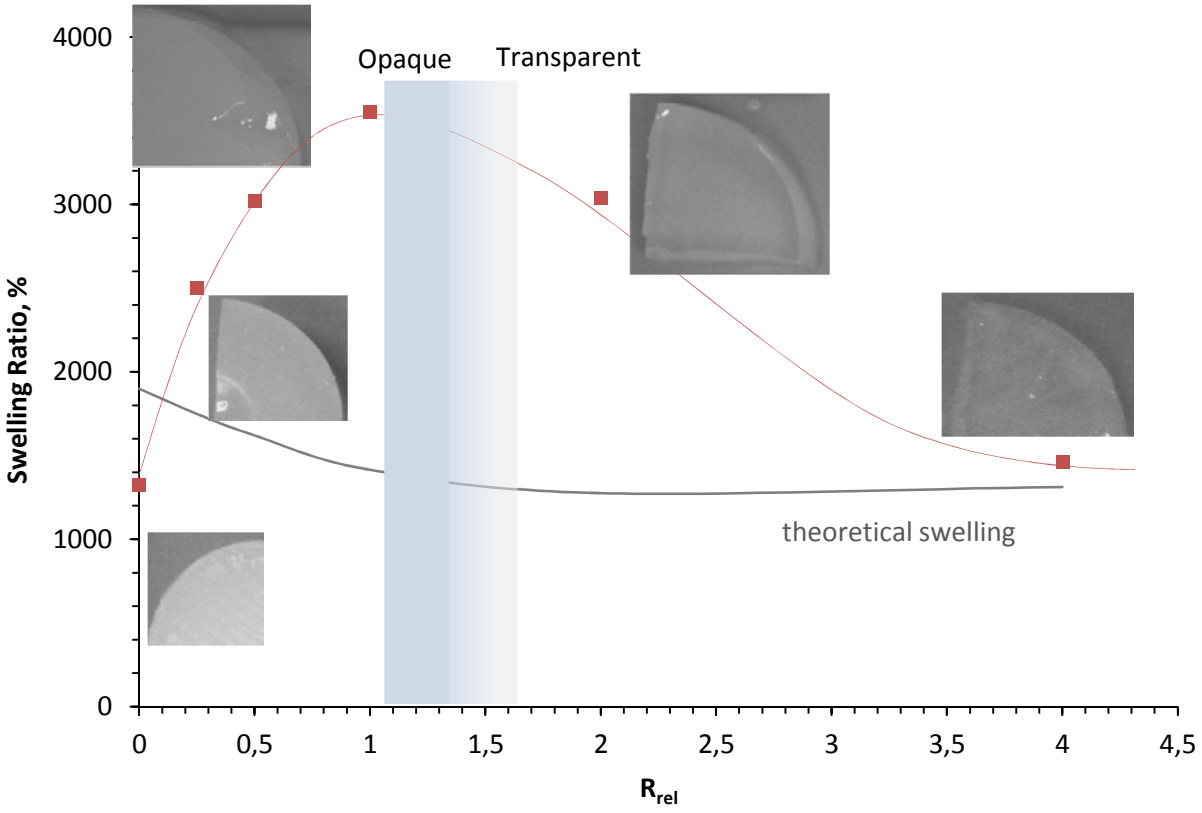

Figure IV. 12 : Swelling ratio of coagulated cellulose prepared from 5_{wt}% cross-linked gels.

We compared %SR of cross-linked coagulated cellulose to the theoretical swelling calculated according to the following approach, considering that the maximal theoretical cross-linking can be at R = 1.5; the excess of ECH, R >1.5, should not participate to the reaction:

For R≤1.5

$$\%SR = \frac{(m_{solution\ cellulose} + m_{ECH}) - (m_{cellulose} + \frac{m_{ECH} \times M_{C3H6O}}{M_{ECH}})}{(m_{cellulose} + \frac{m_{ECH} \times M_{C3H6O}}{M_{ECH}})}$$

For R>1.5

$$\%SR = \frac{(m_{solution\ cellulose} + m_{ECH}) - (m_{cellulose} + \frac{m_{ECH\ for\ R=1.5} \times M_{C3H6O}}{M_{ECH}})}{(m_{cellulose} + \frac{m_{ECH\ for\ R=1.5} \times M_{C3H6O}}{M_{ECH}})}$$

where with "m" we denote substance weight in gram and with "M" it molar weight.

To confirm the results obtained for 5% cross-linked cellulose, especially for the increase of swelling at $0 < R_{rel} < 1$, we also measured the swelling ratio for a 7_{wt}% cellulose. The results for 5_{wt}% and 7_{wt}% are presented in Figure IV. 13. The swelling ratio is less important for 7% than for 5%, as expected (see also (Chang, Zhang, et al., 2010; Zhou et al., 2007)). For cellulose concentration of 7% we also observed an increase of swelling with R_{rel} for $R_{rel} < 1$.

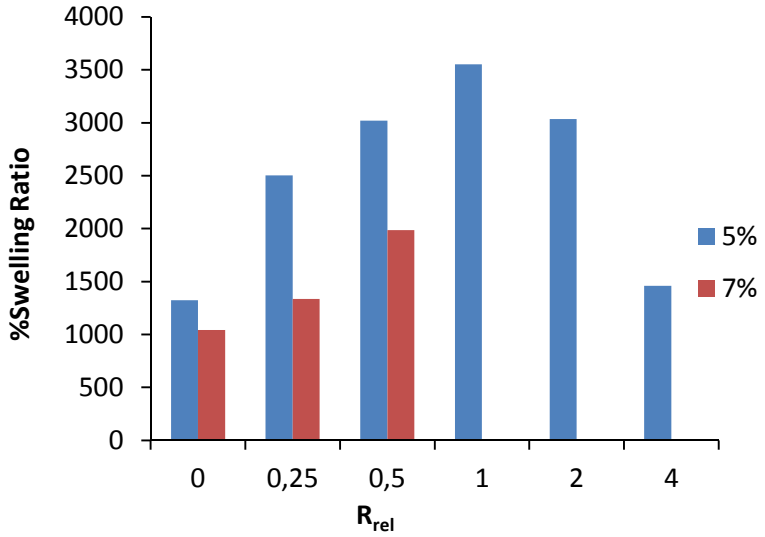

Figure IV. 13 : Comparison of swelling ratio for 5% and 7% coagulated cellulose as a function of relative ECH concentration in reaction, R_{rel}.

While the decrease of swelling with the increase of cross-linker (ECH) concentration is obvious to interpret (case at $R_{rel} > 1$), the increase of swelling with the increase of R_{rel} at $0 < R_{rel} < 1$ is somewhat unexpected. We propose the following qualitative interpretation of this phenomenon, based on the same reasoning as given to explain the delay of gelation with the increase of R_{rel} for low R_{rel} values. Before coagulation, cellulose is forming a gel in NaOH-water. During coagulation of non-crosslinked cellulose, the small pores of the gel are contracting due to cellulose-cellulose preferential interactions (as far as water is cellulose non-solvent) and the formation of hydrogen bonds between hydroxyl groups of cellulose. A low amount of epichlorohydrin which cross-links cellulose chains, acts as a spacer decreasing chains' mobility and preventing the formation of hydrogen bonds. This creates additional pores that are then filled with water, increasing water uptake. Further increase of ECH concentration "brings together" cellulose chains thus decreasing the amount of "new" pores which leads to the decrease of swelling.

The maximum swelling is recorded at $R_{rel} = 1$. We showed previously that for $R_{rel} = 1$, the effective cross-linking ratio equals to 0.66. This result is in agreement with ECH concentration observed for the maximum of delay in cellulose solution gelation (R = 0.5), where there is an important competition between physical and chemical gelation.

2.3 Solvent exchange

In order to dry wet aerocellulose precursor with supercritical CO_2, the fluid in the pores of coagulated cellulose must be compatible with supercritical CO_2. Two ways are possible:

- to coagulate cellulose directly in a fluid compatible with supercritical CO_2 and which also will wash out NaOH, e.g. ethanol
- if cellulose is coagulated in a fluid not compatible with CO_2 (e.g. water), it is necessary to perform solvent exchange: for example, to replace water by ethanol or by acetone. The main requests here are that the "replacing" fluid must be compatible with both the fluid in the pores of cellulose and $scCO_2$.

In both cases, sample porous morphology must be preserved as much as possible to obtain low density porous samples with high specific surface area. In other words, cellulose contraction should be avoided.

After the cross-linked cellulose gel was washed in water, it was then placed in ethanol following the classical procedure of aerocellulose preparation. Unfortunately, cellulose sample strongly contracted. The same happened when coagulated-in-water cross-linked cellulose was placed in acetone. There was then no reason to perform drying with supercritical CO_2; a new "replacing" fluid had to be found.

(Cai et al., 2012) used methanol for making cellulose-silica hybrid aerogels. We decided to explore the behaviour of cross-linked coagulated cellulose in methanol and also in some other fluids, compatible with CO_2, to replace water in swollen cellulose.

Several studies were carried out in literature to correlate the swelling of micro-crystalline cellulose and cotton fibre with the physico-chemical properties of different fluids, protic (El Seoud, Fidale, Ruiz, D'Almeida, & Frollini, 2007) and aprotic (Barton, 1991; Fidale, Ruiz, Heinze, & Seoud, 2008). It was shown that molar volume V_s and Hildebrand parameter $\delta_{Hildebrand}$ give a better understanding of cellulose swelling ratio %SR (Table IV. 1). Water is the best swelling protic solvent as compared to alcohols: the swelling ratio in ethanol is four times lower than in water. Alcohols with smaller size of molecule, like methanol, swell cellulose more than, for example, isopropanol.

Table IV. 1 : Physico-chemical parameters of alcohols (data from (El Seoud et al., 2007)) and of DMSO (data taken from (Fidale et al., 2008)) and cellulose swelling in these fluids.

Solvent	pKa	Vs (cm^3/mol)	$\delta_{Hildebrand}$	%SR
Water	15.7	18.05	47.8	53.5
Methanol	15.5	40.48	29.6	20.8
Ethanol	15.9	58.37	26.5	14.1
Isopropanol	17.1	76.51	23.5	5.8
DMSO	-	71.03	26.7	95.49

The Hildebrand parameter of cellulose equals $\delta_{Hildebrand}$=39.

We studied the influence of the "replacing" fluid on the swelling ratio for coagulated and cross-linked cellulose of different R_{rel}. Cross-linked cellulose coagulated in water was washed in progressive baths of methanol (Figure IV. 14, Figure IV. 15), isopropanol (Figure IV. 16a) or acetone (Figure IV. 16b). Progressive baths means that washing was performed in successive baths containing water and the replacing fluid where the concentration of the latter was progressively increased, up to 100% with the increment of 20%.

Figure IV. 14 displays samples swollen in methanol for different R_{rel}. We observed that initially transparent samples that were swollen in water (with $R_{rel} \geq 2$) became opaque during the solvent exchange step, losing their homogeneous structure when swollen in water.

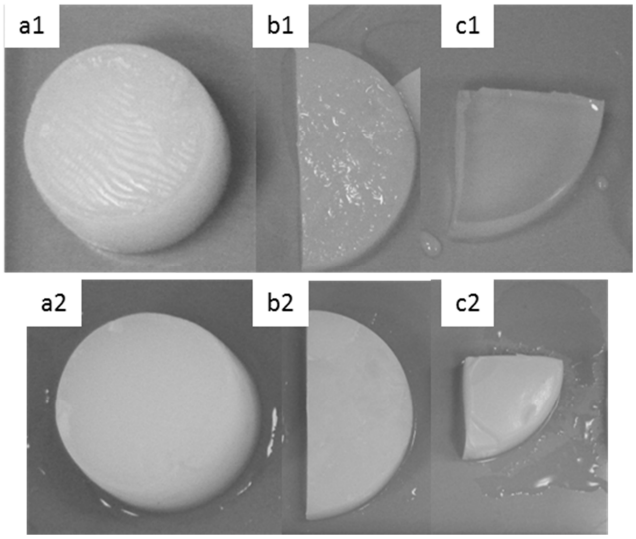

Figure IV. 14 : Influence of methanol on the swelling of 5_{wt}% cross-linked coagulated cellulose. The series 1 (first line) are samples swollen in water used as reference with R_{rel}=0 (a1), R_{rel}=0.5 (b1) and R_{rel}=2 (c1).
The series 2 (second line) are samples swollen in <u>methanol</u> (water exchanged by methanol with progressive baths) R_{rel}=0 (a2), R_{rel}=0.5 (b2) and R_{rel}=2 (c2).

All samples shrink when placed in methanol as expected from Table IV. 1. Figure IV. 15 shows the volume variation of cross-linked coagulated cellulose placed in a methanol bath, for two cellulose concentrations 5 and 7_{wt}%. The maximum volume variation is obtained for the highest R_{rel}, it reaches 70%. Cross-linked cellulose samples lose their faculty of swelling when placed in a different environment than water. This was observed for both 5% and 7_{wt}% cellulose samples. The lowest contraction 10%, was for non-crosslinked cellulose.

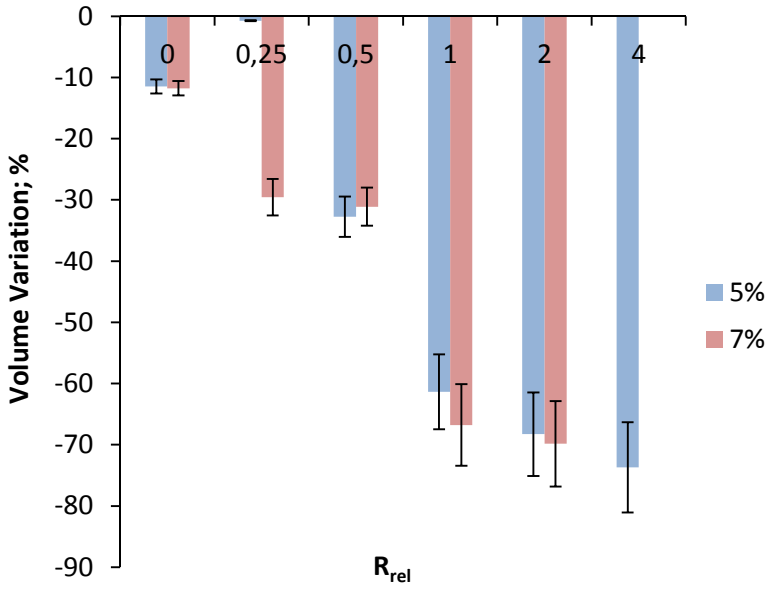

Figure IV. 15 : Volume variation of coagulated cellulose swollen in water to swollen in methanol for 5% and 7_{wt}% cellulose.

Figure IV. 16 compares two others “replacing” fluids, isopropanol and acetone, in terms of their action on cross-linked cellulose swollen in water. Two different techniques of solvent exchange were used:
- a direct one when cross-linked cellulose-swollen-in water is directly placed in an isopropanol or acetone bath;
- with progressive baths, as described above for methanol. Cellulose was placed in successive baths containing water and the second fluid in which the second fluid concentration is progressively increased.

Isopropanol and acetone lead to an important shrinkage of samples for both techniques (Figure IV. 16 first line). Samples become white and distorted (Figure IV. 16a1 and b1). Using gradual solvent exchange only slightly decreases the shrinkage and deformation of samples (Figure IV. 16 a2 and b2).

The next test was to check if the contraction in acetone or isopropanol is reversible or not. To do this, we placed samples swollen either in isopropanol or acetone again into a water bath. All samples re-swell when placed into water and recover their initial shape. The solvent exchange step is reversible and seems not to alter the structure of samples.

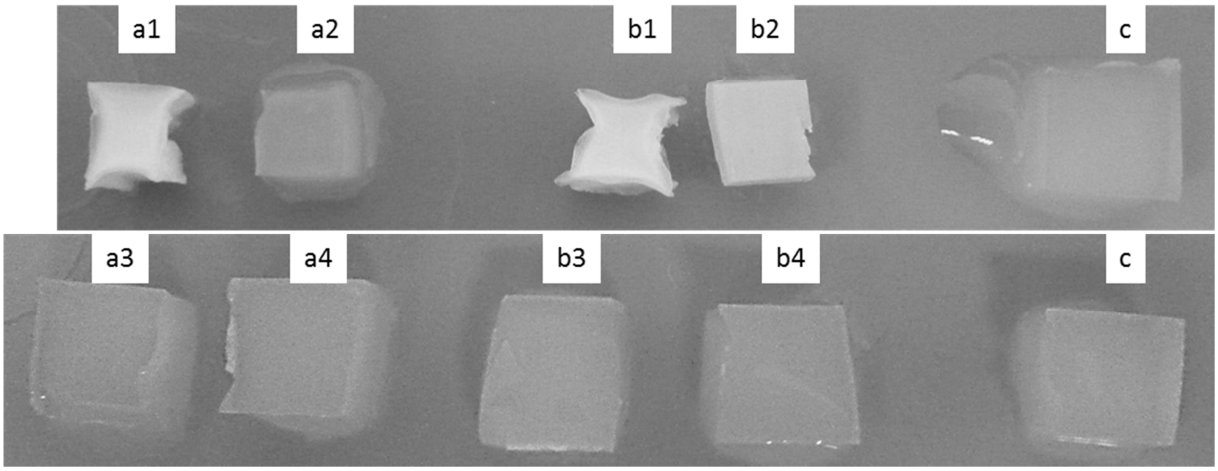

Figure IV. 16 : Influence of "replacing" fluid on the behaviour (first line) of 5_{wt}%cellulose with R_{rel}=2 followed by reswelling in water (second line).
In <u>isopropanol</u> : directly (one bath) (a1), after 3 incremental baths (a2), a1 sample placed in water (a3), a2 sample in placed in water (a4). Reference sample: initial cross-linked cellulose swollen in water (c)
In <u>acetone:</u> directly (one bath) (b1), after 3 incremental baths (b2), b1 sample placed in water (b3), b2 sample in placed in water (b4). Reference sample: initial cross-linked cellulose swollen in water (c)

(Fidale et al., 2008) showed that dimethylsulfoxide, DMSO, is one of the best fluids to swell cellulose with a %SR = 95. We immersed cross-linked cellulose (with R_{rel} = 2) coagulated in water in progressive DMSO baths, and compared to water and methanol (Figure IV. 17). Sample swollen in DMSO does not contract and keeps it transparency (Figure IV. 17b).

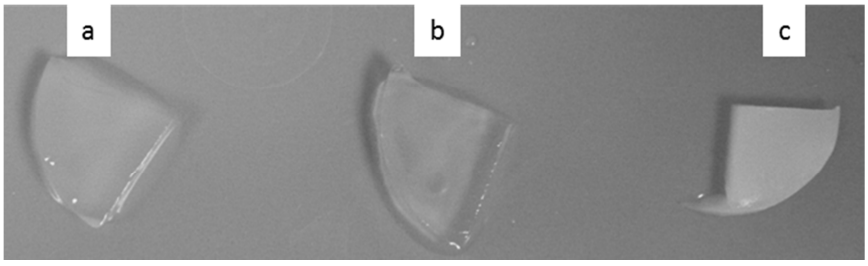

Figure IV. 17 : Influence of DMSO on 5_{wt}% cellulose with R_{rel} = 2: swollen in water used as a reference (a); swollen in DMSO (b) and swollen in methanol (c).

DMSO seems to be the best candidate for the solvent exchange step as it does not alter the structural properties of cross-linked coagulated cellulose. Therefore we investigated the possibility to dry with $scCO_2$ samples swollen in DMSO. DMSO and $scCO_2$ form a monophasic phase at 38°C and 95 bar. The pressure required is higher than that for the mixture ethanol-$scCO_2$ but it is still reachable. However, the main problem is the low melting temperature of DMSO, T_f=19°C. During the depressurization, at the end of supercritical drying process, temperature drops dramatically below 19°C. Even with a heating system around the pipes, DMSO crystallises easily provoking important blockage and an increase of pressure in the

autoclave. It was not possible to make the supercritical drying of DMSO-swollen samples in Persée Mines-ParisTech.

Because of these technical problems we decided to use methanol as a fluid replacing water in cellulose samples and we dried cross-linked samples with various R_{rel} with supercritical CO_2.

3. Properties of cross-linked aerocelluloses

In this section, we studied structural, mechanical and thermal properties of cross-linked cellulose aerogels and their dependence on the relative concentration of epichlorohydrin, R_{rel}.

3.1 Microstructural properties

3.1.1 Bulk and skeletal density

5_{wt}% and 7_{wt}% cross-linked aerocelluloses were characterised in details. First, the bulk density of each sample with various R_{rel} was measured by either mercury pycnometry in the laboratory L2C in the University of Montpellier or by powder pycnometry in Persée-Mines ParisTech. The results are presented in Figure IV. 18. For 5_{wt}% aerocellulose, we compared the two techniques of bulk density measurements. Hg and powder pycnometries give very similar results: ρ_{bulk} increases linearly with the increase of ECH concentration for 5% and 7_{wt}% aerocelluloses. As an example, bulk density of a 5% aerocellulose with R_{rel} = 2 (ρ_{bulk}=0.287 g/cm^3) is twice higher than non-crosslinked aerocellulose (ρ_{bulk}=0.123 g/cm^3). For 7_{wt}% aerocellulose, density increases more sharply with R_{rel} which means that less epichlorohydrin is needed to have higher ρ_{bulk} compared to 5_{wt}%. Density can be tuned by changing the degree of cellulose cross-linking.

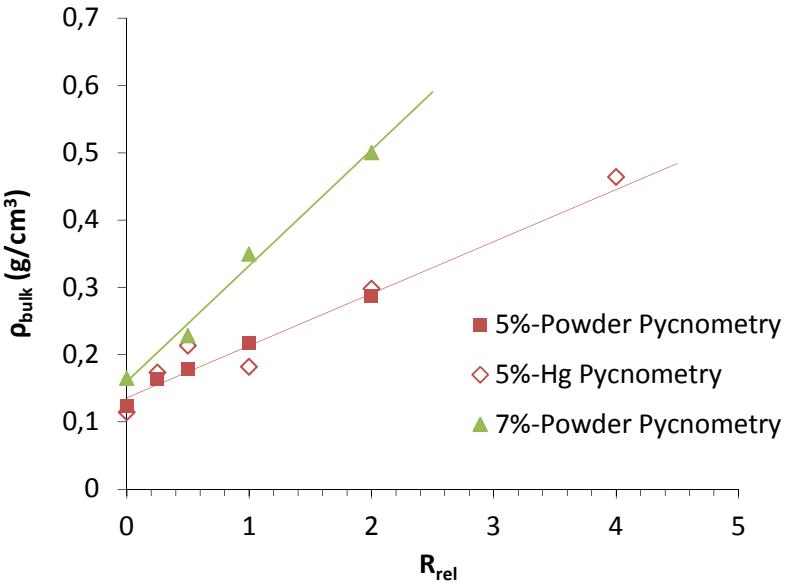

Figure IV. 18 : Variation of bulk density with the relative concentration in ECH, R_{rel}. Bulk density was measured by two different techniques, powder and Hg pycnometry, for 5_{wt}% aerocellulose and by powder pycnometry for 7_{wt}% aerocellulose.

Measurements of cross-linked aerocelluloses skeletal density were carried out by He pycnometry in the laboratory L2C in the University of Montpellier. Data are reported in Table IV. 2. No clear trend is observed as experimental errors are rather important. We obtained an average $\rho_{skeletal} \approx 1.56$ g/cm^3. It is similar to the skeletal density of pure aerocellulose and, in fact, of pure cellulose.

From these data we evaluated the porosity of samples. For 5%, samples with various R_{rel} have a porosity around 90%. No significant evolution is observed with density for $R_{rel} \leq 2$. For 7% samples, porosity is also important, around 80-90%, and it slightly decreases with the density increase.

Table IV. 2 : Bulk and skeletal densities of cross-linked aerocelluloses.

%C	R	ρ_{bulk} (g/cm^3)	$\rho_{skeletal} \pm 0.03$ (g/cm^3)	Porosity
5	0	0.123	1.55	92 %
5	0.25	0.164	1.66	90 %
5	0.5	0.179	1.62	89 %
5	1	0.217	1.58	86 %
5	2	0.287	1.50	82 %
7	0	0.165	1.55	89 %
7	0.5	0.228	1.61	86 %
7	1	0.349	1.52	77 %

3.1.2 Morphology observed by SEM

The influence of the ratio R_{rel} on cross-linked aerocellulose texture was analysed by SEM. Figure IV. 19 displays observations for 5_{wt}% cross-linked aerocelluloses with various R_{rel} from 0 (non-crosslinked) to 4. For R_{rel} = 0.5 (Figure IV. 19b), the morphology appeared slightly denser as compared to non-cross-linked aerocellulose and large macropores usually visible for non-crosslinked aerocellulose (R_{rel} = 0) are less present. For R_{rel} = 2 (Figure IV. 19d) and R_{rel} = 4 (Figure IV. 19e), morphologies are more and more dense. It confirms previous observations on bulk densities. At high R_{rel}, structure seems finer with pores smaller and more homogeneous.

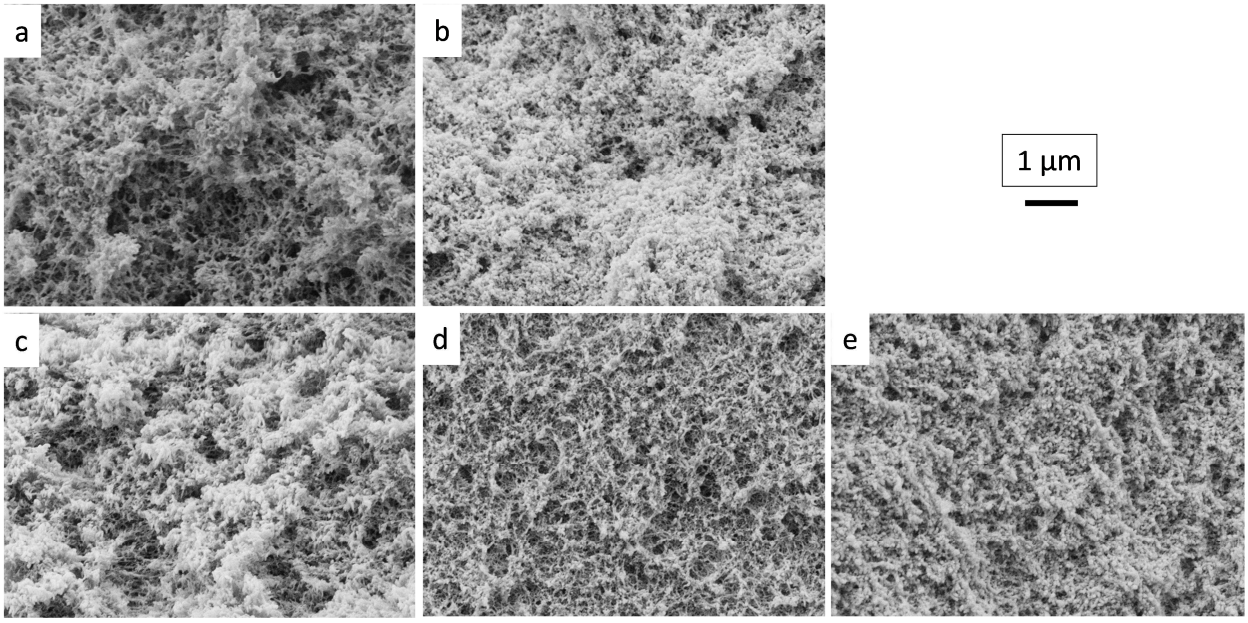

Figure IV. 19 : SEM images of 5_{wt}% cross-linked aerocelluloses with R_{rel} = 0 (a); R_{rel} = 0.5 (b); R_{rel} = 1 (c); R_{rel} = 2 (d) and R_{rel} = 4 (e).

Figure IV. 20 shows SEM observations for 7_{wt}% cross-linked aerocelluloses with R_{rel} from 0 to 1. As for 5_{wt}%, structure becomes more homogeneous and denser with the increase of cross-linker concentration. Pore size distribution seems also to be narrower and large pores of about 500 nm visible in Figure IV. 20a have completely disappeared on Figure IV. 20c.

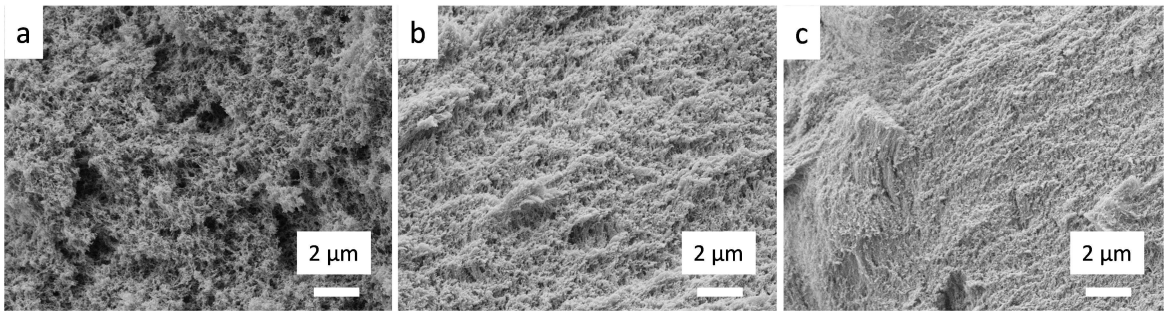

Figure IV. 20 : SEM images of 7_{wt}% cross-linked aerocelluloses with R_{rel} = 0 (a); R_{rel}=0.5 (b); R_{rel} = 1 (c).

3.1.3 Specific surface area

Specific surface areas were studied in the laboratory L2C in the University of Montpellier. Figure IV. 21 displays S_{BET} as a function of the cross-linker concentration R_{rel} for two initial cellulose concentrations of 5 and 7_{wt}%. For 5%, samples with $R_{rel} \leq 1$ present a higher specific surface compared to non-crosslinked aerocellulose. It is probably due to the narrowing of pores and the disappearance of macropores in the structure, observed on SEM images, which create a higher specific surface. For higher $R_{rel} > 2$, S_{BET} is similar or slightly lower than one of non-crosslinked aerocellulose ($R_{rel} = 0$). Density of highly cross-linked aerocellulose is rather

important (above 0.25 g/cm^3) and probably pores walls are thicker than for non-crosslinked aerocellulose which therefore decreases specific surface area.
A similar trend is observed for 7$_{wt}$% cross-linked aerocelluloses (Figure IV. 21). For R_{rel} = 0.5, S_{BET} is higher than that of non-cross linked aerocellulose. S_{BET} then decreases, similarly to 5$_{wt}$%. The role of ECH as a "spacer" at ECH/AGU being close to stoichiometric ratio seems to be confirmed here: for 5%cellulose, specific surface area is increased from 300 to 400 m^2/g which is a clear indication of nanostructuration.

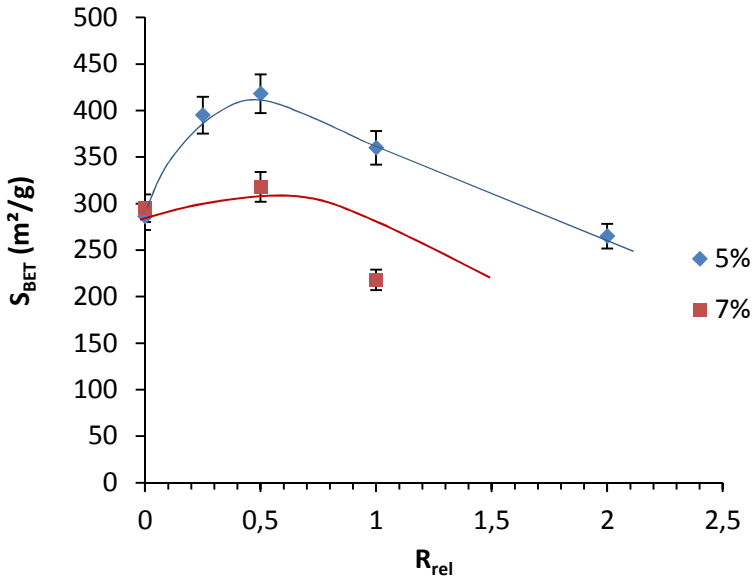

Figure IV. 21 : Variation of the specific surface area for 5% and 7$_{wt}$% cross-linked aerocelluloses with the ratio R_{rel}.

It is interesting that for a particular concentration of cross-linker specific surface area reaches a maximum where a balance is found between pore size distribution (shown later), density and porosity. We compared our results to cellulose acetate aerogels prepared from the cross-linking of cellulose acetate with an isocyanate reagent in the presence of tin-based catalyst (Figure IV. 22) (Fischer et al., 2006; Fischer, 2006).

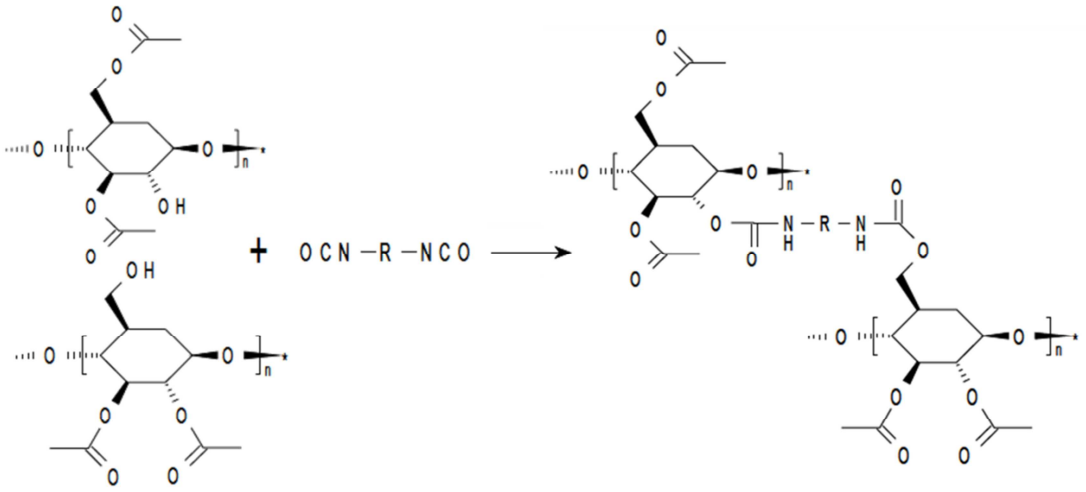

Figure IV. 22 : Cross-linking of cellulose acetate by isocyanate (Fischer, 2006).

Data of cellulose acetate aerogels were taken from (Fischer, 2006) and also from internal reports of the ANR Nanocel Project by Hélène Molnar from Persée Mines-ParisTech. They used the parameter %AC/I which is the mass ratio of cellulose acetate and isocyanate (cross-linker). We re-calculated this value into the equivalent relative concentration of isocyanate, similarly to ECH R_{rel}, according to Equation (IV. 12). Specific surface areas measurements for H.Molnar samples were carried out also in the laboratory L2C of the University of Montpellier according the same procedure described in Chapter II.

$$\%AC/I = \frac{m_{acetate}}{m_{isocyanate}} = \frac{n_{acetate} \times M_{acetate}}{n_{isocyanate} \times M_{isocyanate}} = \frac{1}{R_{rel}} \times \frac{M_{acetate}}{M_{isocyanate}} \qquad \text{(IV. 12)}$$

We plotted the specific surface areas of cellulose acetate aerogels as a function of the corresponding molar ratio R_{rel} (Figure IV. 23). For both 5% or 10_{wt}% cellulose acetate concentrations, a maximum of S_{BET} is also recorded at an optimized R_{rel}.

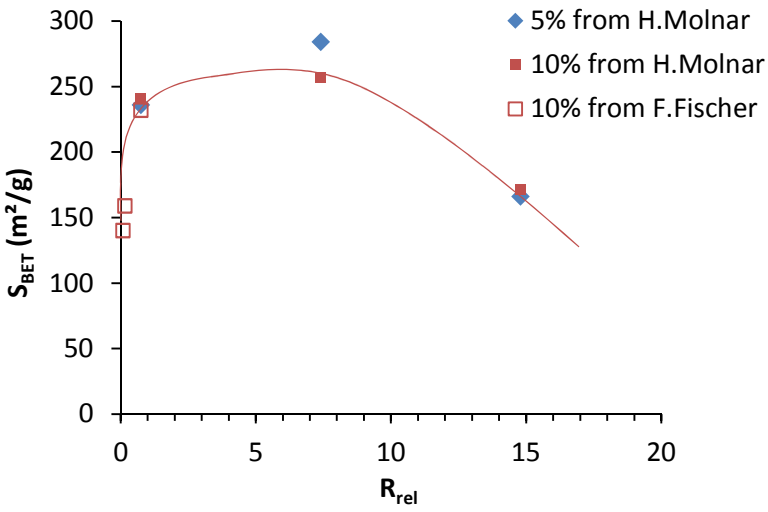

Figure IV. 23 : Specific surface areas of cellulose acetate aerogels as a function of R_{rel}. Data were taken from (Fischer, 2006) and from internal reports in Persée-Mines ParisTech (courtesy of H.Molnar and A.Rigacci).

3.1.4 Pore size distribution

Hg porosimetry was carried out on 5_{wt}% cross-linked aerocelluloses with various R_{rel} in the laboratory L2C. First, the buckling constant, used in the Pirard's theory (Pirard & Pirard, 1997) (c.f. Chapter II) of pores size reconstruction (Equation (IV. 13)), was determined for various R and is given in Figure IV. 24.

$$L = \frac{k}{P^{0.25}} \qquad \text{(IV. 13)}$$

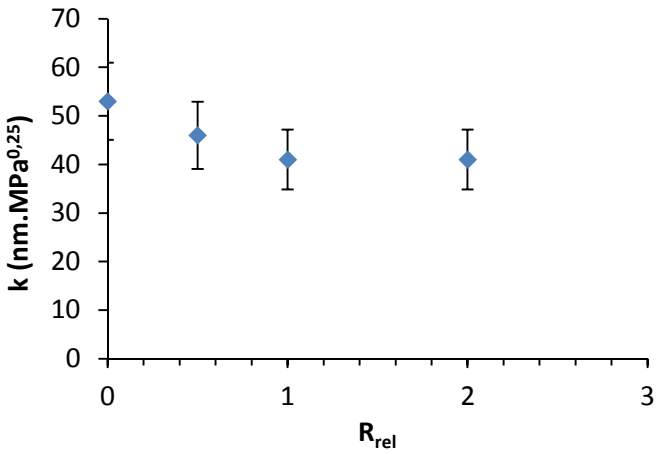

Figure IV. 24 : Buckling constant for cross-linked aerocelluloses.

As presented in Chapter III, the buckling constant for a 5_{wt}% non-crosslinked aerocellulose was determined to be k=56 nm.MPa$^{0.25}$. With the increase of ECH concentration in the reaction (R_{rel}) the buckling constant first slightly decreases and then becomes rather stable around 43 nm at

R > 1. This result allows us to suggest the influence of cross-linking on chains organization in aerocellulose and to predict other trends that will be discussed later.

Let us compare two cases:
A) Aerocellulose is prepared either from physical gels (in NaOH-water solvent) or via direct coagulation from solution (e.g. EMIMAc or EMIMAc + DMSO solvent) and
B) Via chemical cross-linking.

In case A, chains are self-associating whereas in case B chemical cross-linking junction are formed. It has to be noted that as ECH has two reactive functions the functionality of cross-linking junctions is maximum 4 (between two chains) as shown in Figure IV. 25.

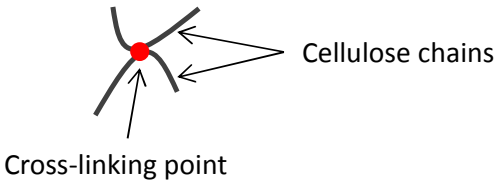

Figure IV. 25 : Schematic example of a cross-linking junction between two cellulose chains (with functionality 4).

The following structures and their evolution with the increase of cellulose concentration and degree of cross-linking are presented in Figure IV. 26:

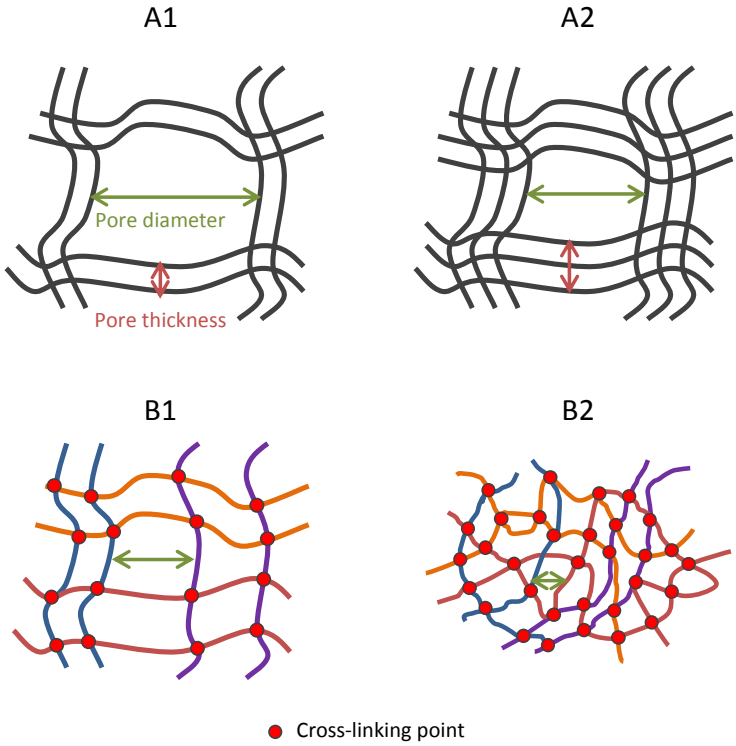

Figure IV. 26 : Schematic presentations of aerocellulose structures.
Case A : via physical gelation or direct coagulation. A1 at low cellulose concentration and A2 at higher cellulose concentration.
Case B: via chemical cross-linking. B1 at low cross-linking ratio and B2 at high cross-linking ratio.

The comparison of cases A and B allows making the following predictions:
- The increase of cellulose concentration from case A1 to case A2 leads to material densification, increase in pore walls thickness and decrease in pore size. This is what was obtained for non-crosslinked aerocelluloses from ionic liquids EMIMAc and EMIMAc/DMSO as described in Chapter III. The increase in buckling constant with cellulose concentration can be indirectly correlated with pore wall thickness and decrease in pore size (Figure IV. 26 A1 and A2).

- If comparing case A1 and B1, cellulose concentration is the same but because of cross-linking junctions cellulose chains are distributed in space in a more homogeneous way. We deduce "thinner" pore walls, what indirectly suggests the result obtained for the buckling constant. We also predict pores smaller in case B1 as compared to A1. This will be studied and discussed in the following paragraphs. The comparison of A1 with B1 suggests that the specific surface of B1 should be higher than that of A1, which was shown in Figure IV. 21.

- The increase of the degree of cross-linking, case B2 vs B1, obviously induces sample densification because of chains elasticity (as obtained in Figure IV. 18). Pore wall thickness should not change which is indirectly confirmed in Figure IV. 24 for the buckling constant. We predict the decrease of pore size.
- Finally, the increase of cellulose concentration and of the degree of cross-linking lead to a rather dense network (Figure IV. 18).

By using Equation (IV. 13), we reconstructed pore size distribution (PSD) of cross-linked aerocelluloses with R_{rel} varying from 0.25 to 2, and we compared them to non-crosslinked aerocellulose (R_{rel} = 0) in Figure IV. 27. All pore size distributions of cross-linked aerocelluloses are narrower and shifted to smaller pores as compared to non-crosslinked aerocelluloses, as it was observed on the SEM images. The result obtained is in-line with the hypothesis on the role of cross-linker: it leads to a more homogeneous structure with smaller pores as compared to non-cross-linked counterpart.
The theoretical porous volume is calculated according to Equation IV.14.

$$V_{p\ theoretical} = \frac{1}{\rho_{bulk}} - \frac{1}{\rho_{skeletal}} \qquad \text{(IV. 14)}$$

The ratio of the measured and theoretical porous volume was determined for each cross-linking ratio and is given in Table IV. 3. At low cross-linker concentration, the ratio is rather high showing that most of pores were characterized. For R=0, the ratio is around 100%. It seems rather impossible since macropores were observed on SEM. It shows that the Hg porosimetry technique has some limitations for fully characterizing pore size distribution. At higher cross-linker concentration, the ratio $V_{p\ measured}/ V_{p\ theoretical}$ decreases, reaching 10-20%. It seems that we might have both large macropores and micropores. The morphology observed by SEM confirms the presence of very small pores. Further experiments for characterizing micropores will be necessary to evaluate more precisely all the porous volume.

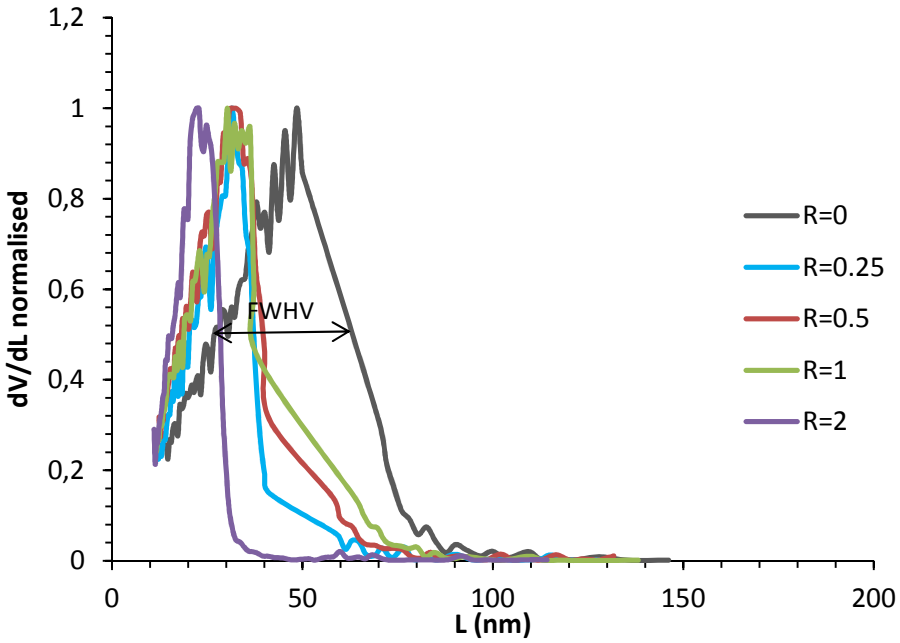

Figure IV. 27 : Pore size distribution by Hg porosimetry for 5$_{wt}$% cross-linked aerocelluloses for R$_{rel}$ from 0 to 2.

More precisely, we determined the maximum and the mean pore diameter $L_{p\ max}$ and $L_{p\ mean}$ and the full width at half value (FWHV) as described in Chapter II. They are reported in Table IV. 3.

Table IV. 3 : Structural properties of 5$_{wt}$% cross-linked aerocelluloses.

%C	R	ρ_{bulk} (g/cm^3)	porosity	S_{BET} (m²/g)	$\frac{V_{p\ measured}}{V_{p\ theoretical}} \times 100$	$L_{p\ max}$ (nm)	FWHV (nm)	$L_{p\ mean}$ (nm)
5	0	0.123	92 %	286	100 %	48	35	35
5	0.25	0.164	92 %	395	61 %	31	17	26
5	0.5	0.179	90 %	418	37 %	32	20	27
5	1	0.217	89 %	360	15 %	32	19	26
5	2	0.287	86 %	265	9 %	25	14	21

$L_{p\ max}$ decreases as soon as cellulose starts to be cross-linked. $L_{p\ max}$ (R_{rel} = 0) = 48 nm drops to $L_{p\ max}$ (R_{rel} = 0.25) = 31 nm. In the same way, $L_{p\ mean}$ decreases from 35 nm to 26 nm. For higher R_{rel}, $L_{p\ max}$ and $L_{p\ mean}$ are still decreasing, as an example R_{rel} = 2 $L_{p\ max}$ and $L_{p\ mean}$ equals to 14 nm and 21 nm respectively.

We compared the width of the distribution between samples of non-crosslinked and of R_{rel} = 0.25-aerocellulose. PSD of cross-linked aerocellulose narrows significantly as the FWHV drops from 35 to 17 nm, confirming the SEM observations. FWHV for R_{rel} = 2 is slightly narrower with 14 nm.

No major difference is observed of $L_{p\ max}$, $L_{p\ mean}$ and FWHV for formulations with R_{rel} = 0.25, 0.5 and 1, probably due to experimental errors. The results obtained confirm the predictions made in Figure IV. 26 on the role of cross-linker on aerocellulose structure. Even being very

rough, Figure IV. 26 describes the main trends on the evolution density, pore size and specific surface in cross-linked vs non-cross-linked cellulose.

Cellulose cross-linking seems to modify structural properties of aerocelluloses, even at low cross-linker concentrations. A formulation 5_{wt}% cellulose-R=0.5 appears very interesting from a structural point of view. It presents a moderate density $\rho_{bulk} = 0.18$ g/cm^3, the highest specific surface area $S_{BET} = 418$ m²/g, a smaller mean pore size $L_{p\ mean} \approx 25$ nm and a narrower pore size distribution compared to non-crosslinked aerocellulose.

3.2 Mechanical properties

Mechanical properties of cross-linked aerocelluloses were studied by uniaxial compression. Strain-stress curves for 5_{wt}% aerocellulose with various relative ECH concentrations R_{rel} from 0 to 2 are plotted in Figure IV. 28. As R_{rel} increases, aerocellulose becomes stiffer as the stress-strain curve is shifted upwards. From these curves, characteristic parameters were determined as Young modulus E, yield stress σ_{yield}, yield strain ε_{yield}, densification strain ε_d and energy absorbed from the beginning of the deformation to 40% strain $W_{40\%}$.

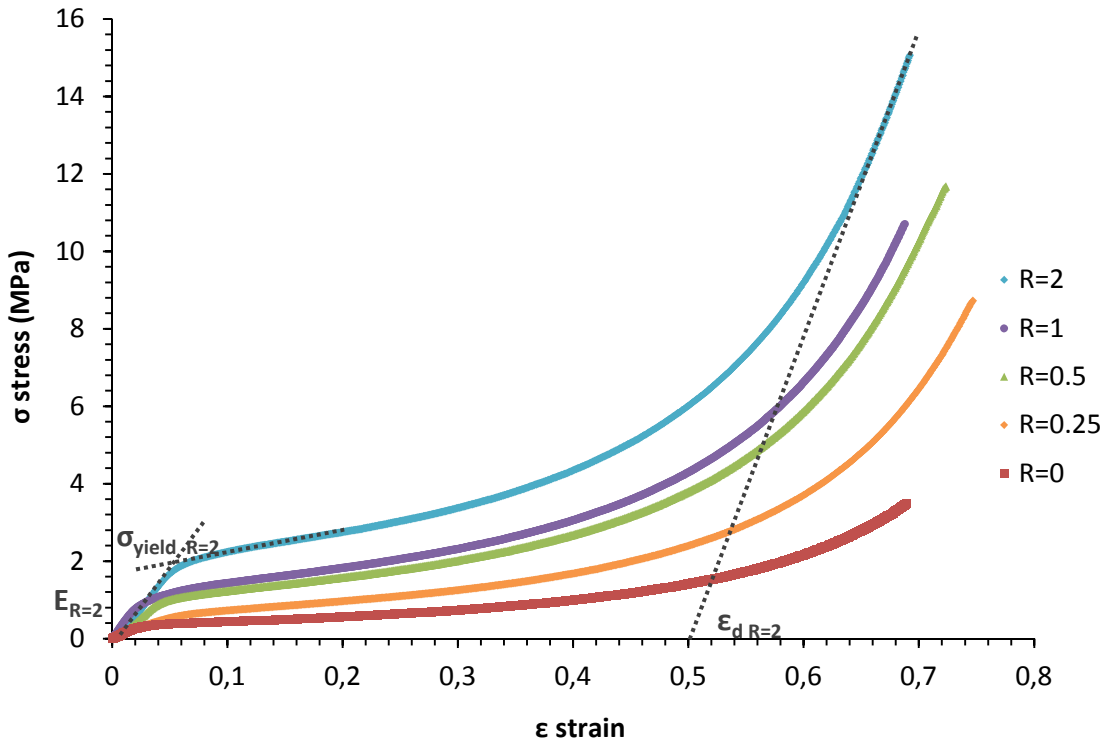

Figure IV. 28 : Stress-strain curves for 5_{wt}% aerocellulose with relative ECH concentrations R_{rel} from 0 to 2.

Table IV. 4 summarises mechanical properties determined from Figure IV. 28. Yield and densification strains seem to remain relatively constant and independent of R_{rel}, around 4-6% and 50% respectively.

Table IV. 4 : Mechanical properties of cross-linked aerocelluloses.

%C	R	ρ_{bulk} (g/cm^3)	E (MPa)	σ_{yield} (MPa)	ε_{yield}	ε_d	$W_{40\%}$ (kJ/m^3)	$W_{\varepsilon d}$ (kJ/m^3)
5	0	0.123	10	0.32	0.037	0.55	213	334
5	0.25	0.164	24	0.56	0.053	0.58	386	800
5	0.5	0.179	29	0.92	0.037	0.52	569	923
5	1	0.217	38	1.0	0.048	0.54	704	1092
5	2	0.287	43	2.2	0.061	0.50	835	1181

By using the model of Gibson and Ashby for foams and Equation (IV. 15), Young moduli and yield stress were plotted as a function of bulk density in Figure IV. 29.

$$E \sim \rho^m \quad \text{(IV. 15)}$$

$$\sigma_{yield} \sim \rho^n \quad \text{(IV. 16)}$$

The exponent m for cross-linked aerocelluloses equals $m = 2.4$ and for non-cross-linked aerocellulose it is $m = 2.8$ data taken from (Gavillon, 2007; Sescousse, Gavillon, & Budtova, 2011; Sescousse, 2010) for aerocelluloses prepared from NaOH-water and ionic liquid solvent. At equal density, e.g. ρ~0.16 g/cm^3, Young modulus increases from 15 for non-cross-linked aerocellulose to 24 MPa for the cross-linked. Cross-linking increases Young modulus by about 50% as compared with aerocellulose made from either physical gelation or direct coagulation.

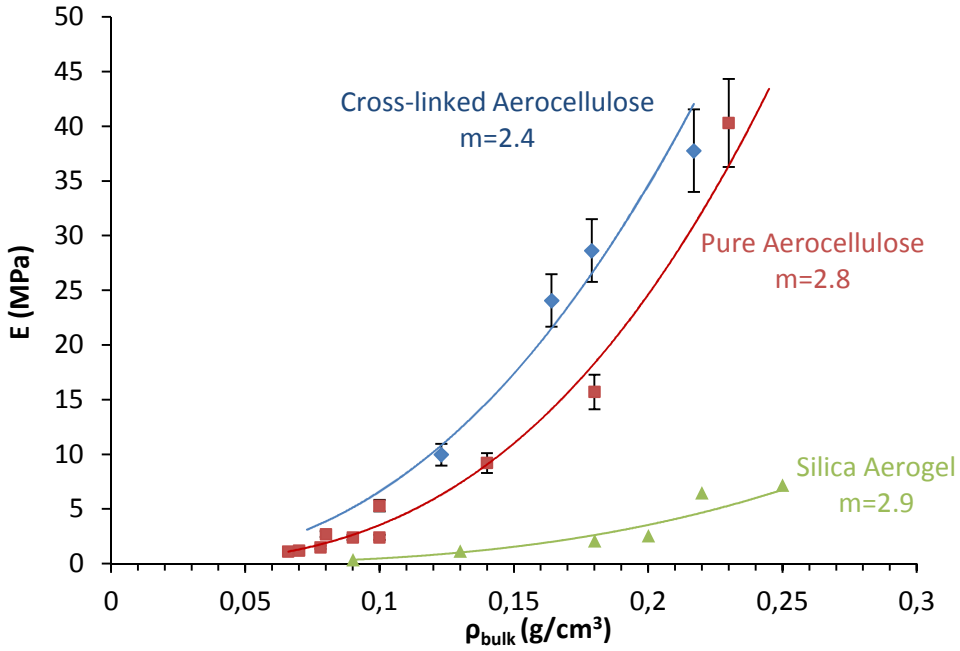

Figure IV. 29 : Young modulus as a function of bulk density for cross-linked aerocellulose. Comparison with non-crosslinked (pure) aerocellulose (data taken from (Gavillon, 2007; Sescousse et al., 2011; Sescousse, 2010)) and silica aerogels (Alaoui, Woignier, Scherer, & Phalippou, 2008).

In Figure IV. 29 the dependence of Young modulus on the density of silica aerogel is also shown. The exponent m = 2.9 similar to some organic aerogels (Pekala, Alviso, & LeMay, 1990) but the values are one order of magnitude lower than the ones of aerocellulose, cross-linked or not.

Yield stress is also plotted versus bulk density in Figure IV. 30. A power-law relationship is obtained according to Equation (IV. 16) with exponent *n*=2.2. Yield stress is slightly higher compared to pure aerocellulose (*n*=1.9). At equal density, e.g. ρ~0.16 g/cm^3, yield stress increases from about 0.4 to 0.6 MPa.

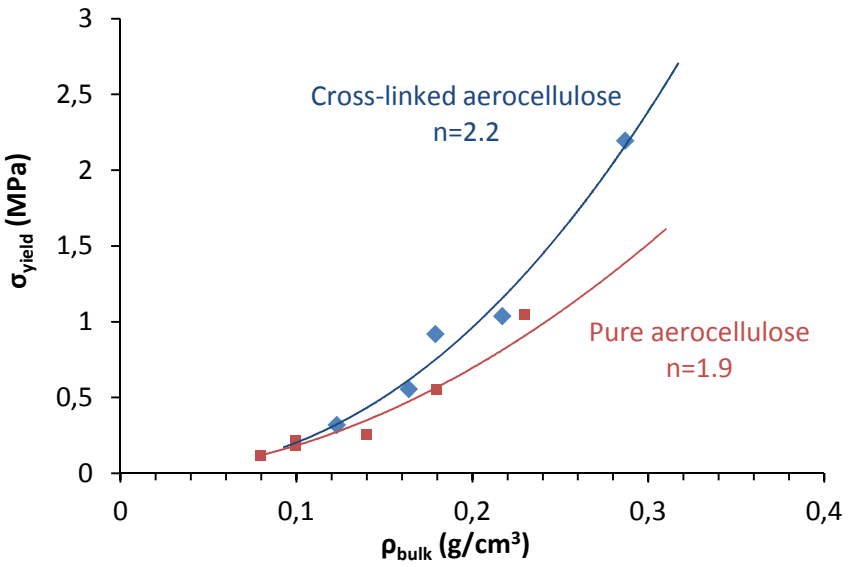

Figure IV. 30 : Yield stress as a function of bulk density for 5$_{wt}$% cross-linked and non-crosslinked (Gavillon, 2007; Sescousse et al., 2011; Sescousse, 2010) aerocelluloses.

Similarly, we compared the absorbed energy until 40% strain for cross-linked and pure aerocelluloses in Figure IV. 31. Both types of aerocelluloses fall on the same power-law relationship $W_{40\%} \sim \rho^{2.2}$. It may be explained by the fact that absorbed energy is highly dependent of material porosity. Cross-linked and pure aerocelluloses have similar porosity at equal density and therefore present similar mechanical behaviour.

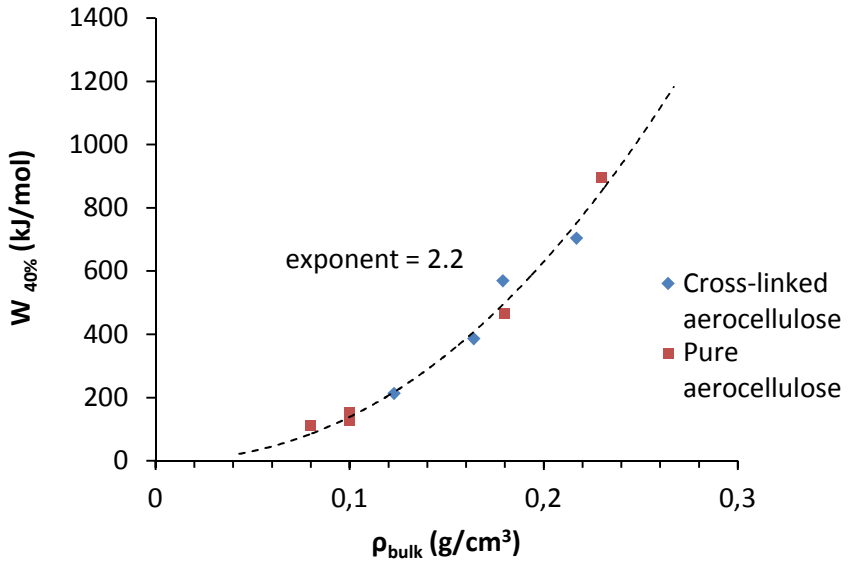

Figure IV. 31 : Absorbed energy $W_{40\%}$ versus bulk density for 5_{wt}% cross-linked and non-crosslinked (Gavillon, 2007; Sescousse et al., 2011; Sescousse, 2010) aerocelluloses.

Summarising, a short study of the mechanical properties of cross-linked aerocellulose showed that both cross-linked and not aerocelluloses have a similar behaviour under a uniaxial compression. However, at equal density, cross-linked aerocelluloses are slightly tougher (higher Young modulus and yield stress) than non-crosslinked ones.

3.3 Thermal properties

The influence of cross-linking on aerocellulose thermal properties was also investigated. The effective thermal conductivity can be split in three contributions (Equation (IV. 17)): the conduction of the solid phase, the conduction of the gaseous phase and the radiative transfer.

$$\lambda_{effective} = \lambda_{solid} + \lambda_{gas} + \lambda_{radiative} \qquad \text{(IV. 17)}$$

The effective thermal conductivities were measured on a Fox 150 heat flow meter in Persée Mines-ParisTech at 20°C (293 K) and are given as a function of bulk density in Figure IV. 32. The measurements were carried out on 5_{wt}% cross-linked aerocelluloses with R_{rel} = 0.25, 1 and 2 and the results for non-crosslinked aerocellulose prepared from NaOH-water solvent are also shown for comparison (30.8 $mW.m^{-1}.K^{-1}$ for 5_{wt}% cellulose and 32.2 $mW.m^{-1}.K^{-1}$ for 7_{wt}%).

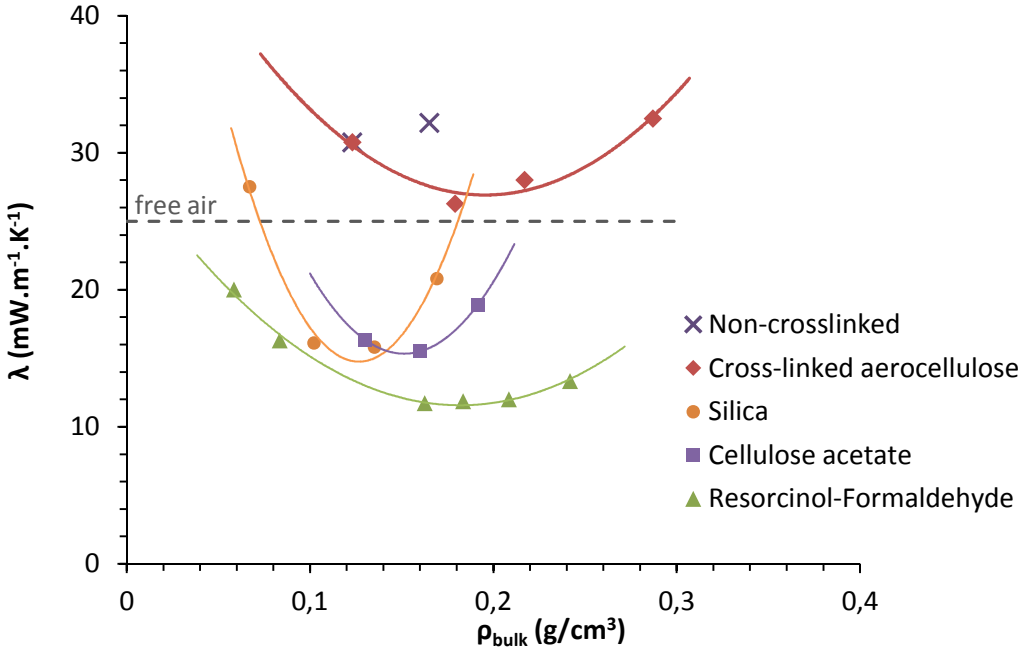

Figure IV. 32 : Effective thermal conductivity versus bulk density for pure and cross-linked aerocelluloses. Comparison with resorcinol-formaldehyde aerogels (adapted from (Ebert, 2011)) and cellulose acetate aerogels (Results from H.Molnar-Courtesy of A.Rigacci).

Figure IV. 32 shows that the dependence of thermal conductivity on density is concave, with a minimum $\lambda_{effective}$=26.2 mW.m^{-1}.K^{-1} for the density around 0.18 g/cm^3 which corresponds to R_{rel} = 0.5. This kind of curve is quite typical for either inorganic aerogels (silica (Bisson, Rigacci, Lecomte, & Achard, 2004)) or organic (resorcinol-formaldehyde or cellulose acetate)

It should be noted that for the same density, thermal conductivity of cross-linked aerocellulose is lower than that of non-crosslinked one. This shows that the idea of cellulose nanostructuring in order to decrease thermal conductivity worked and the optimal conditions were found. Unfortunately, it was not possible to reach the region of thermal super-insulation, with conductivity below 25 mW.m^{-1}.K^{-1}.

We determined the contribution of the conduction solid + gas by measuring conductivity at different temperatures. As the radiative conductivity is proportional to T^3 (Equation I.10), we plotted λ as a function of T^3 and extrapolated at $T \rightarrow 0$ to determine $\lambda_{gas+solid}$ (Figure IV. 33). Data are reported in Table IV. 5 for 5% and 7$_{wt}$% non-crosslinked and cross-linked aerocelluloses.

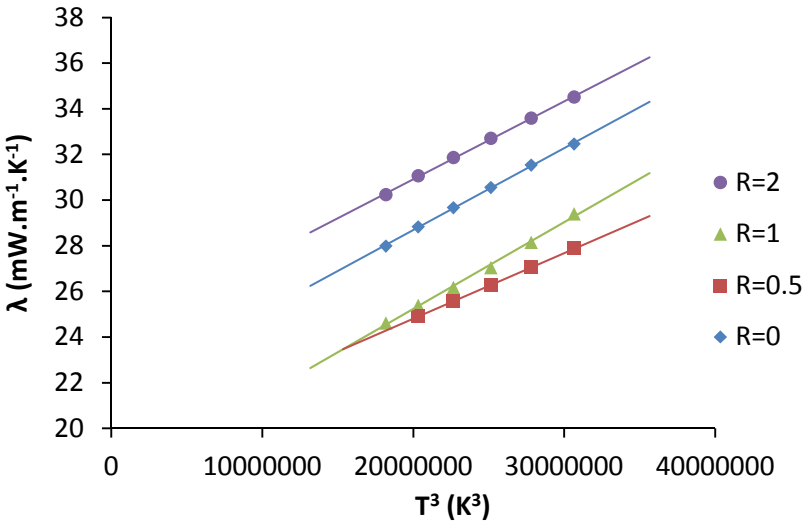

Figure IV. 33 : Thermal conductivity as a function of temperature for 5$_{wt}$% non-crosslinked (R_{rel} = 0) and cross-linked aerocelluloses.

By subtracting $\lambda_{effective} - \lambda_{solid+gas}$, we determined the $\lambda_{radiative}$ contribution. For all formulations, non-crosslinked or cross-linked aerocelluloses, the radiative part represents about 30% of the total conductivity. It does not seem to be influenced by cellulose concentration or ECH concentration R_{rel}. It seems surprising, as it was shown in Chapter I that $\lambda_{radiative}$ is inversely proportional to the bulk density.

Table IV. 5 : Thermal characterisations of pure and cross-linked aerocelluloses

$C_{cellulose}$, ($_{wt}$%)	R_{rel}	ρ_{bulk} (g/cm^3)	$\lambda_{effective}$ (mW.m^{-1}.K^{-1})	$\lambda_{gas+solid}$ (mW.m^{-1}.K^{-1})	%$\lambda_{radiative}$
5	0	0.123	30.8	21.5	30
5	0.5	0.179	26.2	19	28
5	1	0.217	28.0	19	32
5	2	0.287	32.5	24.1	26
7	0	0.165	32.2	23.6	27
7	0.5	0.228	30.7	21.5	30
7	1	0.349	32.8	25.4	23

Figure IV. 34 displays the different thermal contributions: the conduction of solid and gas phases and radiative for 5$_{wt}$% aerocelluloses. As the radiative part seems to be independent on the density, the effective conductivity is mainly driven by solid+gas conduction. $\lambda_{solid+gas}$ also presents a curve with a minimum around $\rho \approx 0.18$ g/cm^3.

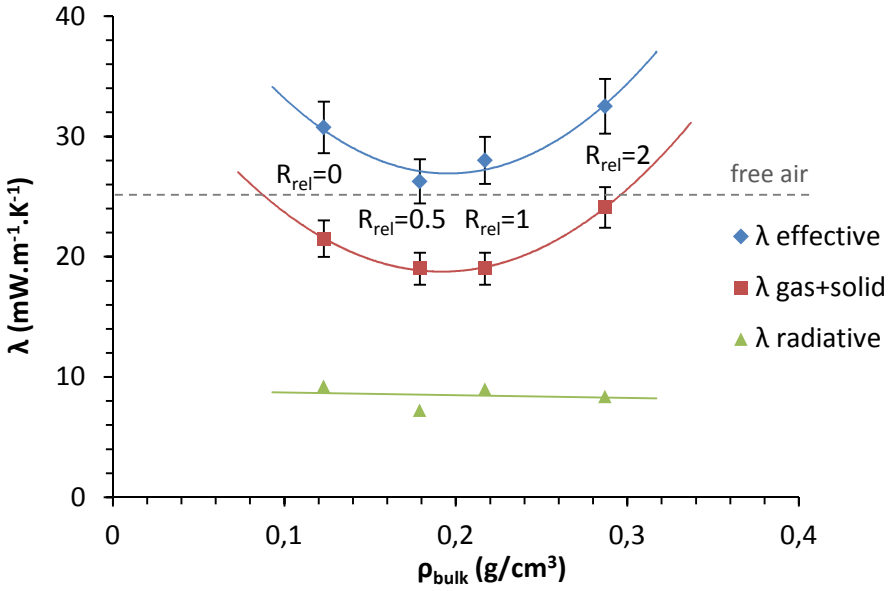

Figure IV. 34 : Effective, solid-gas and radiative conductivity as a function of bulk density for 5_{wt}% aerocelluloses.

The shape of the $\lambda_{solid+gas}$ curve may be explained that at low densities, samples present larger pores which increase the conduction of the gas phase. At high densities, the solid conduction contribution becomes more important as it is directly related to bulk density by a power law $\lambda_{solid} \sim \rho^{1.5}$ (Equation I.6). Therefore there is an optimal density where both the conduction of gas and solid phase are minimized. Unfortunately, we did not have time to determine the contribution of the solid phase by hot-wire at low pressure and temperature in CSTB (c.f. Chapter II) in order to confirm this hypothesis.

The formulation 5_{wt}% cellulose-R_{rel} = 0.5 presents an improved effective conductivity compared to 5_{wt}% non-crosslinked aerocellulose. It may be explained by a decrease in the gaseous conduction. For R_{rel} = 0.5, we showed that mean pore size is about 27 nm (as calculated from the "reconstructed" pore size distribution using Hg porosimetry) vs 35 nm for non-crosslinked aerocellulose, with a narrower pore size distribution. It should be noted that these mean pore size values should be taken with care and can be used only for comparison. First, pore size distribution is obtained in an indirect way (Pirard & Pirard, 1997), and also only part of pores are detected: large pores are not taken into account (about 50%of the total porous volume is effectively measured). What we want to qualitatively demonstrate here is that with the decrease of pore size due to cellulose cross-linking thermal conductivity was decreased. It is highly probable that a certain fraction of large pores (not detected) remained in cross-linked cellulose leading to thermal conductivities higher than of the air.

Similar experiments were carried out for 7_{wt}% non-crosslinked and cross-linked aerocelluloses (Figure IV. 35). The radiative contribution seems to be also constant within experimental errors. A minimum in the solid+gas conduction is observed for the same ECH concentration, R_{rel} = 0.5. The effective conductivity reaches therefore a minimum for R_{rel} = 0.5 with $\lambda_{effective}$ = 30.7 $mW.m^{-1}.K^{-1}$ against 32.2 $mW.m^{-1}.K^{-1}$ for non-crosslinked aerocellulose.

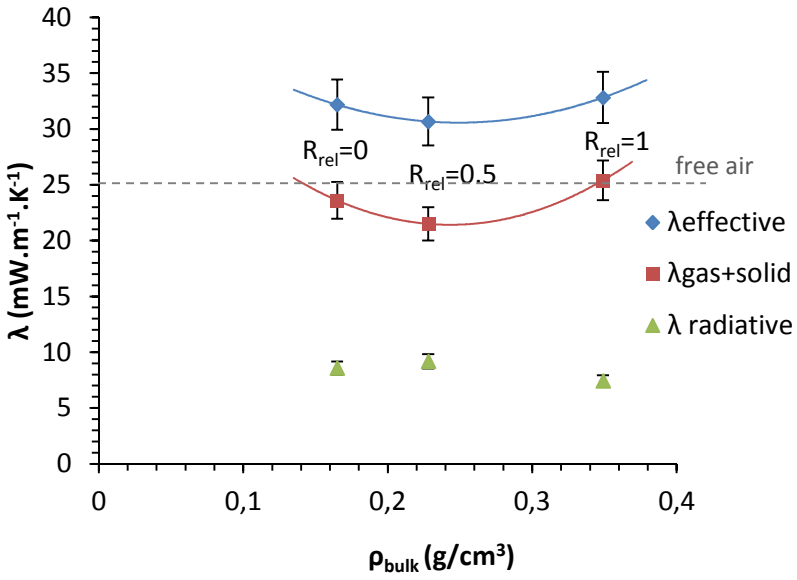

Figure IV. 35 : Effective, solid-gas and radiative conductivity as a function of bulk density for 7_{wt}% aerocelluloses.

The solid conduction for 7_{wt}% non-crosslinked aerocellulose (R_{rel} = 0) was determined by hot-wire technique at -118°C and 10^{-6} hPa by Herbert Sallée in CSTB, Grenoble, and equals λ_{solid}=3.2 $mW.m^{-1}.K^{-1}$. Due to a lack of time, it was not possible to measure the solid conductivity for cross-linked aerocelluloses. We estimated hypothetically the solid conductivity of 7%-R_{rel} = 0.5 aerocellulose of about 5 $mW.m^{-1}.K^{-1}$ (Equation I.6). It represents about 16% of the total conductivity. The gas conduction contributes therefore for the major part of the effective conductivity, with more than 60%. This shows the importance of cellulose nanostructuration.

We showed that cross-linking of cellulose allows producing aerocelluloses with more homogeneous and fine morphology as compared to non-crosslinked counterparts and smaller pore sizes. Optimized formulations, 5_{wt}%-R_{rel} = 0.5 or 7_{wt}%-R_{rel} = 0.5, give improved thermal properties with effective conductivity of 26.2 and 30.7 $mW.m^{-1}.K^{-1}$ respectively. By tuning the morphology it is thus possible to decrease the gas conduction and therefore improve the thermal properties of aerocelluloses. Unfortunately, cross-linked aerocelluloses give conductivities higher than 25 $mW.m^{-1}.K^{-1}$ but allow us a better understanding of the heat flow mechanisms and the importance of reducing the gas conduction contribution.

4. Influence of drying method on the morphology

It was shown previously that cross-linked coagulated cellulose requires a solvent exchange step for being dried by supercritical CO_2. However, this step may lead to sample dramatic contraction thus may modify the morphology. We investigated therefore other types of drying that do not require a solvent exchange. The goal was to keep cross-linked cellulose coagulated in water. We

looked into freeze-drying as this allows direct “drying” of swollen-in water coagulated cellulose. Below we compare three different drying ways of cross-linked coagulated celluloses: supercritical drying (aerogels), freeze-drying (cryogels) and evaporative drying (xerogels).

Freeze-drying is another way to decrease liquid-vapour interfaces in gels. After freezing samples, the solvent is removed by sublimation under low pressure to give a cryogel. Similarly to aerocellulose, we will call these new porous materials cryocelluloses.

Three different types of freezing can be envisaged:
- Fast: samples are placed in a glass beaker (to optimise the heat transfer) and immersed in liquid nitrogen (-196 °C)
- Moderate: samples are placed in a glass beaker are immersed in an ethanol bath cooled down in a freezer (-60°C)
- Slow: samples are directly placed in a freezer (-18°C).

5_{wt}% non-crosslinked and cross-linked (R_{rel} = 2) cryocellulose samples were prepared from these three different freezing processes and are shown in Figure IV. 36. For fast freezing, cross-linked samples tend to crack into small pieces as a result of the thermal shock and water expansion during freezing (Figure IV. 36d). For moderate and slow drying, samples more or less keep their shape (Figure IV. 36c, e, f). After drying, samples obtained from fast freezing, even if they are presented in small pieces, can be easily handled and keep a certain cohesion (Figure IV. 36 a and d). Samples from moderate freezing appear more distorted (Figure IV. 36b, e). From slow freezing, samples have poor mechanical resistance and break very easily when manipulated (Figure IV. 36c). This is slightly less pronounced for highly cross-linked cryocelluloses (Figure IV. 36f).

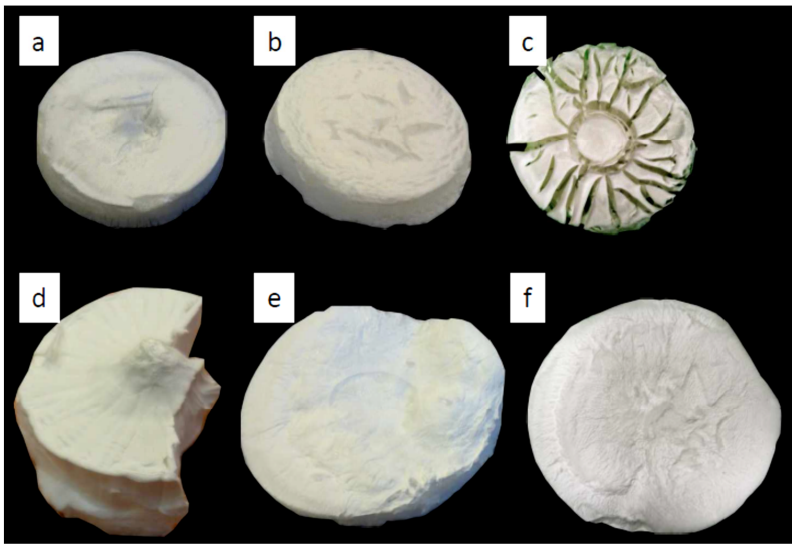

Figure IV. 36 : Different methods of freezing for 5_{wt}% non-crosslinked cryocelluloses: fast (a), moderate (b), slow (c);
and for 5_{wt}% cross-linked with R_{rel} = 2 cryocelluloses : fast (d); moderate (e), slow (f).

These large differences in cryocelluloses visual aspect are due to the solvent expansion during the freezing and essentially to the development of ice crystals. A slow freezing favors the formation of larger ice crystals (Figure IV. 37c) as compared to a fast freezing (Figure IV. 37b). As a result, ice crystals compress the porous structure and large pores are created (Job et al., 2005).

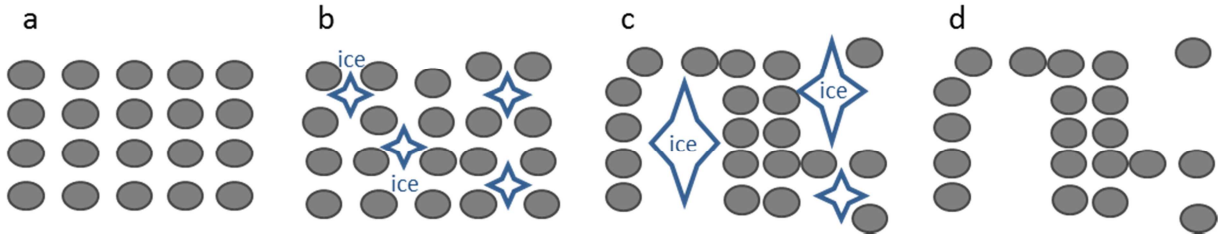

Figure IV. 37 : Ice growth during freezing. Comparison of wet coagulated cellulose (a), after fast freezing (b), slow freezing (c), and cryogel after a slow freezing (d) (adapted from (Job et al., 2005)).

In the following, we used the fast method for freezing for a more detailed analysis of aerocellulose density and morphology.

Cryocelluloses obtained presented large inhomogeneities in their structure for both non-crosslinked and cross-linked samples. Large channels or “megalopores” (pores larger than 10 µm) were visible by SEM (Figure IV. 38), mainly due to ice growth during freezing, as explained previously.

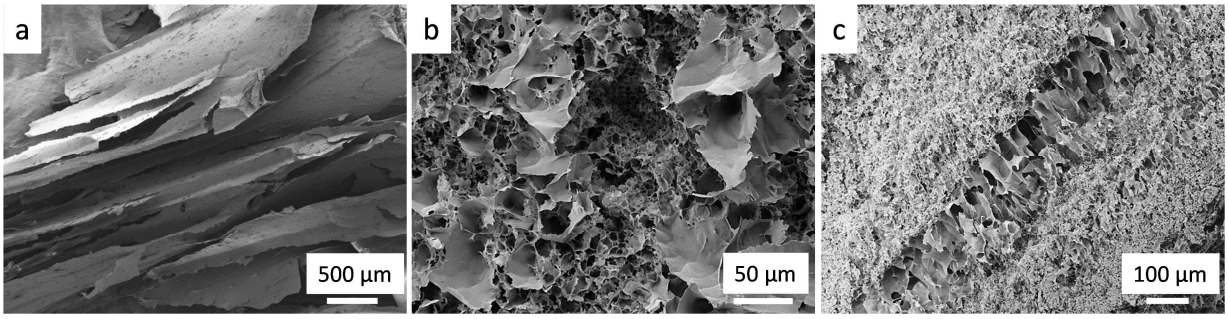

Figure IV. 38 : SEM images of inhomogeneities in 5_{wt}% cryocellulose from non-crosslinked cellulose (a), from cross-linked with R_{rel}=0.5 (b) and from R_{rel}=1 (c).

We investigated the influence of the relative concentration in cross-linker R_{rel} on the morphology of cryocelluloses. SEM images of the most homogeneous parts of samples are given in Figure IV. 39. For non-crosslinked cryocelluloses, the texture presents mainly pores between 1 and 5 µm and sometimes larger pores around 10 µm as it wæs already observed in (Chang, Lue, & Zhang, 2008; Chang & Zhang, 2011; Jin, Nishiyama, Wada, & Kuga, 2004) (Figure IV. 39a). For cross-linked cryocellulose, the morphology is different: cellulose is organized in “sheets” probably due to the fact that thin pore walls do not resist ice crystal growth and thus pores contract. The morphology is not homogeneous with big pores from 1 to 10 µm, and even larger (Figure IV. 39b). The increase of cross-linking decreases pore size in cryocelluloses: for

example, for R_{rel} = 2, pores are below 1 µm (Figure IV. 39d). With this inhomogeneous morphology with very large pores there was no reason to measure thermal conductivity of cryocelluloses.

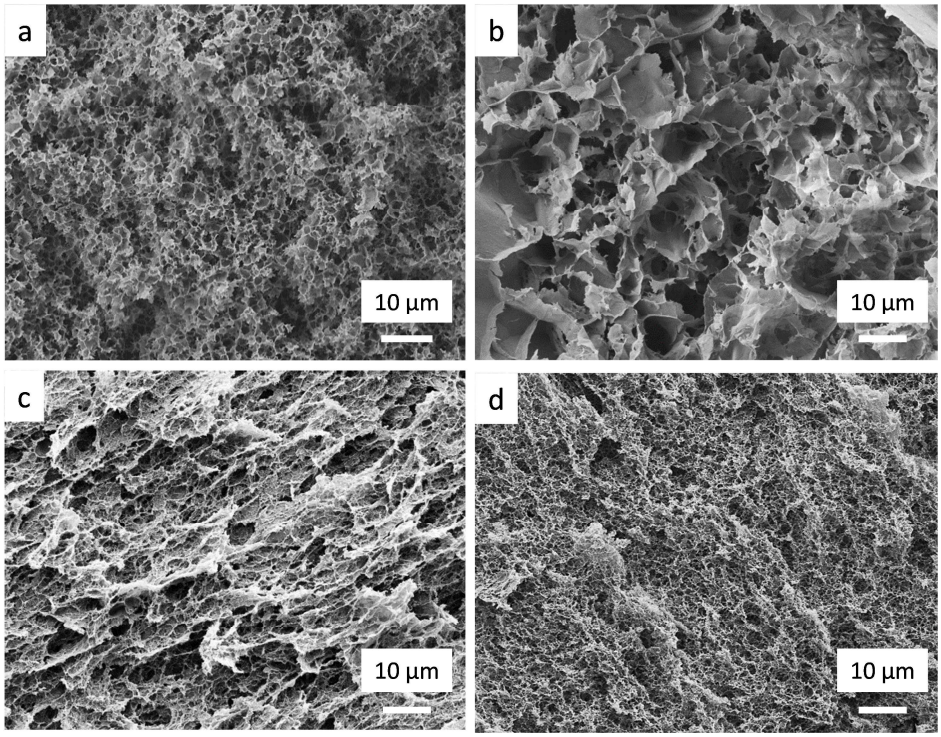

Figure IV. 39 : SEM observations of cryocelluloses from non-crosslinked cellulose (a) and from R_{rel} = 0.5 (b), R_{rel} = 1 (c) and R_{rel} = 2 (d) cross-linked cellulose.

It was interesting to compare three ways of drying of coagulated cellulose, cross-linked or not: supercritical CO_2, freeze-drying and evaporative drying which give aerocellulose, cryocellulose and xerocellulose, respectively. Evaporative drying was performed at room conditions (c.f. Chapter II). We also studied the influence of R_{rel} on some structural properties of cellulose dried in different conditions.

Figure IV. 40 displays 5_{wt}% non-crosslinked and cross-linked cellulose (with R_{rel}=1 and 2) after supercritical CO_2drying, freeze-drying and evaporative drying. Compared to wet samples, all dried materials tend to shrink. Evaporative drying is responsible for a massive shrinkage of all cellulose materials (Figure IV. 40a, b, c) due to strong surface tension between the evaporating liquid and gas and therefore important capillary forces (c.f. Chapter I), and also cellulose-cellulose interactions via hydrogen bonding. For non-crosslinked cellulose, $scCO_2$ and freeze-drying give a similar shrinkage (Figure IV. 40a, b). For cross-linked cellulose, $scCO_2$ drying shrinks samples more significantly than freeze-drying due to contraction during solvent exchange step (Figure IV. 40d, e and Figure IV. 40g, h).

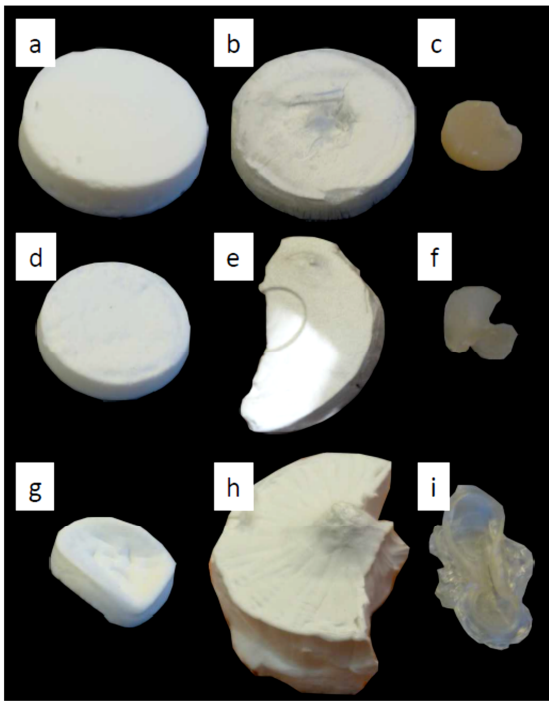

Figure IV. 40 : Influence of drying on 5_{wt}% pure and cross-linked cellulose.
Non-crosslinked cellulose dried by $scCO_2$ (a), freeze-drying (b), evaporative (c).
Cross-linked R_{rel} = 1 cellulose dried by $scCO_2$ (d), freeze-drying (e), evaporative (f).
Cross-linked R_{rel} = 2 cellulose dried by $scCO_2$ (g), freeze-drying (h), evaporative (i).

We measured bulk density for all celluloses presented above (Figure IV. 41) and calculated their porosity (Table IV. 6).

Table IV. 6 : Comparison of structural properties of aerocellulose, cryocellulose and xerocellulose.

Type of drying	$scCO_2$			$N_{2\,liq}$-freeze drying			Evaporative	
R_{rel}	ρ_{bulk} (g/cm^3)	Porosity (%)	S_{BET} (m²/g)	ρ_{bulk} (g/cm^3)	S_{BET} (m²/g)	Porosity (%)	ρ_{bulk} (g/cm^3)	Porosity (%)
0	0.123	92	286	0.108	37	93	1.48	4
1	0.216	86	360	0.042	15	97	1.37	13
2	0.287	82	265	0.055	110	96	1.13	25

As shown previously in Figure IV. 18, bulk density of aerocelluloses increases linearly with the increase of relative concentrations of ECH, R_{rel}. Porosities are around 80-90%. For evaporative drying, densities are much higher than the ones for aerocelluloses, between 1.1 and 1.5 g/cm^3. They slightly decrease with R_{rel} increase and the values are somehow close the density of cellulose (1.55 g/cm^3). The porosity is therefore very low, between 4 and 25%.

Freeze-dried samples have lower bulk densities as compared to aerocelluloses. Pure cryocellulose has $\rho \approx 0.1$ g/cm^3 whereas cross-linked cryocelluloses have bulk densities twice lower $\rho \approx 0.05$ g/cm^3, not depending much on ECH concentration. As freeze-drying shrinks samples moderately, the volume of dried samples is close to the volume of wet samples. Cross-

linked coagulated celluloses ($R_{rel} \geq 1$) are more swollen in water than non-crosslinked counterpart: a larger volume obviously decreases the bulk density. Porosity stands around 95%.

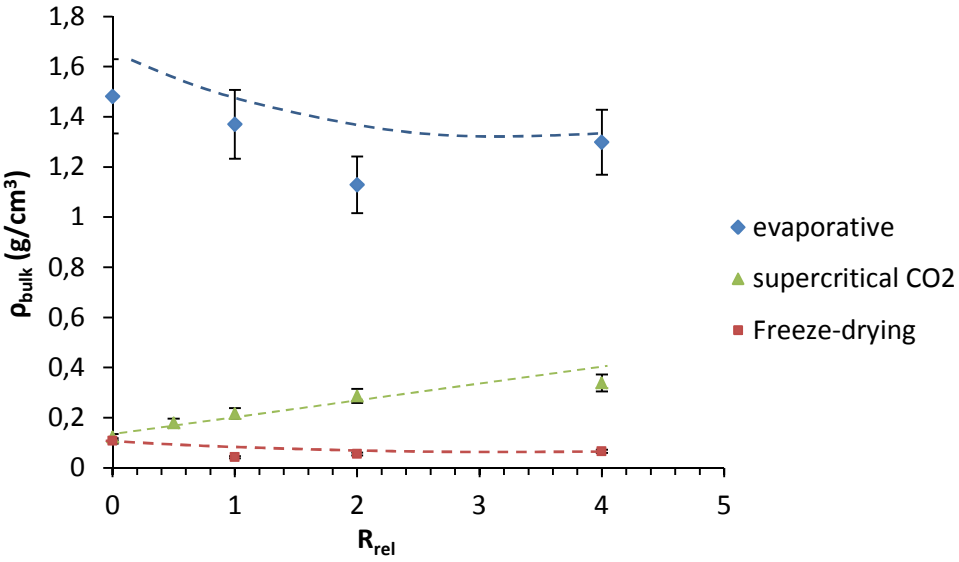

Figure IV. 41 : Bulk density versus relative concentration in cross-linker R_{rel} for 5_{wt}% aerocellulose, cryocellulose and xerocellulose.

Specific surface areas of cryocelluloses were measured in the laboratory L2C in the University of Montpellier. For 5_{wt} % non-crosslinked cryocellulose, we obtained $S_{BET} = 37$ m²/g. This decrease in pores surface, freeze-drying vs supercritical drying, is mainly due to the loss of nanostructure. The value obtained is rather low as compared to results reported in (Jin et al., 2004) where crycellulose was obtained from another solvent, $Ca(SCN)_2$. They obtained S_{BET} around 100 m²/g. For $R_{rel} = 2$ cryocellulose, specific surface area is higher, 110 m²/g. More data are needed to evaluate the influence of R_{rel} on cryocelluloses structural parameters..

Cross-linked cryocelluloses are of interest as they are highly porous and extremely light. In the wet state, they have a high swelling ratio and keep this volume after freeze-drying. They can be interesting for controlled drug release.
Thus, we initiated a collaboration with Diana Ciolacu from the “Petru Poni” Institute of Macromolecular Chemistry in Iasi-Romania to study the incorporation and the release of the procaine from cross-linked cryogels. Studies are currently on-going.

Conclusions

In this chapter, cellulose chemical cross-linking was studied in the view of aerocellulose nanostructuration. Cross-linking was performed in the 8%NaOH-water by epichlorohydrin (ECH). The properties of gelling solutions, of coagulated wet cellulose and of aerocellulose were studied in details. The influence of drying (scCO2, freeze-drying and evaporative drying) on cellulose density and morphology was also briefly investigated.

First, we studied the chemical cross-linking of cellulose in the liquid state by rheology. Dynamic viscoelastic measurements were performed. We determined the times of gelation at different ECH concentrations. We observed that gelation depends on the relative cross-linker concentration R_{rel} (which is the molar ratio of ECH and cellulose). The gelation time of cellulose solutions in the presence of ECH is strongly delayed as compared to physical gelation in 8%NaOH-water, with a maximum at $R_{rel} = 0.5$. It shows a competition between physical and chemical cross-linking. The cross-linker acts as a "spacer" between cellulose chains which are therefore more spatially separated and decreases the probability of chains self-association via hydrogen bonding.
Gelation time of cellulose solutions in the presence of ECH decreases exponentially with temperature with a particular behaviour observed for $R_{rel} = 0.5$ where cellulose solution is slightly less sensitive to temperature increase. It can be explained by the fact that the cross-linker spaces out chains limiting cellulose-cellulose interactions even at high temperatures.

It was not possible to determine accurately the effective cross-linking degree and thus we used the relative concentration of ECH in the reaction, R_{rel}. ^{13}C-NMR gave information on the most favorable position on cellulose hydroxyl groups for cross-linking which is on C_2 and C_3 rather than on C_6.

We characterized coagulated cross-linked cellulose samples by their swelling ratios. They increased dramatically as compared to non-crosslinked counterpart until $R_{rel} = 1$ (%SR≈3500) and decreases at higher R_{rel} values (%SR≈1500). We hypothise that the addition of ECH "separates" cellulose chains which become less mobile and prevent the formation of hydrogen bonds. This creates additional pores filled with water, which increases swelling ratios. At lower R_{rel}, samples were opaque whereas at higher cross-linking ratio, as $R_{rel} \geq 2$, they were completely transparent. The structure of coagulated cellulose with more chemical cross-links is thus more homogeneous than non-crosslinked cellulose.

Coagulated cellulose swollen in water cannot be directly dried by $scCO_2$ and requires a solvent exchange step. Several fluids compatible with $scCO_2$ were investigated and methanol was chosen as the shrinkage of samples was rather limited as compared to ethanol or acetone. A progressive solvent exchange was preferred.

Aerocelluloses were obtained via drying with supercritical CO_2. We studied and correlated structural, mechanical and thermal properties of cross-linked cellulose aerogels and their dependence on the relative cross-linker concentration, R_{rel}.
We showed that bulk density increases linearly with the increase of ECH concentration for 5% and 7_{wt}% aerocelluloses. All pore size distributions of cross-linked aerocelluloses are narrower and shifted to smaller pores as compared to non-crosslinked aerocelluloses. Specific surface area increases from $R_{rel} = 0$ to $R_{rel} = 0.5$ and then decreases at higher ratios. Using Hg porosimetry, pore wall characteristic such as buckling constant was determined. For cross-linked aerocelluloses it is lower than for the non-crosslinked. We suggested to qualitative model describing different ways of structure formation during physical and chemical cellulose gelation. This model predicts the main trends that were observed experimentally.

Cellulose cross-linking seems to modify structural properties of aerocelluloses, even at low cross-linker concentrations. A formulation 5_{wt}% cellulose-$R_{rel} = 0.5$ appears very interesting with a moderate density $\rho_{bulk} = 0.18$ g/cm^3, a higher specific surface area $S_{BET} = 418$ m²/g and a narrower pore size distribution with lower mean pore value compared to non-crossliked aerocellulose.

Mechanical properties of cross-linked aerocelluloses were studied by uniaxial compression. Young moduli and yield stresses increase with bulk density as described by power law dependence: $E \sim \rho^{2.4}$ and $\sigma \sim \rho^{2.2}$. At equal density, cross-linked aerocelluloses are slightly tougher (higher Young modulus and yield stress) than non-crosslinked ones.

Effective thermal conductivity of 5% and 7_{wt}% cross-linked aerocellulose was measured. Minima were observed for both cellulose concentrations at $R_{rel} = 0.5$ confirming that the idea the decrease of thermal conductivity via cellulose nanostructuration due to chemical cross-linking works. The optimal formulations give the effective thermal conductivity of 26.2 and 30.7 mW.m^{-1}.K^{-1} for 5 and 7_{wt}% cellulose with $R_{rel} = 0.5$, respectively. Unfortunately, cross-linked aerocelluloses have the best conductivities higher than the one of the air, 25 mW.m^{-1}.K$^{-1,}$ not allowing the preparation thermal super-insulating material. We suppose that large macropores are still present in cross-linked samples not allowing moving into thermal superinsulation region.

Finally, we compared the influence of drying method, supercritical drying, freeze drying and evaporative drying, on some properties and morphology of chemically cross-linked cellulose. As expected, evaporative drying gives almost non-porous materials. Freeze-dried samples are highly porous and extremely light but present large macropores and inhomogeneities.

Bibliography

Alaoui, A. H., Woignier, T., Scherer, G. W., & Phalippou, J. (2008). Comparison between flexural and uniaxial compression tests to measure the elastic modulus of silica aerogel. *Journal of Non-Crystalline Solids*, *354*(40-41), 4556–4561.

Barton, A. F. M. (1991). *CRC Handbook of Solubility Parameters and Other Cohesion Parameters, 2nd edition*. (CRC Press, Ed.). CRC Press.

Bisson, A., Rigacci, A., Lecomte, D., & Achard, P. (2004). Effective thermal conductivity of divided silica xerogel beds. *Journal of Non-Crystalline Solids*, *350*, 379–384.

Cai, J., Liu, S., Feng, J., Kimura, S., Wada, M., Kuga, S., & Zhang, L. (2012). Cellulose-silica nanocomposite aerogels by in situ formation of silica in cellulose gel. *Angewandte Chemie (International ed. in English)*, *51*(9), 2076–9.

Capitani, D., Alessandro, M., Nobile, D., Mensitieri, G., Sannino, A., & Segre, A. L. (2000). ^{13}C Solid-State NMR Determination of Cross-Linking Degree in Superabsorbing Cellulose-Based Networks, *Macromolecules*, *33*(2), 430–437.

Chang, C., Duan, B., Cai, J., & Zhang, L. (2010). Superabsorbent hydrogels based on cellulose for smart swelling and controllable delivery. *European Polymer Journal*, *46*(1), 92–100.

Chang, C., Lue, A., & Zhang, L. (2008). Effects of Crosslinking Methods on Structure and Properties of Cellulose/PVA Hydrogels. *Macromolecular Chemistry and Physics*, *209*(12),

Chang, C., & Zhang, L. (2011). Cellulose-based hydrogels: Present status and application prospects. *Carbohydrate Polymers*, *84*(1), 40–53.

Chang, C., Zhang, L., Zhou, J., Zhang, L., & Kennedy, J. F. (2010). Structure and properties of hydrogels prepared from cellulose in NaOH/urea aqueous solutions. *Carbohydrate Polymers*, *82*(1), 122–127.

Ciolacu, D., Oprea, A. M., Anghel, N., Cazacu, G., & Cazacu, M. (2012). New cellulose–lignin hydrogels and their application in controlled release of polyphenols. *Materials Science and Engineering: C*, *32*(3), 452–463.

De Miguel, I., Rieumajou, V., & Betbeder, D. (1999). New methods to determine the extent of reaction of epichlorohydrin with maltodextrins. *Carbohydrate Research*, *319*(1-4), 17–23.

Delval, F., Crini, G., Bertini, S., Filiatre, C., & Torri, G. (2005). Preparation, characterization and sorption properties of crosslinked starch-based exchangers. *Carbohydrate Polymers*, *60*(1), 67–75.

Ebert, H.-P. (2011). Thermal Properties of Aerogels. In M. A. Aegerter, N. Leventis, & M. M. Koebel (Eds.), *Aerogels Handbook SE - 23* (pp. 537–564). Springer New York.

El Seoud, O. A., Fidale, L. C., Ruiz, N., D'Almeida, M. L. O., & Frollini, E. (2007). Cellulose swelling by protic solvents: which properties of the biopolymer and the solvent matter? *Cellulose*, *15*(3), 371–392.

Fidale, L. C., Ruiz, N., Heinze, T., & El Seoud, O. A. (2008). Cellulose Swelling by Aprotic and Protic Solvents: What are the Similarities and Differences? *Macromolecular Chemistry and Physics*, *209*(12), 1240–1254.

Fischer, F. (2006). Synthèse et étude de matériaux nanostructurés à base d'acétate de cellulose pour applications énergétiques., *PhD thesis*, Ecole des Mines de Paris.

Fischer, F., Rigacci, A., Pirard, R., Berthon-Fabry, S., & Achard, P. (2006). Cellulose-based aerogels. *Polymer*, *47*(22), 7636–7645.

Gavillon, R. (2007). Préparation et caractérisation de matériaux cellulosiques ultra poreux., *PhD thesis*, Ecole des Mines de Paris.

Hamerstrand, G. E., Hofreiter, B. T., & Mehltretter, C. L. (1960). Determination of the extent of reaction between epichlorohydrin and starch. *Cereal Chem*, *37*, 519 – 524.

Innerlohinger, J., Weber, H. K., & Kraft, G. (2006). Aerocellulose: Aerogels and Aerogel-like Materials made from Cellulose. *Macromolecular Symposia*, *244*(1), 126–135.

Jin, H., Nishiyama, Y., Wada, M., & Kuga, S. (2004). Nanofibrillar cellulose aerogels. *Colloids and Surfaces A: Physicochemical and Engineering Aspects*, *240*(1-3), 63–67.

Job, N., Théry, A., Pirard, R., Marien, J., Kocon, L., Rouzaud, J.-N., Béguin, F., et al. (2005). Carbon aerogels, cryogels and xerogels: Influence of the drying method on the textural properties of porous carbon materials. *Carbon*, *43*(12), 2481–2494.

Jyothi, A. N., Moorthy, S. N., & Rajasekharan, K. N. (2006). Effect of Cross-linking with Epichlorohydrin on the Properties of Cassava (Manihot esculenta Crantz) Starch. *Starch - Stärke*, *58*(6), 292–299.

Luby, P., & Kuniak, L. (1979). Relation between relative reactivity and accessibility of cellulose hydroxyl groups. *Die Makromolekulare Chemie*, *180*, 2379–2386.

Pekala, R. (1989). Organic aerogels from the polycondensation of resorcinol with formaldehyde. *Journal of Materials Science*, *24*, 3221–3227.

Pekala, R. W., Alviso, C. T., & LeMay, J. D. (1990). Organic aerogels: microstructural dependence of mechanical properties in compression. *Journal of Non-Crystalline Solids*, *125*(1–2), 67–75.

Pirard, R., & Pirard, J.-P. (1997). Aerogel compression theoretical analysis. *Journal of Non-Crystalline Solids*, *212*(2-3), 262–267.

Qin, X., Lu, A., & Zhang, L. (2013). Gelation behavior of cellulose in NaOH/urea aqueous system via cross-linking. *Cellulose*, *20*(4), 1669–1677.

Roy, C., Budtova, T., & Navard, P. (2003). Rheological properties and gelation of aqueous cellulose-NaOH solutions. *Biomacromolecules*, *4*(2), 259–64.

Sescousse, R. (2010). Nouveaux matériaux cellulosiques ultra-poreux et leurs carbones à partir de solvants verts., *PhD thesis*, Mines ParisTech.

Sescousse, R., Gavillon, R., & Budtova, T. (2011). Aerocellulose from cellulose–ionic liquid solutions: Preparation, properties and comparison with cellulose–NaOH and cellulose–NMMO routes. *Carbohydrate Polymers*, *83*(4), 1766–1774.

Winter, H., & Chambon, F. (1986). Analysis of linear viscoelasticity of a crosslinking polymer at the gel point. *Journal of Rheology*, *30*(2), 367–382.

Zhou, J., Chang, C., Zhang, R., & Zhang, L. (2007). Hydrogels prepared from unsubstituted cellulose in NaOH/urea aqueous solution. *Macromolecular bioscience*, *7*(6), 804–9.

Chapter V

Cellulose-based porous hybrids prepared in ionic liquids

Introduction

Aerocellulose from pure cellulose (Chapter III) is highly porous with a high specific surface and present a wide range of pores from few tens nanometers to few microns. These macropores are not favorable to superinsulation properties, due to the decrease of the Knudsen effect. Cellulose cross-linking allows improvements in the decrease of macropores but still presents a "high" thermal conductivity of 27 $mW.m^{-1}.K^{-1}$ (Chapter IV).

To limit the formation of macropores and to have a more homogeneous pores distribution, we decided to make interpenetrating networks, one of cellulose and the second one of another polymer. The main idea is that the second polymer will form a network inside the one of cellulose which will result in smaller pores.
Two polymers will be studied:
- lignin as it is a natural partner of cellulose in wood and other lignocellulosic materials
- cellulose acetate as a derivative of cellulose. Cellulose acetate was used for the synthesis of aerogels (Fischer, Rigacci, Pirard, Berthon-Fabry, & Achard, 2006)

As cellulose needs to be processed in solution, a common solvent is required to mix cellulose with a second polymer for preparing cellulose-based hybrids. Ionic liquid, EMIMAc, was chosen as it is known to have not only a high dissolution power for cellulose (Lovell et al., 2010) but also for other polymers, e.g. starch (Liu & Budtova, 2013). However, no data is found in literature on the behaviour of lignin and cellulose acetate in EMIMAc.

We will study in a first part the rheological properties of cellulose acetate-EMIMAc solutions, and of the mixtures of cellulose-cellulose acetate-EMIMAc. We will show potential interactions in the liquid state between these two polymers.

Mixtures of cellulose-cellulose acetate-EMIMAc and cellulose-lignin-EMIMAc will then be coagulated in a non-solvent bath. Cellulose-based hybrids obtained will be dried with supercritical CO_2 and characterized for their structural properties. We will discuss the influence of the addition and the ratio of the second polymer on the final morphology of hybrid aerogels.

Introduction

L'aérocellulose non-réticulée (Chapitre III) est très poreuse mais possède des pores larges, peu favorables pour des propriétés super-isolantes. La réticulation de la cellulose (Chapitre IV) permet d'améliorer la morphologie, qui est plus nano-structurée, et les propriétés thermiques mais qui restent relativement élevées (27 $mW.m^{-1}.K^{-1}$).

La deuxième stratégie pour diminuer la formation de macropores et avoir une distribution de taille de pores plus homogènes est de créer des réseaux interpénétrés : le premier de cellulose et le second à base d'un autre polymère. L'idée principale est que le deuxième réseau sera formé à l'intérieur du réseau de cellulose créant de plus petits pores. Deux polymères ont été étudiés :
- la lignine. C'est un partenaire naturel de la cellulose dans le bois et autres matériaux ligno-cellulosiques.
- l'acétate de cellulose qui est connu pour former un aérogel nano-structuré (Fischer, Rigacci, Pirard, Berthon-Fabry, & Achard, 2006).

La cellulose nécessite d'être mise en forme en solution. Le mélange de cellulose avec un deuxième polymère doit être réalisé en solution dans un solvant commun. Le liquide ionique, l'EMIMAc, a été choisi pour sa grande capacité de dissolution (Lovell et al., 2010) de la cellulose mais aussi d'autres polymères comme l'amidon (Liu & Budtova, 2013). Aucune donnée n'a été trouvée dans la littérature sur le comportement de la lignine et l'acétate de cellulose dans l'EMIMAc.

Les propriétés rhéologiques des solutions d'acétate de cellulose dans l'EMIMAc et des mélanges de cellulose et d'acétate de cellulose dans l'EMIMAc seront étudiées. Les éventuelles interactions entre les deux polymères seront considérées.
Les mélanges à base de cellulose, avec l'acétate de cellulose ou la lignine, seront ensuite coagulés dans un bain de non-solvant. Les hybrides de cellulose obtenus seront séchés par CO_2 supercritique et leurs propriétés structurales seront caractérisées. L'influence de l'ajout d'un deuxième polymère sur la morphologie finale sera discutée.

1. Rheological properties of cellulose acetate/EMIMAc and cellulose/cellulose acetate/EMIMAc mixtures

The first goal of our work was to perform an extended rheological study of cellulose acetate (CA)/EMIMAc solutions: we investigated shear dynamic and steady-state flow in semi-dilute state and polymer hydrodynamic properties in dilute state. We applied theories developed for polymer solutions and compared the results obtained with literature data for cellulose acetates dissolved in other solvents and for cellulose/EMIMAc solutions.

1.1 Dynamic and steady state rheology, Cox-Merz rule

Frequency scans of elastic $G'(\omega)$ and viscous $G''(\omega)$ moduli and dynamic viscosity $\eta^*(\omega)$ were performed for CA/EMIMAc solutions of various polymer concentrations at different temperatures. For each polymer concentration, time-temperature superposition principle was applied and master plots were built by shifting the experimental data by the corresponding a_T values. An example for 7 and 10_{wt}% CA/EMIMAc solutions is given in Figure V. 1; temperatures from 0° to 80°C with a step of 10°C are shown in this plot and the reference temperature is 20°C. a_T parameters used for building master plots for 5, 7 and 10_{wt}% cellulose acetate solutions as a function of temperature are shown in Figure V. 2.

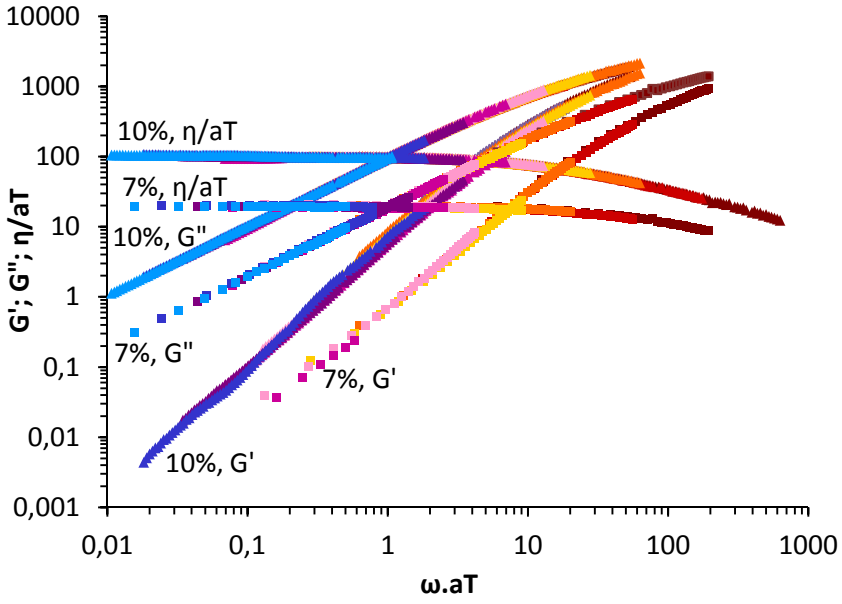

Figure V. 1 : Master plots of G', G" and dynamic viscosity for 7 and 10_{wt}% CA-EMIMAc solution for temperatures from 0° to 80°C with 20°C as a reference.

Figure V. 1 shows that cellulose acetate dissolved in EMIMAc behaves as a classical unentangled polymer solution with $G''>G'$ over the entire frequency range studied (five decades) and with power law exponents $G' \sim \omega^x$ and $G'' \sim \omega^y$ at low frequencies being $x = 1.74$ and $y = 0.97$ for 10% solution; $x = 1.6$ and $y = 0.96$ for 7% solution and $x = 1.59$ and $y = 0.97$ for 5% solution (not shown in order not to overload the graph). The deviation from the theoretical

exponents predicted by Maxwell approach describing visco-elastic response of a fluid, $x = 2$ and $y = 1$, is most probably related to polymer polydispersity.

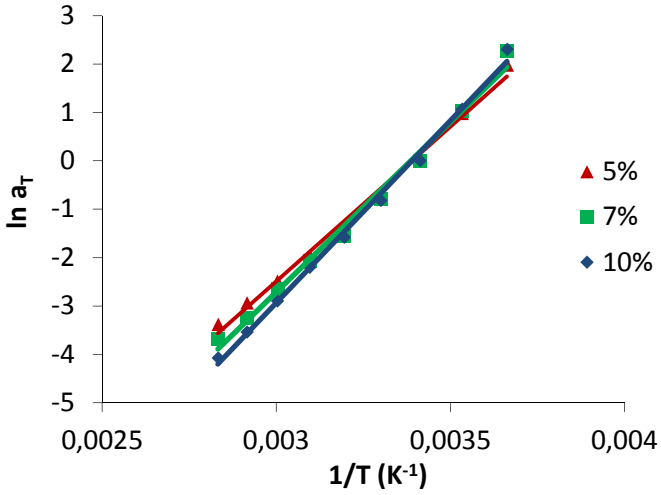

Figure V. 2: a_T shift factor as a function of temperature for 5, 7 and 10$_{wt}$% CA/EMIMAc solutions.

Figure V. 2 shows the shift factor, a_T, as a function of temperature, for three cellulose acetate concentrations, 5, 7 and 10%, all for the reference temperature of 20°C. a_T allows a complete reconstruction of *G'*, *G"* and dynamic viscosity at any temperature and also a determination of the activation energy E_a. The latter is calculated using Arrhenuis law:

$$a_T = \exp\left[\frac{E_a}{R}\left(\frac{1}{T} - \frac{1}{T_{ref}}\right)\right] \quad \text{(V. 1)}$$

where R is ideal gas constant, T is temperature (K) and T_{ref} the reference temperature.

The slopes of $ln(a_T)$ versus $1/T$ shown in Figure V. 2 give the activation energy of 53 kJ.mol^{-1} for 5$_{wt}$%, 58 kJ.mol^{-1} for 7$_{wt}$% and 63 kJ.mol^{-1} for 10$_{wt}$%. These values will be compared later with the ones obtained from steady-state viscosity measurements.

Some examples of steady state flow curves of cellulose acetate/EMIMAc solutions for various concentrations and temperatures are given in Figure V. 3. For all solutions, a Newtonian plateau was observed for at least one-two decades of shear rates. At high viscosities (corresponding to low temperatures and high concentrations) a beginning of shear thinning was observed. It is clear that the viscosity of cellulose acetate/EMIMAc solutions decreases with increasing temperature and decreasing concentration. This behaviour has been already reported for cellulose/EMIMAc solutions (Gericke, Schlufter, Liebert, Heinze, & Budtova, 2009; Sescousse, Le, Ries, & Budtova, 2010). The mean values of viscosity at the Newtonian plateau at all concentrations and temperatures were calculated and used for further analysis.

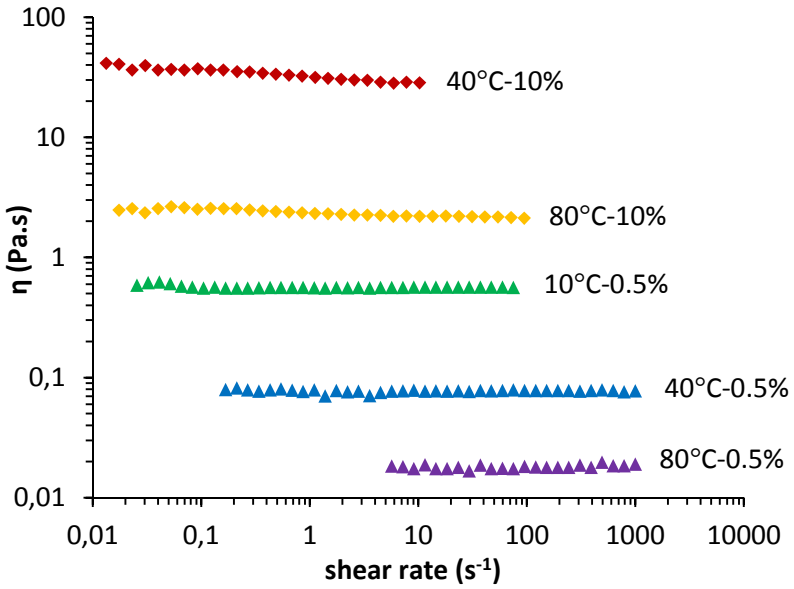

Figure V. 3: Examples of flow curves for cellulose acetate–EMIMAc solutions of different concentrations and temperatures: 10_{wt}% CA at 40°C and 80°C; 0.5_{wt}% CA at 10°C, 40°C and 80°C.

It was interesting to check if cellulose acetate/EMIMAc solutions obey Cox-Merz rule, which is the case of "ordinary" polymer solutions. Frequency dependence of complex viscosity and shear rate dependence of steady-state viscosity are plotted for the same solutions in Figure V. 4. Data sets corresponding to the same polymer concentration/temperature agree perfectly demonstrating that classical polymer theories can be applied to describe the properties of cellulose acetate/EMIMAc solutions.

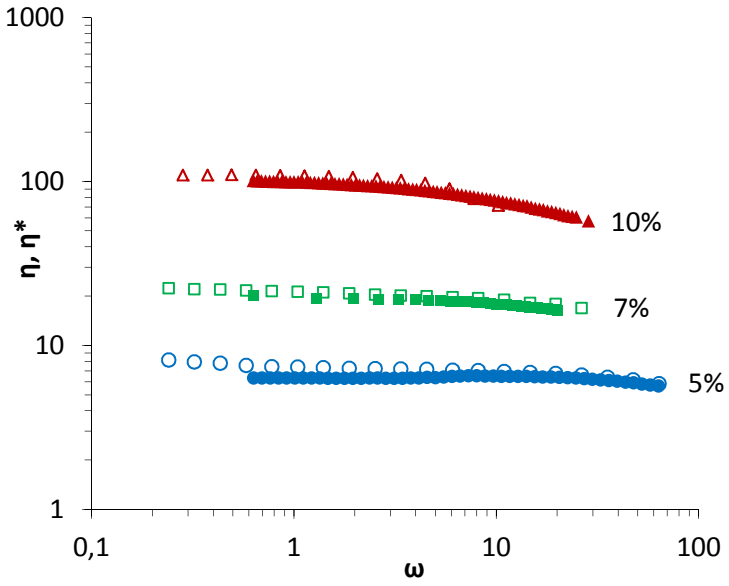

Figure V. 4 : Illustration of Cox-Merz rule for 5, 7 and 10_{wt}% cellulose acetate-EMIMAc solutions at 20°C, dark points correspond to dynamic viscosity and open points to steady state viscosity.

The influence of cellulose acetate concentration C on solution viscosity η_0 (taken as a mean value from Newtonian region) at some selected temperatures is presented in Figure V. 5, solvent viscosities (C = 0) are also included, data are shown in a semi-logarithmic scale. These data will serve a background for the calculation of the intrinsic viscosities and overlap concentrations.

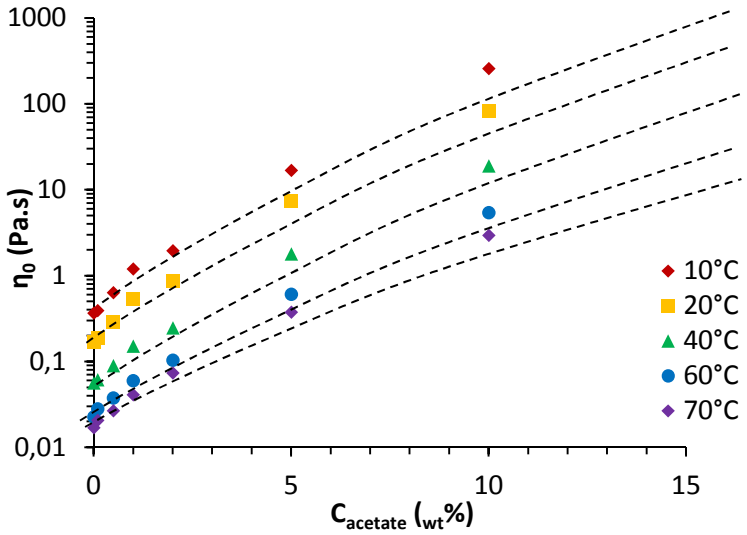

Figure V. 5: Cellulose acetate/EMIMAc Newtonian viscosity as a function of polymer concentration at 10, 20, 40, 60 and 70°C. Dashed lines are given to guide the eye.

1.2 Intrinsic viscosity and overlap concentration as a function of temperature

Polymer intrinsic viscosity $[\eta]$ is an important characteristic of a dissolved polymer as it gives information about the size of the macromolecule and the thermodynamic quality of the solvent. The "standard" method to determine intrinsic viscosity is to use Huggins approach: solution is gradually diluted with the solvent in Ubbelohde capillary viscometer and $(\eta_{rel}-1)/C$ is plotted versus polymer concentration C, where $\eta_{rel} = \eta_{sol}/\eta_{solv}$, η_{sol} and η_{solv} being solution and solvent viscosity, respectively. Intrinsic viscosity is deduced as a limiting value at infinite dilution ($C \rightarrow 0$). Polymer concentration here is expressed in mass per volume units. We used solvent (EMIMAc) density equal to 1.1 g/cm^3 which is a mean value between 1.08 at 90°C and 1.12 g/cm^3 at 20°C (Sescousse, Le, et al., 2010). This small variation of density with temperature can be neglected in the calculation of the intrinsic viscosity in the view of all other accumulated errors.

It was not possible to perform measurements in a capillary Ubbelohde viscometer because EMIMAc is too viscous and too hygroscopic to be studied in contact with the air. We used solution and solvent mean Newtonian viscosity values presented in Figure V. 3. Wolf approach was applied to calculate the intrinsic viscosity (Eckelt et al., 2011; Wolf, 2007) as far as data presented in the classical Huggins plot were somewhat scattered (due to averaging of Newtonian viscosity) and do not allow an adequate $[\eta]$ determination. Briefly, Wolf approach consists in the calculation of the limiting slope of $\ln(\eta_{rel})$ vs C which, according to phenomenological considerations, is identical to the intrinsic viscosity (Wolf, 2007). Being developed for

polyelectrolyte solutions, this approach can also be successfully used for uncharged polymers. Indeed, both Huggins and Wolf approaches gave the same cellulose intrinsic viscosity values for cellulose dissolved in NMMO monohydrate (Eckelt et al., 2011); Wolf approach was also used for determination of amylopectin intrinsic viscosity in EMIMAc (Liu & Budtova, 2013). When possible, we calculated cellulose acetate intrinsic viscosity with both Huggins and Wolf approaches and got the same values.

Figure V. 6 displays cellulose acetate intrinsic viscosity as a function of temperature. The same dependence for microcrystalline cellulose of DP = 300 dissolved in EMIMAc (Gericke et al., 2009) is also shown for comparison. *[η]* decreases with increasing temperature for both polymers. This trend for cellulose esters had already been reported (see, for example, (Flory, Spurr, & Carpenter, 1958; Suzuki, Miyazaki, & Kamide, 1980). The influence of temperature on the intrinsic viscosity was attributed to the change in the unperturbed chain dimension. The slopes of $\Delta(\ln[\eta])/\Delta T$ vary for cellulose acetate with DS = 2.86 and $M_\eta = 9\ 10^4$ from $4.5\ 10^{-3}\ °C^{-1}$ when dissolved in *m*-cresol to $6.6\ 10^{-3}\ °C^{-1}$ in dimethylformamide (Flory et al., 1958); for cellulose acetate with DS = 2.46 and $M_w = 9.5\ 10^4$ dissolved in acetone it was $6.9\ 10^{-3}\ °C^{-1}$ (Suzuki et al., 1980). The slope $\Delta(\ln[\eta])/\Delta T$ obtained for cellulose acetate dissolved in EMIMAc is falling in the same interval as for the ones cited above: $5.9\ 10^{-3}\ °C^{-1}$. For microcrystalline cellulose dissolved in EMIMAc it is twice higher, $1.2\ 10^{-2}\ °C^{-1}$. Cellulose turned out to be much more temperature sensitive than cellulose acetate. At least two reasons explaining this result can be given. One is that cellulose starts to degrade at lower temperatures than cellulose acetate. The second is related to chain flexibility: in general, cellulose esters have higher Kuhn segment length than that of cellulose, they are thus less flexible and may less contract under temperature.

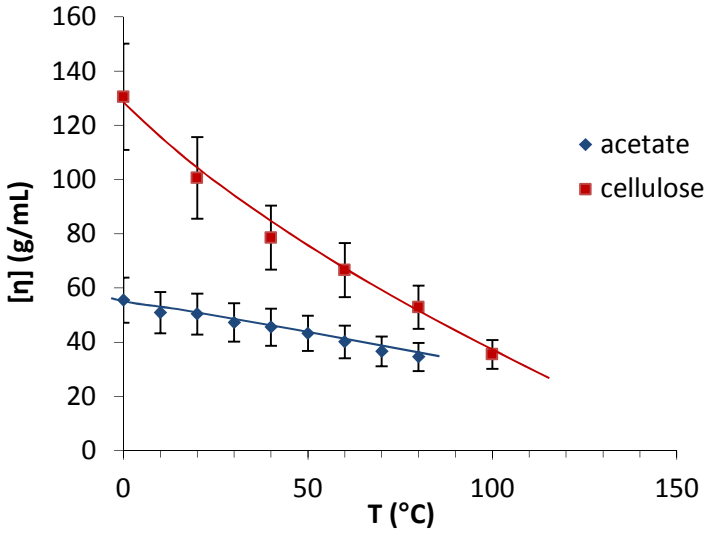

Figure V. 6: Intrinsic viscosity as a function of temperature for cellulose acetate and microcrystalline cellulose (data taken from (Gericke et al., 2009)), both polymers are dissolved in EMIMAc. Lines are given to guide the eye.

Below 50°C the values of cellulose acetate intrinsic viscosities are twice lower than the ones of microcrystalline cellulose dissolved in EMIMAc, despite the fact that both polymers are of a comparable molecular weight. A similar finding, i.e. the decrease of zero shear rate viscosity

with the increase of the degree of acetylation, was reported for cellulose and cellulose acetate of the similar DP dissolved in BMIMCl (Kosan, Dorn, Meister, & Heinze, 2010). It was interpreted by the fact that the increase of degree of acetylation decreases intra- and intermolecular interactions (via hydrogen bonding) between cellulose chains. We suggest that EMIMAc is thermodynamically a better solvent for cellulose than for cellulose acetate. To answer this intriguing question other experimental techniques and more experimental data are needed. The advantage of ionic liquids vs other cellulose solvents is that imidazolium ionic liquids allow dissolution of both cellulose and cellulose acetate and a direct comparison is possible.

Using the intrinsic viscosity obtained, a master plot of specific viscosity $\eta_{sp} = \eta_{rel} - 1$ as a function of $C[\eta]$ for all solution temperatures and concentrations studied was built (Figure V. 7). All experimental points fall very well on one plot. Figure V. 7 shows that in dilute region, viscosity increases slightly stronger than the linear-concentration dependence: the slope in double logarithmic scale is 1.2. The slope of 1.2 – 1.4 had already been reported for various polysaccharide solutions (see, for example,(Morris, Cutler, Ross-Murphy, Rees, & Price, 1981)). In the semi-dilute region, the slope value is 3; at higher concentrations it seems to increase but more data are needed to provide a meaningful value. The change of the slope occurs at $C[\eta] \approx$ 1.4 - 1.5.

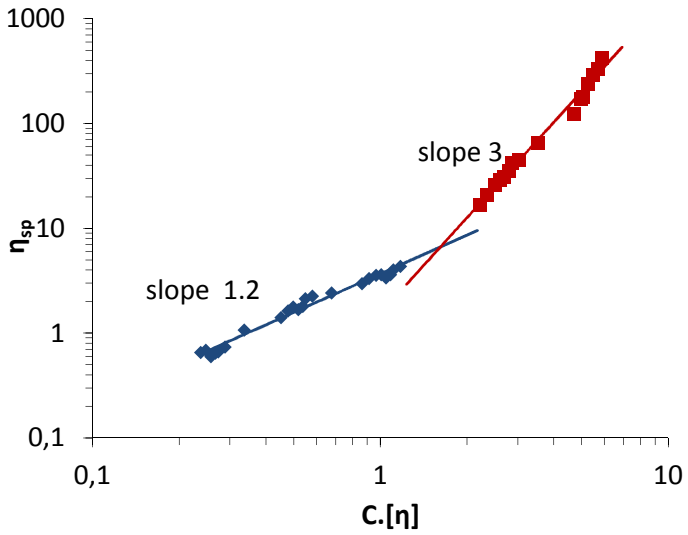

Figure V. 7 : Master plot of specific viscosity vs C[η] for cellulose acetate-EMIMAc solutions for temperatures from 0 to 80°C and concentrations from 0.1 to 10$_{wt}$%.

The overlap concentration C^* divides dilute and semi-dilute concentration regions and is usually defined as the inverse of the intrinsic viscosity $C^* = 1/[\eta]$. According to Figure V. 7 cellulose acetate overlap concentration is roughly $C^* = 1.4/[\eta]$. C^* increases with temperature increase: it varies from ≈ 22 to 36 mg/mL (equivalent to 2 to 3.4%$_{wt}$) for temperatures from 0°C to 80°C, respectively. For comparison, C* = 14 mg/mL was obtained when cellulose acetate was dissolved in dimethylacetamide (neither polymer molecular weight nor exact temperature reported) (Hornig & Heinze, 2008). For cellulose acetate of DS= 2.86 and molecular weight of about 90 000 the overlap concentration varied for temperatures from 20° to 100°C from 3 to 5 mg/mL in DMF, from 4 to 6 mg/mL in m-cresol and from 6 to 9 mg/mL for tetrachloroethane

(Flory et al., 1958); for cellulose acetate of DS = 2.46 and M_w = 9.4 10^4 C* varies from 6 to 8 mg/mL in acetone for temperatures from 10° to 50°C, respectively (Suzuki et al., 1980). In overall, cellulose diacetate overlap concentration values in EMIMAc are higher than those reported in other solvents indicating that m-cresol, tetrachloroethane, DMF and acetone are thermodynamically better solvents for cellulose acetate as compared with EMIMAc.

1.3 Activation energy

Temperature dependence of Newtonian steady state viscosity is usually analysed with the Arrhenius approach, similar to Equation (V. 1): $\eta_0 = A \exp(E_a/RT)$ where A is an adjustable parameter. The activation energy is determined by the slope of $\ln(\eta_0)$ versus $1/T$ when the dependence is linear. Some examples of Arrhenius plots for cellulose acetate-EMIMAc solutions at different concentrations are given in Figure V. 8. As already reported, $\ln(\eta)$ versus $1/T$ dependence for EMIMAc is slightly concave (Gericke et al., 2009; Le, Sescousse, & Budtova, 2011) which is coming from intrinsic properties of EMIMAc. The activation energy may thus depend on the temperature interval selected. Higher is cellulose acetate concentration, less pronounced is the deviation from the Arrhenius law. Since the temperature interval studied is the same for both solvent and polymer solution, we considered that in the first approximation Arrhenius approach can be applied to our data.

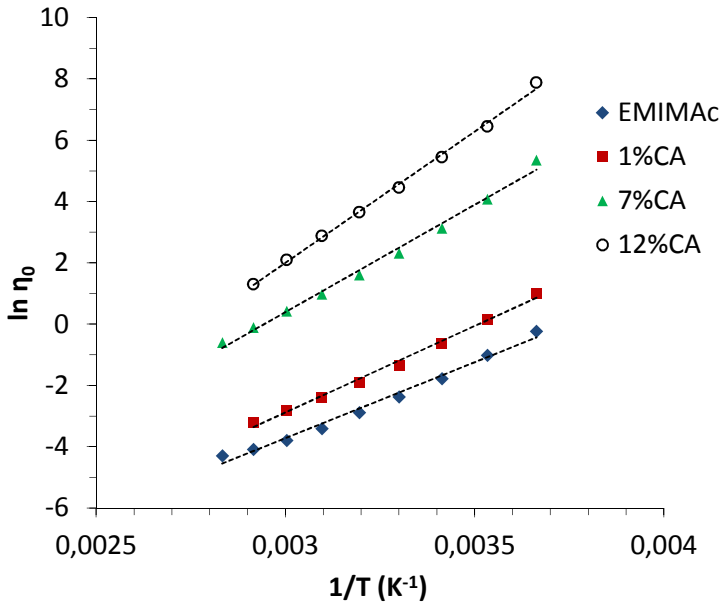

Figure V. 8 : Arrhenius plots for EMIMAc and cellulose acetate/EMIMAc solutions: 1%, 7% and 12%. Lines are linear approximations.

Figure V. 9 displays the activation energy, collected from dynamic and steady state viscosity, as a function of cellulose acetate concentration. It was shown that for microcrystalline cellulose-EMIMAc solutions the activation energy can be described as power-law concentration dependence (Le et al., 2011):

$$E_a = E_a(0) + kC^m \qquad \text{(V. 2)}$$

where $E_a(0)$ is solvent activation energy and k and m are constants.

The best fit gives k = 5 and m = 0.75 (solid line in Figure V. 9). Activation energy values calculated from dynamic data (Figure V. 2) are also shown: they are slightly lower but remain comparable with the ones calculated from steady-state viscosity. The values of the activation energy of viscous flow obtained are quite similar to the ones of microcrystalline cellulose/EMIMAc solutions (Gericke et al., 2009; Le et al., 2011) and of cellulose acetate/BMIMCl solutions (Wang et al., 2011).

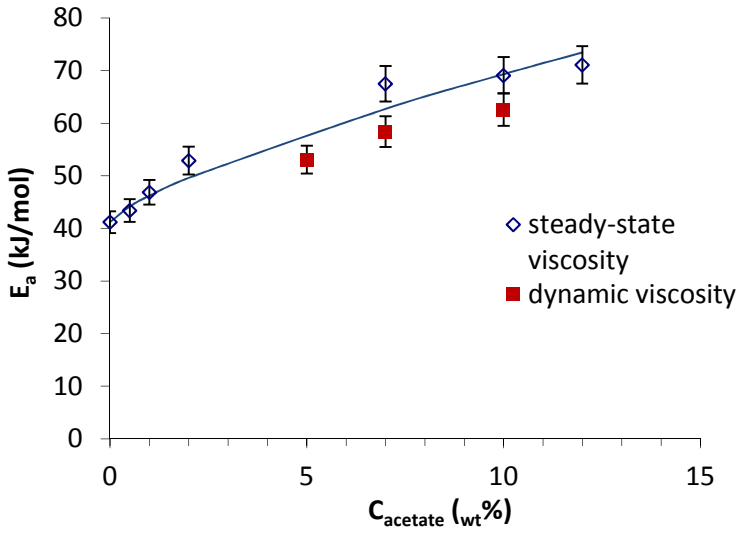

Figure V. 9 : Activation energy as a function of cellulose acetate concentration: points are experimental data (open from steady-state viscosity and dark from dynamic viscosity), line is power-law approximation according to Equation (V. 2).

1.4 Mixtures of cellulose acetate and cellulose in EMIMAc

In this section we study liquid-state properties of cellulose mixed with cellulose acetate in a common solvent, EMIMAc. The first question is if both polymers are miscible without any phase separation. After a careful visual examination of mixtures of various compositions and total polymer concentrations (from 5 to 10_{wt}%) no separation into phases was observed, and this for mixtures stored for several months. Mixture analysis with optical microscopy also did not reveal any inhomogeneities.

The second question is to understand mixture flow properties and viscosity as a function of mixture composition. Mixtures with total polymer concentration of 5 and 10_{wt}% were prepared, both polymers were in semi-dilute regime (the overlap concentration of microcrystalline cellulose varies from $1\%_{wt}$ at 0° to 2.5% at 100°C (Gericke et al., 2009) and for cellulose acetate from 2 to 3.4_{wt}% as shown above). For all mixtures at all temperatures studied a Newtonian plateau was observed on viscosity-shear rate dependences for at least two decades of shear rates. Apparently no structuring under flow occurs in the mixture; it keeps the properties of the individual components (a Newtonian plateau on the flow curves of microcrystalline cellulose-

EMIMAc solution was reported (Gericke et al., 2009; Le et al., 2011) for shear rates similar to the ones at which Newtonian flow was observed for CA-EMIMAc solutions).
In order to deduce if cellulose and cellulose acetate are interacting in the common solvent, viscosity as a function of mixture composition was investigated. Viscosity values were the ones averaged over Newtonian plateau for each mixture composition at a given temperature. The experimental results are compared with the theoretically predicted values η_{mix} calculated according to the additive log-mixing rule (Equation (V. 3)).

$$ln\,\eta_{mix} = \varphi_{cell}\ln\eta_{cell} + \varphi_{CA}\ln\eta_{CA} \qquad \text{(V. 3)}$$

where φ_{cell} and φ_{CA} are weight fractions of cellulose and cellulose acetate ($\varphi_{cell} + \varphi_{CA} = 1$), η_{cell} and η_{CA} Newtonian viscosities of neat cellulose and neat cellulose acetate solutions at the corresponding total polymer concentration in EMIMAc, respectively.

The results are presented in Figure V. 10. For each temperature, the calculated viscosity fits well the experimental data, within the experimental errors. Thus, in the first approximation, we can conclude that cellulose and cellulose acetate co-exist in the solvent without any special interactions. As far as total polymer concentrations studied, 5 and 10_{wt}%, are relatively low, it seems there is no competition for the solvent between the two polymers. Both concentrations are far lower than the maximum concentration of the two polymers that can be dissolved in EMIMAc. No such exact value is known either for cellulose or for cellulose acetate; for cellulose it is predicted to be close to $25\text{-}30_{wt}$% (Lovell et al., 2010); 20_{wt}% cellulose of DP = 515 dissolved in EMIMAc was reported in (Kosan, Michels, & Meister, 2008).

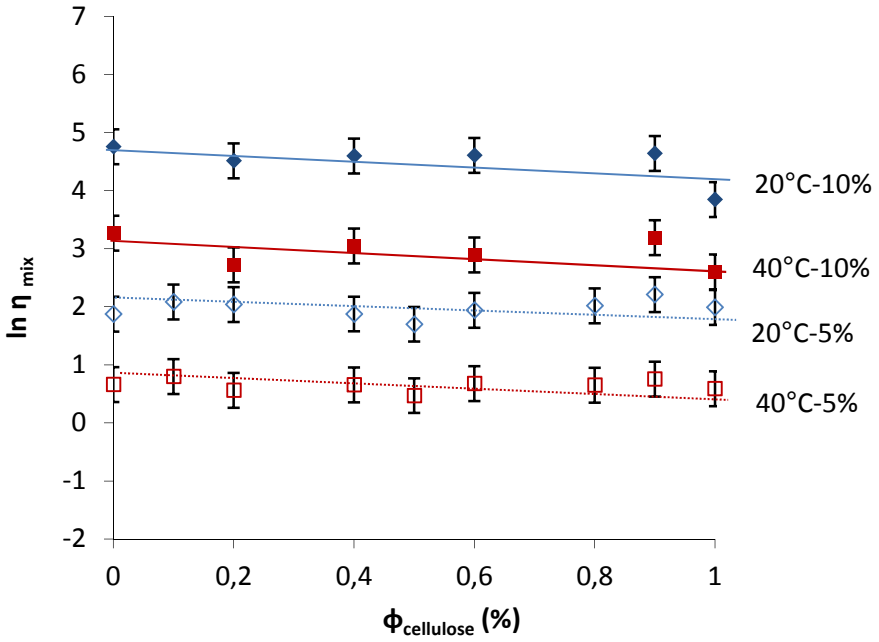

Figure V. 10 : Newtonian viscosity vs cellulose weight fraction in the mixture cellulose-cellulose acetate in EMIMAc with 5% (open symbols) and 10% (filled symbols) total polymer concentration at temperatures of 20°C and 40°C. Lines are calculated viscosity according to the log-mixing rule.

Mixture activation energies were calculated according to Arrhenius law. The results are shown in Figure V. 11 for mixtures with total polymer concentration of 5 and 10_{wt}%. For both types of mixtures E_a vs mixture composition (cellulose weight fraction) is linear confirming our previous conclusion that cellulose and cellulose acetate co-exist in EMIMAc without interacting.

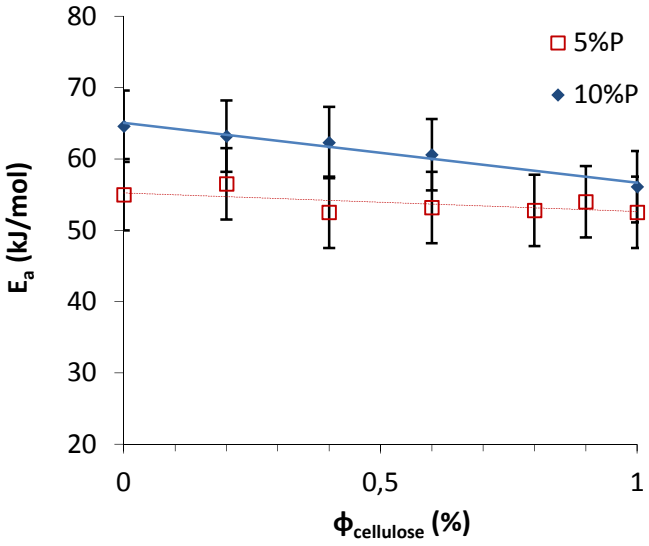

Figure V. 11 : Activation energy as a function of mixture composition for 5% (open symbols) and 10% (dark symbols) total polymer concentration. Lines are linear approximations.

2. Cellulose-cellulose acetate hybrid materials

Solutions of cellulose and cellulose acetate mixed in EMIMAc are then placed in a coagulation bath of water or ethanol. Hybrid materials of various cellulose and cellulose acetate compositions were prepared.

2.1 Hybrid films

First, we studied freeze-dried films from coagulated cellulose-cellulose acetate hybrids. They were prepared from a 10_{wt}% total polymer (cellulose and cellulose acetate) concentration and coagulated in water. They were about 1 mm thick. The morphology of the cross-section of cryo-fractured wet samples of different compositions was observed with SEM (Figure V. 12). Freeze-dried pure cellulose is a “cloudy” network of coagulated cellulose strands (Figure V. 12a); this morphology had already been reported (Sescousse & Budtova, 2009). In the mixture cellulose:CA = 60:40 cellulose acetate is in the minor phase and forms “beads” incorporated in the cellulose matrix (Figure V. 12b). The size of the beads varies from one to a few microns. Being miscible with cellulose in the common solvent in the mixtures with total polymer concentration of 10_{wt}%, cellulose acetate phase separates from cellulose during coagulation. The increase of cellulose acetate concentration in the mixture leads to the formation of an interpenetrated network in the coagulated state (Figure V. 12c). Freeze-dried pure coagulated

cellulose acetate has an inhomogeneous morphology: it forms a cloudy network with beads dispersed in it (Figure V. 12d).

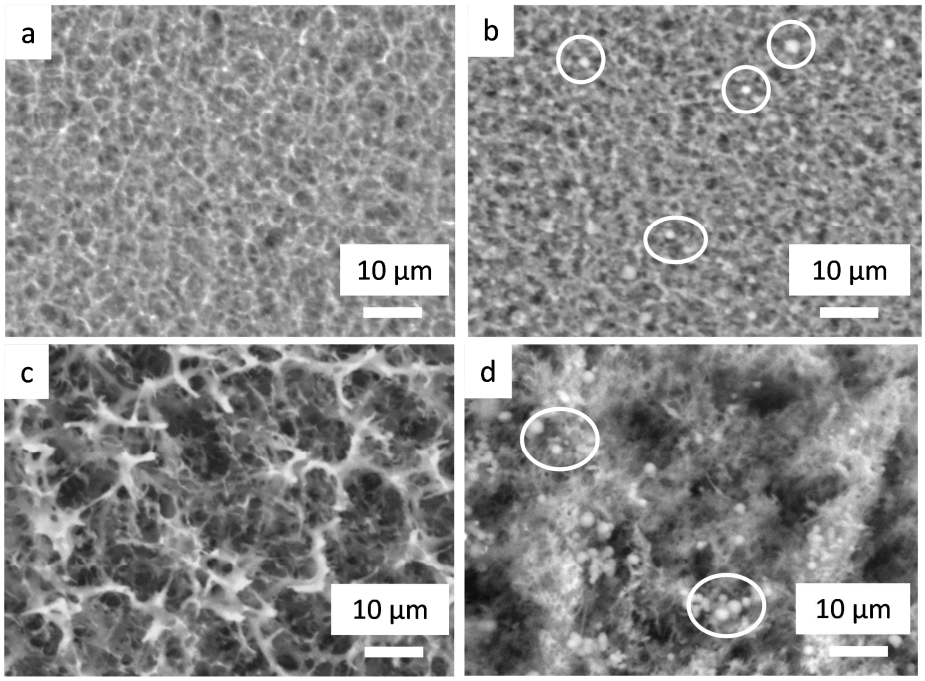

Figure V. 12 : SEM images of cryo-fractured wet cellulose-CA hybrid materials made from mixtures with 10% total polymer concentration: cellulose:CA = 100:0 (a), 60:40 (b), 40:60 (c) and 0: 100 (d). Some cellulose acetate "beads" are outlined for clarity.

2.2 Hybrid monoliths

Following the standard procedure of aerocellulose preparation (coagulation, solvent exchange and $scCO_2$ drying), monoliths of mixed cellulose and cellulose acetate were prepared. Two concentrations were investigated: 5_{wt}% (low concentration) and 10_{wt}% (higher concentration). The coagulation was either in water or ethanol. The solvent exchange, in the case of coagulation in water, was into ethanol. It is not possible to use acetone as cellulose acetate is soluble in this fluid.

First, we started by preparing low concentrations 5_{wt}% hybrids coagulated in water. We varied the composition from pure cellulose (100:0 = C:CA) to pure cellulose acetate (0:100 = C:CA). The cellulose acetate "physical aerogel" has never been reported previously, most of the time chemically cross-linked cellulose acetate aerogels are investigated (Fischer et al., 2006). We prepared different compositions of hybrids: 70:30, 50:50 and 30:70 cellulose (C):cellulose acetate (CA). Figure V. 13 shows coagulated hybrids before drying. For high proportion of cellulose acetate (>50%), these samples do not have cohesion and break in small pieces.

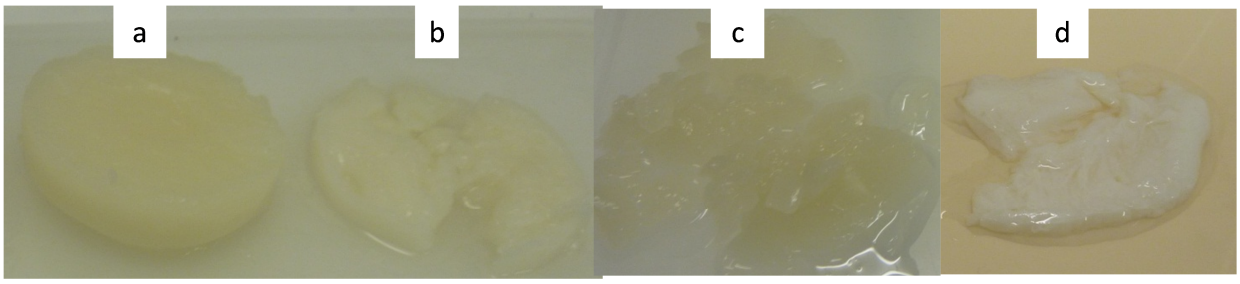

Figure V. 13 : Wet cellulose-cellulose acetate hybrids from a 5% mixture coagulated in water: (a) 70:30, (b) 50/50, (c) 30:70 and (d) 0:100 C:CA.

The morphology of dried hybrids was observed by SEM (Figure V. 14). For pure cellulose acetate (Figure V. 14d) it is a rather complicated structure, with smooth, long but large interpenetrated strands. It is not as mesoporous as aerocellulose with pores of few microns. Hybrids with a larger proportions of cellulose acetate such as 30:70 (Figure V. 14c) or 50:50 (Figure V. 14b) C:CA, have a mixture of smooth and "hairy" beads randomly dispersed. Hairy beads are typical from aerocellulose morphology (see Chapter III) whereas smooth spheres are more similar to cellulose acetate and were already observed in cryofractured samples. However, for 30:70 C:CA cellulose acetate beads have an average size of few µm whereas they are slightly smaller (around 500 nm-1 µm) for the 50:50 composition. For a composition rich in cellulose (70:30 C:CA) aerocellulose-based morphology is observed (Figure V. 14a), cellulose acetate phase is not easily visible. Resuming, a phase separation between rich phase of cellulose and rich phase of acetate was visible after the coagulation and drying with $scCO_2$. With total polymer concentration of 5wt%, either cellulose or cellulose acetate is below their overlap concentration at most of compositions. This does not allow making an interpenetrated network. This leads to poor mechanical properties of hybrids especially because polymer phases are phase separating.

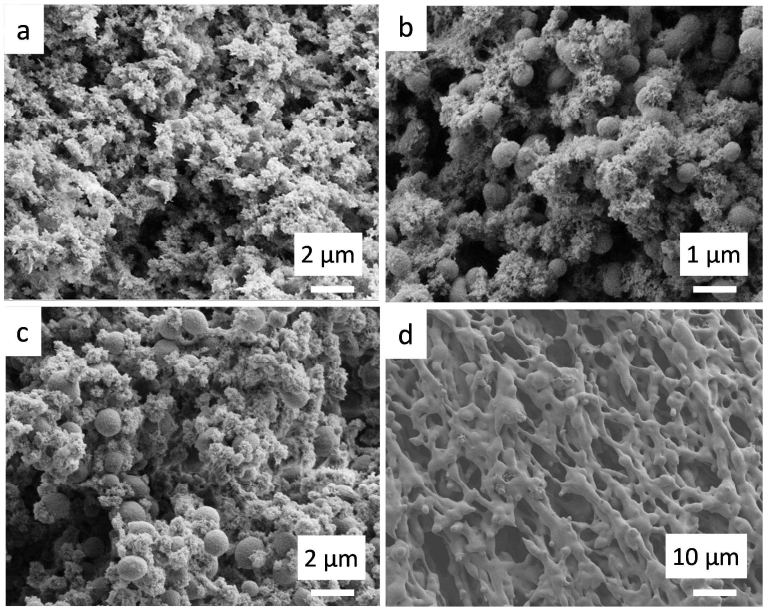

Figure V. 14 : SEM images of dried cellulose-CA hybrid monoliths made from mixtures with 5% total polymer concentration: cellulose:CA = 70:30 (a), 50:50 (b), 30:70 (c) and 0: 100 (d).

By increasing polymer concentration to 10_{wt}%, we were able to form stronger hybrids which do not break. Here we expect the formation of interpenetrated network. Two different coagulation baths were used: water and ethanol. The cellulose acetate "physical aerogel" (without chemical cross-linking) was prepared in each coagulation bath. However, the sample coagulated in water was completely deformed during the solvent exchange phase and we were not able to dry it. The other one in ethanol had not kept its initial shape; it contracted and curved more than other hybrids during the coagulation and the supercritical drying. We will thus focus mainly on hybrids coagulated in ethanol and compare them to the one in water for only two mixture compositions.

Compared to hybrids at 5_{wt}%, 10_{wt}% materials are mechanically much stronger than their 5_{wt}% counterparts and are monolithic (Figure V. 15).

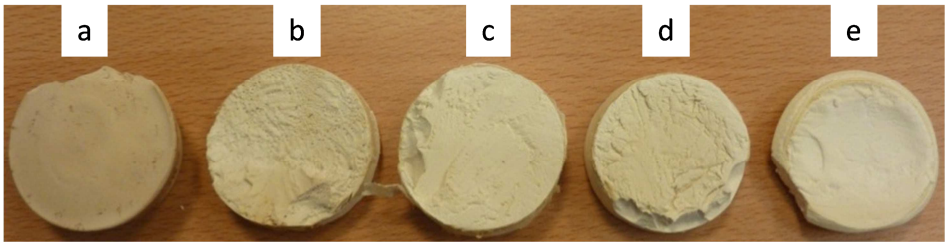

Figure V. 15 : Dried cellulose-CA hybrid monoliths coagulated in ethanol made from mixtures with 10% total polymer concentration: cellulose:CA = 80:20 (a), 60:40 (b), 40:60 (c) and 20: 80 (d), 0:100 (e).

SEM images of the morphology of these hybrids are given in Figure V. 16. Once again the structure of pure cellulose acetate monolith is very complicated with smooth beads and large channels or cavities like alveoles (Figure V. 16e). Hybrid with a high proportion of cellulose (80:20 C:CA) has a classical morphology of aerocellulose and cellulose acetate is not visible (Figure V. 16a). When the concentration of cellulose acetate increases, a mixture of smooth beads of acetate and hairy cellulose structure coexist and the phase separation is clearly visible (Figure V. 16b & c). In Figure V. 16b aerocellulose structure is present but modified and forms "holes" of 5-10 µm in which cellulose acetate beads (1-2 µm) are embedded. Figure V. 16c both types of beads are present, cellulose and acetate, randomly dispersed. Hybrid of 20:80 C:CA composition is made of smooth interpenetrated strands, partly similar to the structure observed for 5_{wt}% pure cellulose acetate (Figure V. 16d).

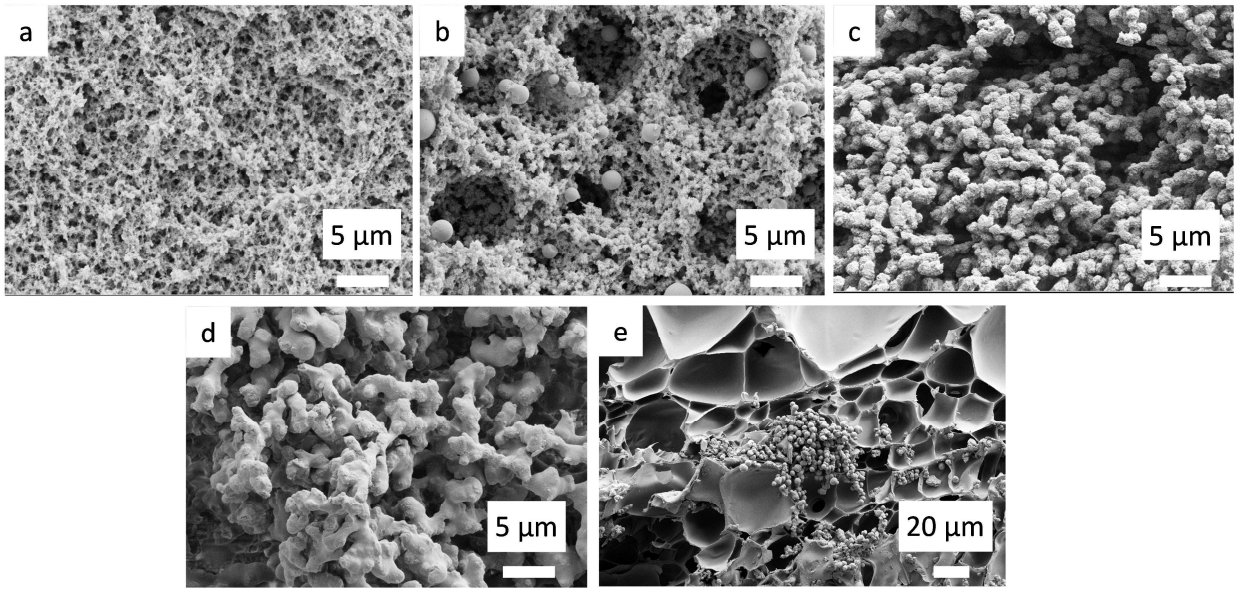

Figure V. 16 : SEM images of dried cellulose-CA hybrid monoliths coagulated in ethanol made from mixtures with 10% total polymer concentration: cellulose:CA = 80:20 (a), 60:40 (b), 40:60 (c) and 20: 80 (d), 0:100 (e).

These hybrids were characterised by bulk density, porosity and specific surface. Skeletal densities were calculated by the ratio of $\rho_{skeletal\ cellulose}$ and $\rho_{skeletal\ acetate}$. $\rho_{skeletal\ cellulose}$ was measured previously (see Chapter III) by He pycnometry and equals 1.55 g/cm^3 and $\rho_{skeletal\ acetate}$ was determined in the frame of ANR Nanocell project and equals 1.35 g/cm^3. Porosity was calculated according to Equation (V. 4).

$$\varepsilon = 1 - \frac{\rho_{bulk}}{\rho_{skeletal}} \qquad \text{(V. 4)}$$

Data are reported in Table V. 1. Pure cellulose acetate monolith has a low porosity compared to aerocellulose. It confirms the SEM observations as it is not highly porous. The intense contraction during coagulation and drying results of an important bulk density.

Table V. 1 : Morphological properties of cellulose-cellulose acetate hybrids.

Mixture composition Cell:CA	C cellulose ($_{wt}$%)	C acetate ($_{wt}$%)	ρ_{bulk} (g/cm^3)	S_{BET} (g/m²)	$\rho_{skeletal}$ (g/cm^3)	Porosity (%)
100:0	10	0	0.262	218	1.55	83
80:20	8	2	0.248	166	1.51	84
40:60	4	6	0.213	131	1.43	85
20:80	2	8	0.164	92	1.39	88
0:100	0	10	0.549	-	1.35	59

The bulk density was plotted as a function of cellulose fraction (Figure V. 17a). For hybrids with at least 40% cellulose, densities are very similar and around 0.23 g/cm^3 regarding the important uncertainty of measurements. For monoliths concentrated with cellulose acetate it is not obvious

to highlight a tendency. Specific surface is more interesting as it seems decreasing linearly with the increase of cellulose acetate proportion (Figure V. 17b). Most probably cellulose acetate phase is not porous (see smooth surface of cellulose acetate beads in Figure V. 16b,c,d) which decreases specific surface area of hybrids.

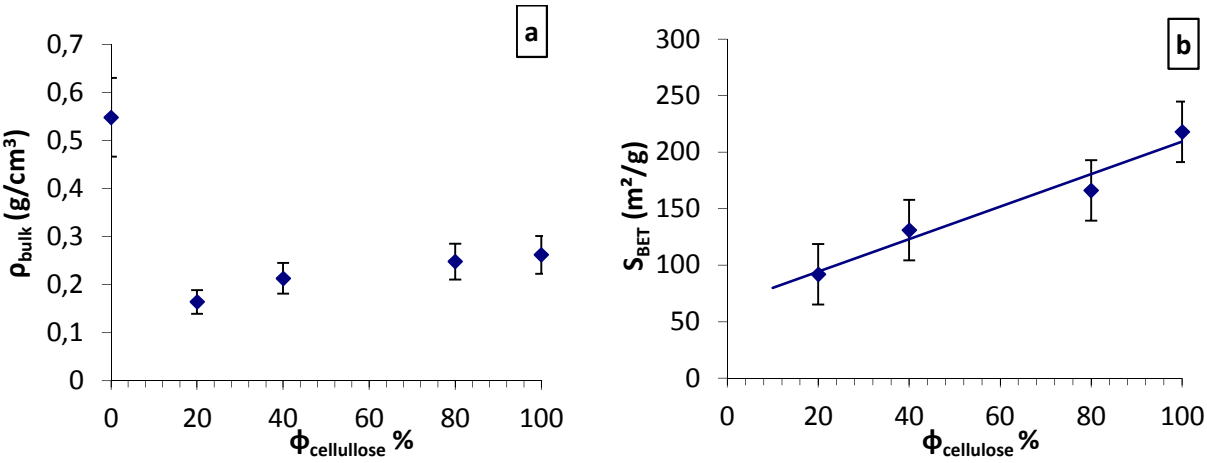

Figure V. 17 : (a) Bulk density and (b) specific surface of 10_{wt}% hybrid monoliths vs cellulose concentration.

Hybrid materials were analysed by FTIR. Figure V. 18 shows FTIR-ATR transmittance spectra of cellulose II (a), cellulose:CA = 60:40 (b), 40:60 (c) and cellulose acetate (d). The characteristic peak of cellulose acetate is at 1720 cm^{-1} corresponding to the C=O bond of acetyl group. This peak is obviously not present in the cellulose II and it increases with the increase of cellulose acetate content. The broad peak at 3300 cm^{-1} is specific of hydroxyl groups linked by hydrogen bonds. It is broad for cellulose II and decreases with the increase of cellulose acetate concentration. For intermediate concentrations (40:60 and 60:40 cellulose:CA) all peaks of cellulose and cellulose acetate are superposed. Neither new chemical bond nor peak shifts were observed.

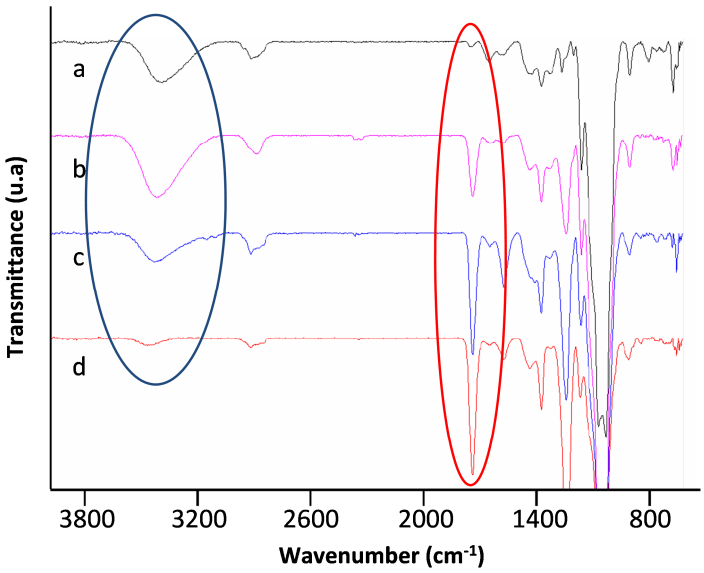

Figure V. 18 : FTIR spectra of 10_{wt}% cellulose-CA hybrid materials with cellulose:acetate ratio of 100:0 (a), 60:40 (b), 40:60 (c), 0:100 (d).

The height *H* of ester peak at 1720 cm^{-1} was evaluated for each hybrid material and plotted as a function of cellulose weight fraction in the mixture (Figure V. 19). *H* decreases linearly with the decrease of cellulose acetate content. This confirms that cellulose and cellulose acetate phase separate during coagulation and polymers are not interacting with each other.

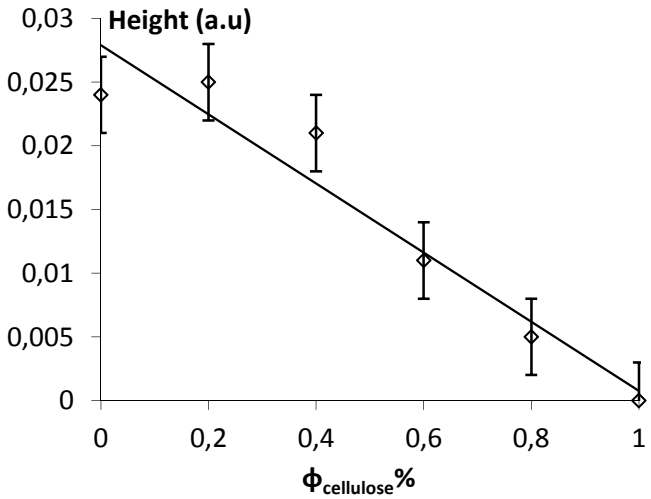

Figure V. 19 : Height of 1720 cm^{-1} peak vs cellulose weight fraction for hybrid materials prepared from coagulated cellulose-CA-EMIMAc, total polymer concentration in the mixtures was 10_{wt}%.

The same procedure was followed for preparing hybrids coagulated in water in which was then exchanged by ethanol before drying with $scCO_2$. Macroscopically, samples have a good cohesion. They have similar properties as hybrids coagulated in ethanol: for example 80:20 ρ_{bulk}=0.252 g/cm^3 and S_{BET}=202 g/m^2; 60:40 ρ_{bulk}=0.237 g/cm^3 and S_{BET}=190 g/m^2. SEM observations are given in Figure V. 20. A phase separation is also visible for equally mixed

hybrids, with cellulose acetate beads embedded an aerocellulose matrix (Figure V. 20b). A complex structure is observed for monoliths highly concentrated with cellulose acetate (Figure V. 20c).

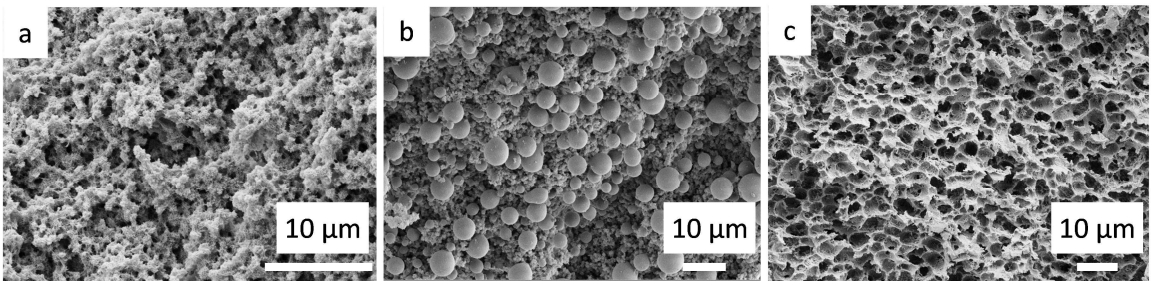

Figure V. 20 : SEM images of dried cellulose-CA hybrid monoliths coagulated in water made from mixtures with 10% total polymer concentration: cellulose:CA = 80:20 (a), 60:40 (b), 20:80 (c).

In all cases, cellulose and cellulose acetate do not form a microscopically homogeneous hybrid. A phase separation occurs with phases rich in cellulose and rich in cellulose acetate. At low concentration of total polymer, hybrids are not cohesive and break easily. The decrease of specific surface area with the increase of cellulose acetate concentration shows that hybrids lose their porosity (especially micro- and mesoporosity) which is not favourable for thermal application. Thus we did not investigate further the mechanical and thermal properties of cellulose/cellulose acetate hybrid monoliths.

3. Cellulose-lignin hybrids

Lignin is a natural partner of cellulose in cell walls of fibers. Each component brings its own properties: mechanical strength from crystalline regions of cellulose; hydrophobicity, binding and protection against microorganisms from lignin. If cellulose is mixed with lignin, will the final hybrid material demonstrate similar synergetic properties as it occurs in a natural fiber?

Different sort of lignin exist: lignosulfonates obtained by the sulfite process or Organosolv (sulfur free and more hydrophobic) with a lower molecular weight (Doherty, Mousavioun, & Fellows, 2011).

Mixtures of cellulose and organosolv lignin in an aqueous 8% NaOH solution has already been studied (Sescousse, Smacchia, & Budtova, 2010). Cellulose-lignin-NaOH-water gels were prepared, coagulated in various aqueous baths, washed in ethanol and dried with $scCO_2$. It was shown that when coagulating an 0.1 M acetic acid bath, 82% of organosolv lignin was “lost”: it was released in the coagulation bath. When coagulated in 1M acetic acid, 65% of lignin was washed out. It seems that organosolv lignin and cellulose do not interact in this solvent. One of the reasons could be the existence of negative electrostatic interactions between cellulose and lignin in 8%NaOH-water.

To avoid negative electrostatic interactions due to the basicity of the solvent, we studied mixtures of cellulose and lignin in ionic liquid EMIMAc. We changed the type of lignin used, Tembec ARBO C12 lignosulfonate, which is soluble in water (1 kg/L) and has a larger molar mass (30 000 g/mol) as compared to organosolv lignin. We tested its solubility in ethanol and in EMIMAc after 24h stirring at room temperature and lignin appears very slightly soluble in alcohol (1g in 100 mL) but completely dissolved in the ionic liquid. Then we prepared a 10_{wt}% total polymer solution in EMIMAc with 7_{wt}% cellulose and 3_{wt}% lignin. Two different coagulation baths were used: water and ethanol. After several washings in the corresponding bath, these two coagulated hybrids present a different color (Figure V. 21a): the pale brown sample is the one coagulated in water and dark brown is the sample coagulated in ethanol. Lignin has been washed out by water which reveals that cellulose and lignin do not form any interpolymer bonds. For the sample coagulated in ethanol, lignin seems staying inside the sample simply because it "coagulated inside" cellulose matrix.

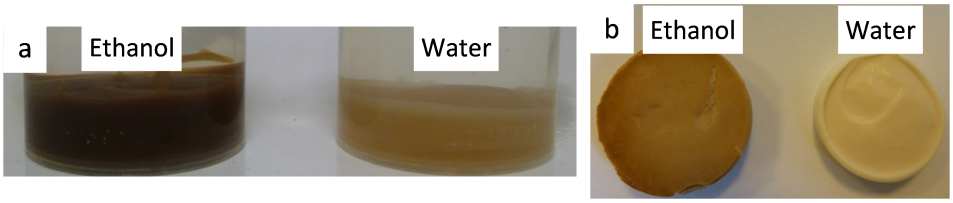

Figure V. 21 : Hybrids cellulose-lignin : (a) wet samples coagulated bath either in water or ethanol, (b) scCO_2 dried samples.

Both samples coagulated in water or in ethanol were dried in supercritical CO_2 (Figure V. 21b) and observed by SEM. Hybrid cellulose:lignin = 70:30 coagulated in water has a classical porous morphology of aerocellulose with hairy and globular structure (compare Figure V. 22a and Figure V. 22b, respectively). However, the overall structure of hybrid is much more porous and "aerated" as compared to aerocellulose (compare Figure V. 22c and Figure V. 22d). Lignin was washed out in water during coagulation which created these inhomogeneities, similar to whatwas already shown in (Sescousse, Smacchia, et al., 2010) for the solvent 8%NaOH-water.

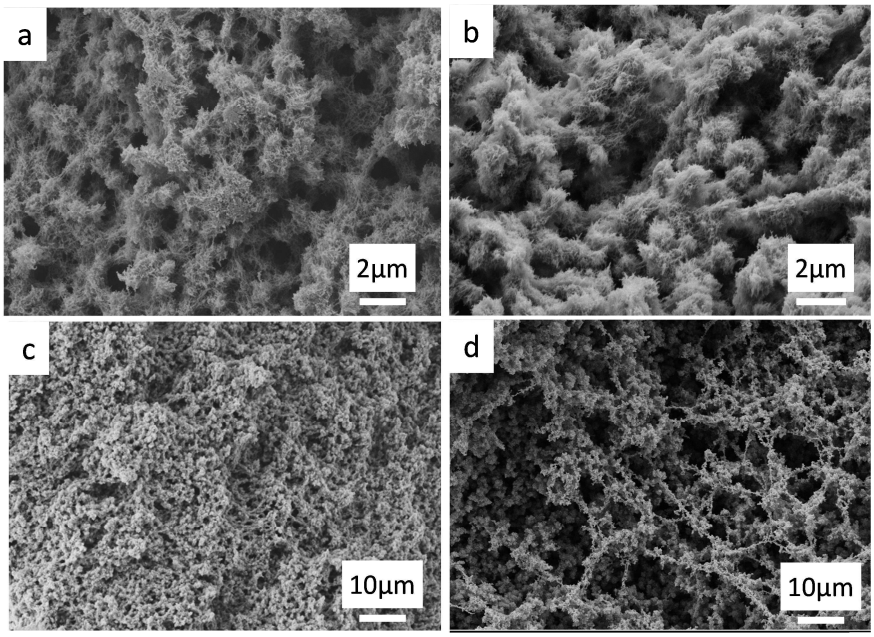

Figure V. 22 : SEM images of dried pure aerocellulose from 10$_{wt}$%cellulose-EMIMAc solution coagulated in water: (a) and (c).
Cellulose-lignin hybrid monoliths made from mixtures with 10% total polymer concentration cellulose:lignin = 70:30, coagulated in water and dried with sc CO_2: (b) and (d).

The bulk density of this "aero-lignocellulose" was 0.187 g/cm^3 (Table V. 2).

Table V. 2 : Bulk density of aero-lignocellulose. (1) Data were taken from (Sescousse, Smacchia, et al., 2010).

%C_{cell}	%C_{lignin}	Coagulation bath	ρ_{bulk} (g/cm^3)
7	0	Water	0.194
7	3	Water	0.187
4	3.3	Acetic acid-water	0.135 (1)
4	8.6	Acetic acid-water	0.1 (1)

The samples coagulated in water were compared with the ones of the same composition but coagulated in ethanol. Their morphology is slightly different (Figure V. 23a, b) as compared to that of aerocellulose (Figure V. 22a),with domains rich with lignin (smooth structure shown with the red circles) and rich in cellulose (hairy globular morphology). These results show that even by using ethanol coagulation bath, cellulose and lignin do not interact together and separate in two phases; similar to what was obtained for cellulose-cellulose acetate mixtures. Due to the lack of the affinity between cellulose and lignin, hybrid samples are mechanically more fragile as compared to aerocellulose.

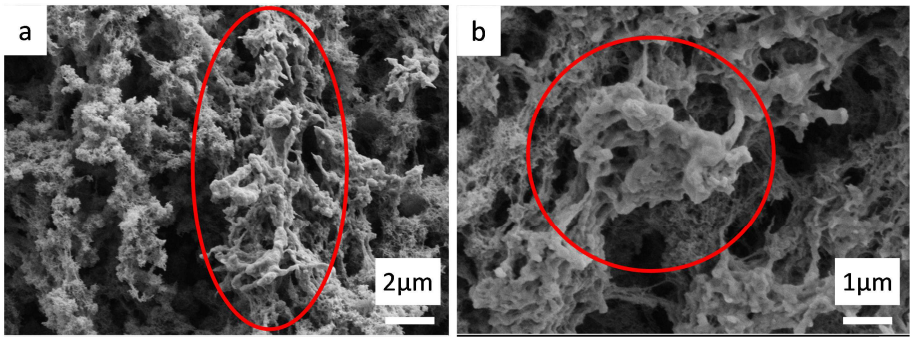

Figure V. 23 : SEM images of cellulose-lignin = 70:30 hybrid monoliths coagulated in ethanol and dried with sc CO_2. Red circles highlight lignin-rich phase.

Conclusions

We investigated the preparation of hybrids from cellulose mixed with other polymers in order to create interpenetrated networks. Two polymers were studied: cellulose acetate and lignin.

For hybrids with cellulose acetate (CA), we first investigated the behaviour of CA in EMIMAc since this has not been reported in literature. A comprehensive study of visco-elastic and flow properties of cellulose acetate/EMIMAc solutions was performed using dynamic and steady state rheology. It was demonstrated that cellulose acetate/EMIMAc behaves as non-entangled (below 10_{wt}%) "ordinary" polymer solution and obeys Cox-Merz rule.
Cellulose acetate intrinsic viscosity in EMIMAc was determined as a function of temperature and compared with the intrinsic viscosity of microcrystalline cellulose in the same solvent. The hydrodynamic size of cellulose acetate macromolecule decreases with temperature increase which indicates the decrease of solvent thermodynamic quality. Intrinsic viscosity decrease with temperature increase is much less pronounced for cellulose acetate dissolved in EMIMAc as compared with cellulose dissolved in EMIMAc, probably because of different chain rigidity. All data fall well on specific viscosity-$C[\eta]$ master plot showing the slope of 1.2 in dilute region and 3 in semi-dilute. The overlap concentration of cellulose acetate in EMIMAc is higher than the one reported for diacetates of similar DS and molecular weights dissolved in other solvents; this indicates that EMIMAc thermodynamic quality is lower than the one of classical inorganic fluids (DMF, tetrachloroethane and acetone).
The activation energy as a function of cellulose acetate concentration is described by power-law dependence. In overall, the rheological properties of cellulose acetate/EMIMAc solutions do not demonstrate any specific interactions between the polymer and the solvent (no gelation or formation of any special structures); they follow the trends already reported for cellulose acetates dissolved in other solvents and thus can be described by classical approaches.

Mixtures of cellulose and cellulose acetate of various compositions with 5 and $10\%_{wt}$ total polymer concentration were prepared in EMIMAc. No phase separation was observed. Newtonian flow of mixtures was recorded for a few decades of shear rates. Mixture viscosity was compared with the calculated values according to the mixing law: no special interactions that could cause the difference between the theoretical and experimental values were detected. It was thus concluded that cellulose and cellulose acetate coexist in EMIMAc at the concentrations studied.

Hybrid materials of various cellulose and cellulose acetate compositions were prepared by coagulating polymers in water or ethanol. FTIR confirmed the absence of the any special interactions between cellulose and cellulose acetate. Various morphologies of samples were obtained as a function of mixture composition. The results show that it is possible to process together cellulose and cellulose acetate but a phase separation between these two polymers occurs during the coagulation process. Porosity decreases and inhomogeneities increase with cellulose acetate concentration increases.

A similar study was performed for cellulose-lignin-EMIMAc mixture. Lignin was washed out by water from cellulose during coagulation step. When coagulated in ethanol, lignin remained inside cellulose network but a phase separation between cellulose and lignin was visible.

Other polymers were also investigated such as starch (Liu & Budtova, 2012) and similar results were obtained: a phase separation between cellulose and the "second" polymer during coagulation. Finally it seems rather difficult to prepare a homogeneous hybrid with cellulose even if both components are well soluble in ionic liquid.

Bibliography

Doherty, W. O. S., Mousavioun, P., & Fellows, C. M. (2011). Value-adding to cellulosic ethanol: Lignin polymers. *Industrial Crops and Products*, *33*(2), 259–276.

Eckelt, J., Knopf, A., Röder, T., Weber, H. K., Sixta, H., & Wolf, B. A. (2011). Viscosity-molecular weight relationship for cellulose solutions in either NMMO monohydrate or cuen. *Journal of Applied Polymer Science*, *119*(2), 670–676.

Fischer, F., Rigacci, A., Pirard, R., Berthon-Fabry, S., & Achard, P. (2006). Cellulose-based aerogels. *Polymer*, *47*(22), 7636–7645.

Flory, P. J., Spurr, O. K., & Carpenter, D. K. (1958). Intrinsic viscosities of cellulose derivatives. *Journal of Polymer Science*, *27*(115), 231–240.

Gericke, M., Schlufter, K., Liebert, T., Heinze, T., & Budtova, T. (2009). Rheological properties of cellulose/ionic liquid solutions: from dilute to concentrated states. *Biomacromolecules*, *10*(5), 1188–94.

Hornig, S., & Heinze, T. (2008). Efficient approach to design stable water-dispersible nanoparticles of hydrophobic cellulose esters. *Biomacromolecules*, *9*(5), 1487–92.

Kosan, B., Dorn, S., Meister, F., & Heinze, T. (2010). Preparation and Subsequent Shaping of Cellulose Acetates Using Ionic Liquids. *Macromolecular Materials and Engineering*, *295*(7), 676–681.

Kosan, B., Michels, C., & Meister, F. (2008). Dissolution and forming of cellulose with ionic liquids. *Cellulose*, *15*(1), 59–66.

Le, K. A., Sescousse, R., & Budtova, T. (2011). Influence of water on cellulose-EMIMAc solution properties: a viscometric study. *Cellulose*, *19*(1), 45–54.

Liu, W., & Budtova, T. (2013). Dissolution of unmodified waxy starch in ionic liquid and solution rheological properties. *Carbohydrate polymers*, *93*(1), 199–206.

Lovell, C. S., Walker, A., Damion, R. a, Radhi, A., Tanner, S. F., Budtova, T., & Ries, M. E. (2010). Influence of Cellulose on Ion Diffusivity in 1-Ethyl-3-Methyl-Imidazolium Acetate Cellulose Solutions. *Biomacromolecules*, 2927–2935.

Morris, E. R., Cutler, A. N., Ross-Murphy, S. B., Rees, D. A., & Price, J. (1981). Concentration and shear rate dependence of viscosity in random coil polysaccharide solutions. *Carbohydrate Polymers*, *1*(1), 5–21.

Sescousse, R., & Budtova, T. (2009). Influence of processing parameters on regeneration kinetics and morphology of porous cellulose from cellulose–NaOH–water solutions. *Cellulose*, *16*(3), 417–426.

Sescousse, R., Le, K. A., Ries, M. E., & Budtova, T. (2010). Viscosity of cellulose-imidazolium-based ionic liquid solutions. *The journal of physical chemistry. B*, *114*(21),

Sescousse, R., Smacchia, A., & Budtova, T. (2010). Influence of lignin on cellulose-NaOH-water mixtures properties and on Aerocellulose morphology. *Cellulose*, *17*(6), 1137–1146.

Suzuki, H., Miyazaki, Y., & Kamide, K. (1980). Temperature dependence of limiting viscosity number and radius of gyration of cellulose diacetate in acetone. *European Polymer Journal*, *16*(8), 703–708.

Wang, B. C., Jiang, G. Sen, Chen, X., Wu, D., Zhang, Y. M., & Wang, H. P. (2011). Rheological Characteristic of Concentrated Cellulose Diacetate Solutions with 1-Butyl-3-Methylimidazolium Chloride as Solvent. *Advanced Materials Research*, *332-334*, 309–312.

Wolf, B. a. (2007). Polyelectrolytes Revisited: Reliable Determination of Intrinsic Viscosities. *Macromolecular Rapid Communications*, *28*(2), 164–170.

Chapter VI

Aeropectin and hybrid pectin-silica aerogels

Introduction

Previous chapters were focused on cellulose and its various aerogels associated.
We saw that cellulose cross-linking gave improved structural, mechanical and thermal properties compared to pure aerocelluloses (Chapter IV). However, a lowest limit of thermal conductivity was reached at 27 $mW.m^{-1}.K^{-1}$.
We investigated also the preparation of interpenetrated cellulose-based networks. We tested two different polymers to mix with cellulose, lignin and cellulose acetate (Chapter V). We showed that, in both cases, cellulose underwent phase separation and it was not possible to obtain homogeneous porous materials.

We decided therefore to explore other types of polysaccharides. After a literature survey (c.f. Chapter I), we explored pectin as a new starting material, as it gave interesting morphological features in (White, Budarin, & Clark, 2010).

In this chapter, we will run a complete study on the structural properties of "aero-pectin" prepared with the similar dissolution-gelation-coagulation route as aerocellulose. We will study bulk and skeletal densities, porosity and specific surface areas. We will discuss and compare pore size distributions given by two different techniques: N_2 desorption (BJH method) carried out in Cemef Mines-ParisTech; and Hg porosimetry performed in the Laboratory Charles Coulomb (L2C) in the University of Montpellier.

Next, we will study mechanical behaviour of aeropectins by uniaxial compression. We will correlate characteristic parameters such as Young modulus and yield stress to bulk densities. We will compare mechanical properties of aeropectins to ones of pure aerocelluloses.

We will measure for the first time thermal conductivity of aeropectin. We will study the conduction of the gaseous and solid phases and we will correlate them to aeropectin porous structure. We will also evaluate the contribution of radiative transfer.

The last part is dedicated to the preparation and characterisation of hybrid pectin-silica aerogels. Silica aerogel is one of the best insulating materials but dusts easily. We will study pectin as a solid backbone in which we will incorporate silica aerogel. Hybrids formed are expected to have better thermal properties than aeropectins and better mechanical behaviour than silica aerogels.

Introduction

Les précédents chapitres se sont focalisés sur la cellulose et les différentes aérocelluloses associées. Il a été montré que la réticulation chimique de la cellulose améliorait les propriétés structurales, mécaniques et thermiques des aérocelluloses (Chapter IV). La meilleure conductivité thermique obtenue a été de 27 $mW.m^{-1}.K^{-1}$. La préparation de réseaux interpénétrés à base de cellulose a aussi été étudiée. Une séparation de phase a été observée conduisant à des matériaux inhomogènes.

D'autres polysaccharides ont été explorés et la pectine présente des propriétés intéressantes (White, Budarin, & Clark, 2010). Dans ce chapitre, une étude complète des propriétés structurales des aérogels de pectine, « aéropectines », sera menée. Les densités, apparente et de squelette, la porosité, la surface spécifique ainsi que les distributions de taille de pores seront mesurées. Deux différentes techniques pour les distributions de pores seront comparées : la porosimétrie au mercure et l'adsorption de N_2 (méthode BJH).

Les propriétés mécaniques seront étudiées par compression uniaxiale. Le module de Young et la contrainte de plasticité seront corrélés à la densité apparente et comparés à l'aérocellulose. L'aéropectine sera caractérisée thermiquement par les mesures de la conductivité totale et des différentes contributions thermiques qui seront discutées en fonction des propriétés structurales.

Ce chapitre abordera également l'élaboration et la caractérisation des aérogels hybrides à base de pectine et de silice. L'aérogel de silice est l'un des meilleurs super-isolants thermiques mais il poudre facilement rendant son utilisation plus difficile. La pectine sera étudiée comme une matrice solide dans laquelle l'aérogel de silice sera formé. Les hybrides pectine-silice devraient présenter de meilleures propriétés thermiques que l'aéropectine et de meilleures propriétés mécaniques que l'aérogel de silice.

1. Microstructural characterisation of aeropectin

1.1 Brief summary of aeropectin preparation

Aeropectin can be prepared via dissolution-gelation-coagulation route (Figure VI. 1), similar to aerocellulose. Only one paper reports on the texture of aeropectin, for only one formulation at 4.8_{wt}% (White et al., 2010). However, a complete study on the structural properties of aeropectins was never performed. In this part, various processing parameters (pH of the solvent, pectin concentration and sources of pectin) of aeropectin preparation were studied and correlated to the microstructure of the final material.

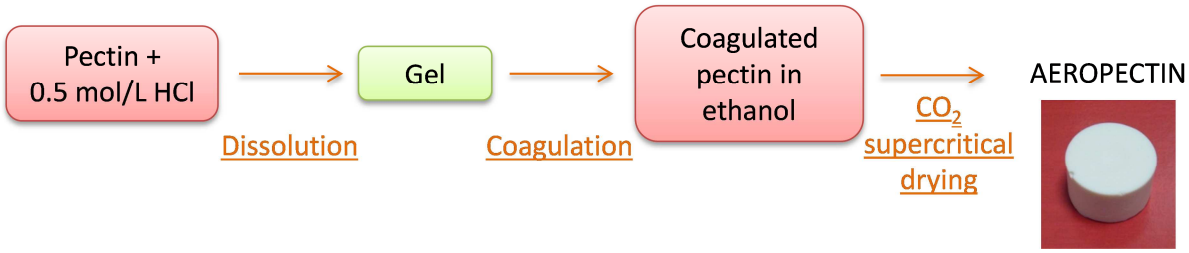

Figure VI. 1 : Preparation of aeropectin.

To be dissolved, pectin is added to an acidic aqueous solution under vigorous stirring (800 rpm) for about 4 to 6 h to ensure a complete dissolution (checked by optical microscopy). The mixture can be relatively viscous; it is thus centrifuged for 20 min at 6000 rpm to remove the maximum of air bubbles. The solution is then placed in moulds and let gelling at room temperature for 24 to 48 h depending on pectin concentration. Pectin gels are coagulated in a 50_{vol} % water and 50_{vol} % ethanol bath. The ratio of ethanol in the coagulation bath is then increased progressively to 100% (by 20% increment) and as a result a 3D network of aeropectin precursor is formed. Coagulated pectin is then dried in supercritical CO_2.

1.2 Effect of pH

It is well known that under acidic conditions pectin gels. It is mainly due to the protonation of most of acidic functions, which favour a stronger H-bonds network. Its pKa is about 2.9. (White et al., 2010) used a very acidic environment for pectin gelation: 0.5 mol/L HCl. We asked ourselves the following questions: what is the optimal pH for preparing pectin gels? What is the influence of pH on the final material morphology?

To answer the first question, we prepared various acidic aqueous solutions from HCl and citric acid and screened pH from 0.2 to 3, to be below the pectin pKa. These solutions were prepared by either diluting a ready solution of HCl 32_{wt} % (10.3 mol/L) in a volumetric flask or dissolving citric acid into water. 4_{wt} % citrus pectin was then dissolved in these solvents and stirred for at least 4 hours. Gelation of solutions at room temperature (22°C) was very different depending on the pH of acidic aqueous solutions. At low pH (<1) gelation was done overnight. For pH>1.5 gelation is not completed and even the rotting of solutions is observed (Table VI. 1). Thus a very low pH<1 is required to produce homogeneous gels from citrus pectin.

Table VI. 1 : Gelation of pectin solutions with various pH of acidic solutions.

C_{acid} (mol/L)	Type of acid	pH of acid solution	Remarks on gelation
0.5	HCl	0.3	Gelation overnight
0.1	HCl	0.9	Gelation overnight
0.05	HCl	1.1	Gelation in 2 days
0.5	Citric acid	1.6	Weak gelation
0.05	Citric acid	2.2	Rotten in 2 days
10^{-3}	Citric acid	3.1	Rotten in 1 day

Only samples prepared from 0.5, 0.1 and 0.05 mol/L HCl and from 0.5 mol/L citric acid will be further studied. All solutions were homogeneous and no air bubbles were visible by the naked eye or by microscopy. Gels were coagulated in 50/50 water/ethanol bath resulting in "alcogels". Coagulation baths were changed regularly and the concentration in ethanol increased to 100% ethanol. Some "holes" or "bubbles" are visible inside the structure of coagulated pectin that was prepared at 0.05 and 0.1mol/L HCl (Figure VI. 2a and c). The corresponding aeropectins also contained "holes" (Figure VI. 2b and d). They were probably created during the introduction of the non-solvent to the gel. One possible explanation is that at slightly higher pH, the gel is weaker due to less H-bonds formed, the structure is thus more easily deformable. For 0.5 mol/L solutions, pectin alcogels seem homogeneous; no bubble is visible inside the structure (Figure VI. 2e).

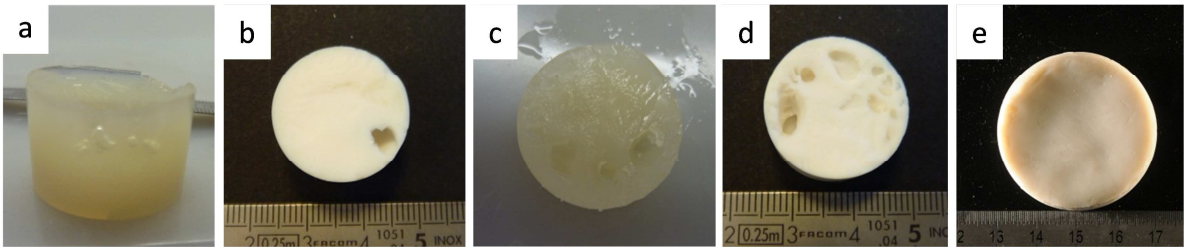

Figure VI. 2 : Alcogel and the corresponding aeropectins: made from 0.05 M HCl (a, b); from 0.1 M HCl (c, d) aeropectin made from 0.5 M HCl (e).

Alcogels were then dried by supercritical CO_2 and aeropectins obtained are presented in Figure VI. 2b, d and e. Their bulk densities were measured with a powder pycnometer Geopyc in Persée-Mines ParisTech (c.f. Chapter II). If aeropectin contained holes, characterisation was performed on parts in the most homogeneous regions. Densities are summarised in Table VI.2. A 4_{wt}% aeropectin has a bulk density of about 0.11 g/cm^3. For 0.05 M and 0.1 M, aeropectin densities are almost the same within experimental errors, when far from holes.

Table VI. 2 : Bulk densities of aeropectins as a function of pH.

C_{acid} (mol/L)	Type of acid	pH of solution before gelation	ρ_{bulk} of aeropectin (g/cm^3)
0.5	HCl	0.3	0.115
0.1	HCl	0.9	0.105
0.05	HCl	1.1	0.108
0.5	Citric acid	1.6	0.0997

The fine structure of these aeropectins was observed by SEM (Figure VI. 3). Here again we avoided regions with large holes. For all aeropectins, a fibrillar structure is observed with pores from few tens to several hundreds of nanometers. It seems that pH does not influence aeropectin morphology on the level of the sizes, seen by SEM.

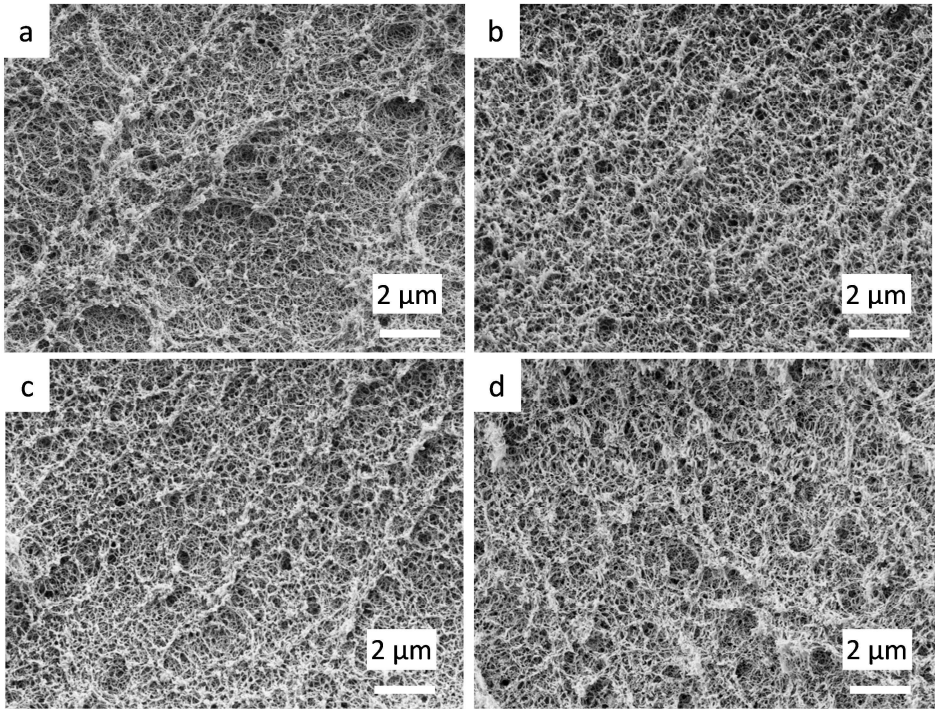

Figure VI. 3 : SEM images of aeropectins prepared from citrus pectin in different acidic solutions, 0.5M HCl (a), 0.1M HCl (b), 0.05M HCl and 0.5 M citric acid (d). Pectin concentration in solution was 4_{wt}%.

In native pectins, the acid functions are either in form of carboxylate COO^- or are esterified $COOCH_3$. For preparing aeropectins, pectin is placed in an acidic solution where all the carboxylate groups will be transformed into carboxylic acids. Figure VI. 4 presents the FT-IR spectra of three different aeropectins prepared from solvents of different pH. For 0.1 and 0.5 mol/L (Figure VI. 4b and c), the signal at 1410 cm^{-1} corresponding to the asymmetrical stretching of carboxylate COO^- has decreased significantly as compared to pure citrus pectin. But for 0.05 mol/L, it decreased only slightly (Figure VI. 4a). The band at 1610 cm^{-1} corresponding to the symmetrical stretching of carboxylate COO^- has disappeared and a shifted band appeared around 1640 cm^{-1}. For 0.05 mol/L, this band is less shifted with a wavelength of

1630 cm^{-1}. The band for C=O in ester and in carboxylic acid group are overlapping and give a higher signal at 1740 cm^{-1}.

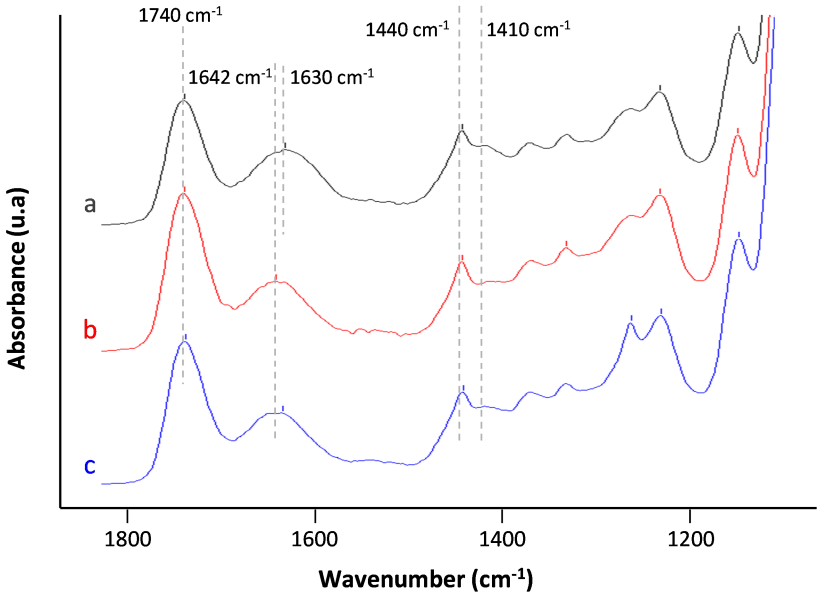

Figure VI. 4 : FT-IR spectra of aeropectins from 0.05 (a), 0.1 (b) and 0.5 (c) mol/L HCl.

It is difficult, just by analyzing FT-IR spectra, to quantify the possible deesterification of pectin during the acidic treatment. (White et al., 2010) claimed (by FT-IR and XPS analyses) this treatment induced a change from a mixed galacturonic acid/methyl esterified pectin to a predominantly galacturonic acid rich pectin.
From this FT-IR analysis, we can conclude that 0.05 mol/L is not enough acidic to undergo a complete acidification as some signals of carboxylate remained. A pH below 1 is thus required for preparing aeropectins. In the following, 0.5 mol/L HCl will be used as pectin solvent.

1.3 Effect of pectin sources and concentration on aeropectin density and morphology

Aeropectins with various concentrations of pectin, from 1% to 6_{wt}%, were prepared from either citrus or apple pectin. Concentrations above 6% have not been tested as the solution was highly viscous and its manipulation is rather difficult. It was not possible to obtain a gel from 1_{wt}% pectin and the coagulation of this solution failed. For pectin solutions of 2 and 3_{wt}% gelation is very slow (few days to a week at room temperature) and gels are weak (Figure VI. 5a & b). For these concentrations, removal from the mould and solvent exchanges were carried with extra care to avoid breaks. For concentrations above 3%, gelation occurs in less than 24h at room temperature (Figure VI. 5c).

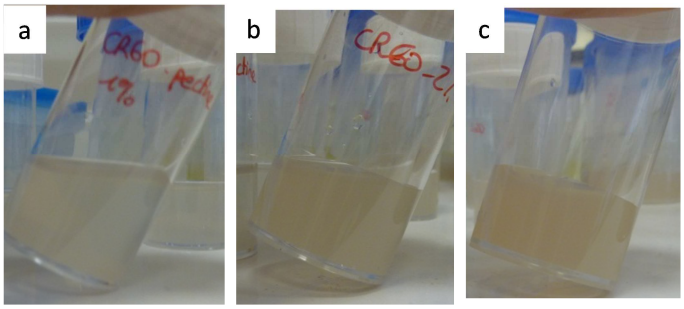

Figure VI. 5 : Pectin gels from 1% (a); 2% (b); and 3_{wt}% (c) citrus pectin after 24 hours at room temperature.

Macroscopically, all samples either from citrus or apple pectins with a concentration in polymer above 2% appear homogeneous, as no macroscopic "channels" are visible. These aeropectins were characterised in details. First, skeletal density of citrus pectin was determined in the laboratory L2C in the University of Montpellier with a He pycnometer and its value is about 1.57±0.03 g/cm^3, close to what is usually found in the literature. Because the skeletal density of apple pectin was not determined, we will use the same value as for citrus pectin. Bulk densities were determined by powder pycnometer Geopyc. Aeropectin density linearly increases with pectin concentration (Figure VI. 6) as it has been already reported for aerocellulose. Porosity is therefore calculated and it is above 90 %.

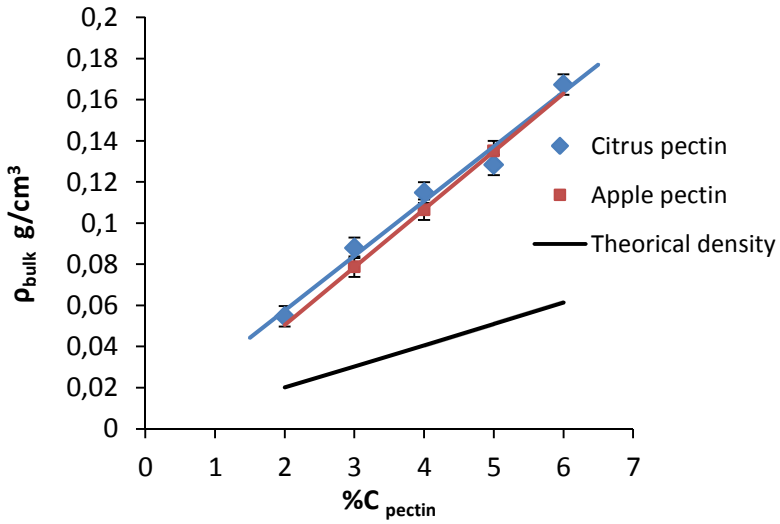

Figure VI. 6 : Bulk densities of aeropectins from citrus and apple pectins as a function of polymer concentration in solution.

Theoretical density was also calculated supposing no volume contraction from gel to dry sample. Densities of aeropectins are higher than the theoretical one, mainly due to contraction during the coagulation and $scCO_2$ drying processes.

No influence of the source of pectin on aeropectin density is observed. For both citrus and apple pectins, a light aeropectin, e.g. 0.08 g/cm^3 for a 3_{wt}% and 0.13 g/cm^3 for a 5_{wt}%, was prepared.

The influence of pectin concentration in solution on aeropectin morphology was analysed by SEM. Figure VI. 7a and b display observations from 3% and 5_{wt}% citrus-based aeropectins. They showed a fibrillar structure with long and entangled strands, as already shown in Figure VI. 3. The morphology at 5% seems denser with pores slightly smaller, which confirms the density values. Aeropectins from apple pectin (Figure VI. 7c) present a very similar morphology as compared to aeropectins from citrus pectin.

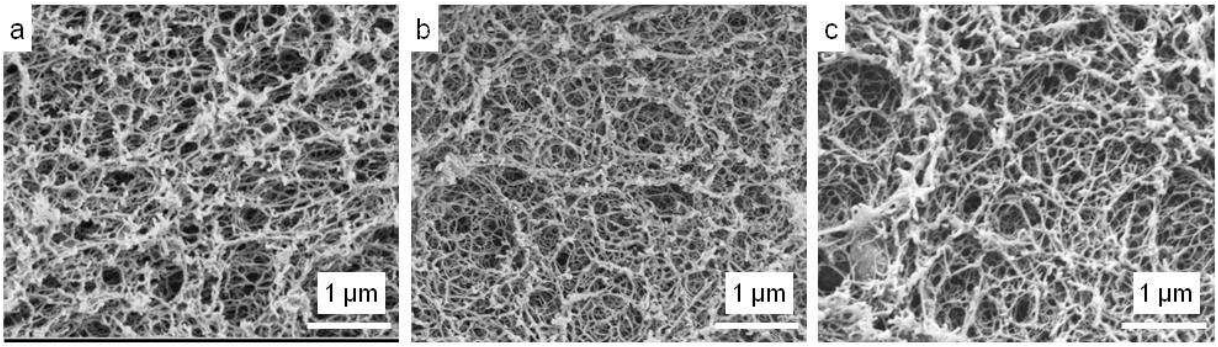

Figure VI. 7 : SEM observations of aeropectins from 3_{wt}% (a) and 5_{wt}% (b) citrus pectin; $3\%_{wt}$ apple pectin (c).

In the following structural characterizations, only citrus aeropectins will be studied. Specific surface areas were measured by the laboratory L2C-Montpellier and pores size distributions (PSD) by two different techniques: Hg porosimetry (L2C-Montpellier) and N_2 desorption (BJH method) (Cemef-Mines ParisTech).

First, specific surface areas were analysed as a function of pectin concentration. They all are around 250 m²/g. It is difficult to see a tendency as a function of pectin concentration due to high experimental errors (10%) and only two polymer concentrations studied (Figure VI. 8). As compared to aerocellulose prepared from cellulose dissolved in 7.6%NaOH-water (Gavillon & Budtova, 2008; Gavillon, 2007) or in 8%NaOH-water (c.f. Chapter III), aeropectins appear to have similar specific surfaces areas as aerocellulose ~250 m²/g (Figure VI. 8).

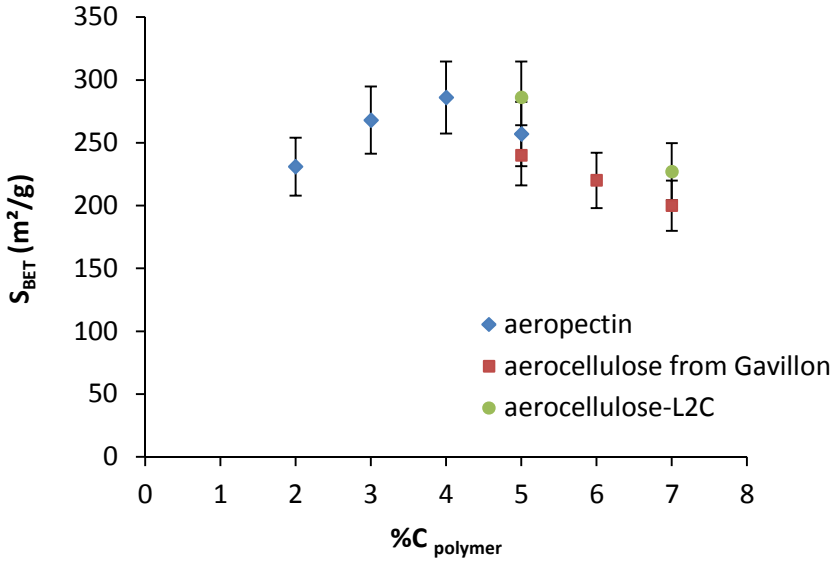

Figure VI. 8 : Specific surface areas vs polymer concentrations for aeropectins and aerocelluloses measured in the laboratory L2C-Montpellier and aerocelluloses from (Gavillon, 2007))

We analysed N_2 adsorption-desorption isotherm, an example for citrus-based aeropectin prepared from 3% solution is given in Figure VI. 9. According to the IUPAC classification, the isotherm is a type IV typical for mesoporous structures (c.f. Chapter II).

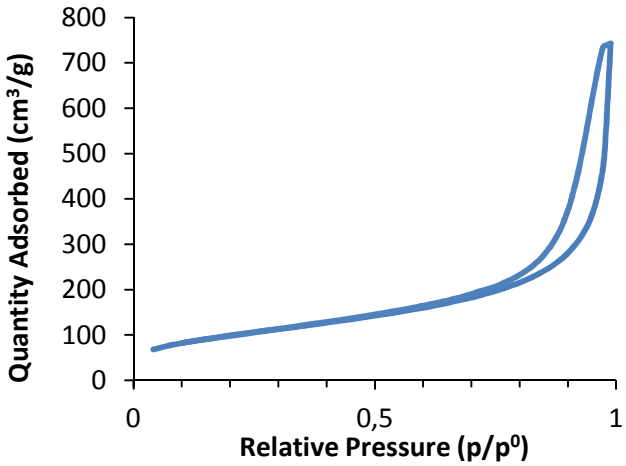

Figure VI. 9 : 3_{wt}% citrus aeropectin N_2 adsorption isotherm.

N_2 desorption is widely used in literature for PSD measurements. (White et al., 2010) reported for the first time aeropectin PSD by using this method (Figure VI. 10). The maximum on pore size distribution is located around 11 nm. However, SEM images of aeropectin clearly show much larger pores (Figure VI. 11). We tried to analyse PSD by SEM image analysis but it was not conclusive as the structure is in three dimensions. Qualitatively we can observe that pores vary from about few tens to few hundred nm. N_2 desorption method does not to fully describe pore size distribution.

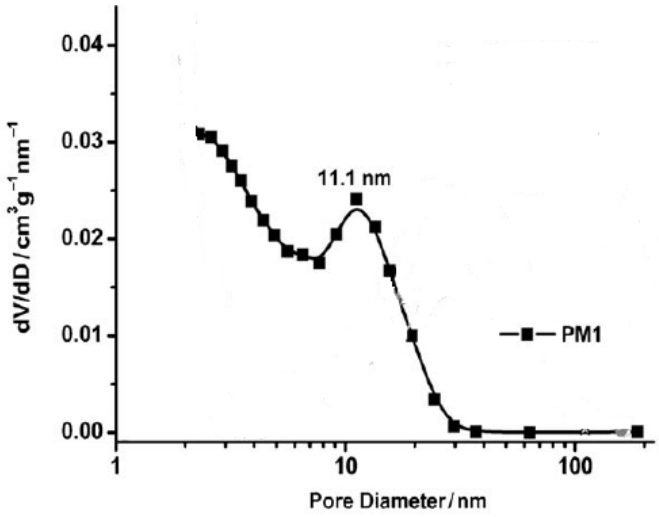

Figure VI. 10 : PSD of 4.8$_{wt}$% aeropectin from (White et al., 2010). Reprinted with permission from (White et al., 2010). Copyright (2010) Wiley.

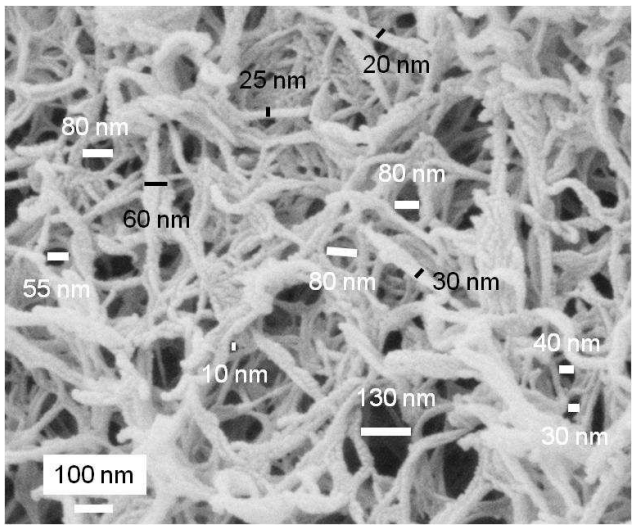

Figure VI. 11 : SEM image of a 5$_{wt}$ % citrus aeropectin. Image analysis of pores and pore wall thickness.

We investigated more deeply the BJH method and compared to Hg porosimetry. For Hg porosimetry, direct determination of pore size distribution is not possible because of pore walls collapse, the same as it was described for aerocelluloses. Pore size distribution was thus built using Pirard approach (Pirard & Pirard, 1997) (c.f. Chapter II):

$$L = \frac{k}{P^{0.25}} \quad \text{(VI. 1)}$$

The buckling constant k was determined in the laboratory L2C in the University of Montpellier: k= 60 nm.MPa$^{0.25}$ for 3$_{wt}$% citrus aeropectin.

Pore size distributions from both techniques, nitrogen adsorption and mercury intrusion, are given in Figure VI. 12.

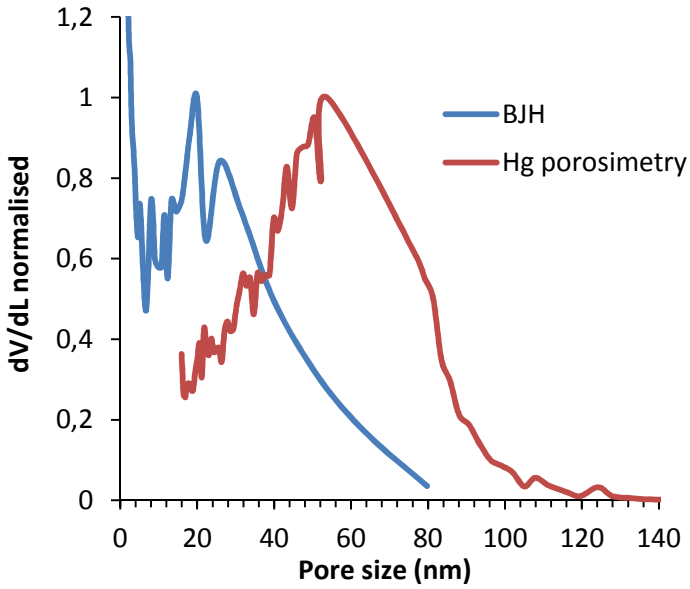

Figure VI. 12 : PSD of 3_{wt}% citrus aeropectin from BJH method and Hg porosimetry.

These two techniques give different PSD. Hg porosimetry uses pressure from 0.01 to 200 MPa and analyses pores from about 15 to 160 nm. N_2 desorption analyses pores from 2 to 80 nm (pressure between 0.1 and 0.01MPa). The main characteristics of each pore size distribution are displayed in Table VI. 3. The theoretical porous volume is calculated according to Equation (VI. 2).

$$V_{p\,theoretical} = \frac{1}{\rho_{bulk}} - \frac{1}{\rho_{skeletal}} \qquad \text{(VI. 2)}$$

Table VI. 3 : Data from PSD of 3_{wt}% citrus pectin by Hg porosimetry and BJH method.

Analysis System	S_{BET} (m^2/g)	$V_{p\ Theoretical}$ (cm^3/g)	$V_{p\ Measured}$ (cm^3/g)	% $V_{p\ measured}$	$Lp_{\ max}$ (nm)	$Lp_{\ mean}$ (nm)	FWHV (nm)	$4V/S_{BET}$ (nm)
Hg porosimetry	268	10.47	5.71	54.5%	54	43	46	85
BJH	268	10.47	1.14	11%	20	11	34	17

We compared the theoretical and the measured porous volume (%V) to evaluate the quantity of porous volume that has been analysed by the two techniques. BJH method analysed only 11% of the total pores volume and Hg porosimetry 54% (Table VI. 3). The complete PSD of aeropectin cannot be obtained by these two techniques. They only give a restricted image of the full aeropectin morphology. An important discrepancy is observed for the maximum of pores size: 54 nm for Hg porosimetry against 20 nm for BJH.

A similar disagreement is observed for $L_{p\ mean}$ between BJH and porosimetry with $L_{p\ mean}$= 11 and 43 nm, respectively.

The BJH method gives a shifted PSD towards smaller pores compared to Hg porosimetry. Hg porosimetry PSD obtained with "Pirard's" approach seems closer to the SEM observations on Figure VI. 11.

Using the Hg porosimetry, the influence of pectin concentration was investigated. First, buckling constants k were determined for each concentration. Figure VI. 13 shows the variation of k with pectin concentration. It increases linearly and equals to $k_{3\%}$ = 60 nm.MPa$^{0.25}$ for 3%$_{wt}$ and $k_{5\%}$ = 76 nm.MPa$^{0.25}$ for 5%$_{wt}$ pectin.

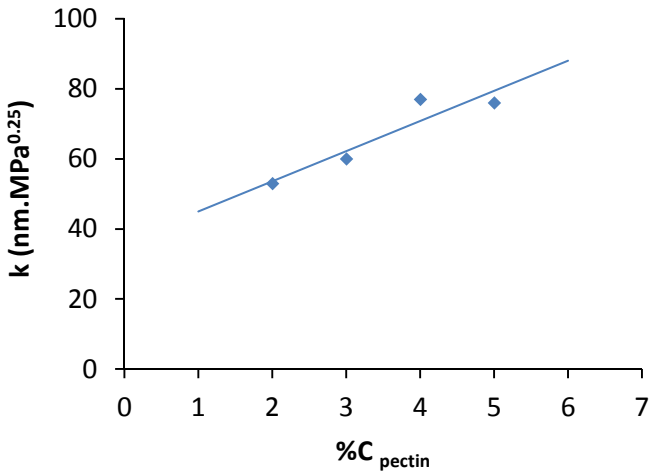

Figure VI. 13 : Variation of the buckling constant with pectin concentration.

SEM images show that the increase of pectin concentration gives smaller pores (Figure VI. 7a & b). We compared PSD of two different pectin concentration 3$_{wt}$% and 5$_{wt}$% (Figure VI. 14). For both concentrations, similar porous volume was measured of about 55-60%. It can be thus estimated that 40-45% of the porous volume is not quantifiy by the Hg porosimetry method and represents the fraction of micropores and large macropores. PSD are centered around 50-55 nm (Table VI. 4). Mean pore size $L_{p\ mean}$ is very similar, about 43-45 nm. The difference is detected in the width of the distribution: at 5$_{wt}$% pectin, PSD is narrower with a full width at half value (FWHV) of 29 nm against 46 nm for 3$_{wt}$%. This is in good agreement with SEM observations.

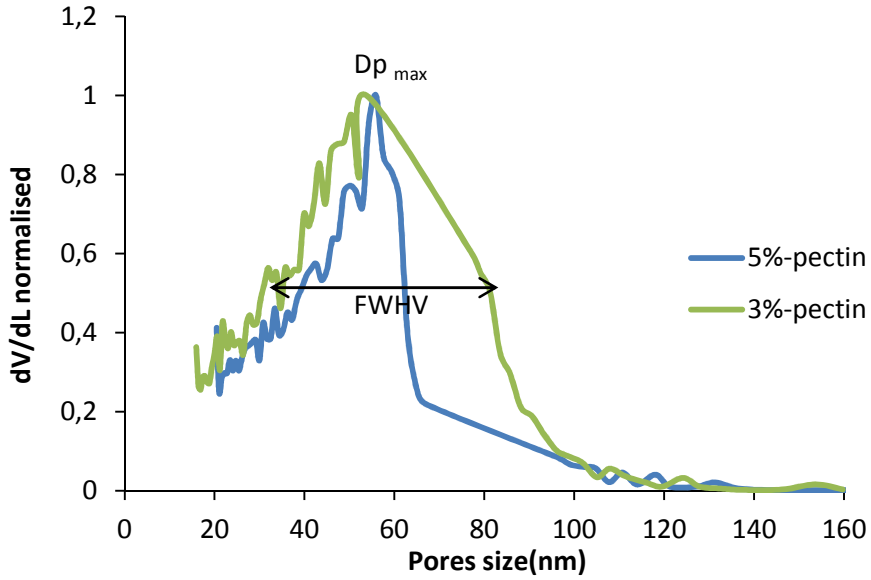

Figure VI. 14 : PSD by Hg porosimetry for 3%$_{wt}$ and 5%$_{wt}$ citrus aeropectins.

Another way to have a mean size of pores is to calculate the quantity $4V_{measured}/S_{BET}$.
The values obtained for 3 and 5% pectin concentrations are given in Table VI. 4 and they seem to overestimate pore mean size: for example, for 3$_{wt}$% aeropectin $4V/S_{BET}$ equals 85 nm.

Table VI. 4 : Data from Hg porosimetry for 3%$_{wt}$ and 5%$_{wt}$ citrus aeropectins.

% C_{pectin}	S_{BET} (m^2/g)	ρ_{bulk} (g/cm^3)	$V_{p\ Theoretical}$ (cm^3/g)	$V_{p\ Measured}$ (cm^3/g)	% $V_{measured}$	$L_{p\ max}$ (nm)	$L_{p\ mean}$ (nm)	FWHV (nm)	$4V/S_{BET}$ (nm)
3 %	268	0.09	10.47	5.71	54.5%	54	43	46	85
5 %	257	0.128	7.17	4.22	59 %	56	45	29	66

As well as for aerocelluloses, aeropectins morphologies can be tuned with polymer concentration.

1.4 Comparison with aerocellulose

In this section, we compare morphology of aerocellulose prepared from a solution of cellulose in 8%NaOH–water and aeropectin. Polymer concentration in solution is the same, 5$_{wt}$%. Table VI. 5 summarizes structural characterizations. Both aerogels have similar densities, specific surface and porosity.

Table VI. 5 : Comparison of structural properties for 5$_{wt}$% aerocellulose and 5$_{wt}$% aeropectin.

Type	ρ_{bulk} (g/cm^3)	$\rho_{skeletal}$ (g/cm^3)	Porosity	S_{BET} (m^2/g)	Lp_{max} (nm)	Lp_{mean} (nm)	FWHV (nm)
5%-aeropectin	0.128	1.57	92 %	257	56	45	29
5%-aerocellulose	0.123	1.55	92 %	286	48	35	35

Pore size distributions for aeropectin and aerocellulose obtained with « reconstructed » mercury porosimetry approach are given in Figure VI. 15. As shown in Chapter III, the buckling constant for 5% aerocellulose equals 56 nm.MPa$^{0.25}$, and for 5% aeropectin 76 nm.MPa$^{0.25}$. Both pore size distributions are centred around 50 nm and have similar mean pore diameter (about 35-45 nm) and FWHV about 30 nm. PSD of aeropectin is slightly shifted towards smaller pores but it is hard to conclude as experimental errors are important. Aerocelluloses and aeropectins morphologies have many similarities.

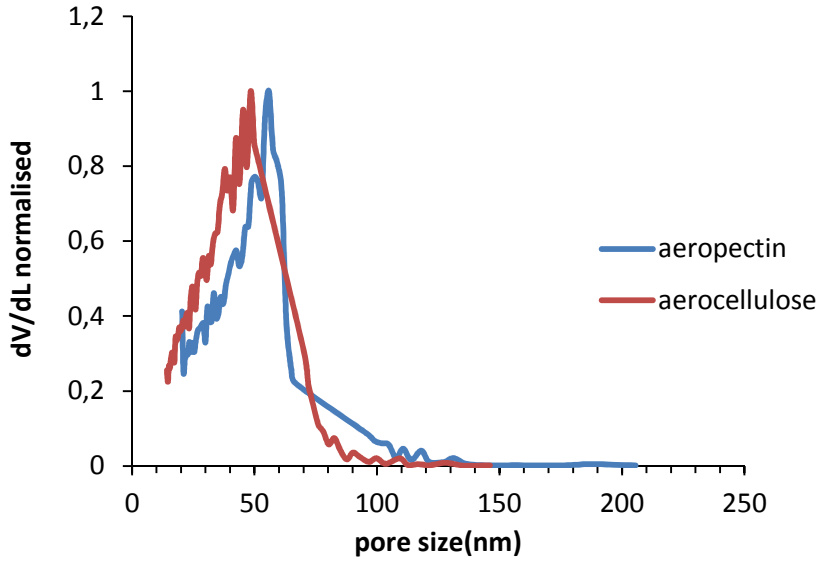

Figure VI. 15 : Comparison of PSD for 5$_{wt}$% aerocellulose and 5$_{wt}$% aeropectin.

2. Mechanical properties of aeropectin

We studied aeropectin mechanical properties by uniaxial compression. Two types of tests were performed (c.f. Chapter II). The first one was at small deformations to evaluate more precisely the Young modulus, and the second test varies strain from 0 to 75% to have the full stress-strain curve. From this curve, different mechanical parameters can be determined such as the yield stress σ_{yield} (beginning of plastic region), the yield strain ε_{yield}, the densification strain ε_d and the energy absorbed by the sample from the beginning of deformation to either 40% strain $W_{40\%}$ or to the densification strain $W_{\varepsilon d}$.

We studied the influence of pectin concentration on aeropectin mechanical behaviour. Figure VI. 16 gives the complete stress-strain curves for 3 different citrus pectin concentrations (3, 4 and 5$_{wt}$%)

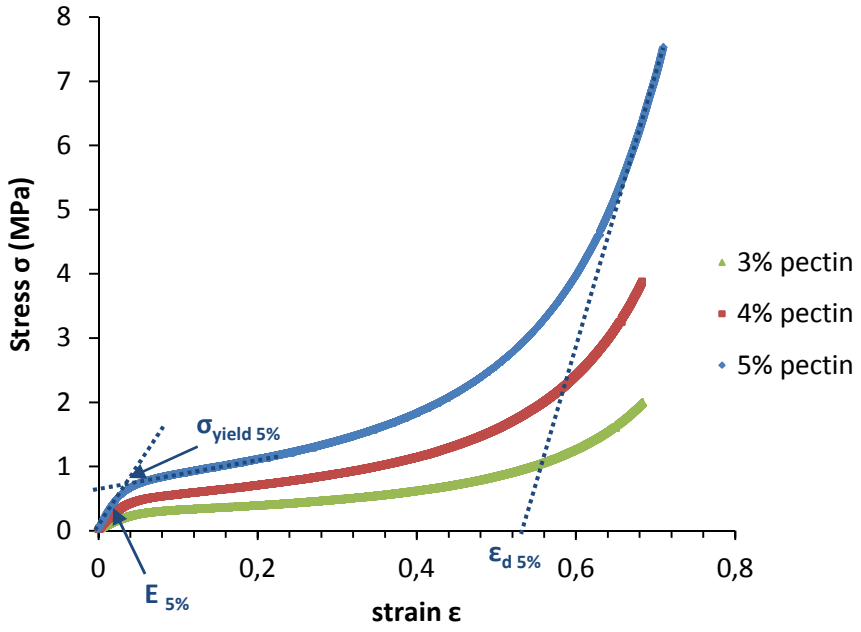

Figure VI. 16 : Stress-strain curve for 3,4 and 5% citrus aeropectins.

Table VI. 6 summarises the mechanical properties of studied aeropectins (3 to 5_{wt}%) determined from Figure VI. 16. Young moduli, yield stress and absorbed energies increase with pectin concentrations. Yield and densification strains seem to remain relatively independent on concentration with values of 4-5% and 50-53% respectively. Mechanical behaviour of aeropectins is quite similar to that of aerocellulose from cellulose dissolved in NaOH-water (data taken from Chapter IV).

Table VI. 6 : Mechanical properties of aeropectins.

%C	ρ_{bulk} (g/cm^3)	E (MPa)	σ_{yield} (MPa)	ε_{yield}	ε_d	$W_{40\%}$ (kJ/m^3)	$W_{\varepsilon d}$ (kJ/m^3)
3% citrus pectin	0.09	4.1	0.21	0.041	0.52	138	217
4% citrus pectin	0.115	5	0.37	0.044	0.51	309	496
5% citrus pectin	0.128	10	0.79	0.053	0.53	455	741
5% cellulose	0.123	10	0.30	0.037	0.55	213	334

Young modulus as a function of bulk density was plotted for aeropectin and presented in Figure VI. 17. By using the model of Ashby and Gibson (Chapter II), the exponent *m* equals to 1.8. Contrary to other type of aerogels, it is close to the ideal foam exponent *m*=2 and below to that of aerogels. However, we shall not speculate about this result because of the narrow interval of aeropectin densities and limited amount of data .

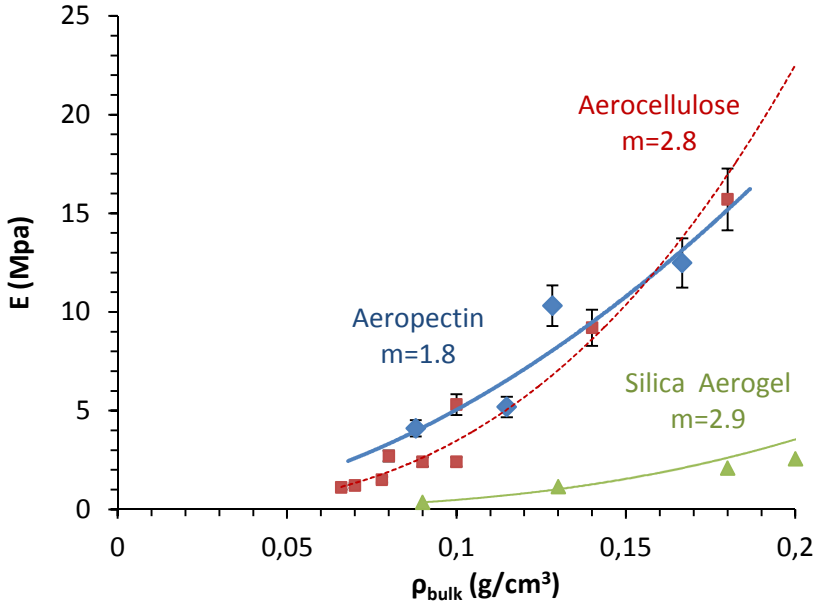

Figure VI. 17 : Comparison of Young modulus for aeropectin, aerocellulose (data taken from from (Gavillon, 2007; Sescousse, Gavillon, & Budtova, 2011; Sescousse, 2010)) and silica aerogel (data taken from (Alaoui, Woignier, Scherer, & Phalippou, 2008)).

Aeropectin was compared to two kinds of aerogels: silica aerogel and aerocellulose. It is clearly mechanically stronger than silica aerogel for all ranges of densities. As an example, at density 0.13 g/cm^3 Young modulus of silica aerogel is ten times lower than that of aeropectin (E= 1.1 MPa, (Alaoui et al., 2008)). Aeropectin and aerocellulose have a very similar mechanical behavior (within the experimental errors) in the range of densities from 0.08 to 0.2 g/cm^3 (e.g. E=10 MPa for a 0.12-0.13 g/cm^3 aerogel) (Table VI. 6).

Yield stress was also plotted versus bulk density (Figure VI. 18) for aeropectin and aerocellulose. For these two aerogels power laws were obtained but their exponent differs greatly: n = 1.9 (recalculated from (Sescousse et al., 2011; Sescousse, 2010)) for aerocellulose and n = 3.2 for aeropectin. At low densities, both aerogels display similar mechanical behavior whereas at higher densities aeropectin present a greater stiffness than aerocellulose. At a density of 0.13-0.14 g/cm^3, aeropectin has a yield stress of 0.8 MPa against 0.3 MPa for aerocellulose (Table VI. 6).

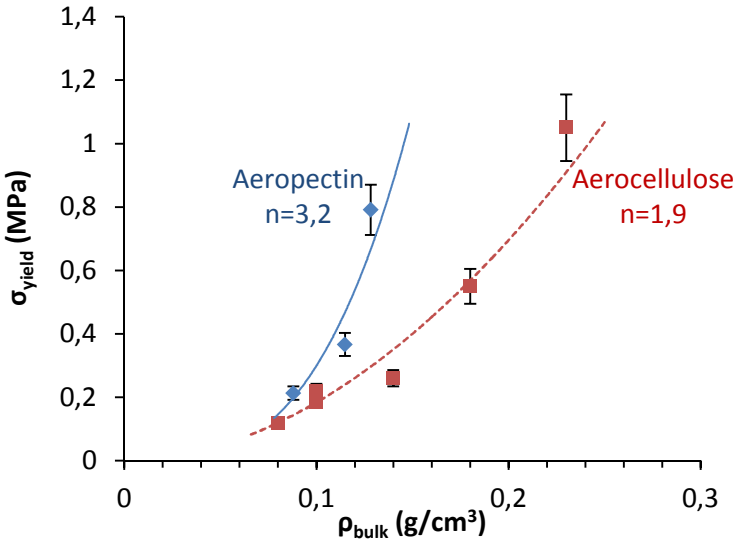

Figure VI. 18 : Comparison of yield stress for aeropectin and aerocellulose (data taken from (Gavillon, 2007; Sescousse et al., 2011; Sescousse, 2010)) as a function of bulk density.

We also compared the energy absorbed during the deformation until 40% strain and until the densification strain (Figure VI. 19). Densification strain ε_d is about 50% for aeropectin (Table VI. 6). $W\varepsilon_d$ is better reflecting the deformation energy, but we also calculated $W_{40\%}$ as this parameter is used in literature on aerogels and allows easier comparison between aerogels. Absorbed energy also follows density power law dependence and exponents are $p = 3.2$ for $W\varepsilon_d$ and $p = 3.1$ for $W_{40\%}$. No significant difference is thus observed between these two energies in terms of concentration dependence and $W_{40\%}$ may be used for comparing mechanical properties with the other aerogels.

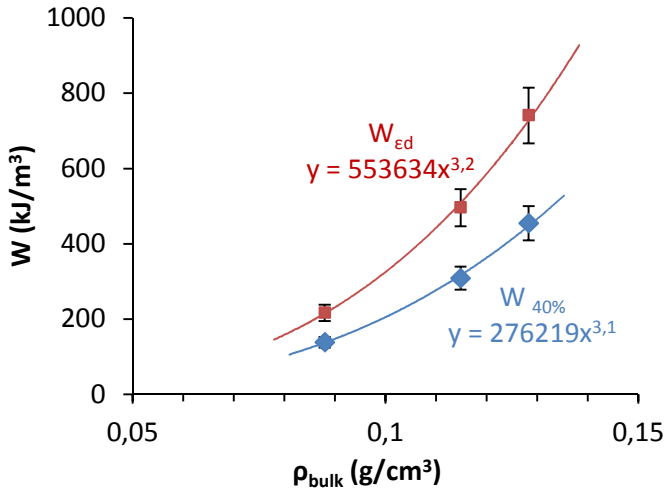

Figure VI. 19 : Absorption energy evaluated at 40% strain or at densification strain.

We compared the absorbed energy during compression test of aeropectin and aerocellulose (Figure VI. 20). As for yield stress, deformation energy is higher for aeropectin than for aerocellulose.

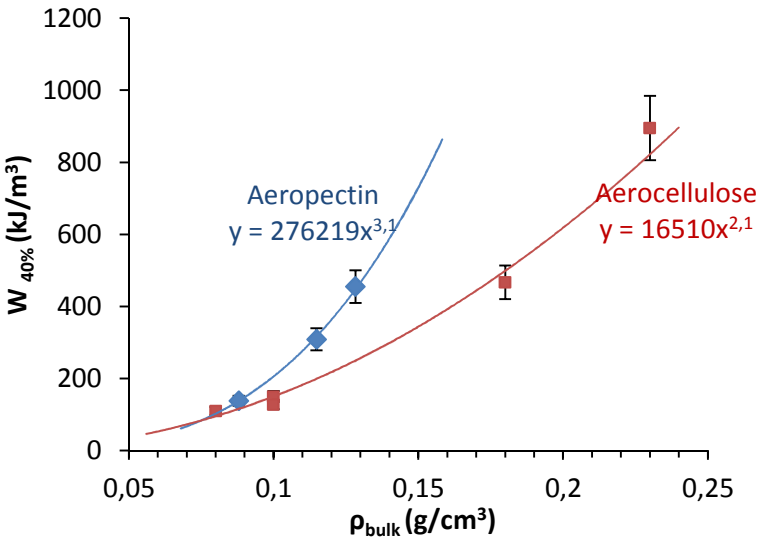

Figure VI. 20 : Comparison of absorbed energy vs bulk density for aropectin and aerocellulose (data taken from (Sescousse et al., 2011; Sescousse, 2010)).

Aeropectin and aerocellulose are alike in terms of structural properties but differ in their mechanical robustness. Aeropectin has a higher stiffness than aerocellulose. It may be explained by the difference in spatial configuration of macromolecules. Cellulose has a β-1,4 linkage whereas pectin has a α-1,4 glycosidic bonds which gives a coiled spring spatial representation. This may modify chain rigidity and thus influence the mechanical properties.

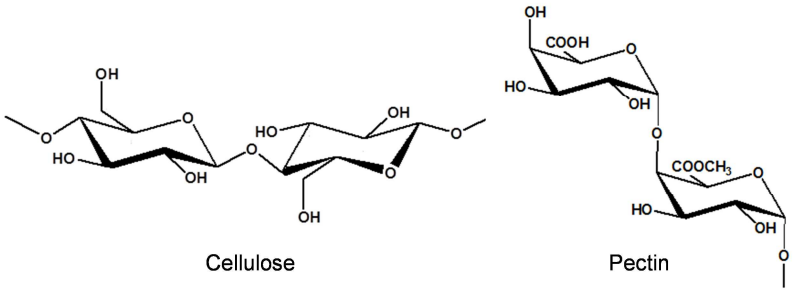

Figure VI. 21 : Schematic representation of cellulose and pectin structure.

3. Thermal properties of aeropectins

The thermal properties of aeropectins were then investigated. As described in Chapter II, the effective thermal conductivity of porous materials has three contributions: the conduction of the solid phase, the conduction of the gas trapped inside the porosity and the radiative heat transfer contribution (Equation (VI. 3)).

$$\lambda_{effective} = \lambda_{solid} + \lambda_{gas} + \lambda_{radiative} \quad \text{(VI. 3)}$$

Each contribution was measured in order to have a better understanding of heat transfer mechanisms within aeropectins. It also gives information on structural parameters to be optimised in order to reach superinsulating properties.
The effective thermal conductivities were measured either on the heat flow meter Fox 150 in Persée-Mines ParisTech or on the heat flow meter Fox 200 adapted to small samples at CSTB at 20°C (293 K). The results from both techniques will be presented.

3.1 Effect of pectin concentration on thermal conductivity

First, we studied the effective thermal conductivity of aeropectins with various bulk densities. Table VI. 7 summarises thermal characterisations of aeropectins and compares with aerocellulose prepared from cellulose dissolved in 8%NaOH-water. The main result is that aeropectins appeared to be thermal super-insulating materials, with thermal conductivity below 0.025 $W.m^{-1}.K^{-1}$. It seems that flow meter Fox 150 slightly overestimates by 20% the thermal conductivity as far as two other different methods used by CSTB, hot wire and heat flow, give the same and lower values as compared to the one obtained with flow meter Fox 150, see aeropectin from 4% (Table VI. 7).

Table VI. 7 : Thermal characterisations of citrus aeropectins.
All conductivities are given in $mW.m^{-1}.K^{-1}$.

Formulation	ρ_{bulk} (g/cm^3)	$\lambda_{effective}$ Fox 150	$\lambda_{effective}$ Fox 200	$\lambda_{effective}$ CSTB hot wire	$\lambda_{gas+solid}$ Fox 150	$\%\lambda_{radiative}$ Fox 150
2% aeropectin	0.05	20.0	-	-	14.5	27%
3% aeropectin	0.09	23.6	-	-	16.3	31%
4% aeropectin	0.115	24.4	20	21	17	30%
5% aeropectin	0.128	25.4	-	-	18	29%
5% aerocellulose	0.123	30.8	-	-	21.5	30%

The effective thermal conductivity as a function of bulk density is plotted in Figure VI. 22; and we compared aeropectin to other different aerogels such as silica aerogel and aerocellulose. Clearly aeropectin is much more insulating than aerocellulose which has a minimum $\lambda_{effective}$ =30 $mW.m^{-1}.K^{-1}$. Compared to silica aerogels, at usual density of aerogel materials (0.1 g/cm^3), aeropectin has a higher thermal conductivity $\lambda_{effective}$ = 22 $mW.m^{-1}.K^{-1}$ against 16 $mW.m^{-1}.K^{-1}$ for silica; but at lower concentrations, citrus aeropectin seems to be even a better thermal insulating material than silica aerogels.

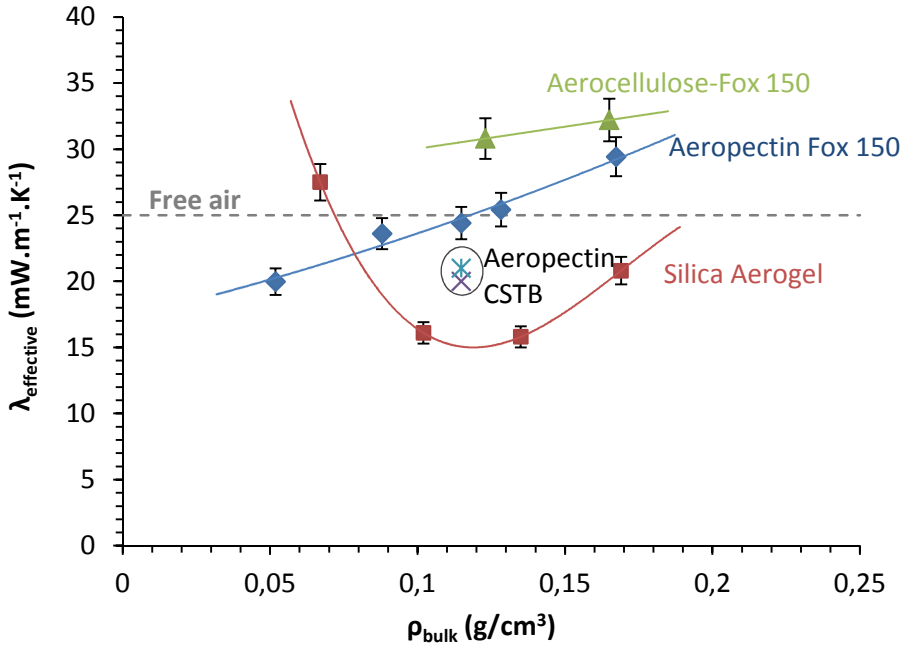

Figure VI. 22 : Thermal conductivity as a function of bulk density for :

- <u>aeropectin</u> measured by heat flow meter Fox 150-Persée Mines ParisTech, by heat flow meter Fox 200- CSTB and by hot wire- CSTB;
- <u>aerocellulose</u> measured by heat flow meter Fox150;
- <u>silica aerogel</u> (data taken from (Bisson, Rigacci, Lecomte, & Achard, 2004)).

It is interesting to note that aeropectin thermal conductivity seems not to reach a minimum in the range of densities 0.05-0.2 g/cm^3 which is the case for several known aerogels (Bisson, Rigacci, Lecomte, & Achard, 2004, Lu, Caps, Fricke, Alviso, & Pekala, 1995). The increase of $\lambda_{effective}$ at very low density, classically visible for silica (Bisson et al., 2004) or resorcinol formaldehyde (Lu, Caps, Fricke, Alviso, & Pekala, 1995) aerogels, was not detected in the case of aeropectins (Figure VI. 22).

3.2 Determination of radiative and conduction contributions

We studied the effect of temperature on thermal conductivity, measured by flow meter Fox 150 and by varying temperature from -10°C to 40°C for pectin concentrations between 2 and 5$_{wt}$% (Table VI. 7). The thermal conductivity was plotted as a function of temperature in power three (Figure VI. 23). The extrapolation to a null temperature suppresses the radiative contribution and gives the conductivity of gas and solid conduction. Figure VI. 23 shows that aeropectin has a conductivity of gas+solid slightly lower than aerocellulose, 18 against 21.5 mW.m^{-1}.K^{-1}, which may explain the difference in the effective thermal conductivity between these two polysaccharide aerogels.

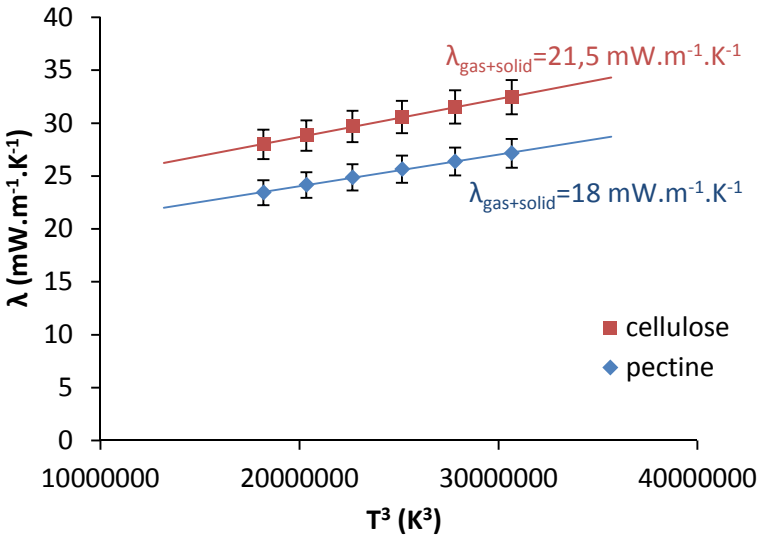

Figure VI. 23 : Variation of thermal conductivity versus temperature of 5_{wt}% citrus aeropectin and 5_{wt}% aerocellulose.

Figure VI. 24 displays the different thermal contributions (radiative and conduction) as a function of citrus aeropectins densities. The conduction of solid and gas decreases with density with the same behavior as the total thermal conductivity. It seems that the conduction is the major part of the heat transfer.

By subtracting the conduction of gas+solid from the effective thermal conductivity, we determined the radiative heat transfer. Values are reported in Table VI. 7. For all concentrations, radiative conductivity represents about 30% and is relatively independent of bulk density (Figure VI. 24). Similarly to aerocellulose (Chapter III), this result is surprising as the radiative conductivity is generally inversely proportional to the bulk density.

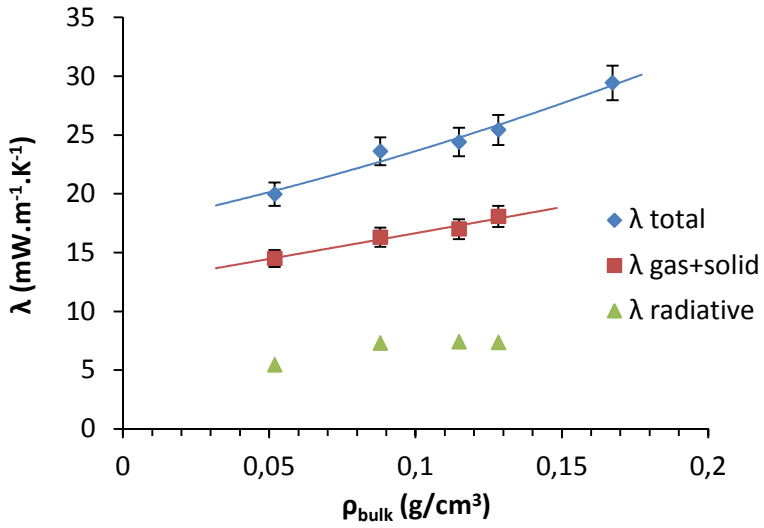

Figure VI. 24 : Influence of density on solid and gas conduction and on radiative transfer.

For 4_{wt}% citrus aeropectin, with the help of CSTB, it was possible to directly determine all contributions to the total thermal conductivity. Experiments at room temperature where the

pressure is decreased to very low values remove the contribution of gas and give the sum of the solid and radiative conductivity. Figure VI. 25 presents the conductivity as a function of pressure. A plateau is observed from about 10 hPa and the conductivity value at the plateau is taken as $\lambda_{solid}+\lambda_{radiative}$ which for 4_{wt}% aeropectin is estimated at 10 $mW.m^{-1}.K^{-1}$. The same experiment was carried out on a 5_{wt}% aerocellulose (from 8%NaOH-water-cellulose solution). Interestingly, for aerocellulose $\lambda_{solid}+\lambda_{radiative}$= 11.5 $mW.m^{-1}.K^{-1}$, which means that only the contribution of the gas phase can explain the difference in effective thermal conductivity between aeropectin and aerocellulose. Nanostructuration of the material is thus an extremely important factor.

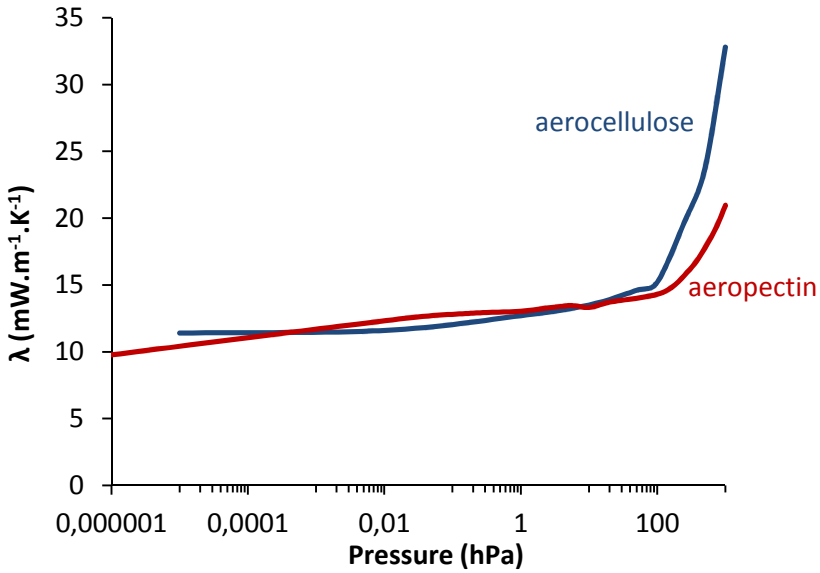

Figure VI. 25 : Variation of thermal conductivity as a function of pressure for a 4_{wt}% citrus aeropectin and a 5_{wt}% aerocellulose.

Table VI. 8 summarises all the thermal data obtained for 4_{wt}% aeropectin. The experiment carried out at low pressure (10^{-6} hPa) and low temperature (-118°C) gives the conductivity of the solid backbone λ_{solid} = 2.8 $mW.m^{-1}.K^{-1}$. λ_{solid} can also be calculated by the subtraction from $\lambda_{effective}$ the $\lambda_{solid}+\lambda_{radiative}$ obtained previously (by $\lambda=f(P)$) with the $\lambda_{radiative}$ determined by $\lambda=f(T^3)$. The obtained λ_{solid} = 2.6 $mW.m^{-1}.K^{-1}$ is in excellent agreement with the direct measurement of the conductivity of the solid backbone.

Table VI. 8 : Different thermal contributions of 4_{wt}% citrus aeropectin. All conductivities are given in $mW.m^{-1}.K^{-1}$.

C_{pectin}	ρ_{bulk} (g/cm^3)	$\lambda_{effective}$ Fox 150	$\lambda_{gaz+solide}$ Fox 150	$\lambda_{radiative}$ Fox 150	$\lambda_{solid}+\lambda_{radiative}$ $\lambda=f(P)$ by CSTB	λ_{solid} $\lambda=f(T)$ by CSTB	λ_{solid} from $(\lambda_s+\lambda_{rad})$ - λ_{rad}	λ_{gas}
4 %	0.115	24.4	17	7.4	10	2.8	2.6	14.2

Schematically, Figure VI. 26 represents the proportion of each thermal contribution in the effective thermal conductivity for aeropectin. The gas conduction counts for more than the half of the total heat transfer.

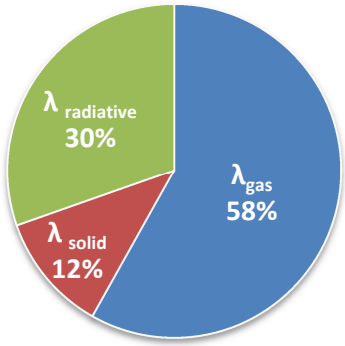

Figure VI. 26 : Distribution of solid and gas conduction and radiative heat transfer in the effective thermal conductivity.

3.3 Thermal conductivity of apple aeropectins

Thermal properties of apple aeropectins were also evaluated. The effective thermal conductivity was measured on heat flow meter Fox150 for 2% and 3_{wt}% apple aeropectin and on heat flow meter Fox 200 adapted to small samples (by CSTB) on the 3_{wt}% aerogel. The results are close to those of citrus aeropectin with $\lambda_{effective}$ = 20.3 and 21.8 mW.m^{-1}.K^{-1} for 2% and 3_{wt}%, respectively (Table VI. 9). Here again the values obtained with flow meter Fox 150 are higher than the conductivity measured with the adapted heat flow meter by CSTB (16 mW.m^{-1}.K^{-1}). The contribution of the gas phase and the solid backbone was also determined by Fox 150. It is slightly lower than for citrus aeropectin, 14 against 16 mW.m^{-1}.K^{-1}. The radiative part seems to be, on the contrary, slightly higher. However, because of the limited amount of data available it is difficult to draw any conclusions. Apple and citrus aeropectins have very similar thermal properties.

Table VI. 9 : Thermal properties of apple aeropectins. All conductivities are given in mW.m^{-1}.K^{-1}.

C_{pectin}	ρ_{bulk} (g/cm^3)	$\lambda_{effective}$ Fox150	$\lambda_{effective}$ Fox 200 CSTB	$\lambda_{gas+solid}$ Fox150	$\%\lambda_{radiative}$ Fox150
2 % apple aeropectin	0.05	20.3	-	13.3	34.5 %
3 % apple aeropectin	0.08	21.8	16	14.3	34.4 %
3% citrus aeropectin	0.09	23.6	-	16.3	31%

Aeropectin is thus the first fully biomass-based, not chemically cross-linked and environmentally friendly polysaccharide material having thermal super-insulating properties and being mechanically robust.

4. Silica-pectin hybrids

Silica aerogel is one of the best insulating materials (λ~ 14 $mW.m^{-1}.K^{-1}$) but it is very fragile and dusts easily. Aeropectin has interesting mechanical properties and a thermal conductivity around 20- 25 $mW.m^{-1}.K^{-1}$. We saw previously that the main contribution to conductivity is due to gaseous phase (Figure VI. 26). Replacing the gaseous phase by a phase which is more insulating that the air, such as silica aerogels, might allow decreasing the effective conductivity of aeropectins.
Thus we studied the preparation of hybrids made of a pectin matrix "filled" with silica aerogel. The goal is double: on one hand to decrease of the thermal conductivity of aeropectin and on the other hand to reinforce silica aerogel with a pectin matrix to avoid dusting. Below the structural and thermal properties of pectin-silica aerogel hybrids are presented.

4.1 Preparation of pectin-silica hybrids

As pectin aerogels have better mechanical properties than silica aerogels, we chose to use aeropectin as a matrix and then to fill the pectin porous structure with silica aerogel.

4.1.1 Approach of impregnation

Two different approaches can be used for preparing hybrid pectin-silica aerogel:

- Mixing pectin solution and silica precursors in the liquid state: the addition of silica precursors to a pectin solution resulting of the simultaneous formation of pectin gel and the condensation of silica ("one pot");

- Impregnation of silica precursors into the pectin gel or into coagulated pectin: diffusion of silica precursors solution into the porous pectin network and an *in-situ* condensation of silica.

The first approach needs a common solvent for mixing silica precursors and pectin.
Pectin is soluble in water at pH below 4 and almost insoluble in alcohols. A silicate aqueous solution will be preferred as a silica source. Formation of homogeneous gels is not always straightforward and strongly depends on the ratio silica-pectin (Agoudjil et al., 2012). This way needs some work in adjusting gelation and formation of interpenetrating network.

We preferred the second approach.
Silica precursor solution at 20_{wt}% in ethanol, referred as P75E20, was kindly provided by PCAS, France. These precursors were prepared by hydrolysis of tetraethoxysilane (TEOS) with a substoichiometric amount of water and under acidic conditions using hydrochloric acid as catalyst. The ratio between the number of moles of water added and the number of moles of TEOS, is called "degree of hydrolysis", and equals 75%.

The preparation of hybrid pectin-silica aerogel is summarised in Figure VI. 27. Citrus pectin gels were coagulated in water-ethanol mixtures and washed in ethanol. Silica precursors were added to coagulated pectin swollen in ethanol (alcogel). It was let diffusing into the pectin for 1 to 48

hours. For facilitating the diffusion of silica, low pectin concentrations were preferred since we showed that they have a larger pore size distribution with larger pores (Figure VI. 14). 2, 3 and 4_{wt}% pectin gels were used. The impregnated sample is then placed in a fresh ethanol bath and ammonia solution (catalyst for silica gelation) is directly added, to avoid a retro-diffusion of silica precursor towards ethanol bath. The catalyst diffuses inside the impregnated pectin where silica can condensate inside the pectin porous structure. After several washing in ethanol, the gel is dried by supercritical CO_2 to give a hybrid pectin-silica aerogel.

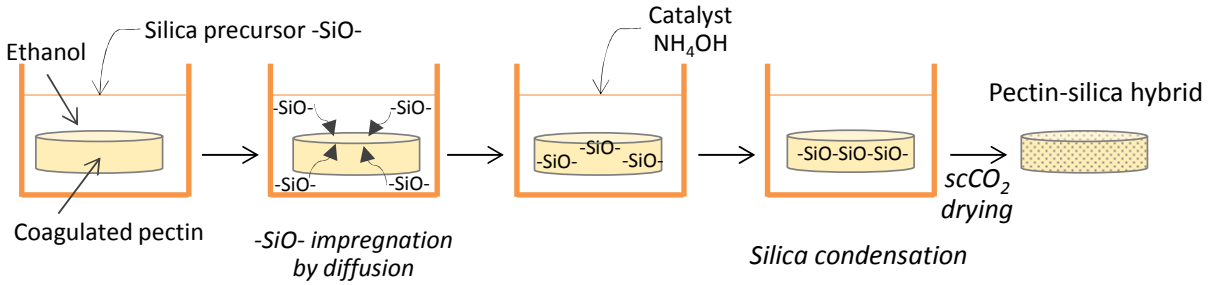

Figure VI. 27 : Preparation of hybrid pectin-silica aerogel.

4.1.2 Experimental conditions for impregnation

To optimise the impregnation, we chose to be in a large excess of silica precursors. A constant mass ratio between silica and pectin was chosen and kept for all hybrid formulations (Equation (VI. 4)). It was fixed at 7.2.

$$Si/P = \frac{mass\ of\ silica\ precursor}{mass\ of\ pectin} = 7.2 \qquad \text{(VI. 4)}$$

P75E20 from PCAS is a silica precursor solution at 20_{wt}% of "SiO_2" in ethanol. The catalyst is a solution of ammonia NH_4OH at 25_{wt}%., we used a standard formulation of silica aerogel, as used in Persée Mines-ParisTech laboratory. Two parameters, the ratio of water to silica *Hyd* (Equation (VI. 5)) and the ratio of catalyst to silica *Cat* (Equation (VI. 6)), were fixed at 4.2 and 0.11 respectively.

$$Hyd = \frac{Nmol\ of\ water}{Nmol\ of\ silica\ SiO_2} \qquad \text{(VI. 5)}$$

$$Cat = \frac{Nmol\ of\ NH_4OH}{Nmol\ of\ silica\ SiO_2} \qquad \text{(VI. 6)}$$

An example of formulation used for the impregnation of pectin alcogel (or coagulated pectin "filled" with ethanol) by silica precursors is given in Table VI. 10.

Table VI. 10 : Formulation of silica aerogel for impregnation of coagulated pectin.

$\%C_{pectin}$	m_{pectin}	Si/C	m_{P75E25}	$m_{ethanol}$	m_{NH4OH} ($25_{wt}\%$)	m_{H2O}	*Cat*	*Hyd*
3%	0.2	7.2	7.2	10.8	0.38	1.52	0.11	4.2

4.2 Study of silica impregnation of pectin alcogel

The important step for preparing pectin-silica hybrid is the impregnation of the pectin alcogel by the precursor solution. It is governed by diffusion. Below we shall estimate silica diffusion coefficients and correlate sample thickness and time needed to completely impregnate pectin with silica sol.

4.2.1 Theoretical calculation of the diffusion time

First, we need to have an estimation of the time necessary for silica precursor molecules (-SiO-) to impregnate the pectin alcogel, from the surface to the heart of the sample. We calculated the diffusion coefficient of –SiO- into a $3_{wt}\%$ pectin network using the results obtained for NaOH diffusing out of cellulose-NaOH-water gel during cellulose coagulation in water, swollen in water sample as described in (Gavillon & Budtova, 2007).
A diffusion coefficient D is given by the Stokes-Einstein formula that relates D and the hydrodynamic size R of the solute (here SiO) (Equation (VI. 7)).

$$D = \frac{k_B T}{6\pi\eta R} \qquad \text{(VI. 7)}$$

Where k_B is the Boltzmann constant, T is temperature and η the viscosity of the medium at temperature T. This equation is developed to describe the motion of a solid sphere in a dilute suspension. In our case, silica precursors are about $8_{wt}\%$ in ethanol and can be considered to be in a dilute state.

The size of silica precursor in the sample (colloidal suspension) P75E20 was determined, in the frame of another project, by the Institut Charles Sadron (Strasbourg, France). 95% of molecules are of 1 nm and less than 5% are larger with a size of 1500 nm, which can be easily removed by filtration of the P75E20 solution. We then estimated R_{SiO} = 1 nm.

In the absence of pectin alcogel, the diffusion coefficient is estimated to be $D_{(Cpectin=0)} = 1.8.10^{-10}$ m²/s at 25°C with $\eta_{ethanol}$= 1.20 10^{-3} Pa.s. As a comparison, NaOH in water diffuses with D= $1.5.10^{-9}$ m²/s (Gavillon & Budtova, 2007). The presence of pectin porous structure will slow down the diffusion of silica precursor. The question here is to estimate how much it will be slowed down without performing experiments.

NaOH diffusion coefficient were measured during cellulose coagulation in water from cellulose-NaOH-water gels of different cellulose concentrations (Gavillon & Budtova, 2007); the main results are given in Table VI. 11.

Table VI. 11 : Diffusion coefficient of NaOH during cellulose coagulation in water at 25°C.

$C_{cellulose}$ ($_{wt}$%)	D_{NaOH} ($\times 10^{-10}$ m²/s)
0	15.1
3	2.09
5	1.42

The cellulose matrix has a great influence on NaOH diffusion coefficient; it is divided by a factor from 7 to 10. Similar decrease of the diffusion coefficient of other molecules (ionic liquid) during coagulation of cellulose in water from cellulose-ionic-liquid solutions were studied in (Sescousse et al., 2011) and presented in Figure VI. 28.

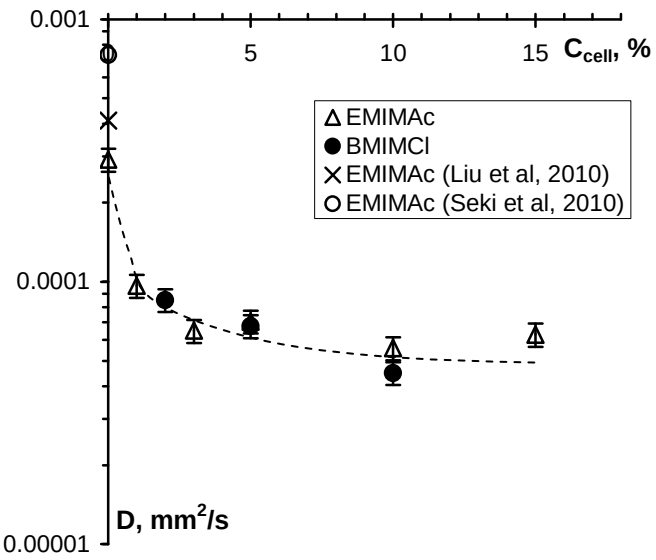

Figure VI. 28 : Diffusion coefficient of EMIMAc and BMIMCl during coagulation of cellulose in water from cellulose-EMIMAc and cellulose-BMIMCl solutions at 22°C as a function of cellulose concentration (Sescousse et al., 2011).

By analogy, we divided the diffusion coefficient of silica precursors at zero pectin concentration by a factor 7 for 3% and 10 for 4$_{wt}$% pectin gels (Table VI. 12).

Table VI. 12 : Distance made by small molecules to diffuse in a 3% or 4% pectin swollen in ethanol.

D_{SiO} ($\times 10^{-10}$ m²/s)	t (h)	1	6	10	24	48
0.25	$L_{3\%}$ (mm)	0.31	0.75	0.97	1.50	2.12
0.18	$L_{4\%}$ (mm)	0.26	0.63	0.81	1.25	1.77

The distance L made by a small molecule diffusing in a medium due to Brownian motion is given by Equation (VI. 8).

$$L = \sqrt{D_{SiO} \times t} \qquad \text{(VI. 8)}$$

where t is the time.
Using this approach, the distances made by silica precursor in pectin alcogels were calculated Table VI. 12. For example, in 24 hours, silica can diffuse 1.5 mm at 25°C.

For further studies, we prepared pectin alcogels with a thickness of 2.5 to 4 mm. The sample was was placed in silica sol in such a way that it allowed diffusion from both sides (Figure VI. 29). We estimated that in 24 to 48 h the impregnation should be complete.

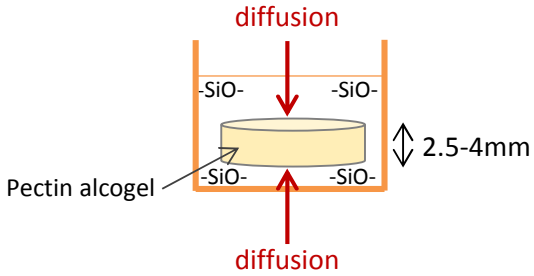

Figure VI. 29 : Schematic representation of pectin alcogel impregnation by silica precursors. Pectin gels are 2.5 to 4 mm thick and slightly "raised" to have diffusion from both sides.

4.2.2 Silica impregnation followed by EDS-SEM analysis

After the impregnation, pectin-silica samples were dried with sc CO_2. Dried hybrid pectin-silica aerogels were studied by SEM with EDS analysis (c.f. Chapter II).
The energy of the X-rays is characteristic of the atomic structure of the element from which they were emitted. The elemental composition of the sample may therefore be determined. An example of X-ray spectrum obtained by EDS is given in Figure VI. 30. The peaks correspond to carbon (K_α 0.5249 keV), oxygen (K_α 0.2774 keV) and silicon ($K_{\alpha\,1,2}$ 1.7398 keV). The number of X-ray detected (peak height) gives the quantity of silicon in the sample.

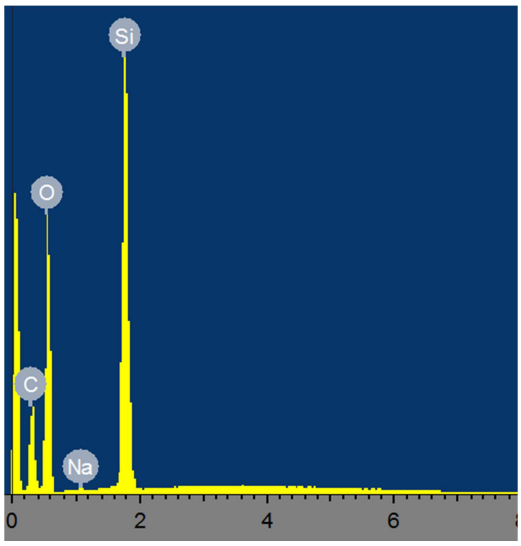

Figure VI. 30 : X-ray spectrum of a 3_{wt}% pectin-silica hybrid analysed by EDS.

We can therefore follow the depth of impregnated silica into the pectin structure by studying the cross-section of the hybrid. In various points of the section, EDS analysis was carried out in various points of sample cross-section and the "scan" of the elemental composition along sample cross-section, from one surface to the opposite one, was obtained. The atomic percentage of silicon was then plotted as a function of sample thickness (Figure VI. 31).

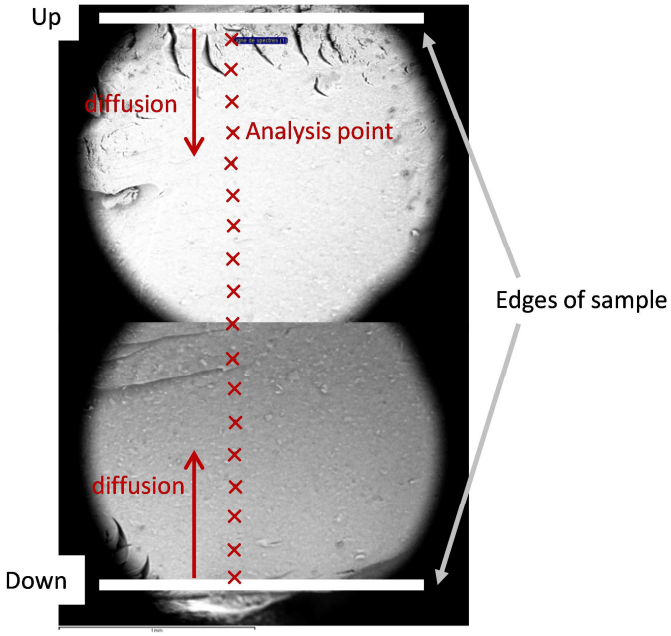

Figure VI. 31 : SEM images for EDS analysis. Scanning of the cross-section of hybrid.

Hybrids were prepared from 3_{wt}% pectin alcogels with various time of impregnation, from 1 to 24 h. The distance of analysis *d* is normalised to the sample thickness. The middle of the sample has *d*=0.5. Figure VI. 32 displays $\%_{atomic}$ of silicon as a function of the distance from sample surface for different times of impregnation. Points are sometimes scattered due to high experimental errors, but some trends can be observed. For short times, such as 1 or 2 hours,

silicon is somewhat present everywhere in the sample but it distribution is not homogeneous. We can observe a minimum of %Si in the middle of the sample, showing a progression of the silica diffusion. After 8 hours, a steady state is established where silicon well distributed in the matrix (%Si ≈ 22%), with a slight decrease for *d* around 0.5. No major difference is observed for longer time of impregnation. It seems that there is saturation in the quantity of silica that can be impregnated into the pectin matrix.

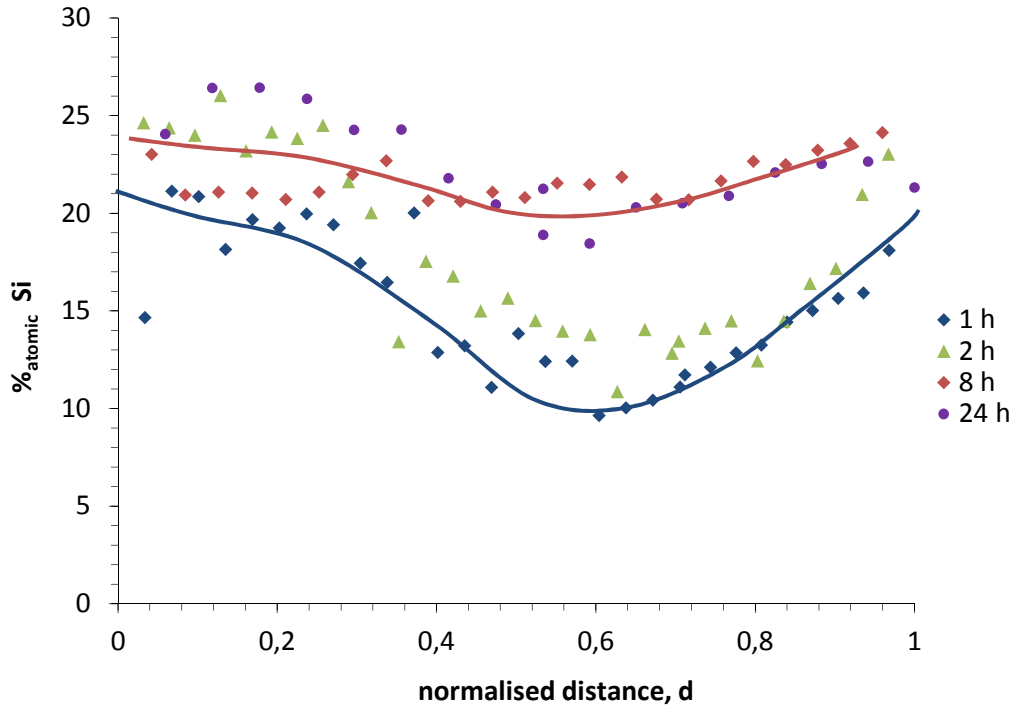

Figure VI. 32 : Silica impregnation of 3_{wt}% pectin versus the normalised distance in the sample.

We repeated these experiments with a more concentrated pectin matrix of 4_{wt}% (Figure VI. 33). Diffusion should be slower as predicted in Table VI. 12. After 24 hours, the impregnation is not homogeneous. An important decrease is observed in the middle of the sample (slightly shifted towards 0.4) with less than 5% of silicon. A longer diffusion time 48 h was investigated. Data are scattered. Similar behaviour as 24 h is observed: silicon does not penetrate effectively into the heart of the sample. 4% pectin matrix is probably too dense and tortuous with smaller pores, which slow down the diffusion inside the structure.

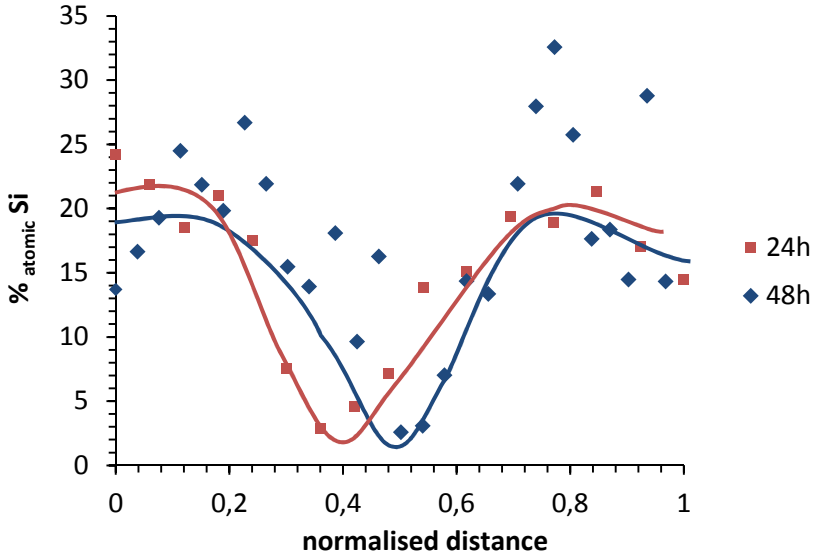

Figure VI. 33 : Silica impregnation of 4_{wt}% pectin versus the normalised distance in the sample for 24 and 48 hours of impregnation.

A homogeneous impregnation of a 3_{wt}% pectin matrix by silica precursors was successfully realised and the dried hybrid pectin-silica aerogel associated was prepared.

4.3 Morphology of dried hybrids

4.3.1 Effect of the time of impregnation

We measured bulk densities and specific surfaces of hybrid pectin-silica aerogel and observed their morphology by SEM.

First, we studied the influence of the duration of impregnation on the structural properties of hybrids. Table VI. 13 summarises data on hybrids prepared from 3_{wt}% pectin alcogels. Data are sometimes scattered and unfortunately we did not have time to reproduce all samples to confirm values.

Table VI. 13 : Structural data on 3_{wt}% pectin-silica aerogel with various times of impregnation.

C_{pectin} ($_{wt}$%)	formulation	time of impregnation (h)	ρ_{bulk} (g/cm^3)	S_{BET} (m²/g)	% Impregnation
3	pure aeropectin	0	0.088	268	-
3	pectin-SiO_2	1	0.107	-	56
3	pectin-SiO_2	2	0.105	567	55
3	pectin-SiO_2	4	0.132	665	69
3	pectin-SiO_2	8	0.136	-	71
3	pectin-SiO_2	10	0.146	700	76
3	pectin-SiO_2	18	0.148	-	77
3	pectin-SiO_2	24	0.134	655	70

Densities were plotted as a function of the impregnation time in Figure VI. 34. They increase until 10 h where they reach a sort of plateau. This means that the quantity of silica possibly introduced into pectin porous structure is saturated even at longer times of impregnation, confirming previous observations by EDS analysis.

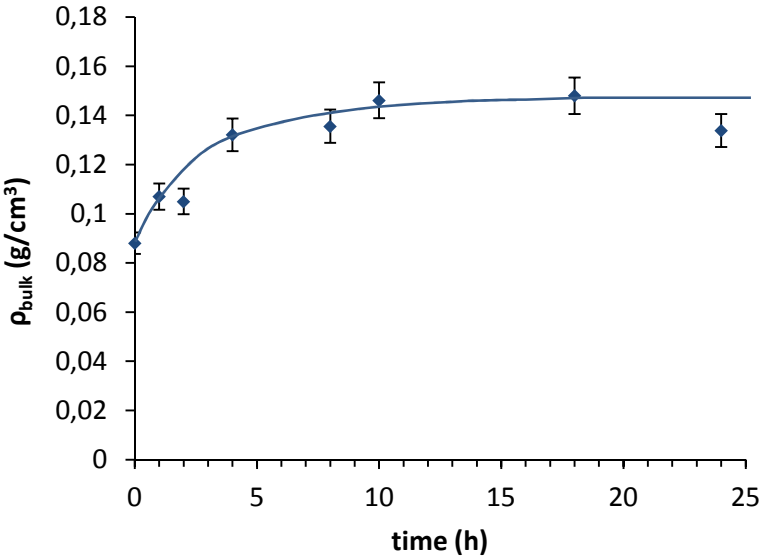

Figure VI. 34 : Bulk density of 3$_{wt}$% hybrid pectin-silica aerogel as a function of time of impregnation.

We compared the amount of silica present in the pectin matrix in the dried state with the theoretical maximum quantity of silica that can be impregnated into pectin.
To do so, we adopted a simplified approach: the volume available for impregnation of silica is the porous volume V_{pores} of aeropectin and silica aerogel impregnated has similar structural properties (bulk and skeletal densities) than non-impregnated silica aerogel.
The porous volume V_{pores} of aeropectin is calculated from the porosity (Equation (VI. 9)).

$$\varepsilon(\%) = \frac{V_{pores}}{V_{total}} = 1 - \frac{\rho_{bulk}}{\rho_{skeletal}} \qquad \text{(VI. 9)}$$

The silica aerogel, obtained by the formulation described in Table VI. 10, was characterized by Noémie Diascorn from the center Persée Mines ParisTech. Its bulk density equals 0.11 g/cm^3 and its skeletal density is known to be around 2.0 g/cm^3 (Phalippou & Kocon, 2008).
The maximum silica mass that can be impregnated into the pectin matrix is given by Equation (VI. 10)

$$m_{silica\ impregnated} = \rho_{silica} \times V_{pores\ \ pectin} \qquad \text{(VI. 10)}$$

We can then evaluate the theoretical density of pectin-silica aerogel according to Equation (VI. 11).

$$\rho_{theoretical} = \frac{m_{silica}}{V_{total}} + \frac{m_{pectin}}{V_{total}} = \frac{\rho_{silica} \times V_{pores\ pectin}}{V_{total}} + \rho_{pectin}$$
$$\rho_{theoretical} = \rho_{silica} \times \varepsilon\ (\%)_{pectin} + \rho_{pectin} \quad \text{(VI. 11)}$$

We define therefore the impregnation yield by the ratio of pectin-silica hybrid bulk density to the theoretical one (Equation (VI. 12)).

$$\%\ Impregnation = \frac{\rho_{hybrid}}{\rho_{theoretical}} \times 100 \quad \text{(VI. 12)}$$

The impregnation yield for different times of impregnation is reported in Table VI. 13. After 1 hour, 56% of silica has already been impregnated. After 10 hours a maximum of filling is reached with a yield of 76%.

Morphology of hybrids was then observed by SEM and is presented in Figure VI. 35 for 1, 4, 8 and 24 h of impregnation, and pure silica aerogel. For 1 h (Figure VI. 35a) the morphology is very similar to pure aeropectin. After 4 h the morphology starts to change, it looks denser but the fibrillar stands are still visible (Figure VI. 35b). At 24 h of impregnation (Figure VI. 35c) the structure is quite different from pure aeropectin. It presents much smaller pores and looks more like a morphology of pure silica aerogel presented in Figure VI. 35d. The nanostructuration visible in the 24 h hybrid shows that silica forms a homogeneous aerogel *in situ* of pectin matrix. It is not possible to distinguish the pectin phase from that of silica aerogel. At this scale, hybrids appear homogeneous.

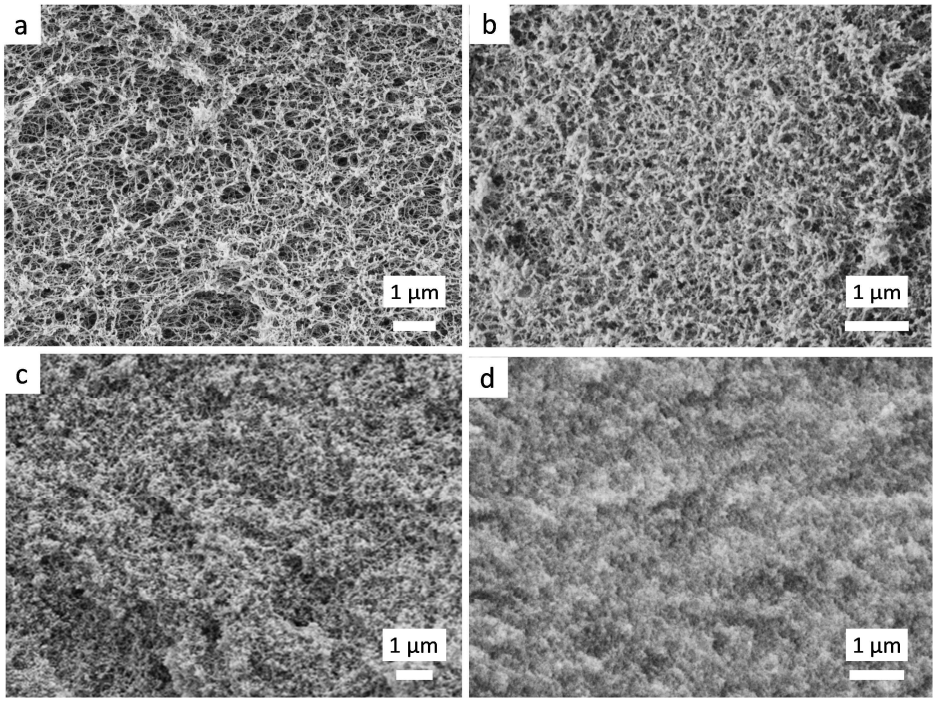

Figure VI. 35 : SEM images of 3_{wt}% pectin-silica hybrids after 1h (a), 8h (b), 24h (c) of impregnation and silica aerogel (d).

We studied the specific surface of hybrids to confirm the presence of nano-structured silica (as it is in aerogel) in the pectin matrix. Specific surface areas of silica aerogels are usually between 600 and 1000 m²/g (Soleimani Dorcheh & Abbasi, 2008). For the silica formulation described in Table VI. 10, the specific surface area was determined by Noémie Diascorn in the Center Persée Mines ParisTech, and S_{BET} = 850-900 m²/g. Table VI. 13 and Figure VI. 36 show an important increase of specific surfaces areas of hybrids as a function of duration of impregnation. Pure 3_{wt}% aeropectin has S_{BET} = 268 m²/g. After 10 hours of impregnation the specific surface saturates around 700 m²/g. Specific surfaces stand between one of pure aeropectin and of pure silica aerogel. This confirms the presence of silica in the form of nanostructured aerogel in the aeropectin matrix.

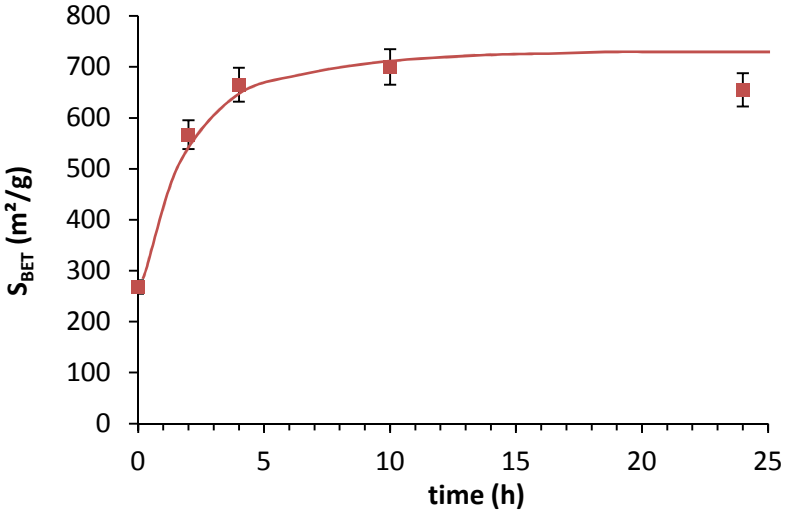

Figure VI. 36 : Specific surface of 3_{wt}% pectin-silica hybrid as a function of impregnation time.

4.3.2 Influence of the pectin matrix and the formulation of silica aerogels

In a second step, we studied the influence of the concentration of the pectin matrix on the impregnation of silica precursors. We compared three different concentrations 2, 3 and 4_{wt}% citrus pectin in Table VI. 14. We also slightly changed the formulation of silica precursor: in the frame of another project, it was shown that the silica aerogel morphology and thermal properties can be optimised by changing the ratio of water and catalyst. The optimised formulation was defined with *Hyd* = 0.88 and *Cat* = 0.059. We called therefore the previous formulation as "standard" and the new one as "optimised". The bulk density of optimised silica aerogel was determined at 0.15 g/cm^3.

Table VI. 14 : Influence of the concentration of citrus pectin matrix on the structural properties of hybrid aerogels for standard and optimized formulations and comparison to pure aeropectins.

Type of pectin	C_{pectin} ($_{wt}$%)	Formulation of silica aerogel	ρ_{bulk} (g/cm^3)	% Impregnation
Citrus	2	pure	0.052	-
Citrus	2	standard	0.118	75
Citrus	2	optimised	0.181	92
Citrus	3	pure	0.088	-
Citrus	3	standard	0.148	77
Citrus	3	optimised	0.214	93
Citrus	4	pure	0.114	-
Citrus	4	standard	0.155	71

We compared bulk densities of hybrids as a function of citrus pectin concentration for the two different formulations of silica aerogels (Figure VI. 37). For both formulations, ρ_{bulk} increases

linearly with concentration. The optimised formulation gives higher bulk density than the standard one.

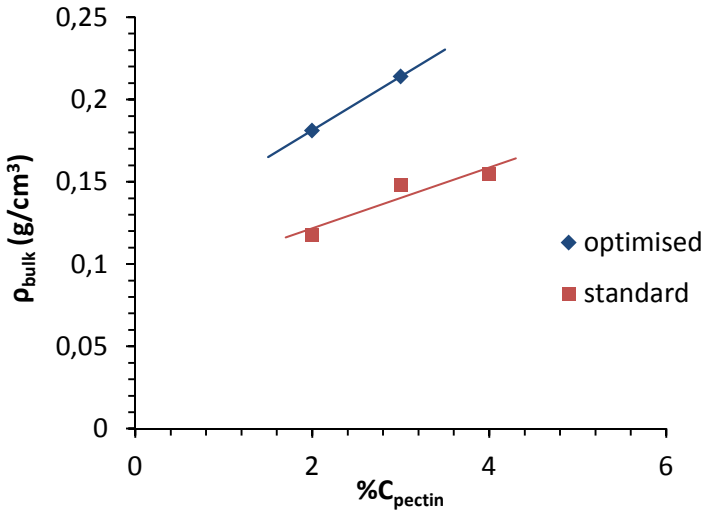

Figure VI. 37 : Bulk density of hybrids as a function of citrus pectin for standard and optimised formulations.

We evaluated the impregnation yields according to Equation (VI. 12) and (Table VI. 14). They are plotted as a function of pectin initial concentration in Figure VI. 38. For the standard formulation of silica aerogel, impregnation yield stands around 75% for the studied pectin concentrations whereas for the optimized formulation the impregnation yield is much higher, above 90%.

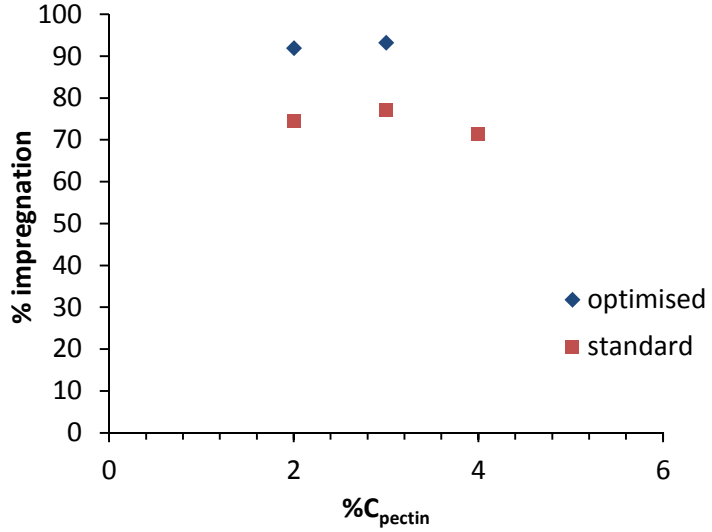

Figure VI. 38 : Impregnation yield as a function of citrus pectin for standard and optimised formulations.

We also investigated the influence of the pectin source on the bulk density and the impregnation ratio of hybrids. We compared citrus and apple pectin matrices for the standard formulation of silica aerogel (Table VI. 15). They give similar bulk density (~ 0.14 g/cm^3) and impregnation

yield (77%). The source of pectin seems not to have an impact on the structural properties of hybrid pectin-silica aerogels.

Table VI. 15 : Influence of the pectin source on the structural properties of hybrid aerogels for standard formulation.

Type of pectin	C_{pectin} ($_{wt}$%)	Formulation of silica aerogel	ρ_{bulk} (g/cm^3)	%Impregnation
Citrus	3	standard	0.148	77
Apple	3	standard	0.141	77

The silica impregnation of pectin network by diffusion is an efficient technique to elaborate pectin-silica hybrid aerogels with interesting structural properties.

4.4 Thermal properties of hybrids

Finally, we tested the different formulations of hybrid pectin-silica aerogels for their thermal properties. We measured their effective as well as their gas and solid conduction thermal conductivities by the heat flowmeter Fox 150 in Persée Mines-ParisTech. We deduced therefore the radiative contribution. We compared $\lambda_{effective}$ measured on the adapted Fox 200 in CSTB (c.f. Chapter II) for two formulations of hybrids. Data are summarised in Table VI. 16.

Table VI. 16 : Thermal properties of hybrid pectin-silica aerogels.

C_{pectin} ($_{wt}$%)	Type of pectin	Formulation of silica aerogels	$\lambda_{effective}$ Fox 150	$\lambda_{effective}$ Fox 200-CSTB	$\lambda_{gas+solid}$ Fox 150	$\%\lambda_{radiative}$
2	apple	pure	20	-	13	34.5 %
2	apple	standard	17	-	13	27 %
3	apple	pure	22	-	14	34 %
3	apple	standard	20	15	14	32 %
3	citrus	pure	24	-	16	31 %
3	citrus	standard	23	20	17	27 %
3	citrus	optimised	20	-	15	25 %

We showed previously that 2$_{wt}$% pectin matrix allows the maximum of silica impregnation. Unfortunately, due to a lack of time only the standard formulation was investigated. The effective thermal conductivity of hybrid 2$_{wt}$% apple pectin-silica aerogel equals λ_{eff} = 17 mW.m^{-1}.K^{-1} and pure 2$_{wt}$% apple aeropectin has λ_{eff} = 20 mW.m^{-1}.K^{-1}. The incorporation of silica aerogel into the pectin matrix improved thermal properties.

We also compared the contribution of the gas and solid phases for pure aeropectin and pectin-silica hybrids. For both samples, $\lambda_{gas+solid}$ ~ 13 mW.m^{-1}.K^{-1}. The incorporation of silica aerogel has decreased pores sizes in the porous structure which has probably decreased the contribution of the gaseous conduction. However, as the density increases with the impregnation of silica aerogel, the solid contribution is more important for hybrid than for aeropectin. The overall

$\lambda_{gas+solid}$ appears to remain almost constant. Unfortunately, it was not possible to measure directly $\lambda_{gas+solid}$ to confirm this hypothesis.
The radiative contribution of 2_{wt}% hybrid is lower (27%) compared to pure aeropectin (34.5%) which can explain the decrease of the effective thermal conductivity (Table VI. 16).

We also studied the influence of the source of pectin and type of silica aerogel formulation on the conductivity of the 3_{wt}% hybrids.
First we compared 3_{wt}% citrus pectin and 3_{wt}% apple pectin matrices for a standard hybrid formulation (Table VI. 16) with pure aeropectins. For 3_{wt}% hybrid apple pectin-silica, the effective thermal conductivity was first measured by Fox 150 which gave λ_{eff} = 20 $mW.m^{-1}.K^{-1}$. It is slightly lower than pure apple aeropectin (22 $mW.m^{-1}.K^{-1}$). When measured by the Fox 200 in CSTB, the effective thermal conductivity is much lower with λ_{eff} = 15 $mW.m^{-1}.K^{-1}$. The overestimation of the Fox 150 in λ_{eff} was already reported for pure aeropectins.
Similarly, 3_{wt}% hybrid citrus pectin-silica with the standard formulation gives λ_{eff} = 23 $mW.m^{-1}.K^{-1}$ by Fox 150 and 20 $mW.m^{-1}.K^{-1}$ by Fox 200-CSTB. It is also lower than pure citrus aeropectin.
For 3_{wt}% citrus pectin matrix, we studied the influence of the silica aerogel formulation. We showed previously than the optimised formulation allows higher silica impregnation ratio. Here the effective thermal conductivity is lower as compared to standard formulation: λ_{eff} = 20 $mW.m^{-1}.K^{-1}$ by Fox 150 vs 23 $mW.m^{-1}.K^{-1}$, respectively.

We measured also the contribution of gas and solid conduction for all 3_{wt}% hybrids. There is no major difference in $\lambda_{gas+solid}$ between pure aeropectins and hybrid pectin-silica aerogels (Table VI. 16). The decrease of the effective thermal conductivity is related to the decrease of the radiative contribution as it was explained for 2_{wt}% hybrids.

The incorporation of silica aerogel into the pectin matrix improved thermal properties of aeropectins. It allows gaining 4-5 $mW.m^{-1}.K^{-1}$ of the effective thermal conductivity.

Conclusions

In this chapter, two types of aerogel-like materials were prepared: aeropectins from apple and citrus pectin and pectin-silica hybrids. Their microstructural, mechanical and thermal properties were investigated and compared.

First, we studied the influence of the acidity of solvent on the structure of pectin gels. We showed that pH has to be lower than 1 to avoid inhomogeneities. The solvent 0.5 mol/L HCl was chosen.

We demonstrated that aeropectin is highly porous (> 90%) and very lightweight. Its bulk density increases linearly with pectin concentration. No significant influence of the pectin source (citrus peel or apple pomace) on bulk densities and texture is observed. SEM observations showed fibrillar structure with long and entangled strands. Specific surface areas are around 250 m^2/g, similarly to non-crosslinked aerocellulose. The pore size distribution done by Hg porosimetry (using Pirard approach) was narrower and shifted to smaller pores at higher pectin concentrations. A 3_{wt}% aeropectin presents a mean pore size of about 43 nm and a width distribution of 46 nm and a 5_{wt}% aeropectin has a similar mean pore size but its pores distribution is narrowed to 29 nm. We compared aeropectin to aerocellulose and showed that both aerogels present many similarities in their morphology.

Mechanical properties of aeropectins were evaluated by uniaxial compression. Young modulus and yield stress followed power law dependence with bulk density, $E \sim \rho^{1.8}$ and $\sigma_{yield} \sim \rho^{3.2}$. At constant density, aeropectin is stiffer than pure aerocellulose (higher Young modulus and yield stress). It may be explained by the difference in spatial configuration of macromolecules between cellulose and pectin.

The thermal properties of aeropectins were also characterised. Apple and citrus-based aeropectins present very similar thermal properties. Effective thermal conductivities decrease with bulk density and the classical increase of $\lambda_{effective}$ at low densities was not recorded for aeropectins. The best thermal conductivity was obtained for 2_{wt}% aeropectin with $\lambda_{effective}$ = 20 $mW.m^{-1}.K^{-1}$. We showed that the contribution of the gaseous phase represents 60% of the total thermal conductivity. The conduction of the solid part of aeropectin in the thermal conductivity was obtained: λ_{solid} = 2.8 $mW.m^{-1}.K^{-1}$. **Aeropectin is thus the first fully biomass-based**, not chemically cross-linked and environmentally friendly polysaccharide material **having thermal super-insulating properties and being mechanically robust**.

We prepared hybrid pectin-silica aerogels in order to further decrease thermal conductivity of aeropectins with the idea of making silica aerogels in the pores of aeropectin. To reach this goal, silica precursor was let diffusing into wet coagulated pectin porous network. The condensation of silica was directly done inside the pectin structure.
In a first part, we studied the influence of the impregnation time and the concentration of the pectin network by EDS analysis. We showed that there was a saturation in the quantity of silica that can be impregnated into the pectin matrix and 10 hours was sufficient to reach this steady

state. The increase of pectin concentration slowed down silica diffusion inside the matrix and 48 h were not enough to reach homogeneous silica distribution over 4_{wt}% pectin.
Bulk densities of hybrid pectin-silica aerogels and impregnation yields were determined for different pectin concentrations and silica aerogels formulations. Impregnation yields are around 75% for standard formulation and 90% for optimised formulation. Specific surface areas of pectin-silica hybrids were higher compared to pure aeropectin,700 m^2/g vs 250 m^2/g, which confirms the presence of nanostructured silica in the pectin network.

Finally, we investigated thermal properties of hybrid pectin-silica aerogels. The incorporation of silica aerogel into the pectin matrix decreased thermal conductivity of aeropectins: it allows gaining 4-5 $mW.m^{-1}.K^{-1}$. The best formulation gave a thermal conductivity of 17 $mW.m^{-1}.K^{-1}$.

Mechanical characterisations still need to be carried out. Qualitatively, we saw that the incorporation of silica aerogel had weakened the pectin matrix. Hybrids appeared more fragile than pure aeropectins. More quantitative data are then required to confirm these observations.

Bibliography

Agoudjil, N., Sicard, C., Jaouen, V., Garnier, C., Bonnin, E., Steunou, N., & Coradin, T. (2012). Design and properties of biopolymer–silica hybrid materials: The example of pectin-based biodegradable hydrogels. *Pure and Applied Chemistry*, *84*(12), 2521–2529.

Alaoui, A. H., Woignier, T., Scherer, G. W., & Phalippou, J. (2008). Comparison between flexural and uniaxial compression tests to measure the elastic modulus of silica aerogel. *Journal of Non-Crystalline Solids*, *354*(40-41), 4556–4561.

Bisson, A., Rigacci, A., Lecomte, D., & Achard, P. (2004). Effective thermal conductivity of divided silica xerogel beds. *Journal of Non-Crystalline Solids*, *350*, 379–384.

Gavillon, R. (2007). Préparation et caractérisation de matériaux cellulosiques ultra poreux., *PhD thesis*, Ecole des Mines de Paris.

Gavillon, R., & Budtova, T. (2007). Kinetics of cellulose regeneration from cellulose--NaOH--water gels and comparison with cellulose--N-methylmorpholine-N-oxide--water solutions. *Biomacromolecules*, *8*(2), 424–32.

Gavillon, R., & Budtova, T. (2008). Aerocellulose: new highly porous cellulose prepared from cellulose-NaOH aqueous solutions. *Biomacromolecules*, *9*(1), 269–77.

Lu, X., Caps, R., Fricke, J., Alviso, C. T., & Pekala, R. W. (1995). Correlation between structure and thermal conductivity of organic aerogels. *Journal of Non-Crystalline Solids*, *188*(3), 226–234.

Phalippou, J., & Kocon, L. (2008). Aerogels : Aspects fondamentaux, *Techniques de l'ingénieur*, 1–24.

Pirard, R., & Pirard, J.-P. (1997). Aerogel compression theoretical analysis. *Journal of Non-Crystalline Solids*, *212*(2-3), 262–267.

Sescousse, R. (2010). Nouveaux matériaux cellulosiques ultra-poreux et leurs carbones à partir de solvants verts., *PhD thesis*, Mines ParisTech.

Sescousse, R., Gavillon, R., & Budtova, T. (2011). Aerocellulose from cellulose–ionic liquid solutions: Preparation, properties and comparison with cellulose–NaOH and cellulose–NMMO routes. *Carbohydrate Polymers*, *83*(4), 1766–1774.

Soleimani Dorcheh, A., & Abbasi, M. H. (2008). Silica aerogel; synthesis, properties and characterization. *Journal of Materials Processing Technology*, *199*(1-3), 10–26.

White, R. J., Budarin, V. L., & Clark, J. H. (2010). Pectin-derived porous materials. *Chemistry (Weinheim an der Bergstrasse, Germany)*, *16*(4), 1326–35.

General Conclusions and Perspectives

General Conclusions

The goal of this thesis was to prepare and characterise new generations of aerogels based on polysaccharides, based on cellulose and pectin. They were prepared via dissolution-coagulation route followed by drying with supercritical CO_2. The main objective was to obtain nano-structured materials and to correlate their morphology to their mechanical and thermal properties.

Three "results" chapters were devoted to the preparation of various types of aerocelluloses and the understanding of their structure-properties relationships.
The elaboration of aerocellulose, cellulose aerogel-like material, was previously studied in different solvents such as NMMO, NaOH-water, and more recently in ionic liquids such as 1-ethyl-3-methylimidazolium acetate (EMIMAc). Aerocellulose is highly porous (density from 0.01 to 0.2 g/cm^3) with a high specific surface (from 200 to 300 m^2/g) but presents a wide range of pores from few tens nanometers to few microns. Our objective was to find new routes for improving aerocellulose morphology towards a nano-structuration and a more homogeneous pore size distribution.

The first route was to investigate the elaboration and the properties of aerocellulose prepared from a new solvent system, EMIMAc/dimethylsulfoxide (DMSO). The use of DMSO as a co-solvent of EMIMAc allowed decreasing solvent viscosity and formation of macropores (due to the formation of bubbles during coagulation). We compared structural and thermal properties of 5_{wt}% aerocelluloses prepared in different solvents: 8%NaOH-water, EMIMAc and 60_{wt}% EMIMAc / 40_{wt}% DMSO. However, the best thermal conductivity was obtained for 5_{wt}% cellulose in 8%NaOH-water, 0.031 W.m^{-1}.K^{-1}. Aerocelluloses, independently of the cellulose solvent, give thermal conductivity higher that of free air (0.025 W.m^{-1}.K^{-1}). It is mainly due the presence of pores with sizes above the free mean path of air (70 nm) and the lack of control in morphology during the coagulation.

The second route for aerocellulose nanostructuration was to chemically cross-link cellulose. Cross-linking was performed in the 8%NaOH-water by epichlorohydrin (ECH). The properties of gelling solutions were studied by dynamic rheology. The gelation time of cellulose solutions in the presence of ECH is strongly delayed as compared to physical gelation in 8%NaOH-water, with a maximum at relative cross-linker concentration $R_{rel} = 0.5$. The result obtained shows a competition between physical and chemical cross-linking and we suggested that the cross-linker is playing a role of a "spacer" preventing cellulose self-association. Higher swelling in water of coagulated cross-linked cellulose was obtained as compared to non-crosslinked cellulose (3500 % vs 1300 %, respectively). We interpreted this phenomenon by formation of "additional" pores due to cross-linker acting as a "spacer", as suggested above. The structure of coagulated cellulose with chemical cross-links was shown to be more homogeneous than of non-crosslinked cellulose.
Aerocelluloses were obtained via a solvent exchange step in methanol followed by drying with supercritical CO_2. Cross-linking of cellulose modify structural properties of aerocelluloses, even

at low cross-linker concentrations. A formulation 5_{wt}% cellulose-R_{rel} = 0.5 appears very interesting with a moderate density ρ_{bulk} = 0.18 g/cm^3, a high specific surface area S_{BET} = 418 m²/g and a narrower pore size distribution compared to non-crosslinked aerocellulose prepared from the same cellulose concentration. Cross-linked aerocelluloses are tougher (higher Young modulus and yield stress) than their non-crosslinked counterparts. The optimal formulations were obtained for R_{rel} = 0.5 which give effective thermal conductivities of 26.2 and 30.7 mW.m^{-1}.K^{-1} for 5 and 7_{wt}% cellulose, respectively. Cellulose cross-linking does indeed lead to aerocellulose nano-structuration which is reflected by the increase of specific surface area and decrease of thermal conductivity.

Another approach for having nanostructured porous materials was to create interpenetrated networks from cellulose mixed with another polymer. Cellulose acetate was chosen because it is known that when cross-linked, it makes highly nano-structured aerogel. Lignin was chosen since it accompanies cellulose in practically all natural fibres making a sort of interpenetrated network. EMIMAc was chosen as a common medium for mixing polymers. First, the rheological studies demonstrated that cellulose acetate/EMIMAc solutions behave as non-entangled (below 10_{wt}%) "ordinary" polymer solution. Cellulose acetate intrinsic viscosity decreases with temperature indicating the decrease of solvent thermodynamic quality. Similar phenomenon was reported in literature for cellulose acetate dissolved in other solvents and cellulose dissolved in EMIMAc. Mixtures of cellulose/cellulose acetate/EMIMAc were also studied by rheology. It was shown that the two polymers (cellulose and cellulose acetate) coexist in EMIMAc without interactions at the concentrations studied.
Hybrid materials were prepared by coagulation of mixtures followed by drying with supercritical CO_2. Various morphologies were obtained as a function of mixture composition. Cellulose and cellulose acetate can be processed together but a phase separation between these two polymers occurs during the coagulation process. Porosity decreases and inhomogeneities increase with cellulose acetate concentration. A similar study was performed for cellulose-lignin (lignosulfonate)-EMIMAc mixture. Lignin was washed out by water from cellulose during coagulation step. When coagulated in ethanol, lignin remained inside cellulose network but a phase separation between cellulose and lignin was visible.

The last chapter is devoted to the preparation and characterisation of new material, aeropectin.
Another type of polysaccharide, pectin, and the preparation of its aerogel "Aeropectin" were investigated. We demonstrated that aeropectin is highly porous (> 90%) and very lightweight. Its bulk density increases linearly with pectin concentration, from 0.05 to 0.17 g/cm^3 for 2_{wt}% and 6_{wt}% pectin concentrations, respectively. No significant influence of the pectin source (citrus peel or apple pomace) was obtained. We compared aeropectin to aerocellulose and showed that both aerogels present many similarities in their morphology but aeropectin has narrower pore size distribution. Aeropectin is slightly stiffer than non-crosslinked aerocellulose (higher Young modulus and yield stress). The best thermal conductivity was obtained for 2_{wt}% aeropectin with $\lambda_{effective}$ = 20 mW.m^{-1}.K^{-1}. Aeropectin is thus the first fully biomass-based, not chemically cross-linked material having thermal super-insulating properties and being mechanically robust.

Perspectives

Here we would like to propose some future work to pursue on polysaccharides-based aerogels. This could hopefully inspire the following research.

Cross-linked aerocellulose presents improved properties. However, the cross-linker used, epichlorohydrin, is rather toxic. Its use and recycling cannot be envisaged for an industrial process. The next step is to find another type of cellulose cross-linker, compatible with cellulose solvents and environmentally friendly.

In this thesis, only high methoxy pectins were used. We can foresee the preparation of aeropectin with low methoxy pectins. The gelation mechanism will be different as explained in Chapter I, as it will take place in an aqueous solution of divalent cations as calcium. The complexation of cations can give a more controlled and finer porous structure.

It was shown in Chapter I that “aeroalginate” has also promising structural properties. It will be interesting to study more deeply the morphology of alginate aerogels and to correlate with mechanical and thermal properties.
Other polysaccharides can be foreseen as carrageenan, chitin or chitosan.

Pectin-silica hybrids were shown to be very promising for thermal super-insulation. Similar studies may be carried out for cellulose-silica hybrid aerogels. The next step could also be polysaccharide hydrophobisation to decrease moisture adsorption. Two projects were recently started in these directions in Mines ParisTech.

We should also like to emphasise that “bio-aerogels” are bio-based, environmentally friendly and present a high potential not only for thermal insulation but also for a large range of other applications such controlled drug release and catalysis.

Aérogels à base de cellulose et de pectine - Vers leur nano-structuration

RESUME : Le but de ce travail de thèse est de développer des aérogels biosourcés, mécaniquement résistants et thermiquement très isolants (voire super-isolants). Les aérogels à base de cellulose, souvent appelés « aérocelluloses », sont connus pour être très poreux et extrêmement légers. Ils présentent en revanche une grande dispersion de tailles de pores, donnant de propriétés thermiques relativement modestes. Nous avons étudié plusieurs approches pour améliorer la morphologie des aérocelluloses: la modification du solvant, la réticulation chimique de la cellulose et la formation d'hybrides avec d'autres polymères. La réticulation de la cellulose a réellement permis d'affiner la structure poreuse de l'aérocellulose vers une nano-structuration ce qui a amélioré la conductivité thermique, s'approchant du domaine de la super-isolation (0.026 $W.m^{-1}.K^{-1}$). Un autre polysaccharide, la pectine, a été utilisé pour préparer un aérogel également poreux et très léger, « l'aéropectine ». L'aéropectine et l'aérocellulose présentent de fortes similitudes dans leur morphologie. Cependant, l'aéropectine possède de meilleures propriétés thermiques, super-isolantes (0.020 $W.m^{-1}.K^{-1}$), grâce à la nano-structuration du réseau poreux. Ces aérogels sont 100% biosourcés avec un faible impact environnemental, et sont très prometteurs non seulement pour l'isolation thermique mais également pour de nombreuses autres applications, telle que la libération contrôlée de médicaments ou la catalyse. La formation d'aérogel de silice à l'intérieur de la structure poreuse d'aéropectine a augmenté la surface spécifique jusqu'à 700 m^2/g et a permis de diminuer la conductivité thermique (0.017 $W.m^{-1}.K^{-1}$).

Mots clés : Cellulose, pectine, bio-aérogel, matériaux poreux, nano-structuration, super-isolation.

Cellulose and Pectin Aerogels - Towards their nano-structuration

ABSTRACT : The work aims at developing a new generation of bio-based aerogels, mechanically robust and thermally very insulating (super-insulating). Cellulose aerogels, called "aerocelluloses", are known to be very porous and ultra-lightweight materials but present a wide range of pores and therefore moderate thermal insulating properties. We studied several approaches for tuning aerocellulose towards a finer and nanostructured morphology: modification of solvent, cellulose crosslinking and formation of cellulose-based hybrids. It was cellulose cross-linking that greatly improved aerocellulose structure towards a nano-structuration, reflected by the increase of specific surface area and the decrease of thermal conductivity, close to super-insulation (0.026 $W.m^{-1}.K^{-1}$). Another polysaccharide, pectin, was used for preparing a highly porous and very lightweight aerogel called "aeropectin". Aeropectin and aerocellulose were compared; they present many similarities in their morphology. However, aeropectin has better thermal properties, reaching super-insulation (0.020 $W.m^{-1}.K^{-1}$). These bio-aerogels are 100% bio-based, environmentally friendly and present a high potential not only for thermal insulation but also for a broad range of other applications such as controlled drug release and catalysis. The formation of silica aerogel directly inside the porous structure of aeropectin increased the specific surface area up to 700 m^2/g and decreased thermal conductivity (0.017 $W.m^{-1}.K^{-1}$).

Keywords : Cellulose, pectin, bio-aerogel, porous material, nano-structuration, super-insulation.

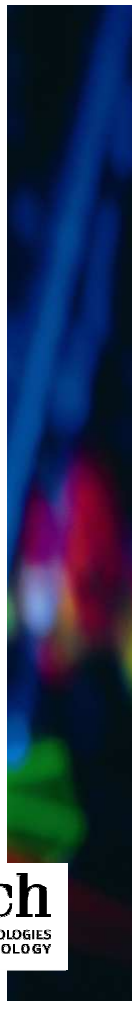

MINES ParisTech

ParisTech
INSTITUT DES SCIENCES ET TECHNOLOGIES
PARIS INSTITUTE OF TECHNOLOGY